SOVIET PHYSICS

JETP

A translation of the Journal of Experimental and Theoretical Physics of the USSR.

SOVIET PHYSICS JETP VOL. 35 (8), NO. 4, pp 577-742 APRIL, 1959

ON THE ZENITH ANGLE DISTRIBUTION OF HIGH-ENERGY EXTENSIVE AIR SHOWERS

V. V. GUSEVA, G. T. ZATSEPIN, and G. B. KHRISTIANSEN

P. N. Lebedev Physics Institute, Academy of Sciences, U.S.S.R.; Moscow State University

Submitted to JETP editor January 7, 1958

J. Exptl. Theoret. Phys. (U.S.S.R.) **35**, 833-837 (October, 1958)

A cloud chamber ~ 600 cm^2 in area and a hodoscope consisting of a large number of counters were used to study the zenith-angle distribution of extensive air showers initiated by ultra-high-energy primaries of ~ 10^{17} ev. The data obtained indicate that, contrary to accepted ideas, such showers are past the stage of maximum development at mountain altitudes.

A direct study of the longitudinal development of extensive air showers (EAS) is extremely difficult. At the same time, the position of the maximum in EAS, which depends on the character of nuclear interactions of ultra-high-energy particles, is of considerable interest. The present experiment set out to provide an estimate of the absorption, at mountain altitudes, of extremely energetic EAS initiated by particles of $\geq 10^{17}$ ev, from their zenith-angle distribution.

The measurements were carried out at 3860 m, using a small cylindrical cloud chamber 30 cm in diameter with an illuminated region 6 cm deep, in conjunction with a hodoscope array described in reference 1 (cf. Fig. 1). The hodoscope made it possible to locate the axes of the EAS with respect to the chamber, and to determine the total number of particles in individual showers.

Since the direction of the particle flux in EAS is nearly vertical, the cloud chamber was placed horizontally.* The effective area of the chamber for vertical flux was 615 cm^2. The pictures were taken from above, the lens axes of the stereoscopic camera forming an angle of 30° with the vertical.

An electric field was used to split the particle tracks to enable us to distinguish shower particles from those arriving at random.* For that purpose the field was switched off after a relatively long delay of ~ 10^{-2} sec with respect to the trigger pulse.

The measure of splitting corresponding to shower particles was found in a separate experiment, in which we determined the splitting of the track of single charged particles, which triggered the chamber. Measurements on the tracks of particles which did not trigger the chamber and which were recorded in random expansions has shown that, on the average, not more than 0.3 random tracks per picture exhibited the splitting accepted as the identification of shower particles.

Altogether 75 EAS were recorded by the array. All tracks of shower particles in the chamber were relativistic.

The distribution of EAS with respect to the number of tracks observed in the cloud chamber is given in Table I. The density spectrum of shower particles measured by the hodoscope[1] and the data of Table I, yield the following features of EAS: the mean shower-particle density averaged over the density spectrum,† the number of cases in which no shower particle fell upon the chamber, and the number of cases when one, two, etc. particles fell upon the chamber. These results are given below

---

*The chamber was placed in a light plywood hut with a lid 3.5 g/cm^2 thick. The thickness of the top glass of the chamber amounted to 1.5 g/cm^2.

*Following a suggestion of N. G. Birger.

†The densities are based on a chamber area of 615 cm^2.

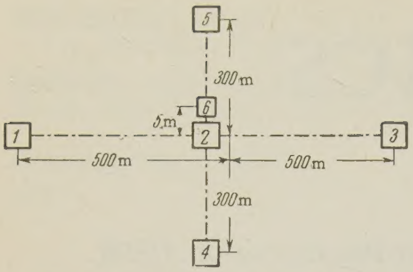

FIG. 1. Plan of the array. 1, 2, 3, 4, 5 – groups of hodoscope counters (for details cf. reference 1); 6 – cloud chamber.

for the hodoscope and the cloud chamber:

	$\bar{\rho}$	$\overline{e^{-\rho}}$	$\overline{\rho e^{-\rho}}$
Cloud chamber measurements	4±1.3	0.5±0.1	0.24±0.05
Hodoscope measurements	3.4	0.34	0.20

It can be seen from the above that there is good agreement between the statistical data obtained by means of the cloud chamber and hodoscope respectively.

The axis position and the total number of particles for nine showers with the largest number of tracks in the cloud chamber are given in Table II.

TABLE II

No. of event	Number of shower-particle tracks in the chamber	Total number of particles in the EAS	Position of the axis (Distance from the cloud chamber, m)
1	6	10^8	200
2	6	$5\cdot10^7$	160
3	12	10^8	170
4	11	10^8	190
5	7	$5\cdot10^8$	700
6	26	10^8	100
7	26	$8\cdot10^8$	250
8	20	$5\cdot10^7$	90
9	80	$2\cdot10^8$	100

It can be seen that in all nine cases the cloud chamber was at the periphery of the high-energy EAS.

The photographs of shower particles enable us to study the angular distribution of shower particles at the periphery of EAS.

The direction of the tracks was determined by projecting the pictures through the same camera which was used for photography.[2]

TABLE I

Number of particles observed in the chamber	Number of showers	Number of particles observed in the chamber	Number of showers
0	28	9	0
1	22	10	0
2	13	11	1
3	2	12	1
4	1	—	—
5	1	>20	1
6	2	26	1
7	1	26	1
8	0	~80	1

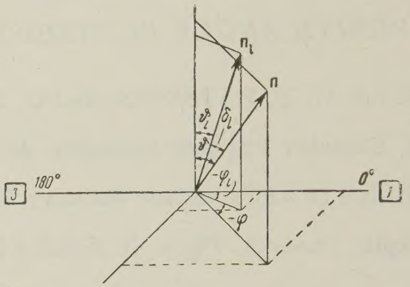

FIG. 2. Angles used in the determination of the mean direction of shower tracks (n) and the deviation of individual tracks (n_i) from it. $\bar{\vartheta}$, $\bar{\varphi}$ – angles determining the mean direction; ϑ_i, φ_i – angles determining the direction of individual particles; δ_i – angles characterizing the deviation of individual tracks from the mean direction. 1 and 3 – hodoscope counter groups (cf. Fig. 1).

The direction of each trajectory was found by measuring the zenith and azimuth angles ϑ_i and φ_i (cf. Fig. 2). These were used in turn to determine the mean direction of the shower particle flux and the deviation of single trajectories from the mean in each measured shower. The mean direction was defined as a vector, the Cartesian components of which are

$$\overline{l_i\cos\vartheta_i}\,;\quad \overline{l_i\sin\vartheta_i\cos\varphi_i}\,;\quad \overline{l_i\sin\vartheta_i\sin\varphi_i}$$

where the index i refers to individual tracks.*

The deviation of individual tracks from the mean direction is characterized by the angle δ_i (Fig. 2) between the mean direction and the track.

The angular distribution of shower particles is characterized by the angle $(\overline{\delta^2})^{1/2}$.

Results of the corresponding calculations are given in Table III.

It should be noted that the mean direction of the shower particle flux at the periphery of EAS is very nearly vertical. Clearly, the axes of these showers should be even closer to the vertical. In spite of poor statistics, it is possible to draw conclusions about the zenith-angle distribution of the recorded showers. Let us assume that the zenith-angle distribution Y(v) is of the form $A\cos^x\theta$, where $A = (x+1)/2\pi$, so that

---

*The factor $l_i = s_0/(S_0\cos\vartheta_i + s_0\sin\vartheta_i)$, where S_0 is the area of the horizontal cross section of the chamber, and s_0 the area of the vertical cross-section along the diameter, takes into account the detection probability of particles going at an angle ϑ_i to the vertical.

$$\iint A \cos^x \theta \sin \theta \, d\theta \, d\varphi = 1.$$

We shall apply now Bayes' Theorem to find the distribution function of the variable x and its most probable value. According to this theorem, the distribution of x is given by the expression

$$P(x, \theta_1, \theta_2, \theta_3 \ldots) = C(x+1) \prod_{i=1} \cos^x \theta_i \sin \theta_i,$$

where it is assumed all values of x have the same a priori probability, and that the probability of occurrence of an angle between $\overline{\theta}_i$ and $\overline{\theta}_i + d\overline{\theta}_i$ under the assumption of a $\cos^x \theta$ distribution is given by the expression

$$[(x+1)/2\pi] \cos^x \theta_i \sin \theta_i \, d\theta_i.$$

TABLE III

No. of event	No. of particles, n	θ, (deg)	φ, (deg)	$\overline{(\delta^2)}^{1/2}$, deg
1	6	25	−150	31
2	6	15	+ 53	28
3	12	16	− 65	32
4	11	14	−156	18
5	7	25	− 51	10
6	26	5	+110	26
7	26	18	+ 20	30
8	>20	≈30	+135	—
9	~80	≈40	+150	—

The function $P(x, \theta_1, \theta_2 \ldots \theta_9) \equiv P(x)$ is shown in Fig. 3. It enables us to find the most probable value of x and its error: $x = 11^{+4.5}_{-3.5}$. The zenith angle distribution is therefore very steep. This is confirmed also by the distribution of the angle φ (Table III). According to Table III, the distribution is uniform; it is almost independent of the bias of the experimental setup,[7] which detects with a higher probability showers with axes lying in the vertical plane passing through the line 1 — 2 — 3 (Fig. 1), i.e., with φ close to 0 and 180°.

It is interesting to compare the measured zenith angle distribution of EAS with that calculated according to the electromagnetic cascade theory for showers of similar energies. The zenith-angle distribution of the axes of showers with the number of particles $N > 10^8$* calculated according to the cascade theory is shown in Fig. 4. The experimental distributions $\cos^x \theta$ for $x = 7.5$ and $x = 15.5$ are included. A large discrepancy is seen between the experimental and theoretical distributions.

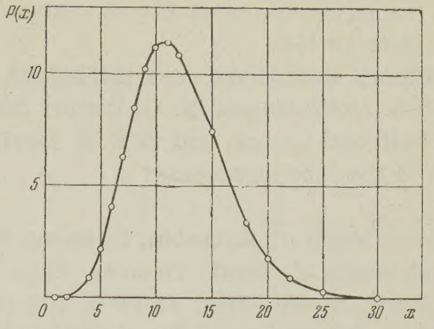

FIG. 3. Distribution function P(x) of the exponent x in the expression for the zenith angle distribution of recorded showers ($\cos^x \theta$). The y axis represents the probability of a given x in arbitrary units.

It is known[6] that the absorption mean free path for shower particles is given by the expression $\lambda = \kappa t/x$, where κ is the exponent of the size spectrum, and t is the depth of the observation level. According to reference 1, $\kappa = 2.1$ for large showers with $N \sim 10^8$; for the Pamir station $t = 650\ \text{g/cm}^2$. For the found values of x we have, therefore, $\lambda = 124^{+58}_{-36}$ which does not contradict the analogous results obtained recently at sea level[6] for showers of the same energy.

The experimental data indicate therefore that EAS initiated by high-energy primaries are, even at mountain altitudes, far beyond the maximum of their development, contrary to accepted ideas. More detailed experiments on the longitudinal development of high-energy showers would be therefore of considerable interest.

In conclusion we wish to give an estimate of the energy of electrons at the periphery of EAS from the values of $\overline{(\delta^2)}^{1/2}$ given in Table III.

From the multiple-scattering theory we have for $E \ll \beta$ (where β is the critical energy, equal to 72 Mev for air), $\overline{(\vartheta^2)}^{1/2} = 19\ \text{Mev}/(E_\beta)^{1/2}$.

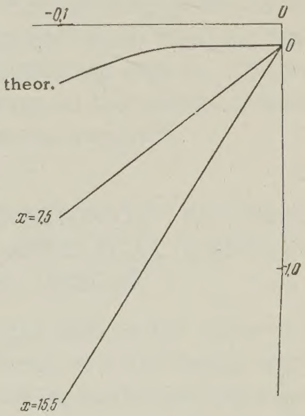

FIG. 4. Comparison between the theoretical and experimental zenith angle distribution of the axes of EAS with the number of particles $N \geq 10^8$ at the depth of 19 radiation units. The x axis represents log cos v, the y axis – log Y(v).

---

*This corresponds, according to the cascade theory, to $\sim 10^{17}$ ev primary energy at 3860 m altitude.

From Table III we obtain for E values on the order of 10 to 20 Mev.

The authors wish to express their deep gratitude to N. A. Dobrotin and N. G. Birger for their valuable help and advice, and to E. S. Levit who took part in the measurements.

---

[1] Antonov, Vavilov, Zatsepin, Kutuzov, Skvortsov, and Khristiansen, J. Exptl. Theoret. Phys. (U.S.S.R.) **32**, 227 (1957), Soviet Phys. JETP **5**, 172 (1957).

[2] Groshev, Dobrotin, and Frank, Dokl. Akad. Nauk SSSR **3**, 287 (1936).

[3] S. Z. Belen'kii, **Лавинные процессы в космических лучах** (Cascade Processes in Cosmic Rays), Gostekhizdat 1948.

[4] G. T. Zatsepin and L. I. Sarycheva, Dokl. Akad. Nauk SSSR **99**, 951, (1954).

[5] Dobrotin, Zatsepin, Rozental', Sarycheva, Khristiansen, and Eidus, Usp. Fiz. Nauk **49**, 185 (1953).

[6] G. T. Zatsepin, Dissertation, Moscow, Phys. Inst. Acad. Sci. 1950.

[7] G. Cocconi, Phys. Rev. **72**, 350 (1947).

Translated by H. Kasha
181

SOVIET PHYSICS JETP VOLUME 35(8), NUMBER 4 APRIL, 1959

INELASTIC SCATTERING OF 300-Mev POSITIVE AND NEGATIVE π MESONS BY PHOTOGRAPHIC EMULSION NUCLEI

G. E. BELOVITSKII

P. N. Lebedev Physical Institute, Academy of Sciences, U.S.S.R.

Submitted to JETP editor March 29, 1958

J. Exptl. Theoret. Phys. (U.S.S.R.) **35**, 838-844 (October, 1958)

We report on the results of measurements of the inelastic scattering cross sections, angular distributions, and energy spectra of 300-Mev π^+ and π^- mesons inelastically scattered by photographic emulsion nuclei. Some other characteristics of inelastic scattering were also obtained.

A study of the interaction of π mesons with nuclei can yield important information about the spatial distribution and energy spectra of nucleons in the nucleus, as well as the magnitude of the potential for a meson-nuclear reaction and its dependence on π-meson energy. Moreover, experimental data on interactions between π mesons and nuclei can be used to check various model representations of the nature of π-meson interaction with nucleons in a nucleus. In particular, it is possible to evaluate the validity of the hypothesis that nucleons inside a nucleus and free nucleons interact with π mesons in an identical manner.

The interactions of π mesons of different energies (mostly π^- mesons) with various nuclei have been the object of a whole series of investigations.[1-9].

The present investigation dealt with the inelastic scattering of 300 ± 15 Mev π^+ and π^- mesons by emulsion nuclei. NIKFI-R and Ilford G-5 photographic plates $400\,\mu$ thick were used. For several reasons the NIKFI plates contained 1.6 times as many light nuclei (O, C) as the G-5 plates (per unit area). The number of nuclei per cm^3 in the NIKFI emulsion (minus hydrogen) was $\sim 7.5 \times 10^{22}$. The conditions under which the photographic plates were irradiated and examined were described before.[8] The results obtained are based on an analysis of 5000 inelastic interactions (stars), due to π^+ and π^- mesons, found when the photographic plates were examined "by area."

We classified as inelastic scattering those interactions (stars) in which, besides a scattered π^+ or π^- meson, the track of at least one other charged particle was observed (in this case the minimum energy transferred by the meson to the nucleus equals ~20 Mev). In this investigation the contribution of other $\pi^\pm$-meson interactions were included in the total cross section. The presence of a scattered charged π meson in a star with an energy > 60 Mev was determined by measuring the ionization (grain density) in the tracks of the secondary particles forming the star. To identify lower-energy π mesons and to determine the energies of the mesons identified by grain density, it was necessary to make still further measurements of Coulomb scattering. These measurements were reliable only for particle tracks $> 1500\,\mu$ long. Therefore, it was not possible to specify all stars containing inelastically scattered mesons (with an energy < 60 Mev).

Only tracks more than $2000\,\mu$ long, having a grain density corresponding to mesons with an energy over 10 Mev, were used to construct the energy spectra of the scattered mesons. Coulomb scattering was measured on a spring stand with a very low noise level, $\overline{D}_{\text{noise}}(200\,\mu) = 0.02\,\mu$, described by Belovitskii et al.[10] The total error attributed to false-scattering effects was $0.1\,\mu$. Third differences[11] were used for the calculation of multiple scattering angles. The average statistical accuracy in the energy measurement of scattered mesons was 16%.

1. DETERMINATION OF THE CROSS SECTION FOR INELASTIC SCATTERING OF 300-Mev π^+ AND π^- MESONS

Experimental data on the ratio of inelastically scattered mesons without charge exchange to the total number of inelastic interactions were obtained from a study of 1622 stars due to π^- mesons and 1377 stars due to π^+ mesons on NIKFI plates and 286 stars due to π^- mesons on G-5 plates. Inelastic scattering occurred in (45 ± 2)% of π^- mesons and in (40 ± 2)% of π^+ mesons. A value

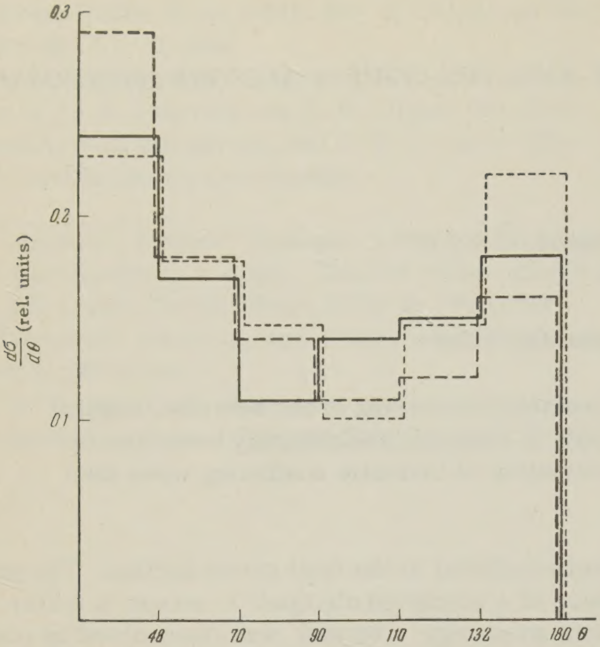

FIG. 1. The angular distribution for inelastically scattered mesons with energies > 60 Mev. The solid line is for π^- mesons (640 tracks), the broken line for π^+ mesons (481 tracks, NIKFI plates), and the dotted line for π^- mesons (95 tracks, G-5 plates).

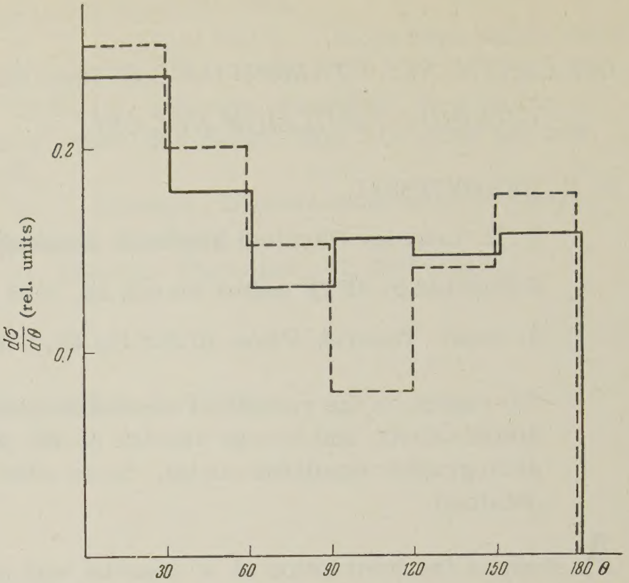

FIG. 2. The angular distribution for inelastically scattered mesons with energies over 10 Mev. The solid line is for π^- mesons (129 tracks), and the dashed line for π^+ mesons (85 tracks).

of (38 ± 4)% was obtained for π^- mesons in G-5 plates. Thus, the percentages of inelastically scattered π mesons of both signs were about the same for both kinds of emulsions.

Combining these data with the data of Dulkova et al.[8] on mean free paths for inelastic interactions of $\pi^\pm$ mesons of identical energy on identical photographic plates, we obtain 200 ± 32 and 185 ± 33 mbn for the cross section for inelastic scattering of π^- and π^+ mesons respectively. When the fraction of inelastically-scattered mesons was being computed, a correction was made for unidentified stars with tracks fue to π mesons with energies up to 60 Mev. In this connection, the fraction of mesons with energies of from 10 to 60 Mev was determined by comparing the number of 10- to 60-Mev mesons that had been identified by measuring grain density and Coulomb scattering with mesons of higher energy. The fraction amounted to (15 ± 5)% of the number of observed scattered mesons. In the case of π^- mesons, this correction should be increased by another 5% to account for slow π^- mesons with energies < 10 Mev. This last correction arose from the fact that in the stars due to π^- mesons we observed the emission of 11 π^- mesons that were stopped in the emulsion (with energy < 10 Mev) and in turn caused nuclear fission. No such correction was made where π^+ mesons were involved, because in the stars due to them not a single case was observed in which a π^+ meson was emitted and was stopped in the emulsion to bring about $\pi^+ \rightarrow \mu^+$ decay.

In order to obtain the total number of inelastic interactions involving π^- mesons, a correction was also made for the number of π^- mesons that "perished in flight" and hence were not observed during our examination of the area. This correction amounted to 5% of the total number of stars observed.[8]

It should be noted further that interactions in which only a scattered meson was detected were also predominantly inelastic. It was found that a considerable amount of energy (up to 200 Mev) could be transferred to a nucleus by a meson without any loss of heavy charged particles by the nucleus. Only the maximum value of the corresponding correction can be determined from the data of Dul'kova et al.,[8] this correction alters the inelastic scattering cross section only slightly.

2. ANGULAR DISTRIBUTIONS FOR INELASTICALLY-SCATTERED π^+ AND π^- MESONS

Figures 1 and 2 show the angular distributions for inelastically scattered π^+ and π^- mesons in the laboratory coordinate system (the data are related to equal solid angles). Figure 1 gives the distribution for mesons with energies > 60 Mev (NIKFI and G-5 plates), and Fig. 2 gives the distribution for mesons with energies > 10 Mev as identified by measuring Coulomb scattering and grain density (NIKFI plates). We see that the angular distributions presented in Fig. 1 and 2 have a similar shape for mesons of equal sign.

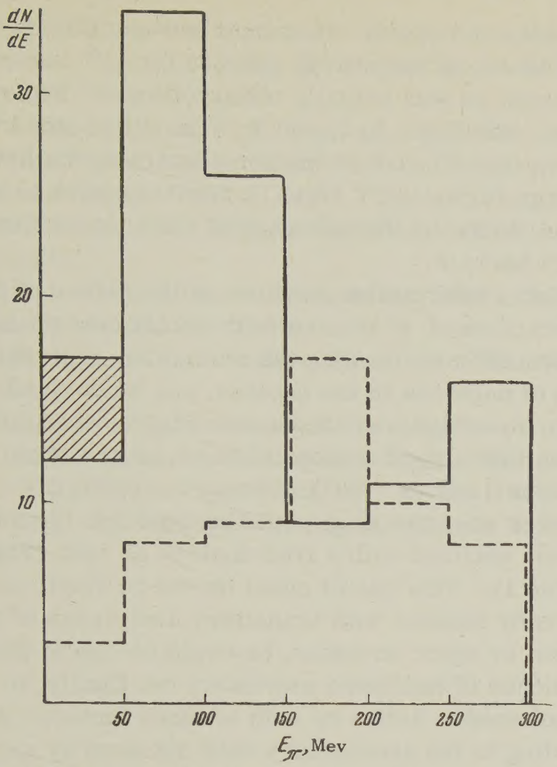

FIG. 3. The energy spectra of inelastically scattered mesons. The solid line is for π^- mesons, the dashed line for π^+ mesons.

The ratio of forward scattered mesons, (angles < 90°) to back scattered (angles > 90°) ones was 1.48 ± 0.14 and 1.5 ± 0.33 for π^+ mesons for both energy groups and 1.15 ± 0.1 and 1.19 ± 0.23 for π^- mesons. From these ratios it follows that the preponderance of forward scattering is notably greater for π^+ mesons than for π^- mesons. The angular distributions should also have included the cases mentioned above where the inelastic scattering of mesons was not accompanied by charged-particle emission. Inclusion of these examples would somewhat increase the proportion of mesons scattered forward.

3. THE ENERGY SPECTRA OF INELASTICALLY-SCATTERED π^+ AND π^- MESONS

Figure 3 shows the energy spectra for inelastically scattered π^+ and π^- mesons. Energy is plotted along the abscissa, the number of occurrences dN/dE along the ordinate. The π^- spectrum was corrected for slow π^- mesons with energies < 10 Mev (the shaded part of the histogram in Fig. 3). No such correction was made for the π^+-meson spectrum. The π^--meson energy spectrum has a maximum for E = 50 to 100 Mev. The maximum in the π^+ meson spectrum is shifted toward the larger energies. The average energy was 133 and 168 Mev for scattered π^- and π^+ mesons respectively.

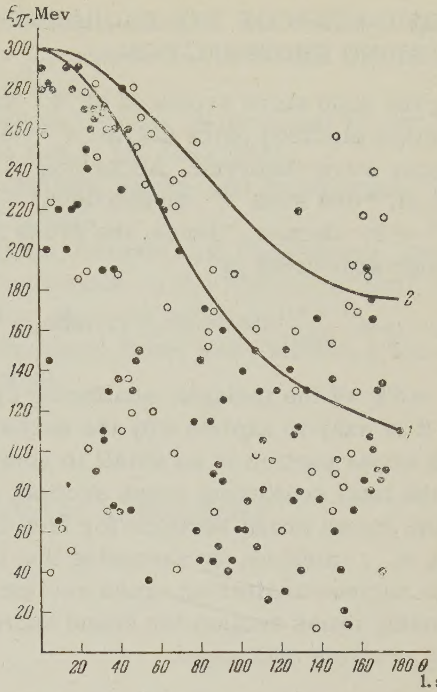

FIG. 4. Relation between the energy of a scattered meson and the scattering angle (laboratory coordinate system). Experimental data: ● is for π^- mesons; and ○ – for π^+ mesons. Curves 1 and 2 were computed for the elastic scattering of 300-Mev π mesons by protons and deuterons respectively.

The average meson energy for three angular intervals is presented in the table. A significant difference is seen to exist between the π^+ and π^- mesons. The average energy of scattered π^+ mesons changes only slightly from one angular interval to another. In the case of π^- mesons, on the other hand, the average energy doubles in the same range. It should be noted, however, that the data for π^+ mesons is based on less statistical material and therefore lacks sufficient accuracy.

Energy and pion charge	Scattering angle in degrees		
	0–60°	60–120°	120–180°
π^+—300 Mev	188	163	152
π^-—300 Mev	194	103	95

Figure 4 presents a more detailed independence between the meson energy E and its scattering angle θ. Here every scattered meson has a corresponding point in the (E, θ) plane. Also shown on the figure are the computed curves for the elastic scattering of 300-Mev mesons by free nucleons and deuterons. For scattering angles less than 90°, not a single case was observed where the energy of a meson noticeably exceeded the energy of a meson scattered by a free nucleon, whereas for scattering angles > 120° the fraction of such cases is fairly high, attaining ~ 20%.

4. DETERMINATION OF THE EXCHANGE-SCATTERING CROSS SECTION

Among the 5000 stars produced by π^+ and π^- mesons, three electron pairs due to $\pi^0 \rightarrow e^+ + e^- + \gamma$ decay were observed. According to Lindenfeld et al.[12] one such π^0 meson decay occurs per 80 $\pi^0 \rightarrow 2\gamma$ decays. Hence, the cross section for exchange scattering is

$$\sigma_{\pi^\pm \rightarrow \pi^0} \approx \left(\frac{3\times 80}{5000}\right) 450 \approx (20 \pm 12)\,\text{mbn},$$

which is ~5% of the inelastic scattering cross section. It is easy to explain why the exchange scattering cross section is so small in comparison with the total scattering cross section, on the basis of the known cross sections for free nucleon scattering of π mesons, by assuming that the ratio of the free nucleon scattering cross section to the corresponding cross section for bound nucleon scattering remains unchanged.

5. ANALYSIS OF THE RESULTS

The pronounced foward scattering of 300-Mev $\pi^\pm$ mesons by free nucleons[13] is absent from the angular distributions for scattered mesons (Figs. 1 and 2). Also, the average energy of the scattered mesons proved to be substantially less than that computed (~220 Mev) on the assumption that the mesons experience one collision in the nucleus. All of this is indicative of the fact that a considerable number of the scattered mesons experience more than one collision in the nucleus.

Mesons were observed among the scattered mesons that had been formed as the result of the absorption of a primary π meson by a nucleon pair, with subsequent internal production of a π meson by one of the nucleons. It was possible to identify such examples during the analysis of the interactions of π^+ mesons with nuclei. In particular, the emission of slow π^- mesons, generated mostly through the above mechanism, was observed in stars due to π^+ mesons. We found that ~10% of the inelastically scattered π mesons were created in this way.

The existence of some kind of difference between the interactions of π^+ and π^- mesons with nuclei, as indicated in the table, is of considerable interest. This difference may be due to the unequal number of protons and neutrons in the heavy nuclei composing the emulsion (Ag, Br). Because of this inequality, the number and geometric arrangement of the collisions experienced by π^+ and π^- mesons in heavy nuclei may prove not to be identical. If this is so, then it would be natural to expect a noticeable difference between the angular distributions and energy spectra for π^+ and π^- mesons, as was actually observed in our experiment (see Figs. 1, 2, and 3). The difference between the π^+ and π^- meson spectra in the low energy region ($E < 10$ to 15 Mev) appears to have been caused by the influence of the nuclear Coulomb barrier.

Some information concerning the nature of the interaction of π mesons with nuclei, and possibly information concerning the momentum distribution of nucleons in the nucleus, can be derived from an analysis of the data in Fig. 4. It is obvious that a good number of the back scattered mesons (angles > 90°) possess substantially greater energies than would be expected if each meson collided with a free nucleon at rest (Fig. 4, Curve 1). This result could be due to single collisions by mesons with transitory complexes of two, three, or more nucleons, or could be due to the influence of nucleonic movement or, finally, to simultaneous action by both of these factors. According to the preliminary data obtained by us, the probability of collisions between 300-Mev mesons and a deuteron in the nucleus amounts to ~2 to 3% of the total cross section for inelastic scattering, or about half of the observed effect.

If the second hypothesis is correct, it must follow that nuclear nucleons can possess a maximum kinetic energy of 50 to 60 Mev. This value is twice the magnitude usually taken for the nuclear model (the degenerate Fermi gas of non-interacting particles). Evidence that high-energy nucleons exist in the nucleus is also provided by several experiments with high-energy particles.[14] Therefore, it is not improbable that the observed effect is caused by the combined action of the factors described above.

It is our intention to compute the inelastic scattering of 330-Mev π mesons by emulsion nuclei with the Monte Carlo method, the assumption being that there are individual meson-nucleon collisions in the nucleus. The angular and energy distributions obtained in this way will be compared with the experiment.

In conclusion, the author wishes to express his gratitude to I. M. Frank for several helpful suggestions made when the investigation was being performed and to A. P. Lagena and O. N. Pavlova for their help with the measurements.

---

[1] Bernardini, Booth and Lederman, Phys. Rev. 83, 1075 (1951).

[2] G. Goldhaber and S. Goldhaber, Phys. Rev. 91, 467A (1953).

[3] Nikol'skii, Kudrin, and Ali-Zade, J. Exptl. Theoret. Phys. (U.S.S.R.) **32**, 48 (1957); Soviet Phys. JETP **5**, 93 (1957).

[4] A. H. Morrish, Phil. Mag. **45**, 47 (1954).

[5] Dzhelepov, Ivanov, Kozodaev, Osipenkov, Petrov, and Rusakov, J. Exptl. Theoret. Phys. (U.S.S.R.) **31**, 923 (1956); Soviet Phys. JETP **4**, 864 (1957).

[6] E. L. Grigor'ev and N. A. Mitin, Dokl. Akad. Nauk. SSSR **103**, 219 (1955).

[7] M. Blau and M. Caulton, Phys. Rev. **96**, 150 (1954).

[8] Dul'kova, Romanova, Sokolova, Sukhov, Toletov, and Shafranova, Dokl. Akad. Nauk. SSSR **107**, 43 (1956); Soviet Phys. "Doklady" **1**, 154 (1956).

[9] A. E. Ignatenko, CERN, Symposium **2**, 313 (1956).

[10] Belovitskii, Golovin, and Sukhov, Приборы и техника эксперимента (Instrum. and Meas. Engg.) **1**, 102 (1956).

[11] Biswas, George, Peters, and Swamy, Nuovo cimento Suppl. **12**, 369 (1954).

[12] Lindenfeld, Sachs, and Steinberger, Phys. Rev. **89**, 531 (1953).

[13] Mukhin, Ozerov, and Pontecorvo, Report at the Joint Conference on the Physics of High Energy Particles, Moscow (1956).

[14] Brueckner, Eden, and Francis, Phys. Rev. **98**, 1445 (1955).

Translated by A. Skumanich
182

SOVIET PHYSICS JETP VOLUME 35(8), NUMBER 4 APRIL, 1959

CHANGE OF SATURATION MAGNETIZATION AND OF ELECTRICAL RESISTANCE OF IRON-NICKEL ALLOYS UNDER HYDROSTATIC COMPRESSION AT LOW TEMPERATURES

E. I. KONDORSKII and V. L. SEDOV

Moscow State University

Submitted to JETP editor April 23, 1958

J. Exptl. Theoret. Phys. (U.S.S.R.) **35**, 845-853 (October, 1958)

The changes of saturation magnetization and of electrical resistance of binary iron-nickel alloys, with nickel contents 38 and 45%, under the influence of pressure, have been studied. Measurements were made in the temperature range 1.7 to 77°K in fields up to 7000 Oe. It was established that the limiting values of the saturation magnetization and of the electrical resistance for $T \to 0$ change under hydrostatic compression, and that the signs of the changes are opposite for the two quantities. These limiting values also change upon increase or decrease of the field in strong magnetic fields, and the differential magnetic susceptibility in the region of magnetic saturation does not vanish at $T \to 0$. The ratio of the change of the limiting value of the saturation magnetization to the change of the limiting value of the electrical resistance under the influence of pressure, and the corresponding ratio under the influence of field, are close to each other.

In theories of ferromagnetism based on the model of a nonconducting lattice of hydrogen-like atoms,[1] the specific saturation magnetization σ_0 at absolute zero is equal to $n\mu$, where n is the number of atoms in unit mass, and where μ is the Bohr magneton. The product $n\mu$ obviously is independent of temperature and pressure. In this case the dependence of the specific spontaneous magnetization σ_S on pressure for $T \neq 0$ is attributed to the influence of the pressure on the exchange integral, and through it on the Curie temperature.

In that theory of metallic ferromagnetics that takes account of interaction between the valence electrons and the conduction electrons (the s-d exchange model of Vonsovskii[2] and the Zener model[3]), the possibility of an influence of pressure upon σ_0 is not excluded; for in this case one considers changes in the values of exchange integrals that affect the resultant magnetic moment, equal to the sum of the magnetic moments of the lattice and of the conduction electrons. There are other cases, also, in which an influence of pressure on the specific magnetization at absolute zero is obviously not excluded — cases in which there are several magnetic subsystems, in particular compounds or alloys in which there are magnetic sublattices.

In band theory, the value of σ_0 is connected with the distribution of electrons among shells (in metals of the iron group, the 3d and 4s shells). Under the influence of pressure, this distribution can change, and a simultaneous change should occur in σ_0 and in the electric resistivity ρ. However, ρ can change also if the change of σ_0 is caused only by changes of the exchange integrals, since magnetic inhomogeneities have an influence on the movement of conduction electrons.

Until recently, the investigation of the influence of pressure on the saturation magnetization of ferromagnetic metals was carried out at or above room temperature.[4] The influence of uniaxial tension on saturation magnetization has been investigated from nitrogen temperatures to the Curie point.[5] The observed changes were interpreted as an indirect effect, caused by a shift of the Curie point under pressure.

The present work was undertaken for the purpose of studying the effect of pressure and field on the saturation magnetization and electrical resistance of ferromagnetic metals and alloys at low (hydrogen and helium) temperatures, and of estimating the influence of these factors on the saturation magnetization at absolute zero. In this article we present results obtained in a study of binary iron-nickel alloys containing 38 and 45% nickel. These alloys were chosen for the reason that iron-nickel alloys of such compositions exhibit, at high temperatures, a larger number of

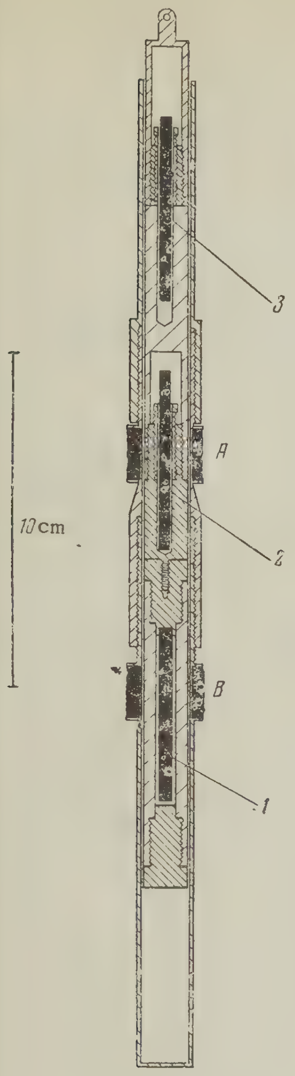

FIG. 1. Arrangement of specimens and coils for measurement of the effect of pressure on the magnetic flux through a specimen.

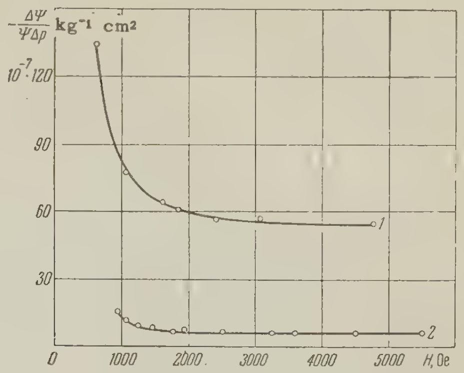

FIG. 2. Relative change or magnetic flux under the influence of pressure at various fields, for iron-nickel alloys: 1) 38% nickel; 2) 45% nickel (T = 20.4°K).

interesting effects than do ferromagnetic metals, and become magnetized to saturation in comparatively small fields; this is convenient for investigations at elevated pressures.

SPECIMENS AND METHOD OF MEASUREMENT

For the measurements of the change of saturation magnetization and electrical resistance under the influence of pressure, the specimens used were cylinders with length $l = 55$ mm and diameters from 3 to 3.5 mm. The differential magnetic susceptibility was measured on cylindrical specimens with $l = 200$ mm and $d = 8$ mm. Before the measurements, the specimens were annealed in vacuum at 1000° for a period of 6 to 8 hours, with subsequent slow cooling in the furnace.

Pressures from 1700 to 1900 kg/cm^2 were produced with a bomb of beryllium bronze, by the freezing of water, in accordance with the method proposed by Lazarev and Kan.[6] The magnitude of the pressure was controlled with the aid of a resistance strain gauge, on the basis of the elastic change of external diameter in the middle part of the bomb. What was measured was the relative change of resistance of the gauge upon freezing of the water. The precision of measurement of the magnitude of the pressure by this method is 3%.

The change of magnetic flux through the test coils was recorded with a photoelectric fluxmeter, constructed according to a system like that described in reference 7. A 15-maxwell change of magnetic flux in the specimen produced a deflection of one division on the scale of the instrument (the critical resistance of the fluxmeter system was 10,000 ohms).

Figure 1 shows the arrangement of the specimens and test coils. Three identical specimens, rigidly fastened to one another, are capable of displacement along the axis of coils A and B, which have 2400 turns apiece and are connected in series. If the system of specimens is so displaced that specimen 2 takes the place of specimen 1 and that specimen 3 takes the place of specimen 2, the magnetic flux through the test coils does not change. If specimen 1 is subjected to pressure, then in such a displacement of the system a change of magnetic flux will be recorded.

The differential susceptibility κ was measured by the following method: to a specimen in a constant magnetic field there was applied an additional magnetic field ΔH, of order 100 Oe, from a special "submagnetizing" coil, which was wound on the outside surface of the liquid-helium dewar; the latter was placed inside the liquid-nitrogen dewar. The test coil consisted of two coaxially arranged sections, connected in series in such a way that in the absence of a specimen, the signals from the two sections upon application of ΔH canceled each other. The magnitude of the observed effect was proportional to the difference between the numbers

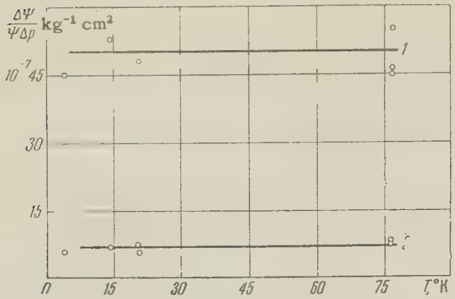

FIG. 3. Relative change of magnetic flux at saturation under the influence of pressure, for iron-nickel alloys of compositions: 1) 38% nickel; 2) 45% nickel; H = 4500 Oe.

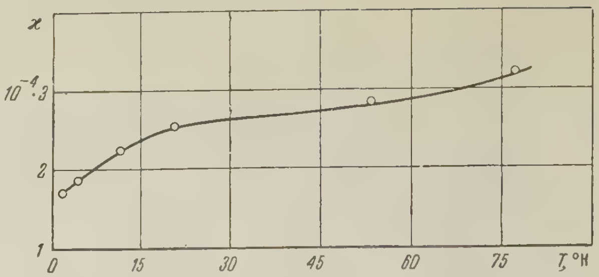

FIG. 5. Dependence of the differential magnetic susceptibility on temperature for an iron-nickel alloy with 38% nickel; H = 6700 Oe.

of turns of the inside and outside sections, which in our case was 6300 turns.

The measurement of the electrical resistance under pressure was carried out by the method described in reference 6. The magnitude of the pressure in this case was determined from the shift of of the transition temperature of tin in the superconducting state.

The properties mentioned above were determined for temperatures from 1.7 to 77°K. Magnetic fields up to 7000 Oe were obtained with a solenoid with water cooling. In the middle part of the solenoid, the change of field over a distance of 80 mm along the axis did not exceed 1%.

RESULTS OF THE MEASUREMENTS

In Figs. 2 and 3 are shown curves that describe the variation of $\Delta\Psi/\Psi\Delta p$ with field at 20.4°K, and with temperature at field $H = 4500$ Oe, respectively; here $\Delta\Psi$ is the magnitude of the change of magnetic flux Ψ in the specimen upon change of the pressure by amount Δp. Within the precision of the measurements, $\Delta\Psi/\Psi\Delta p$ does not vary with temperature over the range 4.2 to 77°K; it does not approach zero as $T \to 0$.

The values of $\Delta\Psi/\Psi\Delta p$ are related to the values of interest to us, namely the values of $\Delta\sigma/\sigma\Delta p$, where $\Delta\sigma$ is the change of specific magnetization σ upon change of the pressure by Δp. The relation is

$$\frac{\Delta\Psi}{\Psi\Delta p}=\frac{\Delta\sigma}{\sigma\Delta p}-\frac{1}{3V}\frac{\Delta V}{\Delta p}. \qquad (1)$$

For the alloy studied, the coefficient of compressibility $\frac{1}{V}\frac{\Delta V}{\Delta p} = -12 \times 10^{-7}\ \mathrm{cm}^2/\mathrm{kg}$; thus the second term in the right member of (1) has a sign opposite to that of the observed value of $\Delta\Psi/\Psi\Delta p$ in both alloys. It follows from this that the value of $\Delta\sigma/\sigma\Delta p$ also does not approach zero as $T \to 0$; consequently, the value of σ_0, for the alloy studied, changes under the influence of pressure.

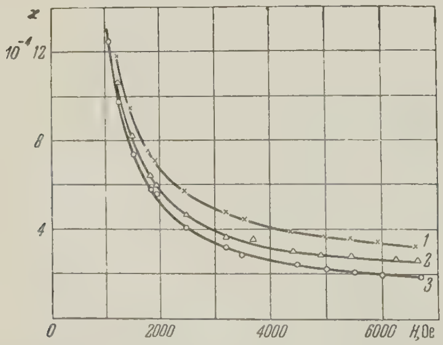

FIG. 4. Dependence of the differential magnetic susceptibility in strong fields upon the field intensity at various temperatures, for a nickel-iron alloy 38% nickel. 1) T = 77°; 2) T = 20.4°; 3) T = 4.2°K.

In Fig. 4 are shown curves that describe the variation with field of the magnitude of the differential susceptibility $\kappa = \Delta I/\Delta H$ in strong fields at various temperatures. The dependence of κ on temperature at $H = 6700$ Oe is described by the curve shown in Fig. 5; from the course of the curve it is clear that κ does not approach zero as $T \to 0$. Hence, as will be shown below, it can be concluded that the value of σ_0, for the alloy studied, changes not only under the influence of pressure, but also under the action of a magnetic field.

In Figs. 6 and 7 are shown curves that describe the variation with temperature of the values of $\Delta R/R_0\Delta p$ and $\Delta R/R_0\Delta H$, respectively. Here ΔR is the change of electrical resistance, in the strong magnetic field region, upon change of pressure by amount Δp or of field by amount ΔH; R_0 is the electrical resistance at normal pressure and at

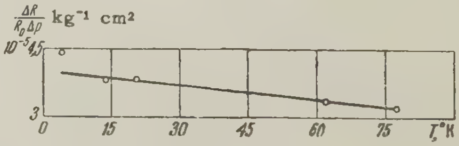

FIG. 6. Dependence on temperature of the relative change of electrical resistance of iron-nickel alloys with 38% nickel under the influence of pressure.

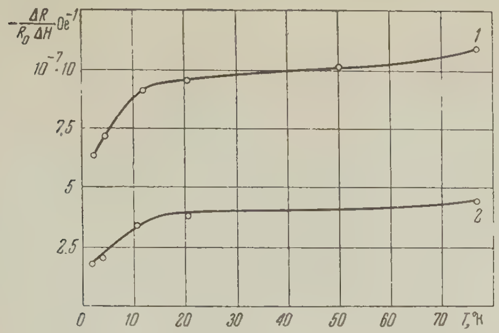

FIG. 7. Dependence on temperature of the relative change of electrical resistance of an iron-nickel alloy [composition: 1) 38% nickel; 2) 45% nickel], for small increments of the magnetic field at strong magnetic fields (in the range of the paraprocess).

4.2°K. From the course of the curves in Figs. 6 and 7 it is clear that the quantities $\Delta R/R_0\Delta p$ and $\Delta R/R_0\Delta H$ do not approach zero as $T \rightarrow 0$. The existence at $T \rightarrow 0$ of residual values of one of these quantities ($\Delta R/R_0\Delta H$) had already been established.[8,9]

Table I gives numerical values of some of the measured quantities. Table II gives their limiting values, obtained by linear extrapolation to $T = 0$ of the part of the corresponding curves belonging to the interval 1.7 to 4.2°K; the values $(\Delta I/\Delta H)^*_{p0}$ and $(\Delta R/R\Delta H)^*_{p0}$ were obtained by linear extrapolation to zero of the part lying in the interval 20.4 to 53°K (cf. Figs. 5 and 7).

DISCUSSION OF RESULTS

We shall first show that the existence of residual values of κ and $\Delta R/R_0\Delta H$ at $T \rightarrow 0$ cannot be considered a consequence of the change of volume of the lattice under the action of the magnetic field. The latter possibility is not excluded, since for the alloy studied $(\Delta V/V\Delta H)_{T=0} = -(\delta\Delta\sigma/\Delta p)_{T=0} \neq 0$ (δ is the value of the density). The differential susceptibility is

$$\varkappa = \left(\frac{\partial I}{\partial H}\right)_p = \delta\left(\frac{\partial \sigma}{\partial H}\right)_p - \frac{1}{V}\left(\frac{\partial V}{\partial H}\right)_p I = \delta\left[\left(\frac{\partial \sigma}{\partial H}\right)_p + \left(\frac{\partial \sigma}{\partial p}\right)_H I\right] \tag{2}$$

With the aid of known thermodynamic relations, it is easy to obtain

$$\left(\frac{\partial \sigma}{\partial H}\right)_p = \left(\frac{\partial \sigma}{\partial H}\right)_V - \delta\left(\frac{\partial \sigma}{\partial p}\right)_H^2 \Big/ \frac{1}{V}\left(\frac{\partial V}{\partial p}\right)_H. \tag{3}$$

By substituting (3) in (2), we get

$$\varkappa = \delta\left(\frac{\partial \sigma}{\partial H}\right)_V - \left[\delta^2\left(\frac{\partial \sigma}{\partial p}\right)_H^2 \Big/ \frac{1}{V}\left(\frac{\partial V}{\partial p}\right)_H\right] + \delta\left(\frac{\partial \sigma}{\partial p}\right)_H I. \tag{4}$$

TABLE I

Ni content in the alloy specimens	T,°K	$\frac{1}{\Psi}\left(\frac{\Delta\Psi}{\Delta p}\right)_H\cdot 10^7$, kg^{-1} cm^2	$\left(\frac{\Delta I}{\Delta H}\right)_p\cdot 10^4$, G·Oe^{-1}	$\frac{1}{R_0}\left(\frac{\Delta R}{\Delta p}\right)_H\cdot 10^5$, kg^{-1} cm^2	$\frac{1}{R_0}\left(\frac{\Delta R}{\Delta H}\right)_p\cdot 10^7$, Oe^{-1}
38%	1.7	—	1.71±0.07	—	— 6.6±0.35
	4,2	—50±8	1.88±0.07	4.5 ±0,3	— 7.3±0.35
	11.3	—	2,25±0,1	—	— 9,1±0.35
	14.5	—50±8	—	3,7 ±0.2	—
	20.4	—50±8	2.5 ±0.1	3.8 ±0.2	— 9,6±0.35
	53	—	2,8 ±0,1	3.5 ±0.2	—10,2±0,5
	77	—50±8	3,2 ±0.1	3.2 ±0,2	—10,9±0.5
	293	—	11,7 ±0.3	—	—
45%	1.7	—	—	—	— 1,8±0,2
	4.2	— 7±1.5	—	1.35±0.2	— 2,15±0,2
	11.3	—	—	1.4 ±0.2	— 3,5±0.2
	14.5	— 7±1,5	—	—	—
	20.4	— 7±1,5	—	1,4 ±0.2	— 3.85±0.2
	53	—	—	—	—
	77	— 7±1.5	—	—	— 4,5±0.5

TABLE II

	For alloy Ni content 38%	For alloy Ni content 45%		For alloy Ni content 38%	For alloy Ni content 45%
$\delta\sigma_0$, G	1370	1380	$\left(\frac{\Delta I}{\Delta H}\right)^*_{p0}\cdot 10^4$, G·Oe^{-1}	2.33	—
$R_0\cdot 10^4$, Ω	3,12	1,88	$\frac{1}{R_0}\left(\frac{\Delta R}{\Delta p}\right)_0\cdot 10^5$, kg^{-1} cm^2	4.0	1,35
$\frac{1}{\Psi}\left(\frac{\Delta\Psi}{\Delta p}\right)_0$ 10^7 kg^{-1} cm^2	—50	—7	$\frac{1}{R_0}\left(\frac{\Delta R}{\Delta H}\right)_{p0}\cdot 10^7$, Oe^{-1}	—6,20	—1.4
$\left(\frac{\Delta I}{\Delta H}\right)_{p0}$ 10^4 G·Oe^{-1}	1,62	—	$\frac{1}{R_0}\left(\frac{\Delta R}{\Delta H}\right)^*_{p0}\cdot 10^7$, Oe^{-1}	—9.1	—

The first term in parentheses describes the changes of specific magnetization σ (in strong fields) that are connected with orientation of the spins (paraprocess) and with increase of the number of electrons contributing to ferromagnetism, purely as a result of the action of the field (at constant volume). The second term describes the changes of σ that are connected with an increase of the number of electrons contributing to ferromagnetism, or with their orientation, in consequence of a change of volume of the lattice. The third term, which is equal to the second term of (2), describes a trivial change of the magnetic moment density that is connected with a change of volume of the body in consequence of magnetostriction. By inserting in (4) the values of $\delta\partial\sigma/\partial p$ obtained from our measurements and the value of $\partial V/V\partial p$, we can estimate the influence of volume magnetostriction on κ. The calculation gives, for the alloy with 38% nickel, the value 0.46×10^{-4} for the second term and -0.1×10^{-4} for the third in formula (4). Both terms together amount to about 20% of the value of κ at 4.2°. Thus the main part of κ at $T \rightarrow 0$ is determined by a direct and not an indirect effect of the field on σ_0.

The relative change of electrical resistance under the influence of pressure is

$$\frac{\Delta R}{R\Delta p} = \frac{\Delta \rho}{\rho \Delta p} - \frac{1}{3}\frac{\Delta V}{V\Delta p}. \tag{5}$$

Here $\Delta\rho$ is the change of specific electrical resistance upon change of the pressure by Δp. The second term, for the alloy studied, amounts to $4 \times 10^{-7}\ \mathrm{cm}^2\,\mathrm{kg}^{-1}$, i.e., about 1% of the measured value of $\Delta R/R\Delta p$ at $T = 4.2°\mathrm{K}$.

The relative change of electrical resistance in strong magnetic fields (in the paraprocess region) under the action of the field is

$$\left(\frac{\Delta R}{R\Delta H}\right)_p = \frac{1}{\rho}\left(\frac{\Delta\rho}{\Delta H}\right)_V + \left[\frac{1}{\rho}\left(\frac{\Delta\rho}{\Delta p}\right)_H \left(\frac{\Delta V}{\Delta H}\right)_p \Big/ \left(\frac{\Delta V}{\Delta p}\right)_H\right] - \frac{1}{3V}\left(\frac{\Delta V}{\Delta H}\right)_p. \tag{6}$$

The second term in this expression is analogous to the second term in (4) and represents the change of specific electrical resistance connected with a change of volume of the lattice on magnetization. By inserting values of $\frac{1}{V}\left(\frac{\Delta V}{\Delta H}\right)_p = -\delta\left(\frac{\Delta\sigma}{\Delta p}\right)_H$ and of $\frac{1}{V}\left(\frac{\Delta V}{\Delta p}\right)_H$, it is easy to estimate the magnitude of the second and third terms. The calculation gives, for the alloy with 38% nickel, the value $-2.5 \times 10^{-7}\ \mathrm{Oe}^{-1}$ for the second term and $-2 \times 10^{9}\ \mathrm{Oe}^{-1}$ for the third. The larger of these values amounts to about 40% of the value of $(\Delta R/R\Delta H)_p$ at $T = 4.2°\mathrm{K}$. For the alloy with 45% nickel, we find correspondingly -0.16×10^{-7} and -0.5×10^{-9}. Thus the ultimate changes of electrical resistance with increase of field at strong fields, as $T \rightarrow 0$, cannot be explained entirely on the basis of the effect of volume magnetostriction. With the aid of formulas (1) and (4) to (6) and of the data obtained in the experiment, it is easy to find the limiting values at $T \rightarrow 0$ of the quantities of interest to us: $\frac{1}{\sigma_0}\left(\frac{\Delta\sigma}{\Delta p}\right)_0$, $\frac{1}{\rho_0}\left(\frac{\Delta\rho}{\Delta p}\right)_0$, $\delta\left(\frac{\Delta\sigma}{\Delta H}\right)_{V0}$, and $\frac{1}{\rho_0}\left(\frac{\Delta\rho}{\Delta H}\right)_{V0}$. These values are given in Table III. The values of $\delta\left(\frac{\Delta\sigma}{\Delta H}\right)_{V0}$ and $\frac{1}{\rho_0}\left(\frac{\Delta\rho}{\Delta H}\right)_{V0}$ are calculated by formulas (4) and (6); $\delta\left(\frac{\Delta\sigma}{\Delta H}\right)^*_{V0}$ and $\frac{1}{\rho_0}\left(\frac{\Delta\rho}{\Delta H}\right)^*_{V0}$ are obtained if in these formulas we insert, instead of $\left(\frac{\Delta I}{\Delta H}\right)_{p0}$ and $\frac{1}{R_0}\left(\frac{\Delta R}{\Delta H}\right)_{p0}$, $\left(\frac{\Delta I}{\Delta H}\right)^*_{p0}$ and $\frac{1}{R_0}\left(\frac{\Delta R}{\Delta H}\right)^*_{p0}$ from Table II. Also given in Table III are the ratios of the limiting values mentioned; and in the last line, for comparison, is given the ratio $\left(\frac{R_{20} - R_0}{R_0}\right) \Big/ \left(\frac{I_{20} - I_0}{I_0}\right)$, which describes the relation between the changes of electrical resistance and of saturation magnetization upon change of temperature in the hydrogen temperature range.[10]

With the aid of the values of $(\Delta\sigma/\sigma\Delta p)_0$ and $(1/\rho_0)(\Delta\rho/\Delta p)_0$ given in Table III, it is possible to estimate the values of the dimensionless quantities $n_\sigma = \left(\frac{\Delta\sigma}{\sigma}\right)_0 \Big/ \frac{\Delta a}{a}$ and $n_\rho = \left(\frac{\Delta\rho}{\rho}\right)_0 \Big/ \frac{\Delta a}{a}$, where $\Delta a/a$ is the fractional change of the lattice constant of the alloy under the influence of pressure Δp; $\Delta a/a \approx \frac{1}{3}\Delta V/V$. For the alloys under consideration, $\Delta a/a \approx 4 \times 10^{-7}\Delta p$. By use of the values of quantities given in Table III, we get for the alloy with 38% nickel, $n_\sigma \approx 15$ and $n_\rho \approx 100$; and for the alloy with 45% nickel, $n_\sigma \approx 2.5$ and $n_\rho \approx 30$.

From a consideration of the quantities given in Table III it is clear that whether it is a pressure or a field that is acting, an increase of σ_0 is accompanied by a decrease of ρ_0 and vice versa. The values of the ratios $\left(\frac{\Delta\rho}{\rho\Delta p}\right)_0 \Big/ \left(\frac{\Delta\sigma}{\sigma\Delta p}\right)_0$, $\left(\frac{\Delta\rho}{\rho\Delta H}\right)_{V0} \Big/ \left(\frac{\Delta\sigma}{\sigma\Delta H}\right)_{V0}$, and $\frac{R_{20} - R_0}{R_0} \Big/ \frac{I_{20} - I_0}{I_0}$ are of a single order and close to one another; this

TABLE III

	For alloy Ni content			For alloy Ni content	
	38%	45%		38%	45%
$\left(\frac{\Delta\sigma}{\sigma\Delta p}\right)_0 \cdot 10^7$, kg^{-1} cm^2	—54	—11	$\frac{1}{\rho_0}\left(\frac{\Delta\rho}{\Delta H}\right)^*_{V0} \cdot 10^7$, Oe^{-1}	—6.62	—
$\delta\left(\frac{\Delta\sigma}{\Delta H}\right)_{V0} \cdot 10^4$, G·Oe^{-1}	1.26	—	$\left(\frac{\Delta\rho}{\rho\Delta p}\right)_0 \Big/ \left(\frac{\Delta\sigma}{\sigma\Delta p}\right)_0$	—7.4	—11.8
$\delta\left(\frac{\Delta\sigma}{\Delta H}\right)^*_{V0} \cdot 10^4$, G·Oe^{-1}	2.0	—	$\left(\frac{\Delta\rho}{\rho\Delta H}\right)_{V0} \Big/ \left(\frac{\Delta\sigma}{\sigma\Delta H}\right)_{V0}$	—4.1	—
$\frac{1}{\rho_0}\left(\frac{\Delta\rho}{\Delta p}\right)_0 \cdot 10^5$, kg^{-1} cm^2	4.0	1.3	$\left(\frac{\Delta\rho}{\rho\Delta H}\right)^*_{V0} \Big/ \left(\frac{\Delta\sigma}{\sigma\Delta H}\right)^*_{V0}$	—4.6	—
$\frac{1}{\rho_0}\left(\frac{\Delta\rho}{\Delta H}\right)_{V0} \cdot 10^7$, Oe^{-1}	—3.7	—1.3	$\frac{(R_{20}-R_0)}{R_0} \Big/ \frac{(I_{20}-I_0)}{I_0}$	—5.45	—6.7

points to the existence of a close connection between the changes of σ_0 and of ρ_0. We note that at fields of 6000 to 7000 Oe, the differential susceptibility κ decreases with increase of field somewhat faster than does $\Delta\Psi/\Psi\Delta p$ (cf. Figs. 2 and 4), and therefore in stronger fields the ratios mentioned should become even closer.

The existence of a connection between the changes of σ_0 and of ρ_0 under the influence of pressure and field indicates that the value of σ_0, like that of ρ_0, depends on the state of the conduction electrons. Changes of σ_0 and ρ_0 may be caused by: (1) transitions of electrons from the s to the d shell on compression of the lattice, or contrary transitions on increase of magnetic field; (2) change of the spontaneous magnetization of the d electrons as a result of the influence of pressure or field on the magnitude of the d-d exchange integrals, when there is uncompensated antiferromagnetism in the alloy and some of the exchange integrals (d_{Ni}-d_{Fe} or d_{Ni}-d_{Ni} and d_{Fe}-d_{Fe}) are negative; (3) change of the spontaneous magnetization of the s electrons as a result of the influence of pressure or field on the magnitude of the s-d exchange integral.

In the first case the observed signs of the changes in σ_0 and ρ_0 receive a simple explanation;* however, the reason for the large effect of pressure on σ_0 in the 38% alloy remains an open question. It also remains an open question why, in the alloys with 30 to 40% nickel (which according to our data show the largest changes of σ_0 under the influence of pressure), there are also observed appreciable changes of the spontaneous magnetization under uniaxial tension in the vicinity of the Curie point.[5] In the second case there is an explanation for the connection that exists between the change of σ_0 and the shift of the Curie point under the influence of pressure; however, it is more difficult to explain the connection between the changes of σ_0 and of ρ in this case. The possibility is not excluded that in the changes of σ_0 and ρ_0 under the influence of pressure and field, all the causes indicated above play a role.

---

*We note that if the changes of σ_0 and ρ_0 under the influence of pressure are mainly due to the first cause, there arises a possibility of using the values of the ratio $(\Delta\rho/\rho\Delta p)_0/(\Delta\sigma/\sigma\Delta p)_0$ for a rough estimate of the number x of conduction electrons belonging to one atom of the alloy. This estimate gives, for the alloy with 38% nickel, the value

$$x \approx \frac{\rho_0}{\mu N}\frac{\Delta\sigma_0}{\Delta\rho_0}(0.62\, A_{Fe} + 0.38\, A_{Ni}) \approx 0.2.$$

---

[1] F. Bloch, Z. Physik **74**, 295 (1932); C. Møller, Z. Physik **82**, 559 (1933); T. Holstein and H. Primakoff, Phys. Rev. **58**, 1098 (1940).

[2] S. V. Vonsovskii and Ia. S. Shur, Ферромагнетизм (Ferromagnetism), OGIZ, 1948.

[3] C. Zener, Phys. Rev. **81**, 440 (1951); **82**, 403 (1951); **83**, 299 (1951); **85**, 324 (1952).

[4] M. Ebert and A. Kussman, Physik. Z. **38**, 437 (1937); K. H. v. Klitzing and J. Gielessen, Z. Physik **146**, 59 (1956).

[5] K. P. Belov, J. Tech, Phys. (U.S.S.R.) **19**, 1032 (1949); Izv. Akad. Nauk SSSR, Ser. Fiz., **16**, 420 (1952); Физика металлов и металловедение (Physics of Metals and Metal Research) **2**, 447 (1956).

[6] B. G. Lazarev and L. S. Kan, J. Exptl. Theoret. Phys. (U.S.S.R.) **14**, 439 (1944).

[7] S. P. Kapitza, J. Tech. Phys. (U.S.S.R.) **25**, 1307 (1955).

[8] J. Smit, Physica **17**, 612 (1951).

[9] K. P. Belov and A. V. Ped'ko, J. Exptl. Theoret. Phys. (U.S.S.R.) **33**, 815 (1957), Soviet Phys. JETP **6**, 628 (1958).

[10] Kondorskii, Galkina, and Chernikova, J. Exptl. Theoret. Phys. (U.S.S.R.) **34**, 1070 (1958), Soviet Phys. JETP **7**, 741 (1958).

Translated by W. F. Brown, Jr.
183

SOVIET PHYSICS JETP VOLUME 35(8), NUMBER 4 APRIL, 1959

*THE $n + p \to \pi^0 + d$ REACTION FOR NEUTRONS OF 600 Mev EFFECTIVE ENERGY AND THE CHARGE-INDEPENDENCE HYPOTHESIS**

V. B. FLIAGIN, V. P. DZHELEPOV, V. S. KISELEV, and K. O. OGANESIAN

Joint Institute for Nuclear Research

Submitted to JETP editor April 30, 1958

J. Exptl. Theoret. Phys. (U.S.S.R.) 35, 854-867 (October, 1958)

The angular distribution and total cross section for the production of π^0 mesons in the $n + p \to \pi^0 + d$ reaction have been measured for 600-Mev neutrons. The experimental arrangement permitted the recording of coincidences between the deuteron and one of the π^0-meson decay quanta. Gamma quanta were recorded with a scintillation-counter telescope containing a lead converter. The deuterons were analyzed by means of a multichannel magnetic spectrometer. The angular distribution, $(0.220 \pm 0.222) + \cos^2\theta$ (in the c.m.s.), and the total cross section for the reaction, $(1.5 \pm 0.3) \times 10^{-27}$ cm^2, confirm the charge-independence hypothesis.

INTRODUCTION

One of the foundations of the contemporary phenomenolgical theory of strong interactions is the hypothesis of charge invariance of nuclear forces. An elementary analysis shows that none of our present experimental knowledge of strong interactions conflicts with this hypothesis. The most promising method of proving the conservation of isotopic spin at high energies is an exact quantitative study of pion production processes. We can obtain valuable information in this connection by comparing the pion production cross sections in the reactions

$$p + p \to \pi^+ + d, \qquad (1)$$

$$n + p \to \pi^0 + d. \qquad (2)$$

In 1952 Yang pointed out that if isotopic spin is conserved in meson-nucleon interactions the differential cross sections for the given reactions should obey the simple relation

$$\sigma_2(\theta) = \frac{1}{2}\sigma_1(\theta). \qquad (3)$$

In other words, the pions produced in reactions (1) and (2) should have identical angular distributions while the total cross sections should have the ratio 2:1.

Reaction (1) has been studied in detail by many workers (see the review in reference 1 as well as references 2 to 6) and we now possess information concerning this reaction from threshold up to proton energies of 900 Mev. The synchrocyclotron of the Joint Institute for Nuclear Research has been used to investigate this reaction systematically in the energy region 460 to 900 Mev.[4-6]

There are many difficulties associated with the study of reaction (2) compared with (1). These result mainly from the small intensity of the neutron beams, the broad neutron energy spectrum and, finally, the relative difficulty of identifying the reaction, since one of the produced particles (the π^0 meson) is neutral and decays practically instantaneously. These conditions are apparently the principal reason that only two studies of reaction (2) have thus far been reported in the literature (references 7 and 8) and at only a single neutron energy of 400 Mev. In reference 7 only the π^0-meson angular distribution was determined; the result obtained was $(0.20 \pm 0.06) + \cos^2\theta$. In reference 8 measurements of both the angular distribution and the total cross section were given. It must be pointed out, however, that whereas the latter article gave the total cross section with accuracy ~20% ($\sigma_t = (0.41 \pm 0.07) \times 10^{-27}$ cm^2), the accuracy of the angular distribution was clearly inadequate. As a whole these experiments with the given accuracy provided evidence of the fulfillment of Yang's relation.[3]

The investigations which will be described here were performed for the purpose of testing the charge independence of meson-nucleon interactions through a study of reaction (2) at an energy considerably above the meson production threshold.

EXPERIMENTAL METHOD

Because of the relatively weak neutron beam obtained from the synchrocyclotron (3×10^4 cm^{-2}

---

*Reported in November, 1957 at the third session of the Scientific Council of the Joint Institute for Nuclear Research.

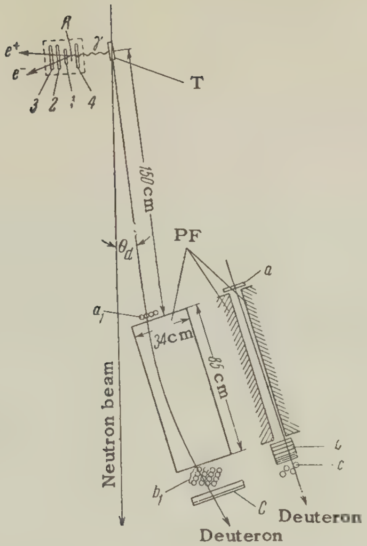

FIG. 1. Experimental arrangement. C) – Pb converter, T) – target (CH_2 or C), PF – pole faces of electromagnet; 1, 2, 3, 4) – scintillation counters

sec^{-1}) the experimental method and the apparatus must be as efficient as possible. We therefore used a system of recording the coincidence between the deuteron and only a single γ quantum from the π^0-meson decay. With 600-Mev neutrons this setup possesses an efficiency that is greater by a factor of several tens than that employed in reference 7, where three telescopes were used to register the simultaneous production of two γ quanta and the deuteron.

For deuteron momentum discrimination we used a magnetic spectrometer which permitted the definition of a relatively narrow energy interval in the primary neutron spectrum. The experimental procedure also took into account the necessity of excluding particles from the reaction

$$n + p \rightarrow \pi^0 + n + p, \tag{4}$$

which could seriously distort the results. This was easily accomplished by the method of using the magnetic spectrometer in the deuteron-recording channel.

A diagram of the experimental setup is shown in Fig. 1. The neutron beam passed through a collimator in the form of a vertical slit and struck a polyethylene (CH_2) or graphite (C) target. The effect due to hydrogen was determined from the difference of the CH_2 and C effects. For different deuteron-energy intervals (different angular intervals in the center-of-mass system) two different pairs of targets were used (with CH_2 thicknesses of 6 g/cm^2 and 2 g/cm^2) in order to minimize the corrections for multiple scattering of deuterons in the targets. The graphite and polyethylene targets contained the same number of carbon nuclei. The results obtained with targets of different thicknesses agreed in general.

The γ quanta from π^0-meson decay were registered by a telescope set up in the direction of π^0-meson motion in the laboratory system. The telescope consisted of three scintillation counters (with diameters of 90, 120 and 125 mm) preceded by a lead converter of 7 mm thickness and 90 mm diameter. The fourth counter, which was in front of the converter, was connected in anticoincidence with the others and served to reduce the background from charged particles. The scintillation counters contained solutions of terphenyl in toluene or phenylcyclohexane, the containers of which were made of duraluminum or plexiglas.

To eliminate the influence of the magnetic field, the photomultipliers were screened by iron 5 mm thick. Additional screening was provided by the external iron jackets of the counters. The effectiveness of the screening was tested by the γ count with the magnetic field on and off. At the high voltage of the photomultipliers the telescope plateau was about 200 v with a slope of not more than 10%. The energy threshold of the γ-ray telescope, which was determined by the thickness of the scintillators, was quite low (~25 Mev). The low threshold was necessary in order to minimize the variation of telescope efficiency as the gamma-ray energies varied within the limits $140 \leq E_\gamma \leq 400$ Mev.

THE MAGNETIC SPECTROMETER

The spectrometer was constructed with an electromagnet of 18,000 Oe maximum field and 60 mm gap. An analysis of all the required experimental conditions (the required energy and angular resolutions, maximum efficiency with minimum background, minimum number of channels, etc.) led to the spectrometer shown in Fig. 1.

The fast-deuteron detectors were thin-walled (0.15 mm steel) counters filled with methylal (CH_2OCH_3) operating with "limited proportionality" at high voltages (1700 to 2100 v). These counters were arranged in three groups along the deuteron trajectory close to the edges of the pole faces. Figure 1 shows the counter system for registering deuterons in coincidence with a single γ-ray telescope. When permitted by the geometry, the time required for the measurements was reduced by the use of two such systems with a common target. The counters of groups a and b had the following dimensions:

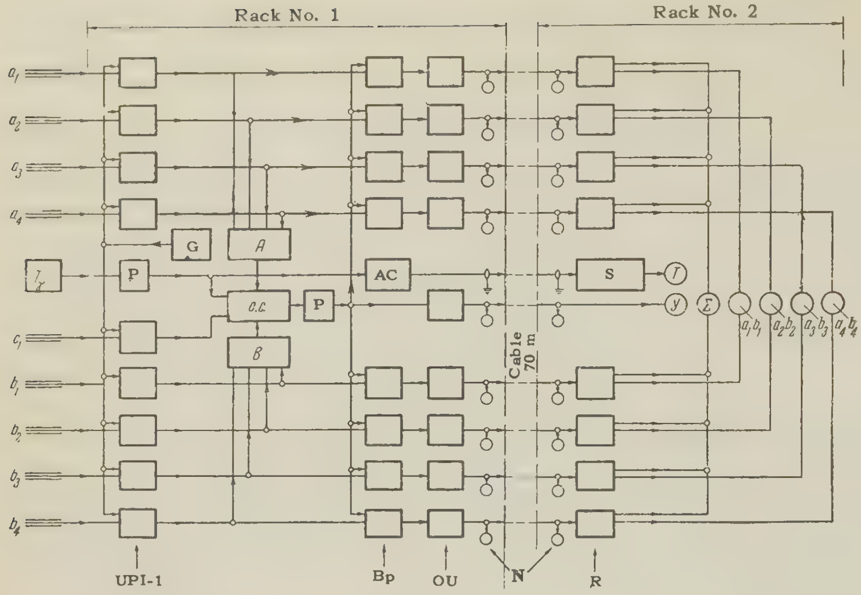

FIG. 2. Block diagram of the electronic circuit. T_γ) γ telescope, P) pulse-shaping univibrator, G) test-pulse generator, AC) amplifier and cathode follower, S) scaler, N) neon lamps; the rest of the notation is explained in the text.

diameter 10 mm and length 100 mm; the dimensions of group c were 18 and 300 mm, respectively.

The coincidence combinations of counters were based on the required form of the resolution curve. Each counter of group a was connected in coincidence with only a single tray of counters b (four counters) and with all the counters of group c. The energy resolution was thus determined by the width of a single counter of a and of a single row of group b. For each angle the readings of four coincidence groups of type $a_i + b_i$ were added. The angular resolution of the system, as determined by the width of counter tray a, was selected to be 1.5° in the laboratory system.

The angle at which deuterons were registered was varied by shifting the counter groups a and b along the edges of the pole faces. The entire interval of deuteron angles (with 14° maximum laboratory-system angle of deuteron emission) was covered in two positions of the magnet with respect to the neutron beam.

The counters were adjusted on the deuteron trajectory by means of a current-carrying filament in the magnetic field. For most angles the error in the cross section that was associated with the adjustment of the counter positions did not exceed 1 or 2%, but the error was 7% for four c.m. angles of deuteron emission into the backward hemisphere. This relatively large error resulted from the fact that for different neutron energies the deuterons have very close energies in the laboratory system. The relative positions of counters a and b gave only the energy threshold, which corresponded to ~550-Mev neutrons. The maximum deuteron energy was determined by the upper limit of the neutron spectrum.

A block diagram of the electronic circuit of the spectrometer is shown in Fig. 2.* Pulses from counters a, b and c were fed to standard UPI-1 pulse-converting amplifiers with a passband of 1 Mc and gain of 10^4, in the output stages of which 4 or 5×10^{-7}-sec 8-volt pulses were formed. The total number of amplification channels for the two systems of gas-filled counters was 18 (Figs. 1 and 2 show only one of these systems). Signals formed in UPI-1 were "split" in each channel except channel c and were fed to the mixer (A or B) and bandpass circuit Bp. Standardized pulses from the two mixers, γ-ray telescope, and selecting counters c were fed to a fourfold coincidence circuit cc (resolving time 5×10^{-7} sec), which sent a master pulse to the bandpass circuits Bp. The latter passed pulses from gamma-deuteron coincidences to "slow" output univibrators (OU) and almost completely prevented accidental ground pulses from reaching these univibrators.

The required combinations of discharged coordinated counters following the passage of a particle were selected by the relays R in the plate circuits of the output univibrators. These combinations and their sums were counted by electromechanical counters (T, Y, Σ, a_1b_1, a_2b_2 etc.).

CONTROL EXPERIMENTS

1. To verify that the particles registered by the spectrometer were actually deuterons we measured

---

*For a portion of the electronic equipment of our spectrometer we used the circuits placed at our disposal by the designers of the multi-channel γ-ray spectrometer developed at the Laboratory for Nuclear Problems.[9]

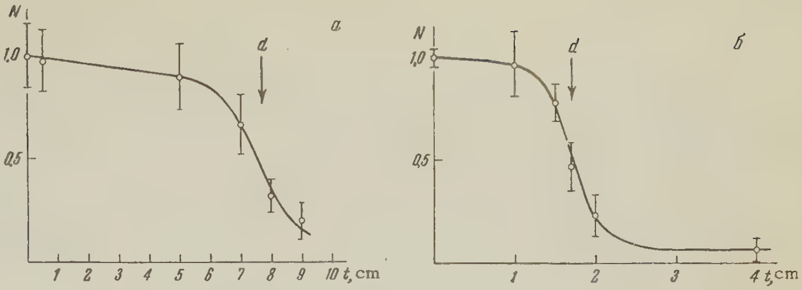

FIG. 3. Curves of deuteron absorption in copper. a) $\theta_d = 6°$; b) $\theta_d = 9°$.

the absorption curves of these particles in copper for two angles of π^0-meson emission, $\theta_\pi^* = 34$ and 146°.* The resulting curves (Fig. 3) leave no doubt that the events recorded by the apparatus were coincidences between γ quanta and deuterons. The steep slopes of the curves are located exactly at the centers of the range distributions which can be expected from the kinematics of the reaction (the arrows d in Fig. 3). The range of protons with the same momentum is approximately double the range of the deuterons.

2. The use of a magnetic field to register deuterons and the selected energy threshold (E_π = 550 Mev) permits the complete exclusion of particles from reaction (4) for most investigated π^0-meson angles. The angular range where such extraneous particles are absent corresponds to deuterons emitted forward in the c.m. system and having "large" momentum in the laboratory system [in Fig. 4 the branches of the curve that lie above the limit of possible momenta of protons from reaction (4)]. It also follows from Fig. 4 that, on the contrary, in the "small" momentum region corresponding to deuterons emitted "backward" in the c.m. system (the branches of the curves that lie below the dotted line) a proton contribution is possible. Four points in this region were measured on the π^0-meson angular distribution curve (at $\theta_\pi^* = 27$, 34, 40 and 50°). For two of these angles ($\theta_\pi^* = 34$ and 50°) the percentage of protons coinciding with π^0 mesons was determined by means of filters placed in front of counters c. Reaction (4) was easily distinguished because of the different ranges of deuterons and protons with the same momentum. The measurements indicated a small proton component: For $\theta_\pi^* = 34°$ it was $(6.5 \pm 5.9)\%$ and for $\theta_\pi^* = 50°$ it was $(0.2^{+5.7}_{-0.2})\%$ of the principal effect [reaction (2)]. For the other two angles the percentage was determined by linear interpolation and extrapolation of the data.

3. In order to verify that the recorded γ quanta are actually decay products of π^0-mesons from reaction (2) we have investigated the angular correlation of the γ quanta and deuterons. This experiment was performed at $\theta_\pi^* = 108°$. The results are shown in Fig. 5, where the abscissas are the angles between the telescope axis and the direction of π^0-meson motion. The curve in the figure was calculated for a mean neutron energy of 600 Mev. The correlation is clearly observed.

EFFICIENCY OF THE γ-RAY TELESCOPE

The telescope when pointed in the direction of π^0-meson motion registered the most energetic γ quanta resulting from decays (from 150 to 400 Mev, depending on the angle of observation). To determine the relation between the telescope efficiency k_γ and γ-quantum energy, we performed additional experiments on the passage of fast electrons through converters of different thicknesses. The results of these experiments make it considerably easier to calculate the efficiency. When

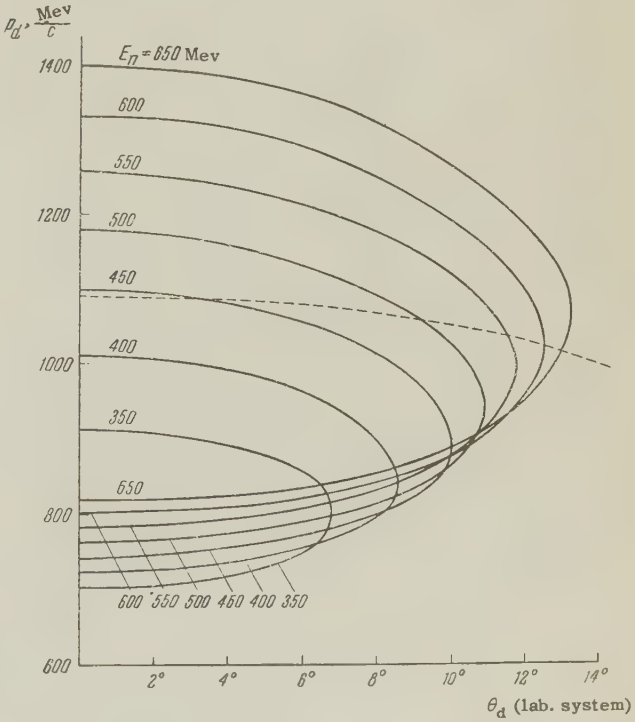

FIG. 4. Momentum of deuterons from reaction (2) as a function of their laboratory system emission angle and incident neutron energy. Dotted line – maximum momentum of protons from the reaction n + p → π^0 + n + p, E_n = 650 Mev.

---

*Here and henceforth the symbol * denotes angles in the c.m. system of colliding nucleons.

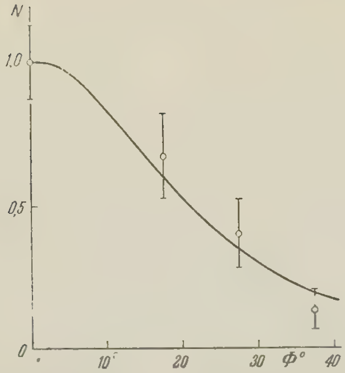

FIG. 5. Counting rate as a function of the angle Φ between the telescope axis and the direction of π^0-meson motion. The solid curve represents the function $(1-\beta^2)/(1-\beta\cos\Phi)^2$.

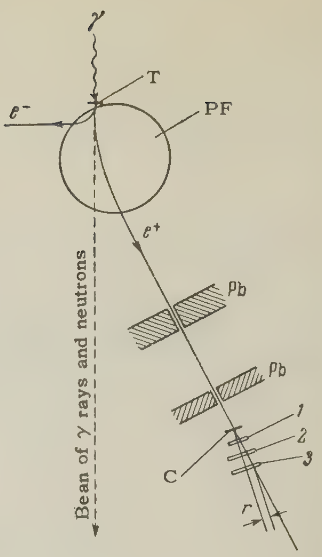

FIG. 6. Diagram of experiments for determining γ-telescope efficiency. T) Pb target (t = 2 mm), PF) pole faces of electromagnet, C) Pb converter of variable thickness; 1, 2, 3) scintillation counters.

experiment gives us the probability of registering an electron q^- and of a positron q^+ the probability of registering the pair is easily determined to be

$$\eta = 1-(1-q^-)(1-q^+). \tag{5}$$

The probability W of electron-positron pair production is easily calculated from the experimental cross sections[10] for γ-ray absorption (where we can neglect the Compton effect and, with even greater justification, the photoelectric effect for energies on the order of 100 Mev). The probability product ηW gives the telescope efficiency for γ rays of a given energy.

Figure 6 is a diagram of the experiment for determining q. The lead target produced electrons of the required energy by converting γ rays, which are always present in high-energy neutron beams. These γ rays are derived from the π^0 mesons produced in the internal target of the synchrocyclotron. The conversion electrons were deflected by the magnetic field, passed through the collimator of 2 cm diameter and entered the telescope (anticoincidence counter 4 (Fig. 1) was removed in these experiments). This experiment compared the telescope counting rate when the converter was used with the primary electron beam intensity. The variable parameters were the converter thickness t, the positron energy E^+, and the distance r from the center of the last scintillator to the beam axis.

In calculating the probability of recording a pair the quantities calculated by means of (5) were averaged over a number of values of E^+, r, and the converter area. In this calculation it was assumed that the telescope possesses identical efficiency for electrons and positrons of different energies. Integration of the telescope efficiency (the product ηW) over the converter thickness t gives the coefficient k_γ for a given γ-ray energy. Because of the geometry employed (large converter area), a fraction of the electrons may not reach the rear counter even if emitted from the converter in the direction of the γ rays. As a result some portions of the converter are less efficient. Therefore the effective solid angle is smaller than the actual angle viewed by the converter in the telescope.

The results for k_γ, reduced to the effective solid angle, which in the majority of measurements was 8.5×10^{-2} radians, are given in Table I.

The accuracy of the relative efficiencies was quite high (above 5%). In measurements of the absolute yield of reaction (2) the error in the absolute value of k_γ was reduced by the use of an unusually small converter (4 mm thickness, 60 mm diameter).

By means of the foregoing method of calculating the efficiency, we also determined corrections for its dependence on the distance between the telescope and target (in measurements at small angles the telescope was moved away from the target so that the neutron beam would not strike its walls).

TABLE I

θ^*_π, degrees	27 – 49	94	132	146	152	164
Average γ-ray energy (lab. system), Mev	400	280	200	173	163	150
Telescope efficiency, k_γ	0.61	0.58	0.56	0.54	0.53	0.51

The efficiency ratio of the two γ-ray telescopes used in the experiments was measured separately. For this purpose one telescope was replaced by the other at one of the test angles (the apparatus recorded the reaction $n + p \rightarrow \pi^0 + d$). From the ratio of the counting rates in these two instances, $N_1 : N_2 = 0.97 \pm 0.05$, it can be inferred that the telescopes possessed nearly identical efficiency, despite the small difference of geometry.

MEASUREMENTS

In each series of measurements the effect of the CH_2 and C targets was determined with and without the presence of the converter. As a control, the background was also measured in the absence of the target. The effect produced by the reaction under investigation was determined by the difference

$$A = (N^{c}_{CH_2} - N^{nc}_{CH_2}) - (N^{c}_{C} - N^{nc}_{C}). \qquad (6)$$

Here N is the counting rate for different targets. The superscripts c and nc denote "with converter" and "no converter", respectively.

Under the given experimental conditions the counting rates for the thin targets (2g/cm² CH_2) which were used in most of the measurements had the following average values:

TABLE II

Target	Counting rate with converter, pulses/hour	Counting rate without converter, pulses/hour
CH_2	12	3
C	3	1.5
Background	~0.5	~0.5

The results show that a carbon target produces a relatively small effect. This fact is of independent interest since it indicates a characteristic of π^0-meson production in reaction (2) with nucleons of complex nuclei. In the given experiment the smallness of N^{c}_{C} compared with $N^{c}_{CH_2}$ played a very important part, since it enabled us to obtain results of sufficiently high accuracy in a reasonable period of time.

Measurements in which we introduced an artificial delay of pulses fed from the telescope to the common coincidence circuit (cc in Fig. 2) showed that accidental coincidences of pulses from the telescope and spectrometer were responsible for most of the count in the absence of the converter. The rise of the background and of the count without the converter as well as the reduced useful effect due to the necessity of separating the telescope from the target in measurements at angles close to 0° and 180° were the principal difficulties in measurements near these angles.

For measurements of deuteron absorption in copper and the determination of the contribution of particles from reaction (4), it was very important to take into account the background of accidental coincidences of the entire system with the last layer c of spectrometer counters. This background was determined by shifting counters c away from the deuteron trajectory.

REDUCTION OF EXPERIMENTAL RESULTS

The relative counting rates for different angles of deuteron emission are proportional to

$$A(\theta_d) \sim \int_0^\infty \sigma(\theta_d^*, E_n)\,[d\cos\theta_d^* / d\cos\theta_d] \times \xi_d(\theta_d, E_n)\,\xi_\pi(\theta_d^*, E_n)\,N_n(E_n)\,dE_n. \qquad (7)$$

Here θ_d^* is the c.m. deuteron angle, θ_d is the deuteron angle in the laboratory system, $\sigma(\theta_d^*, E_n)$ is the c.m. differential cross section of reaction (2), $\xi_d(\theta_d, E_n)$ is the curve of spectrometer resolving power, $N_n(E_n)$ is the energy spectrum of the neutron beam (known from reference 11), $\xi_\pi = k_\gamma(1-\beta^2)/[1-\beta\cos\Phi(E_n)]^2$ is the efficiency of π^0-meson registration, where Φ is the angle between the telescope axis and the π^0-meson path (laboratory system), β is the π^0-meson velocity (laboratory system) and $k\gamma$ is the telescope efficiency for γ rays (see above). All quantities are given in arbitrary units. The function $(1-\beta^2)/(1-\beta\cos\Phi)^2$ expresses in relative units the angular distribution of γ rays from the decay of π^0 mesons.

The resolving power curves $\xi_d(\theta_d, E_n)$ are determined from the spectrometer geometry and target dimensions. These curves were first calculated analytically for a parallel incident beam; the results were then integrated numerically over the angles of deuteron entrance into the spectrometer. The calculation took into account the finite dimensions of the target and counters. The resolving power curves obtained in this manner had the shape of trapezoids with rounded corners.

It is impossible to determine exactly the form of the function $\sigma(\theta^*, E_n)$ from measurements performed with a relatively broad neutron spectrum and a detector with constant energy threshold. In the present experiments, in order to overcome this difficulty, the angular distribution of products of reaction (2) and the absolute value of the total cross section were obtained for an average effective value of neutron energy. It was assumed that the angular distribution of reaction products is independent of neutron energy in the energy range covered by the detector, i.e., that

$$\sigma(\theta^*, E_n) = f(\theta^*)\,\sigma(E_n). \tag{8}$$

Using (8) in (7), we obtain

$$A(\theta_d) \sim \int_0^\infty f(\theta_d^*)\,\frac{d\cos\theta_d^*}{d\cos\theta_d}\,\xi_d\xi_\pi\sigma(E_n)\,N_n(E_n)\,dE_n$$

$$= \int_0^\infty N(E_n)\,\sigma(E_n)\,dE_n. \tag{9}$$

In the second integral $N(E_n)$, the meaning of which is clear from the equation, has the same dimensions as the neutron spectrum, so that it can be called the effective neutron spectrum. This new designation is introduced for simplicity in what follows. Figure 7 shows a neutron beam energy spectrum[11] measured with a magnetic spectrometer and a typical effective neutron spectrum.

Since the integrand contains the still undetermined function $f(\theta_d^*)$ the experimental results were treated by the method of successive approximations. In the first approximation it was assumed that the neutron energy spectrum can be represented by a straight line at the height of its maximum (at 600 Mev). The angular distribution is then easily obtained by means of the simplified equation which follows from (9):

$$f_1(\theta_d^*) \sim A(\theta_d)\,/\,[d\cos\theta_d^*\,/\,d\cos\theta_d]\,\xi_\pi(\theta_d^*). \tag{10}$$

$f_1(\theta_d^*)$ obtained in this manner was already close to its final form. The second approximation was determined from the first approximation by taking into account the neutron-energy dependence of all quantities in (9). Corrections to the first approximation amounted to less than 8% for all π^0-meson angles and were occasioned mainly by the earlier assumption regarding the shape of the spectrum. The calculation could thus be confined to the second approximation for $f(\theta^*)$.

It must be noted that the angular distribution thus obtained depends on the assumed form of the excitation function $\sigma(E_n)$ for the given reaction. For the purpose of determining the sensitivity of the results to the form of this function the cross sections were calculated for several angles using two extremely different excitation functions: (1) One excitation function describing the cross section for meson production in reactions (1) and (2) at low energies was

$$\sigma \sim 0.14\eta + 1.0\eta^3, \tag{11}$$

where η is the c.m. meson momentum; (2) the other excitation function for reaction (1) with 460 to 660 Mev protons is that given in references 4 to 6.

The calculations showed that the angular distribution is insensitive to the form of $\sigma(E_n)$. For a number of angles there is a variation of less than 5% in the ratio of the cross sections obtained using the two different functions. The second form for the energy dependence of the cross section will be used for the final results given in the present article.

Figure 8 gives the final angular distribution measurements for π^0 mesons from reaction (2). The indicated errors include the following: errors in determining the relative efficiency k_γ (~5%) as well as in measurement of the relative number of protons from reaction (4) at small angles (6%), errors associated with the arangement of the spectrometer counters (1 to 7%), inaccurate determination of relative telescope efficiency (5%), and statistical experimental errors. The solid curve in Fig. 8 was obtained by the method of least squares and represents the expression

$$f(\theta^*) = (0.220 \pm 0.022) + \cos^2\theta^*. \tag{12}$$

TOTAL CROSS SECTION MEASUREMENT

Using the known angular distribution $f(\theta^*)$ (in relative units) the total cross section for the

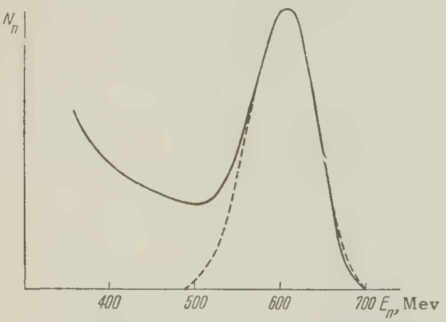

FIG. 7. Solid curve – energy spectrum of neutron beam, broken line – effective neutron spectrum.

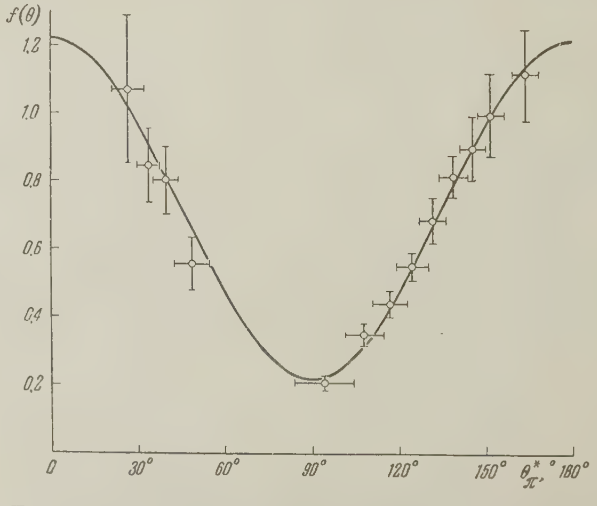

FIG. 8. Angular distribution (c.m. system) of π^0 mesons from the reaction $n + p \rightarrow \pi^0 + d$ with 600-Mev Neutrons.

TABLE III

Energy of incident nucleon, Mev	Reaction	Angular distribution	Total cross section 10^{-27} cm²	Reference
580	$p+p\rightarrow\pi^{+}+d$	$(0.216\pm0.033)+\cos^2\theta^*$	3.10 ± 0.24	[2]
600	$n+p\rightarrow\pi^{0}+d$	$(0.220\pm0.022)+\cos^2\theta^*$	$1.5\ \pm0.3$	Present experiment
660	$p+p\rightarrow\pi^{+}+d$	$(0.23\ \pm0.03)+\cos^2\theta^*$	$3.1\ \pm0.2$	[5]
610	$p+p\rightarrow\pi^{+}+d$		3.15 ± 0.22	

reaction in question could be obtained by measuring the differential cross section in absolute units for one of the angles. This was accomplished through simultaneous measurement of the counting rate for the given reaction and the counting rate for recoil protons produced in the same target through elastic n-p scattering, the cross section for which is given in reference 12. Recoil protons were registered by one of the γ-ray detectors while excluding the anticoincidence cirucit and the converter. It was thus unnecessary to redetermine the relative efficiency of the telescopes used in the experiment. To permit direct use of the (n-p)-scattering data the proton detector contained an absorber which furnished an energy threshold (E_{th}) identical with that of the detector in reference 12. The proton counting rate was determined at laboratory system angle 60°, since in reference 12 the differential cross section for n-p scattering was determined most exactly at that angle.

If the effective energy is defined as the argument of the excitation function $\sigma(E_n)$ at $\sigma(E_n) = \overline{\sigma}$, where

$$\overline{\sigma} = \frac{\int\limits_0^\infty \sigma(E_n)\, N(E_n)\, dE_n}{\int\limits_0^\infty N(E_n)\, dE_n}, \tag{13}$$

our experiment determines the differential cross section at the effective energy (E_{eff}) to be

$$\frac{d\sigma(\theta_d^*)}{d\Omega} = \frac{d\sigma_{np}}{d\Omega}\,\frac{\Delta\Omega_p}{\Delta\Omega_d}\,\frac{A_\pi}{A_p}\;\frac{\int\limits_{E_{th}}^\infty N_n(E_n)\, dE_n}{\int\limits_0^\infty N'(E_n)\, dE_n}, \tag{14}$$

where $d\sigma_{np}/d\Omega$ is the laboratory system elastic (n-p)-scattering cross section; $\Delta\Omega_p$ and $\Delta\Omega_d$ are the solid angles seen by the proton and neutron detectors, respectively; A_π and A_p are the counting rates for π^0 mesons produced in reaction (2) and for recoil protons from elastic n-p collisions; $N_n(E_n)$ is the neutron spectrum; $N'(E_n)$ is the effective neutron spectrum for reaction (2), suitably normalized [unlike the unnormalized $N(E_n)$].

Following the previously-described method, Eq. (14) was used to determine the absolute cross section for reaction (2) at $\theta_\pi^* = 138°$. In determining the recoil proton flux A_p a correction was introduced for the π^+ mesons produced in n-p collisions. According to reference 12, this correction was 17%.

The differential cross section obtained by means of (14) is entirely independent of the form of the excitation function $\sigma(E_n)$. However, the effective energy to which the cross section refers varies somewhat with $\sigma(E_n)$. Calculations show that the effective energy at $\theta_\pi^* = 138°$ changes from 590 to 605 Mev for the two forms of $\sigma(E_n)$ given in the preceding section. The final value of the total cross section for reaction (2), which is given below, refers to an effective neutron energy of 600 ± 10 Mev.

From the obtained angular distribution $f(\theta^*)$ and the absolute cross section at $\theta_\pi^* = 138°$ the total cross section is given by

$$\sigma_t = (1.5 \pm 0.3)\cdot 10^{-27}\ \text{cm}^2$$

The error in this cross section includes in addition to the statistical error of measurement (7.5%) the following: errors in determining the total and differential cross sections for elastic n-p scattering (12 and 6.5% respectively), errors in measuring the absolute efficiency of the γ-ray telescope (10%) and of the magnetic spectrometer (7%), the error in determining the relative efficiency of the telescopes (5%), and the error in extrapolating the angular distribution to large and small angles (2%).

DISCUSSION OF RESULTS

Let us examine our results from the point of view of charge invariance. For this purpose we shall compare our data with the measurements given in the literature for the angular distribution and total cross section for reaction (1) at energies close to 600 Mev. The data are summarized in Table III.

The table shows that the angular distributions of π mesons from reactions (2) and (1) at similar energies are the same with a good degree of accuracy. However, the total cross sections at practically equal energies differ by a factor of 2.

It may be noted here that reference 6 gives a somewhat larger value of the constant in the angular distribution of π^+ mesons from reaction (1) at proton energies of 633 and 660 Mev. However, when the energy dependence of this constant that is given in reference 6 is extrapolated to 600 Mev we obtain a value close to ours for reaction (2). Thus the experimental results obtained for reaction (2) and a comparison with the results for reaction (1) at identical nucleon energy (600 Mev) show that Yang's relation is fulfilled, thus confirming the charge invariance hypothesis for meson-nucleon interactions.

Independently of the existence of charge invariance, the rapid growth of the cross section for reaction (2) with increasing energy and the shape of the angular distribution permit us to infer that at 400 to 600 Mev π^0 mesons are produced principally in the p state. This conclusion is not in conflict with the conservation of isotopic spin. In addition, the fact that it is satisfied for meson-nucleon interactions permits the direct application to reaction (2) of a number of laws known for reaction (1). For instance, we can state that the energy dependence of the total cross section for reaction (2) is of resonant character similar to that which was established for reaction (1) in references 5 and 6. Furthermore, in experiments on the asymmetry of π^+-meson emission in reaction (1), which were recently performed using a polarized proton beam,[13] a d-wave component was detected. This can also be applied to reaction (2).

It is known that for a number of transitions that are accompanied by the emission of π mesons in the d state the angular distribution is characterized by the presence of a term that is proportional to $\cos^4\theta$.* An attempt to detect this term through the representation of our experimental results by the polynomial $a + \cos^2\theta^* + \cos^4\theta^*$ showed that the coefficient of $\cos^4\theta^*$ is small and is determined with an error which is twice its own magnitude. Similar results for reaction (1) were previously given in reference 5. The authors of reference 13 state that their data are also in agreement with the assumption of small amplitudes for transitions with the emission of π^+ mesons in s and d states compared with the amplitude of the transition ${}^1D_2 \rightarrow {}^3S_1p_2$ (in Rosenfeld's notation[1]).

When our results are considered in connection with the recently advanced hypothesis[14] of the existence of a pseudoscalar π_0^0 meson with zero isotopic spin and mass close to that of an ordinary π meson, we cannot exclude the possibility that the former are produced in the reaction $n + p \rightarrow \pi_0^0 + d$. But the data permit us to infer that the given reaction would yield a relatively small number of π_0^0 mesons, if any, compared with the yield of π^0 mesons.* In this connection it must be remembered that the relatively small probability of the production of the hypothetical π_0^0 mesons could result from the resonant character of ordinary π^0-meson production in reaction (2) (with $T = 3/2$, $J = 3/2$).

The authors wish to thank Iu. D. Baiukov, M. S. Kozodaev, A. A. Markov, A. N. Sinaev, and A. A. Tiapkin for valuable suggestions regarding the electronic equipment of the spectrometer. They also wish to thank L. I. Lapidus and B. M. Pontecorvo for their continued interest, as well as M. M. Kuznetsov for assistance with the construction of the apparatus.

[1] A. H. Rosenfeld, Phys. Rev. **96**, 139 (1954).

[2] C. E. Cohn, Phys. Rev. **105**, 1582 (1957).

[3] Batson, Culwich, and Riddiford, Preprint, Birmingham, England.

[4] Meshcheriakov, Neganov, Bogachev, and Sidorov, Dokl. Akad. Nauk SSSR **100**, 673 (1955).

[5] M. G. Meshcheriakov and B. S. Neganov, Dokl. Akad. Nauk SSSR **100**, 677 (1955).

[6] B. S. Neganov and L. B. Parfenov, J. Exptl. Theoret. Phys. (U.S.S.R.) **34**, 767 (1958), Soviet Phys. JETP **7**, 528 (1958).

[7] R. H. Hildebrand, Phys. Rev. **89**, 1090 (1953).

[8] R. A. Schluter, Phys. Rev. **96**, 734 (1954).

[9] Baiukov, Kozodaev, Markov, Sinaev, and Tiapkin, Приборы и техника эксперимента (Instruments and Measurements Engineering) (in press).

[10] De Wire, Ashkin and, Beach, Phys. Rev. **83**, 505 (1951).

[11] Kiselev, Oganesian, Poze, and Fliagin, J. Exptl. Theoret. Phys. (U.S.S.R.) **35**, 812 (1958), Soviet Phys. JETP **8**, 564 (1959).

[12] Iu. M. Kazarinov and Iu. N. Simonov, J. Exptl. Theoret. Phys. (U.S.S.R.) **31**, 169 (1956), Soviet Phys. JETP **4**, 161 (1957).

[13] Akimov, Savchenko, and Soroko, J. Exptl. Theoret. Phys. (U.S.S.R.) **35**, 89 (1958), Soviet Phys. JETP **8**, 164 (1959).

[14] A. M. Baldin, Nuovo cimento **8**, 569 (1958).

Translated by I. Emin
184

---

*We do not give a more exact quantitative estimate of the π_0^0-meson yield, which could in principle be obtained by using our data, since any such estimate would require a specific assumption regarding the form of the π_0^0-meson angular distribution.

SOVIET PHYSICS JETP VOLUME 35(8), NUMBER 4 APRIL, 1959

ELECTRON CAPTURE AND LOSS IN COLLISIONS OF FAST CARBON AND OXYGEN ATOMS WITH GAS MOLECULES

Ia. M. FOGEL', V. A. ANKUDINOV and D. V. PILIPENKO

Physico-Technical Institute, Academy of Sciences, Ukrainian S.S.R.

Submitted to JETP editor April 8, 1958

J. Exptl. Theoret. Phys. (U.S.S.R.) **35**, 868-874 (October, 1958)

The electron capture and loss cross sections have been measured for carbon and oxygen atoms with energies between 10 and 65 kev in collisions with He, Ne, Ar, Kr, Xe and H_2, N_2 and O_2 molecules. The electron capture cross section for fast atoms increases with increasing electron affinity. The electron loss cross section for fast atoms is a non-monotonic function of the first ionization potential of the atom. Massey's adiabatic criterion is found to apply for electron capture by fast atoms. The value of the constant a in these processes is 3 A.

INTRODUCTION

In an earlier work[1] we have measured the electron capture and loss cross sections for collisions between fast hydrogen atoms and gas molecules. It is of interest to extend this investigation to other atoms in order to determine the influence of the electron affinities of the fast atoms on the electron capture cross section σ_{0-1} and the effect of the ionization potential on the electron loss cross section σ_{01}. It is reasonable to expect that the main effect will be due to the configuration of the electron shell of the fast atom. However, the possibility is not excluded that there will be a correlation between the cross sections σ_{0-1} and σ_{01} and the binding energy of the electron in the negative ion which is formed and the binding energy of the electron which is detached from the fast atom.

In the present work these problems were studied by measuring the cross sections σ_{0-1} and σ_{01} for fast carbon and oxygen atoms. These atoms were chosen on the basis of the following considerations: (1) the electron affinity of H, C and O atoms is an increasing function which takes on the following values 0.75, 1.13 and 1.48 ev;[2] (2) the ionization potentials are the same in H and O, but the electron shell configurations are different ($1s^1$ and $1s^2\ 2s^2\ 2p^4$ respectively); (3) the ionization potential of the C atom is smaller than that of the H and O atoms.

RESULTS OF THE MEASUREMENTS AND DISCUSSION

The experimental setup for investigating electron capture and loss in fast atoms and the method of measuring σ_{0-1} and σ_{01} has been described in detail in reference 1.

A beam of fast C and O atoms was obtained by neutralizing C^+ and O^+ ions which passed through a mercury-vapor target.[3] The optimum target thickness was chosen (of the order of 10^{15} atoms/cm^2) and it was verified experimentally that the energy loss of the C^+ and O^+ ions in the target was very small.

The electron capture and loss cross sections were measured for C and O atoms with energies between 10 and 65 kev in collisions with He, Ne, Ar, Kr, Xe and the molecules H_2, N_2 and O_2. The values of σ_{0-1} and σ_{01} for each energy were obtained by averaging two measurements. The cross sections were computed for particles of a gas, i.e. for molecular gases consisting of one kind of gas molecule. The random error in these measurements of σ_{0-1} and σ_{01} was ±15%. The error in the measurement of the energy of the C and O atoms was ± 3%.

Figures 1 to 8 show the cross sections σ_{0-1} and σ_{01} as functions of the energy and velocity of the C and O atoms for atomic and molecular gases. An examination of these curves indicates the following.

1. For the majority of atom-molecule pairs, σ_{0-1} and σ_{01} increase with increasing energy of the C and O atoms. For the pairs O-Xe, O-Kr, and C-Xe, however, σ_{0-1} passes through a maximum as the energy is increased. For O-Ar and C-Kr the curve $\sigma_{0-1} = f(E)$ reaches a plateau at the extremity of the energy region.

2. σ_{0-1} and σ_{01} are fairly sensitive functions of the type of gas particle. For the $C^0 \rightarrow C^-$ and

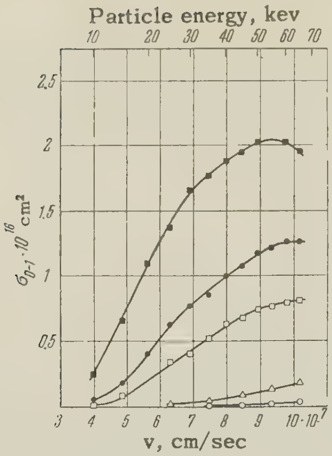

FIG. 1. Electron capture cross sections for carbon atoms in inert gases: ■) Xe, ●) Kr, □) Ar, △) Ne, ○) He.

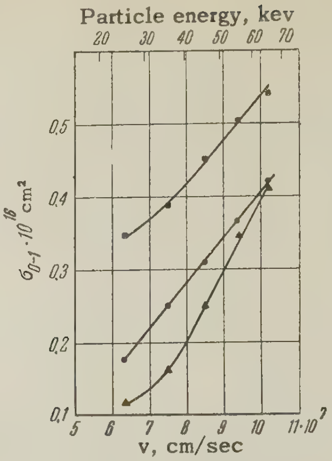

FIG. 2. Electron capture cross sections for carbon atoms in molecular gases: ●) H_2, ▲) N_2, ■) O_2.

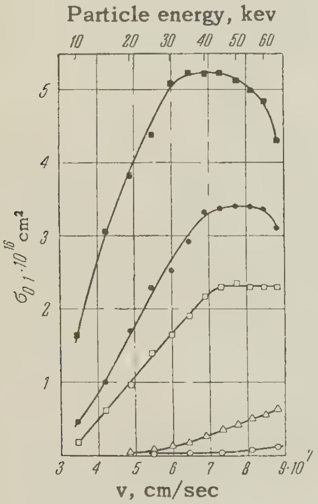

FIG. 3. Electron capture cross section for oxygen atoms in inert gases: ■) Xe, ●) Kr, □) Ar, △) Ne, ○) He.

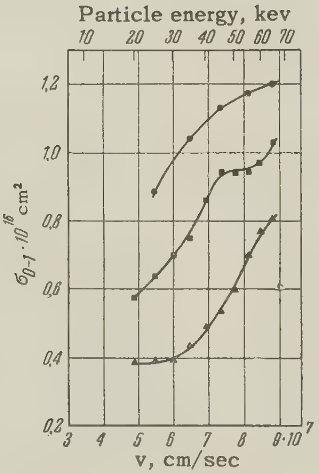

FIG. 4. Electron capture cross section for oxygen atoms in molecular gases: ●) H_2, △) N_2, ■) O_2.

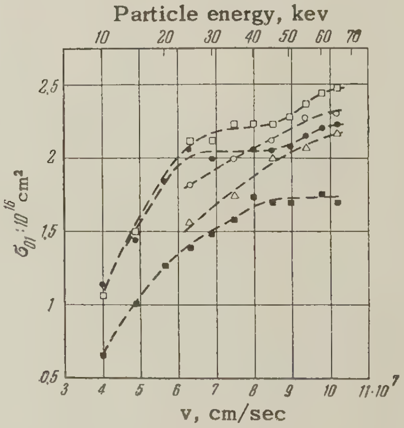

FIG. 5. Electron loss cross section for carbon atoms in inert gases: ■) Xe, ●) Kr, □) Ar, △) Ne, ○) He.

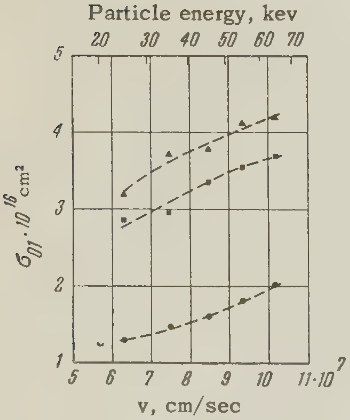

FIG. 6. Electron loss cross sections for carbon atoms in molecular gases: ●) H_2, ▲) N_2, ■) O_2.

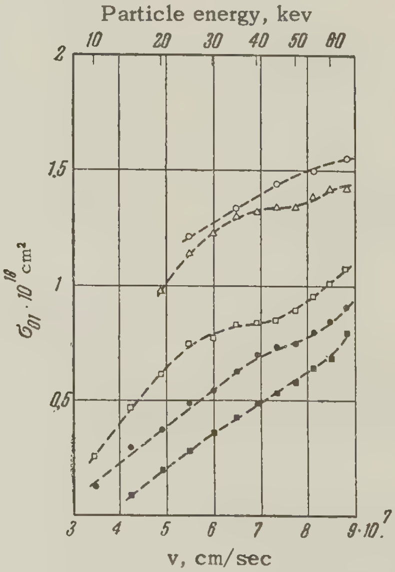

FIG. 7. Electron loss cross section for oxygen atoms in inert gases: ■) Xe, ●) Kr, □) Ar, △) Ne, ○) He.

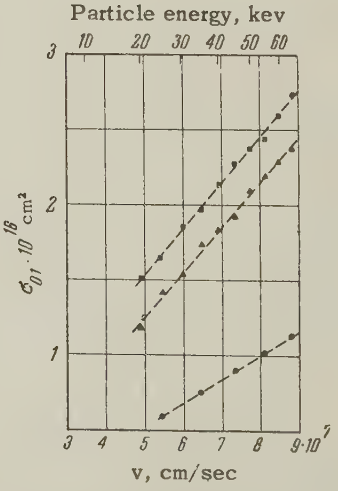

FIG. 8. Electron loss cross sections for oxygen atoms in molecular gases: ●) H_2, ▲) N_2, ■) O_2.

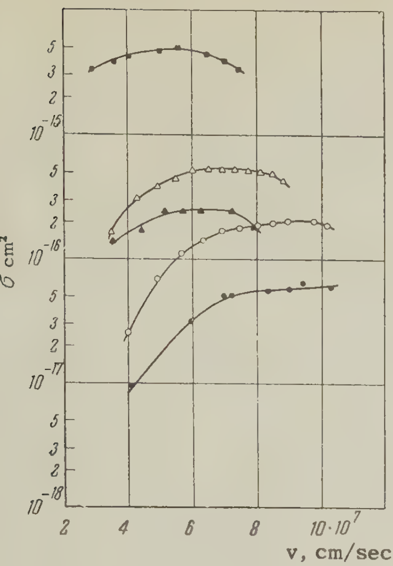

FIG. 9. Electron capture cross sections: ■) σ_{01}, ▲) σ_{0-1}, ●) σ_{1-1} for carbon; △) σ_{0-1}, ○) σ_{1-1} for oxygen (in Xe).

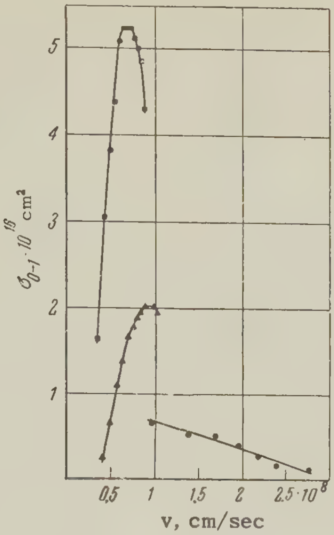

FIG. 10. Cross sections for the capture of one electron in atoms: ■) O, ▲) C, ●) H (in Xe).

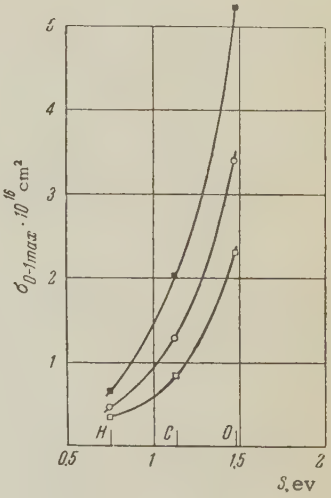

FIG. 11. The dependence of $\sigma_{0-1\,\max}$ on electron affinity: □) Ar, ○) Kr, ■) Xe.

$O^0 \rightarrow O^-$ reactions in inert gases the values of σ_{0-1} are the same at the same atomic velocities and fall off monotonically as the atomic number of the inert gas is reduced. For $O^0 \rightarrow O^+$ reactions, on the other hand, σ_{01} increases as the atomic number of the inert gas is reduced. In the $C^0 \rightarrow C^+$ reactions these cross sections are nonmonotonic functions of the atomic number of the gas. In molecular gases, a monotonic dependence of cross section on atomic number of the gas is observed only for σ_{01} in the $O^0 \rightarrow O^+$ reactions, in which case this quantity increases with the atomic number.

3. The cross sections σ_{0-1} and σ_{01} are also functions of the type of fast atom. σ_{0-1} is larger for O atoms than for C atoms. On the other hand σ_{01} is smaller for O atoms than for C atoms.

4. For O atoms in the light inert gases He and Ne and the molecular gases N_2 and O_2, σ_{01} is greater than σ_{0-1}; in the heavier inert gases Ar, Kr, and Xe, it is smaller. In the case of C atoms $\sigma_{01} > {}_{0-1}$ for all gases except Xe, in which case $\sigma_{01} \approx \sigma_{0-1}$.

The literature contains no data concerning the $C^0 \rightarrow C$ and $O^0 \rightarrow O$ reactions; thus we cannot make a comparison of these results with other experiments.

It is of interest to compare σ_{0-1} and σ_{01} with other electron capture and loss cross sections in carbon and oxygen. The data available in the literature allow a comparison between σ_{0-1} and σ_{1-1} for capture of two electrons by C^- and O^+ ions[4] for all the gases investigated and with the cross section σ_{01} for capture of one electron by C^+ ions[5] in Ar, Kr, Xe, and H_2.

In Fig. 9 are shown the quantities σ_{01}, σ_{0-1}, and σ_{1-1} as functions of the carbon velocity and σ_{0-1} and σ_{1-1} for oxygen (target atom, Xe). It is evident from these curves that the electron capture cross sections for carbon obey the relation $\sigma_{01} > \sigma_{0-1} > \sigma_{1-1}$ which also applies for the capture cross sections in hydrogen (cf. reference 1). σ_{01} is approximately two orders of magnitude greater than σ_{0-1} and σ_{1-1}. σ_{0-1} is two or three times greater than σ_{1-1}. The ratio $\sigma_{0-1}/\sigma_{1-1}$ is smaller for oxygen than for carbon. The characteristics of the electron capture cross section for carbon and oxygen in Xe also apply to other target gases.

Certain conclusions may be drawn from a comparison of σ_{0-1} in H, C and O atoms. In Fig. 10 are shown $\sigma_{0-1}(v)$ curves for H, C and O atoms in Xe;* these curves illustrate the strong dependence of σ_{0-1} on the fast atom. It is apparent from this figure that the highest electron capture cross section is found in O; the cross section in C is somewhat smaller and the smallest values for this cross section are found in H atoms. Similar relations are found for other target atoms. The dependence of σ_{0-1} on the type of fast atoms may be related to the binding energy of the level at which electron capture takes place, i.e., the electron affinity. It is reasonable to assume that σ_{0-1} will increase with increasing electron affinity. The curves shown in Fig. 11, which give the maxi-

---

*The function $\sigma_{0-1}(v)$ for H atoms was plotted from the data of reference 1.

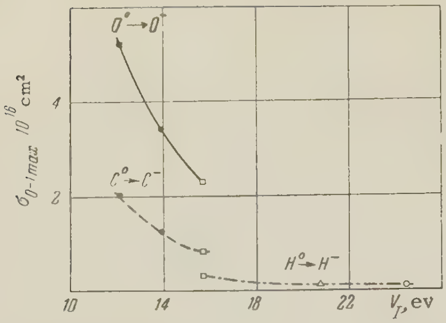

FIG. 12. The dependence of σ_{0-1max} on the ionization potential of the target atom: ■) Xe, ●) Kr, □) Ar, △) Ne, ○) He.

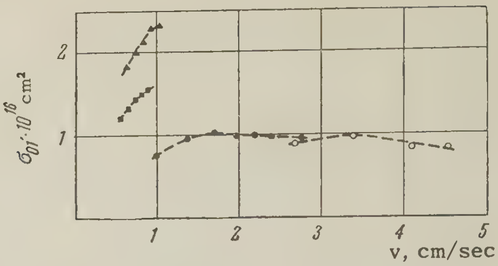

FIG. 13. Electron loss cross sections for fast atoms: ▲) C, ■) O, ●) H, ○) He (in He).

mum value of σ_{0-1} as a function of electron affinity, are plotted for Ar, Kr, and Xe and show the rapid growth in σ_{0-1} as the electron affinity of the fast atom increases; these curves tend to support the suggestion made above. The monotonic increase in σ_{0-1} as a function of electron affinity is not disturbed by the fact that the electron is captured at the 1s level in H and at the 2p level in C and O.

The effect of the target atom on σ_{0-1} can be characterized by the binding energy of the electron which is detached, i.e., the first ionization potential of the target atom. Curves showing the dependence of the maximum value of σ_{0-1} on the first ionization potential of the target atoms are plotted for the fast atoms H, C and O in Fig. 12. As is apparent from this figure, σ_{0-1} falls off monotonically with increased binding energy of the detached electron. The points for the $H^0 \to H^-$, $C^0 \to C^-$ and $O^0 \to O^-$ reactions lie on three different curves, reflecting the effect of the electron affinity of the fast atoms.

A comparison of the cross section σ_{01} for different fast atoms is shown in Fig. 13, where the function $\sigma_{01}(v)$ is shown for H, C, O and He atoms in He.* As is apparent from this figure, there is no relation between σ_{01} and the first ionization potential of the fast atom. Although the first ionization potential of the He atom is considerably greater than that of the H atom, σ_{01} is about the same in these atoms; it should be noted that the detached electrons come from the same shell in both atoms (the 1s shell). H and O atoms have the same ionization potential, but σ_{01} in the O atom is higher than in the H atom. It is possible that in this case there is an effect due to the electron shell from which the electron is detached (1s for the H atom and 2p for the O atom). It is only in the C and O atoms that there is an increase in σ_{01} as the ionization potential is reduced. The detached electrons in both atoms come from the 2p shell. The inequality $(\sigma_{01})_H < (\sigma_{01})_O < (\sigma_{01})_C$ is observed for all the gases which were investigated.

It has been established in reference 1 that the maxima on the curve $\sigma_{0-1}(v)$ for $H^0 \to H^-$ reactions are located in correspondence with the Massey adiabatic criterion $a|\Delta E|/hv_{max} \approx 1$ (a is the distance over which the interaction forces between the colliding particles operate, ΔE is the resonance defect and v_{max} is the ion velocity corresponding to the maximum cross section), where the quantity a changes slightly for different targets, varying about the mean value 3 A. Using the maxima on the curves for $\sigma_{0-1}(v)$ for C atoms and O atoms (cf. Figs. 1 and 3) it is possible to estimate the constant a for the $C^0 \to C^-$ and $O^0 \to O^-$ reactions in Ar, Kr and Xe.

If the quantity a is the same for different atom-molecule pairs, it follows from the Massey adiabatic criterion that $v_{max} \sim |\Delta E|$. A graph of the function $v_{max} = f(|\Delta E|)$, plotted for all atom-molecule pairs in which maxima are observed on the $\sigma_{0-1}(v)$ curve is shown in Fig. 14. In plotting these curves we have assumed that all

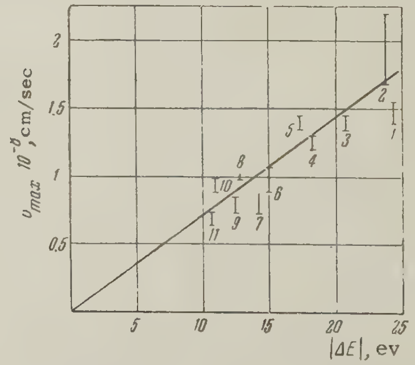

FIG. 14. The quantity v_{max} as a function of resonance defect: for $H^0 \to H^-$ in: 1) N_2, 2) He, 3) Ne, 4) O_2, 5) H_2, 6) Kr; for $O^0 \to O^-$ in: 7) Ar, 9) Kr, 11) Xe: for $C^0 \to C^-$ in: 8) Kr, 10) Xe.

---

*The curves $\sigma_{01}(v)$ are plotted from the data given in reference 6.

particles which participate in the $A^0 \rightarrow A^-$ reactions are in ground states. The resonance defects for $H^0 \rightarrow H^-$ reactions in molecular gases were computed under the assumptions that the molecular ion which is formed dissociates into atomic particles. The vertical spreads indicate the error in the determination of v_{max}. In this case, when the curve $\sigma_{0-1}(v)$ reaches a plateau the corresponding vertical section on Fig. 14 has no upper or lower limits.

As is evident from Fig. 14 the points for all $A^0 \rightarrow A^-$ reactions for which maxima are observed on the $\sigma_{0-1}(v)$ curves lie about a line which corresponds to $a \approx 3\,A$. The quantity a is found to be approximately constant not only for processes such as $A^0 \rightarrow A^-$ but also for processes in which one or two electrons are captured by singly charged positive ions; with the sole difference that the mean value of a is 8 A (reference 7) for ordinary charge-exchange processes (capture of one electron) and 1.5 A (reference 8) for double charge-exchange (capture of two electrons). Thus, the available experimental data indicate that the Massey adiabatic criterion applies in all investigations of electron capture by fast particles which have been carried out.

N. V. Topolia participated in these measurements.

In conclusion, we take this opportunity to thank A. K. Val'ter for his continued interest in this work.

---

[1] Fogel', Ankudinov, Pilipenko, and Topolia, J. Exptl. Theoret. Phys. (U.S.S.R.) **34**, 579 (1958), Soviet Phys. JETP **7**, 400 (1958).

[2] L. M. Branscomb, Negative Ions, Advances in Electronics and Electron Physics, Vol. IX, Academic Press, New York 1957.

[3] Fogel', Krupnik, and Ankudinov, J. Tech. Phys. (U.S.S.R.) **26**, 1208 (1956).

[4] Fogel', Mitin, and Koval', J. Exptl. Theoret. Phys. (U.S.S.R.) **31**, 397 (1956), Soviet Phys. JETP **4**, 359 (1957).

[5] H. B. Gilbody and J. B. Hasted, Proc. Roy. Soc. (London) **A238**, 334 (1956).

[6] S. K. Allison, Phys. Rev. **109**, 76 (1958).

[7] J. B. H. Stedeford and J. B. Hasted, Proc. Roy. Soc. (London) **A227**, 466 (1955).

[8] Fogel', Mitin, Kozlov, and Romashko, J. Exptl. Theoret. Phys. (U.S.S.R.) **35**, 565 (1958), Soviet Phys. JETP **8**, 390 (1959).

Translated by H. Lashinsky
185

SOVIET PHYSICS JETP VOLUME 35(8), NUMBER 4 APRIL, 1959

TEMPERATURE DEPENDENCE OF THE PARAMAGNETIC SUSCEPTIBILITY OF NICKEL-ZINC FERRITES

V. I. CHECHERNIKOV and Iu. D. VOLKOV

Moscow State University

Submitted to JETP editor May 5, 1958

J. Exptl. Theoret. Phys. (U.S.S.R.) 35, 875-879 (October, 1958)

We have investigated the temperature dependence of the paramagnetic susceptibility of nickel-zinc ferrites. The results of the measurements are in good agreement with theory.

1. Numerous investigations of ferromagnetic metals and alloys at high temperatures $T \gg \Theta_f$ (where Θ_f is the ferromagnetic Curie point) have shown that their paramagnetic susceptibility obeys the Curie-Weiss law. The definite dependence on alloy composition which was established for the Curie-Weiss constant C and thus for the magnetic moment played an important part in the development of paramagnetic theory.

The temperature dependence of the paramagnetic susceptibility of ferrites cannot be described even approximatly by the Curie-Weiss law. The law that is obeyed by the paramagnetic susceptibility of ferrites was first established theoretically by Néel.[1] In Néel's theory the reciprocal of the susceptibility $1/\chi$ is a hyperbolic function of the temperature T:

$$1/\chi = 1/\chi_0 + T/C_N - \sigma/(T-\Theta), \qquad (1)$$

where the constants σ, Θ, $1/\chi_1$ represent the following:

$$\Theta = nC_N\lambda\mu\,(2+\alpha+\beta), \qquad (2)$$

$$\sigma = n^2C_N\lambda\mu\,[\lambda(1+\alpha) - \mu(1+\beta)]^2, \qquad (3)$$

$$1/\chi_0 = n\,(2\lambda\mu - \lambda^2\alpha - \mu\beta). \qquad (4)$$

Here C_N is the atomic constant for magnetic Fe^{3+} ions; λ and μ are the numbers of these ions in sublattices A and B, respectively; n, α, and β are constants of the molecular field associated with the sum of the exchange integrals corresponding to interactions of the types AB, AA and BB, respectively. It has been shown[2,3] that Néel's equation (1) is a sufficiently good description of the experimentally observed paramagnetic properties of simple ferrites.

The dependence of the parameters C and Θ in the Curie-Weiss law on composition has played an important part in the development of paramagnetic theory, especially regarding the paramagnetism of alloys. At the present time we have no information regarding the dependence of the parameters in Néel's equation on the composition of mixed ferrites (ferrite alloys). Moreover, it would be of great interest to determine whether ferrites possess a transition region at temperatures very close to the Curie point where the magnetic susceptibility would depend on the magnetic field strength as in the case of ferromagnetic metals.[4] The present work was undertaken to answer the questions that have been indicated.

2. The temperature dependence of the paramagnetic susceptibility of ferrites was investigated with the apparatus described in reference 4. We investigated the mixed nickel-zinc ferrites $Fe_2O_3 \cdot (1-z)\,NiO \cdot z\,ZnO$, where z varied from 0 to 1. The ferrites were compressed under a pressure of 3 tons/cm^2 and were baked at 1300°C for 3 hours, after which they were cooled slowly inside the furnace. The uniformity of the ferrites was then checked. Several samples were prepared from a ferrite of a given composition; these were investigated over a broad temperature range and the values of the susceptibility were compared. Repeated heating and cooling of the samples during the investigation did not affect the results; this was evidence of the absence of any phase transformation in the given temperature range.

Figure 1 shows the temperature dependence of the reciprocal of the molar susceptibility for all of the ferrites that we investigated from 300 to ≈ 1500°K. The curves of $1/\chi$ as a function of T are concave to the temperature axis. The curvature decreases gradually as more zinc oxide is added to the nickel ferrite and we have an almost linear dependence for a pure zinc ferrite. As already stated, in Néel's theory of ferrites the temperature dependence of the paramagnetic susceptibility obeys Eq. (1). Unfortunately the numerical values of the constants in the equation are not given by Néel's theory and must be determined

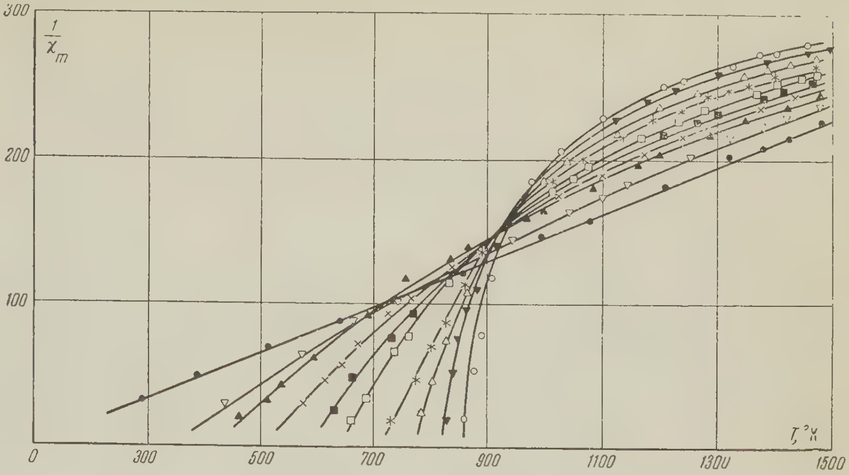

FIG. 1. Temperature dependence of the reciprocal susceptibility for the following ferrites: ○ – $Fe_2O_3 \cdot NiO$; ▼ – $Fe_2O_3 \cdot 0.9NiO \cdot 0.1ZnO$; Δ – $Fe_2O_3 \cdot 0.8NiO \cdot 0.2ZnO$; * – $Fe_2O_3 \cdot 0.7NiO \cdot 0.3ZnO$; □ – $Fe_2O_3 \cdot 0.6NiO \cdot 0.4ZnO$; ■ – $Fe_2O_3 \cdot 0.5NiO \cdot 0.5ZnO$; × – $Fe_2O_3 \cdot 0.4NiO \cdot 0.6ZnO$; ▲ – $Fe_2O_3 \cdot 0.3NiO \cdot 0.7ZnO$; ∇ – $Fe_2O_3 \cdot 0.2NiO \cdot 0.8ZnO$; ● – $Fe_2O_3 \cdot ZnO$.

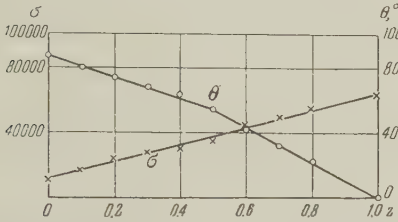

FIG. 2. Dependence of the constants σ and Θ on the percentage of zinc oxide.

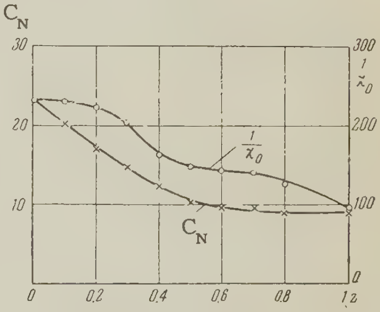

FIG. 3. Dependence of the constants C_N and $1/\chi_0$ on the percentage of zinc oxide.

experimentally. We obtained these constants by the method of successive approximations which was suggested by Néel[1] and which was described by us in detail in reference 3. It must be noted that when the constants obtained in this way are substituted into Néel's equation and the corresponding curves are plotted, the latter may not agree with the experimental curves from which the constants were determined by the graphical method referred to above. The degree of divergence of the curves can characterize the correctness of Néel's equation in each individual case.

Figures 2 and 3 show the dependence of the constants Θ, C_N, and $1/\chi_0$ on the percentage of ZnO in the ferrite. We note that while Θ and C_N decrease as the zinc oxide content increases, σ, on the other hand, increases. C_N must evidently indicate to some extent the magnitude of the paramagnetic moment. Figure 3 shows that as the amount of zinc oxide increases, C_N decreases. The reduction of C_N and thus of the paramagnetic moment evidently results from the fact that the addition of zinc, which supplies electrons, reduces the uncompensated spins of electrons in the 3d shell of nickel ions.

The downward slope of the Θ vs. z curve can be attributed to the fact that zinc ions mainly enter sublattice A and affect the exchange interaction in this sublattice. A reduction of the molecular-field constant α follows, accompanied by a reduction of Θ. It must be remembered that the constant C_N and the product $\lambda\mu$, which determine Θ, are also decreased as z increases. We can attempt to explain the increase of σ with z by assuming that the molecular-field constant n and thus the exchange interaction between sublattices increases with the number of zinc ions. It also follows from Néel's theory that σ, unlike the other constants, is quadratically dependent on n. In this connection it should be noted that, as Néel's calculations[5] for nickel-zinc ferrites have shown, the molecular field constant n has a tendency to increase with the amount of zinc oxide.

With an increase in the ZnO content $1/\chi_0$ decreases, but in a less complicated manner than Θ and C_N (Fig. 3).

Figure 4 shows the relation between $1/\chi$ and T for a few ferrites. The dashed curves were plotted from Néel's equation using the constants that had been obtained, while the solid curves were plotted from experimental data. At high temperatures the theoretical and experimental curves practically coincide. It should be noted especially that the agreement of the experimental and theoretical curves occurs for all ferrites of the nickel-zinc system although the shapes of the curves of $1/\chi$ as a function of T are extremely different. In all cases Néel's law is verified for ferrites over a broad temperature range, from approximately 850 to 1500°K. We must also note

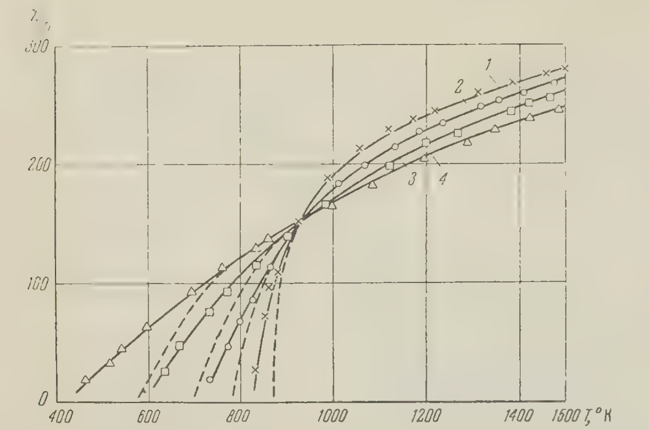

FIG. 4. Temperature dependence of the reciprocal susceptibility for the ferrites: 1 – $Fe_2O_3 \cdot 0.9NiO \cdot 0.1ZnO$; 2 – $Fe_2O_3 \cdot 0.7NiO \cdot 0.3ZnO$; 3 – $Fe_2O_3 \cdot 0.5NiO \cdot 0.5ZnO$; 4 – $Fe_2O_3 \cdot 0.3NiO \cdot 0.7ZnO$.

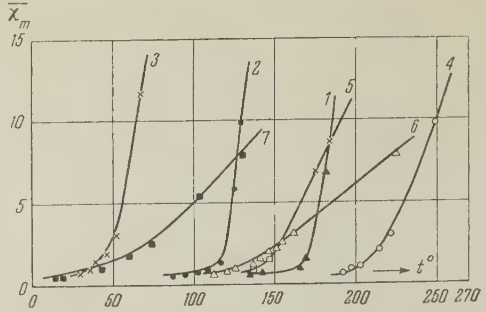

FIG. 5. Temperature dependence of the reciprocal susceptibility for ferrites. Temperature interval T = 650° + t° for 1 – $Fe_2O_3 \cdot 0.9\,NiO \cdot 0.1\,ZnO$, 2 – $Fe_2O_3 \times 0.8NiO \cdot 0.2ZnO$; 3 – $Fe_2O_3 \cdot 0.7NiO \cdot 0.3ZnO$; temperature interval T = 400° + t° for 4 $Fe_2O_3 \cdot 0.6NiO \cdot 0.4ZnO$, 5 – $Fe_2O_3 \cdot 0.5NiO \cdot 0.5ZnO$; temperature interval T = 300° + t° for 6 – $Fe_2O_3 \cdot 0.4NiO \cdot 0.6\,ZnO$, 7 – $Fe_2O_3 \cdot 0.3NiO \cdot 0.7ZnO$.

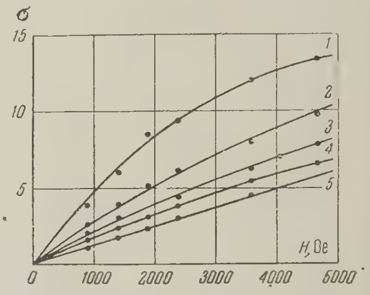

FIG. 6. Magnetization curves of the ferrite $Fe_2O_3 \cdot 0.5\,NiO \cdot 0.5\,ZnO$ at different temperatures: 1 – 537°, 2 – 547°, 3 – 550°, 4 – 553°, 5 – 556°K.

that near the ferromagnetic Curie point the theoretical and experimental curves do not agree and that this disagreement is most pronounced near Θ_f. We note that a similar behavior has been observed in pure ferrites such as Ni, Co, and Fe ferrites, according to Fallot and Maroni.[2] We believe that these discrepancies are caused to a considerable extent by the effect of short-range magnetic ordering especially in the immediate vicinity of the ferromagnetic Curie point. Inhomogeneity of the samples also probably contributes to the disagreement of theory and experiment.

3. To investigate the ferromagnetic transition region we measured the paramagnetic susceptibility at temperatures close to the ferromagnetic Curie point (Fig. 5). Very near Θ_f peculiar "tails" are seen, where the magnetic susceptibility depends on the magnetic field H as well as on temperature. Figure 6 shows a few isothermal magnetization curves (σ as a function of H) for one of the ferrites, where σ is the specific magnetization. Near Θ_f the magnetization curves are seen to be essentially linear; the departure from linearity increases as Θ_f is approached. At a sufficient distance from Θ_f the curves approximate straight lines and the paramagnetic susceptibility ceases to depend on the magnetic field. Similar behavior is observed in the other ferrites that were investigated.

An analysis of the experimental curves has shown that the dependence of σ on H near Θ_f can be represented analytically by

$$H = a\sigma + b\sigma^3, \tag{5}$$

where a and b are coefficients that depend on P and T.

In Fig. 6 Eq. (5) is represented by solid curves while the experimental values are given by dots. With suitably selected constants Eq. (5) is seen to give a satisfactory description of the experimental results. The experiments show that for all of the investigated ferrites the coefficient a increases linearly with temperature. The coefficient b is comparatively small and increases with temperature just as in the case of ferromagnetic metals.

In conclusion the authors wish to thank Professor E. I. Kondorskii and D. I. Volkov for their participation in a discussion of the results.

---

[1] L. Neel, Ann. phys. 3, 137 (1948).

[2] M. Fallot and P. Maroni, J. phys. et radium 12, 256 (1951).

[3] D. I. Volkov and V. I. Chechernikov, Научн. докл. Высш. школы (Scientific Reports of the Higher Schools) 1, 2 (1958).

[4] D. I. Volkov and V. I. Chechernikov, Izv. Akad. Naul SSSR, Ser. Fiz. 21, 1111 (1957) [Columbia Techn. Transl. 21, 1099 (1957)].

[5] L. Neel and P. Brochet, Compt. rend. 230, 280 (1950).

Translated by I. Emin
186

SOVIET PHYSICS JETP VOLUME 35(8), NUMBER 4 APRIL, 1959

INTERACTION OF 80 to 300 Mev π^+ MESONS WITH LIGHT NUCLEI

G. A. BLINOV, M. F. LOMANOV, Ia. Ia. SHALAMOV, V. A. SHEBANOV, and V. A. SHCHEGOLEV

Submitted to JETP editor May 6, 1958

J. Exptl. Theoret. Phys. (U.S.S.R.) 35, 880-886 (October, 1958)

A 17-liter bubble chamber was used to study the interaction of π^+ mesons with nuclei. The cross-sections for scattering, absorption, charge-exchange scattering, and production of charged mesons were measured. The processes of absorption and charge-exchange scattering are discussed.

A bubble chamber filled with a mixture of freons CCl_2F_2 and $CClF_3$ was used for experiments on the interaction of 80 to 300 Mev π^+ mesons with the working liquid in the chamber. The cross sections for charge-exchange scattering and star production, and the total cross section for elastic and inelastic scattering in collisions between π^+ mesons and C, F, and Cl nuclei were measured for ten energy values throughout the range. Six events in which charged π mesons had been produced by π^+ mesons were observed in the 210 to 300 Mev range. The cross section for charge-exchange scattering was found to increase by a factor of two over the 80 to 200 Mev range, attaining 10% of the geometrical cross section. The star-production cross section reaches a maximum in the vicinity of 180 Mev. Experiments were carried out on the interaction of 260 Mev protons stopping in the chamber.

A comparison of the stars accompanying the charge-exchange scattering events with those produced in interactions of protons with C, F, and Cl nuclei shows that the charge-exchange scattering on light nuclei is a result of the interaction between the incident π^+ meson and a single nucleon of the nucleus. An analysis of the absorption stars and comparison with proton-produced stars shows that, in the energy range investigated, the absorption of π^+ mesons results predominantly from a single interaction between the π^+ meson and a proton-neutron pair. This process occurs in 60 to 70% of the events involving 200-Mev π^+ mesons.

1. EXPERIMENTAL METHOD

The experiments were made with the synchrocyclotron of the Nuclear Research Laboratory of the Joint Institute for Nuclear Research. The π^+-meson beams were obtained by bombarding polyethylene targets with the external proton beam.[1] A π^+ meson beam of given energy traversed the freon bubble chamber having an observation volume of $50 \times 22 \times 15$ cm^3. The construction and operation of the chamber have been described in an earlier publication.[2] The working liquid used in this series of experiments consisted of a mixture of 54% (per weight) freon 12 (CCl_2F_2) and 46% freon 13 ($CClF_3$). The chamber operated at +28°C. The working liquid density was equal to 1.12 g/cm^3. When the chamber was triggered, its pressure fell from 38 to 10 or 13 atmos in about 15 milliseconds. The fact that the pressure dropped to a predetermined level ensured a good stability of the chamber sensitivity, and made it possible to choose quickly the working conditions during the experiments. The operating cycle of the chamber varied from 16 to 40 sec in different experiments. A stereoscopic camera using two parallel films, with a lens base of 103 mm and mean reduction equal to 11.6 was used for photography.

Since the π^+ mesons lost by ionization about 80 Mev in traversing the chamber, it was possible to study the interaction of π^+ mesons of various energies using a single beam. The chamber volume was divided for that purpose into four regions by means of a grid on the internal side of plexiglass windows. The grid simplified also considerably coordinate measurements in the chamber.

Three series of measurements were conducted, with the initial energy of π^+ mesons in the beam (before entering the chamber) equal to 320, 234, and 130 Mev respectively. The 320 Mev and 230 Mev beams were obtained choosing the field of the deflecting magnet so that the maximum beam intensity was attained for a given thickness of the polyethylene target bombarded by protons. The secondary π^+ meson beam was produced mainly as the result of the $pp \rightarrow d\pi^+$ reaction. It was difficult to find experimentally the maximum intensity of the 130 Mev beam and the corresponding setting of the magnetic field was calculated.

The energy of π^+ mesons in the first beam

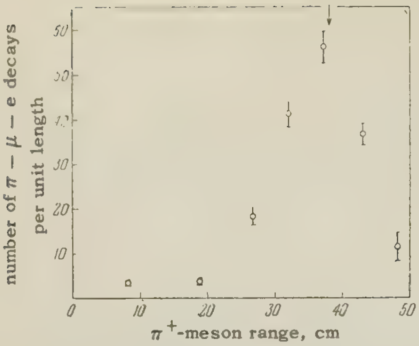

FIG. 1. Dependence of the number of $\pi-\mu-e$ decays per unit length on the π^+-meson range.

TABLE I. Cross-sections for various interactions of π^+ mesons with C, F, and Cl nuclei expressed in terms of the mean geometrical cross-section

π^+ meson energy, Mev	σ_e/σ_{geom}*	σ_a/σ_{geom}	σ_s/σ_{geom}
77	0.045 ± 0.020	0.393 ± 0.050	0.491 ± 0.056
100	0.068 ± 0.023	0.502 ± 0.055	0.807 ± 0.068
136	0.064 ± 0.025	0.537 ± 0.064	0.904 ± 0.084
157	0.101 ± 0.028	0.629 ± 0.068	1.056 ± 0.089
177	0.092 ± 0.023	0.572 ± 0.058	1.108 ± 0.083
197	0.078 ± 0.019	0.549 ± 0.051	1.144 ± 0.081
224	0.107 ± 0.022	0.447 ± 0.059	0.973 ± 0.092
245	0.099 ± 0.020	0.439 ± 0.053	1.050 ± 0.087
264	0.124 ± 0.020	0.365 ± 0.041	1.032 ± 0.079
283	0.098 ± 0.016	0.375 ± 0.042	0.886 ± 0.067

*Only statistical errors are given.

(320 Mev) was found from the kinetics of the reaction $pp \rightarrow d\pi^+$ taking into account the ionization losses in the polyethylene target and in the layer of air between the target and the chamber. The energy of π^+ mesons in the other beams was obtained from the energy of the first beam and the relative magnetic field intensities. The energy of the third beam calculated in that way (130 Mev) is in a good agreement with that found from the range-energy relation R(E). The range of π^+ mesons in the chamber was measured by counting the number of π-μ-e decays along the π^+-meson path. The results are shown in Fig. 1, where the arrow indicates the π^+-meson range calculated from the range-energy curves under the assumption that the energy of the π^+ mesons was 130 Mev before entering the chamber.

Possible admixture of other particles in the π^+-meson beam was taken into account in counting the number of π^+ mesons traversing the chamber. Proton and electron tracks were easily distinguished by their ionization and multiple scattering, so that their presence did not introduce any errors. The admixture of μ mesons in the 130-Mev beam amounted to 13%. This value was found from the pictures by means of data on the range of π and μ mesons. We did not determine the fraction of μ mesons in the other beams, but used the results of Mukhin et al.[1] who conducted experiments in identical conditions. Data on the admixture of μ mesons were taken into account in calculating the cross sections. In addition, a correction was applied for the π^+ mesons removed from the beam by multiple scattering.

Only π^+ mesons entering the chamber at not more than 5° to the beam axis and not less than 7 cm from the top and bottom wall of the chamber were counted. The π^+ mesons that underwent an interaction were identified by their ionization, multiple scattering, or π-μ-e decay. In several cases π^+ mesons were identified by the characteristic increase of ionization and multiple scattering along the track. Only the events in which the sum of the scattering angle projections in the two pictures was larger than 10° were used for measuring the scattering cross-section. The adoption of this criterion prevented the errors due to the multiple scattering and decay of π mesons in flight.

The large dimensions of the bubble chamber and the relatively high density of the filling liquid ensured a high efficiency of photon detection through pair production. It was therefore possible to measure separately the cross sections for star production and charge-exchange scattering ($\pi^+ \rightarrow \pi^0$). In the reduction of the data, events in which the disappearance of a π^+ meson was accompanied by one or two conversion pairs with their apex directed towards the point in which the interaction took place were interpreted as charge-exchange scattering. The accuracy with which the pair followed the direction of the photon amounted to ±3 or 5° and was determined from the mean angle of multiple scattering of the electrons and

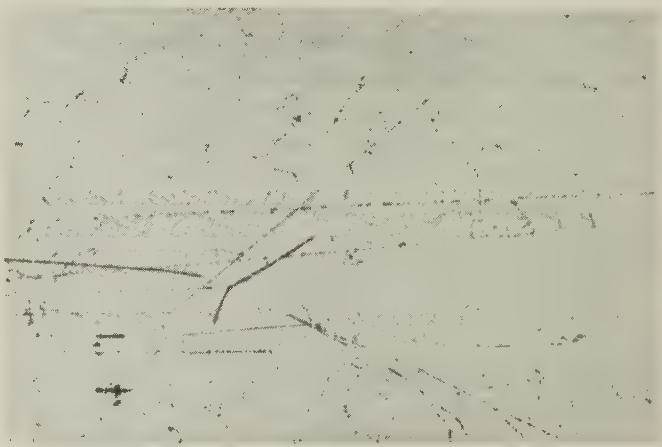

FIG. 2. Photograph of a charge-exchange scattering event. The conversion pair is produced by a photon emitted from the two-pronged star.

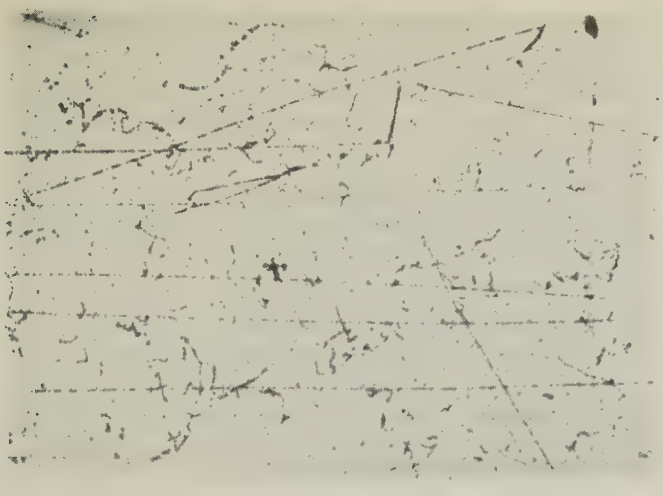

FIG. 3. A charge-exchange scattering event. Two conversion pairs are visible.

the mean angle between the momentum of the photon and of the pair.

The efficiency of π^0-meson detection in the chamber was calculated by two methods. In the first, the probability of the materialization of photons within a sphere 5 cm in radius was calculated using the known value of the radiation length, equal to 21.2 cm for the case of the freon mixture used, under the condition that the angle between the direction of emission of photons and the film plane was $\leq 30°$. The calculation showed that the probability that a conversion pair will be observed in this volume is 0.21. The detection efficiency for charge-exchange scattering events is then $0.21\ N_0/N_1$, where N_0 is the total number of pairs produced in the total volume of the chamber, and N_1 is the number of pairs found within a sphere 5 cm in radius.

In the second method we studied the characteristic features of the stars accompanying charge-exchange scattering events. It was found that in the majority of cases the energy of protons in these was less than 30 or 40 Mev. The multiplicity distribution of stars unaccompanied by a conversion pair is similar to that of stars associated with exchange scattering. One can assume, therefore, that all stars with a low energy yield correspond to exchange scattering events, i.e., that the detection probability of π^0 mesons is given by the ratio of the number of stars accompanied by a conversion pair to the total number of low-energy stars. Both methods yielded similar results for the π^0-meson detection efficiency, which was found to be equal to 0.50 ± 0.11.

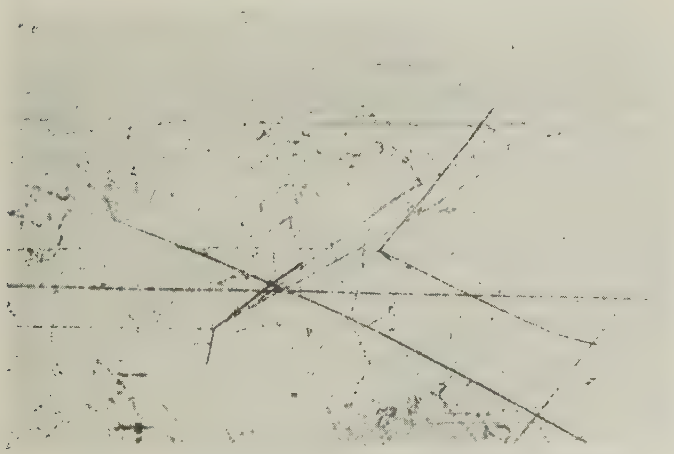

FIG. 4. A charge-exchange scattering event. A π^0-meson decays according to the scheme $\pi^0 \to e^+ + e^- + \gamma$.

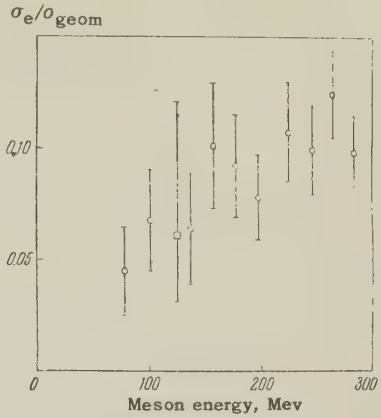

FIG. 5. Energy dependence of the charge-exchange scattering cross sections of π^+ mesons. ○ – this experiment, □ – (π^-, C) according to reference 10.

2. RESULTS AND DISCUSSION

About 7000 pairs of photographs were taken while the chamber was exposed to the π^+ beams. 193 exchange-scattering events and six charged-meson production events were detected in the energy range from 80 to 300 Mev. In the scanning of 3000 pictures, 4460 various interaction events of π^+ mesons with nuclei were observed. Examples of the pictures are shown in Figs. 2 to 4.

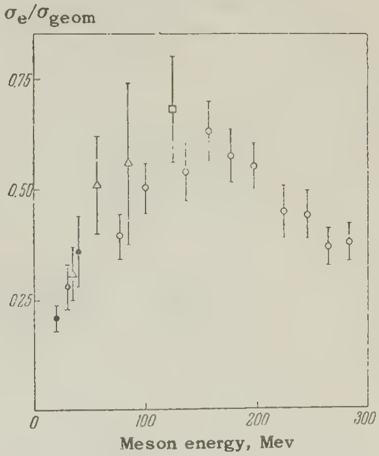

FIG. 6. Energy dependence of the star-production cross-sections of π^+ mesons. ○ – this experiment, □ – (π^-, C),[10] △ – (π^+ Al),[5] ● – (π^+, Be).[7]

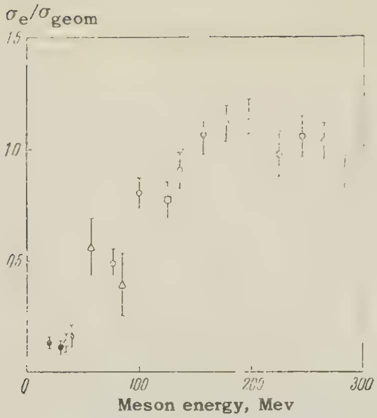

FIG. 7. Energy dependence of the total cross section for elastic and inelastic scattering of π^+,mesons. ○ – this experiment, □ – (π^-, C).[10] △ – (π^+, Al),[5] ● – (π^+, Be).[7]

The observed energy dependence of the various types of interaction of π^+ mesons is given in Table I. In this table σ_e denotes the exchange scattering cross section, σ_a is the star production (absorption) cross-section, and σ_s is the total cross section for elastic and inelastic scattering. The measured value of the latter was somewhat low, since we considered only those scattering events in which the sum of the scattering angle projections in both pictures was larger than 10°. All cross sections in the table are expressed in terms of the mean geometrical cross-section of the C, F, and Cl nuclei, equal to 483×10^{-27} cm^2. This value was calculated assuming a nuclear radius of $1.40 \times 10^{-13} A^{1/3}$. The energy dependence of the cross-sections σ_e, σ_a σ_s, constructed using the data of Table I, is shown in Figs. 5 to 7.

The multiplicity distribution of stars was studied in order to elucidate the mechanism of the charge-exchange scattering of π^+ mesons and their absorption by nuclei. Charged star products were recorded starting with 10 to 20 Mev proton energy. Most detailed data on the multiplicity distribution were obtained for 220 to 300-Mev π^+ mesons. These data are given in Table II, which contains the distributions of the sum of absorption and charge-exchange processes (row 1) and of each of them separately (rows 2 and 3). The meaning of the fourth row will be given below.

a. Charge-Exchange Scattering

The charge-exchange scattering of π^+ mesons on free nucleons takes place in the $\pi^+ n \rightarrow \pi^0 p$ reaction. The character of this process on a nucleus can be determined by comparing the stars accompanying charge-exchange events with those produced in interactions between protons of corresponding energy and the nuclei. The conditions for the production of stars as the result of development of nucleonic cascades may be similar in both cases, since the interaction mean free path of π^+ mesons in the energy range under consideration is small compared with the size of the nucleus and the interaction mean free path of protons in it.

Data on the stars produced by protons were obtained in the course of a special proton-beam experiment using the same chamber filling as in the experiments with π^+-meson beams. 280-Mev protons were chosen to ensure their stopping at

TABLE II. Relative multiplicity distribution of stars associated with charge-exchange and absorption of 220 to 300-Mev π^+ mesons

Type of event	Multiplicity (number of prongs)					
	0	1	2	3	4	5
Absorption and charge-exchange stars	5.6±0.8	24.2±1.8	39.4±2.4	22.2±1.8	7.6±1.0	~1
Charge-exchange stars	18.5±3.9	52.0±6.2	28.0±4.6	1.5±1.2	—	—
Absorption stars F(n)	2.6±0.7	17.8±3.0	42.3±2.8	27±2.2	9.3±1.3	—
Distribution f(n + 1)	<1	10.8±1.5	51.1±3.2	33.7±2.6	4.4±0.9	—

TABLE III. Relative multiplicity distribution f(n) of stars associated with inelastic scattering of 115 to 220-Mev protons

Proton energy Mev	Multiplicity (number of prongs)			
	0	1	2	3
143±27	11.3±2.0	54.8±4.4	30.5±3.2	3.4±1.1
195±25	10.3±2.0	47.7±4.3	36.6±3.7	5.3±1.4
115–220	10.8±1.5	51.1±3.2	33.7±2.6	4.4±0.9

the end of the chamber. The multiplicity distribution of stars of various energies is given in Table III. It follows from the table that the distribution is independent of the energy over the measured range. We can conclude from the data obtained at lower proton energies that the multiplicity distribution is slightly different from that of Table III. The maximum, nevertheless, remains in the vicinity of one-prong stars.

Comparing the multiplicity distribution of stars associated with the exchange scattering of π^+ mesons (Table II, row 2) with that of proton-produced stars (Table III) one can notice a close similarity between the two. This fact shows that the charge-exchange scattering from nuclei is due to a single collision between the incident π^+ meson and a neutron of the nucleus.

The angular distribution of photons in the charge-exchange scattering of 264 ± 15 Mev and 245 ± 15 Mev π^+ mesons was estimated from the forward/backward ratio in 67 events. This was found to be equal to 1.76 ± 0.30, which indicates clearly anisotropy of the exchange scattering and of the π^+-meson scattering from free protons in the energy range investigated.

Difficulties connected with the identification of π^- mesons in the chamber did not permit us to estimate with reasonable accuracy the efficiency of the charge-exchange process ($\pi^+ \rightarrow \pi^-$). The cross-section for this process, judging from the two cases observed, is of the order of 10^{-27} cm^2 per fluorine nucleus.

b. Production of Stars

The absorption of π^+ mesons by nuclei was studied earlier in greater detail at energies below 100 Mev by means of emulsions and cloud chambers.[4-7] An analysis of the stars produced as the result of the absorption of < 100 Mev π^+ mesons showed that, in not less than 60% of cases, π^+ mesons are absorbed by proton-neutron pairs according to the scheme $\pi^+ + (pn) \rightarrow pp$.

The contribution of this process to the absorption of π^+ mesons in the energy range investigated in the present experiment can be assessed from a study of the multiplicity distribution of stars. The data for 220 to 300-Mev π^+ mesons were analyzed in detail. It can be seen from Table II that two- and three-pronged stars are observed most often in absorption events. This fact can be explained assuming that, as in the low-energy range, the absorption follows the scheme $\pi^+ + (pn) \rightarrow pp$, and using the data on the interaction of protons with nuclei. In fact, since the angle between the protons emitted in the reaction is large (150 to 180°), one only of the fast protons interacts, on the average, in the nucleus. The energy of these protons is close to that used in the auxiliary experiment employing a proton beam. One can expect therefore that the multiplicity distribution of stars produced in the absorption of π^+ mesons is $F(n) = f(n+1)$, where $f(n)$ is the proton distribution.

It follows from Table II that the distributions $F(n)$ and $f(n+1)$ are very similar (rows 3 and 4). This strengthens the assumption that the reaction $\pi^+ + (pn) \rightarrow pp$ plays a predominant role in the absorption of 230 to 300-Mev π^+ mesons by nuclei. An additional analysis of the multiplicity distribution of stars as a function of π^+-meson energy in the 80 to 300 Mev range showed that the distribution is almost independent of energy. It follows therefore that the absorption of π^+ mesons by (p-n) pairs is the main absorption process over the whole range.

It was found by a comparison of the number of events corresponding to the reaction $\pi^+ + (pn) \rightarrow pp$ with the total number of stars and with the known degree of transparency of nuclei for protons that, for 200-Mev π^+ mesons, the absorption by (p-n) pairs in the first interaction occurs in 60 to 70% of cases.

c. Production of Charged π Mesons by π^+ Mesons

Six events in which charged π mesons were produced by π^+ mesons were observed in the 210 to 300 Mev range. The cross section calculated from these is $(0.7 \pm 0.3) \times 10^{-27}$ cm^2 per fluorine nucleus. This value is close to that obtained in experiments using a helium-filled diffusion chamber[8] and is also in agreement with the results of experiments using hydrogen.[9]

It is interesting to note that in one only of the six cases an accompanying proton is emitted. Its energy was found to be 40 Mev. This fact indicates that, in the production process, the incident meson collides more often with a virtual meson than with a nucleon.

In conclusion, the authors would like to thank A. A. Tiapkin for a discussion of the results, V. P. Dzhelepov for enabling us to carry out the experiments, and to V. P. Rumiantseva and K. A. Zaitsev for help in the reduction of data.

---

[1] Mukhin, Ozerov, and Pontecorvo, J. Exptl. Theoret. Phys. (U.S.S.R.) 31, 371 (1956), Soviet Phys. JETP 4, 237 (1957).

[2] Blinov, Lomanov, Meshkovskii, Shalamov, and Shebanov, Приборы и техника эксперимента (Instruments and Meas. Eng.) **1**, 35 (1958).

[3] Blinov, Krestnikov, and Lomanov, J. Exptl. Theoret. Phys. (U.S.S.R.) **31**, 762 (1956), Soviet Phys. JETP **4**, 661 (1957).

[4] Byfield, Kessler, and Lederman, Phys. Rev. **86**, 17 (1952).

[5] J. Tracy, Phys. Rev. **91**, 960 (1953).

[6] G. Bernardini and F. Levy, Phys. Rev. **84**, 610 (1951).

[7] F. H. Tenney and J. Tinlot, Phys. Rev. **92**, 974 (1953).

[8] Kozodaev, Suliaev, Filippov, and Shcherbakov, J. Exptl. Theoret. Phys. (U.S.S.R.) **31**, 701 (1956), Soviet Phys. JETP **4**, 580 (1957).

[9] V. B. Zinov and S. M. Korenchenko, J. Exptl. Theoret. Phys. (U.S.S.R.) **34**, 301 (1958), Soviet Phys. JETP **7**, 210 (1958).

[10] J. O. Kessler and L. M. Lederman, Phys. Rev. **94**, 689 (1954).

Translated by H. Kasha
187

SOVIET PHYSICS JETP VOLUME 35(8), NUMBER 4 APRIL, 1959

BREMSSTRAHLUNG FROM π MESONS INTERACTING WITH NUCLEI

M. F. LOMANOV, A. G. MESHKOVSKII, Ia. Ia. SHALAMOV, V. A. SHEBANOV, and A. F. GRASHIN

Submitted to JETP editor May 6, 1958

J. Exptl. Theoret. Phys. (U.S.S.R.) **35**, 887-893 (October, 1958)

Bremsstrahlung from π^+ mesons in a nuclear force field was observed in a freon bubble chamber in the course of study of the interactions of π^+ mesons of energies from 80 to 300 Mev with carbon, fluorine, and chlorine nuclei. The bremsstrahlung cross section both in the cases of inelastic and elastic scattering of π^+ mesons amounts, on the basis of 20 observed events, to $(4.5^{+1.2}_{-2.0}) \times 10^{-27}$ cm^2 per fluorine nucleus in the energy range indicated above. Three events have been observed of bremsstrahlung accompanying the absorption of a π^+ meson by a nucleus, and two events have been observed which may be attributed to bremsstrahlung accompanying charge exchange scattering of π^+ mesons by nuclei. The bremsstrahlung cross section for various nuclear processes has been calculated in the quasi-classical approximation. The values of the cross sections computed from these formulas are in good agreement with the experimental results.

1. INTRODUCTION

BECAUSE of the strong nuclear interaction between π mesons and nucleons, bremsstrahlung from π mesons, i.e., the emission of γ quanta arising as a result of a change of velocity or of a loss of charge, must be determined primarily by nuclear rather than Coulomb forces. Bremsstrahlung in a nuclear force field from mesons of various energies has been treated in several theoretical papers.[1-4] In particular, Solov'ev[3] has discussed bremsstrahlung from π mesons at energies close to the π-meson rest energy. It was found that the bremsstrahlung cross section in this energy range should in order of magnitude amount to approximately 10^{-28} cm^2 per nucleon.

The relatively large theoretically-expected value of the bremsstrahlung cross section for π mesons in a nuclear force field makes it probable that this phenomenon should be observed experimentally. However, up until now no bremsstrahlung from π mesons has been found experimentally. In the present work bremsstrahlung from π mesons was found in the course of study of the interactions of π^+ mesons with light nuclei in the range of energies close to the rest energy.

The experiments were carried out in the external π^+-meson beam of the synchrocylclotron of the Laboratory for Nuclear Problems of the Joint Institute for Nuclear Research. π^+ mesons of definite energy were introduced into a freon bubble chamber[5] whose useful observation volume amounted to approximately 17 l. The working liquid in the chamber was a mixture of two freons — CCl_2F_2 and $CClF_3$. Bremsstrahlung γ quanta were observed by means of conversion into electron-positron pairs. The energies of the charged products of the interaction of π^+ mesons in the chamber were determined mainly from the range of the particles. The range curves have been computed earlier[5] according to the theory of ionization losses. In some cases the energy of π mesons after interaction was found by measuring the ionization losses along the length of the tracks or by multiple scattering. The remaining details of the method are given in the paper by Blinov et al.[6]

2. CLASSIFICATION OF THE VARIOUS FORMS OF BREMSSTRAHLUNG AND COMPETING PROCESSES

We shall distinguish the following cases of bremsstrahlung that can result from the interaction of π mesons with nuclei.

1. Radiation arising during inelastic scattering of π mesons by nuclei. In this case the principal track of the π meson in bubble-chamber photographs shows a kink at the point of interaction, and at the same time the photograph shows an electron-positron pair pointing towards the kink. The scheme of the process $\pi^+ + A \rightarrow \pi^+ + \gamma + A'$, where A and A' are the initial and final states of the nucleus. The transformation of nucleus A into nucleus A' is accompanied by the emission of protons and neutrons from nucleus A, which in the majority of cases can be seen in the photograph as proton tracks leaving the point of interaction. Such a photograph can alternately be in-

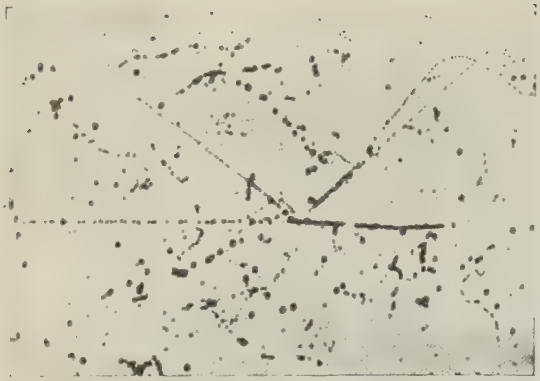

FIG. 1. Bremsstrahlung accompanying inelastic scattering.

FIG. 2. Bremsstrahlung accompanying scattering (elastic or inelastic).

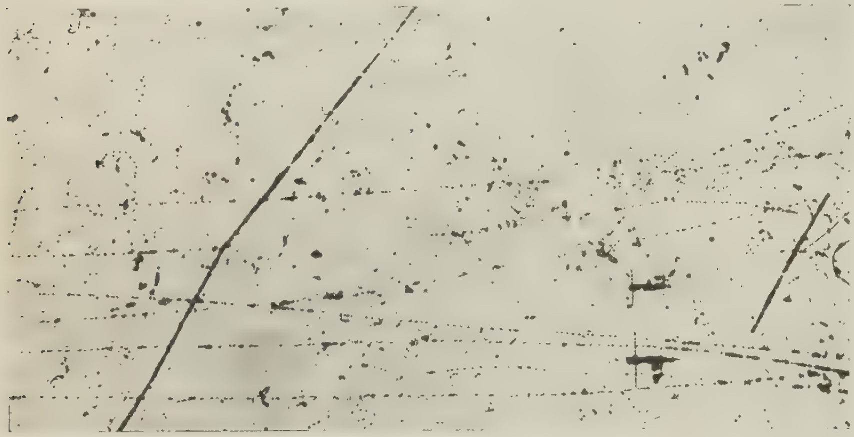

FIG. 3. Bremsstrahlung accompanying absorption.

terpreted as the creation of a neutral π meson in accordance with $\pi^+ + A \rightarrow \pi^+ + \pi^0 + A'$, with subsequent decay of the π^0 meson into two γ quanta, only one of which is converted within the region of observation. One may discriminate between this competing process and bremsstrahlung on the basis of the following energy considerations. We denote the kinetic energy of the π meson before interaction by E_0, after interaction by E_1, and the energy of the protons leaving the nucleus by E_p. It is then evident that if the following condition is fulfilled

$$E_0 - (E_1 + E_p) < \mu c^2,$$

where μ is the π^0-meson mass, this event should be attributed to bremsstrahlung. The inverse condition

$$E_0 - (E_1 + E_p) > \mu c^2$$

can be evidence either of the process $\pi^+ + A \rightarrow \pi^+ + \pi^0 + A'$, or of bremsstrahlung, and therefore such cases require additional investigation.

2. Radiation arising during elastic or diffraction scattering of a π meson by a nucleus in accordance with the scheme $\pi^+ + A \rightarrow \pi^+ + \gamma + A$. In the photographs this case differs from the preceding one by the absence of proton tracks at the kink, and by a relatively small angle of scattering of the π meson. Just as in the preceding case, a competing process is the process of creation of a π^0 meson by a π^+ meson according to the reaction $\pi^+ + A \rightarrow \pi^+ + \pi^0 + A'$, under the condition that the transformation of nucleus A into nucleus A′ is not accompanied by visible tracks of reaction products, so that the measured value is $E_p = 0$. It is evident that if the inequality $E_0 - E_1 < \mu c^2$ is satisfied, the event should be attributed to bremsstrahlung.

3. Radiation arising when a π meson is absorbed in accordance with $\pi + A \rightarrow \gamma + A'$. In the photograph the π-meson track ends in a star or disappears ("prongless" star). At the same time the photograph shows a pair directed towards the center of the star or towards the end of the track. A competing and a considerably more probable process in this case is the process of charge-exchange scattering of the π^+ meson in accordance with the reaction $\pi^+ + A \rightarrow \pi^0 + A'$ under the condition that, as in the preceding two cases, only one of the two γ quanta into which the π^0 meson decays is converted within the region of observation. As before, discrimination between these two processes is possible only in individual cases, on the basis of energy considerations.

4. Radiation arising in charge-exchange scattering of the π^+ meson according to the reaction $\pi^+ + A \rightarrow \pi^0 + \gamma + A'$. The track of the π meson ends in a star or stops, while electron-positron pairs directed toward the point of interaction can be seen in the photograph. If three pairs can be seen in the photograph, then the process $\pi^+ + A \rightarrow \pi^0 + \pi^0 + A'$ is possible, i.e., the creation of a π^0 meson accompanied by a simultaneous charge exchange of the π^+ meson is possible, with only three of the four γ quanta from the π^0 meson decay being converted.

In all the above four cases the bremsstrahlung can be distinguished from the competing process not only on the basis of energy balance, but also by considering the angular distribution of the γ quanta. As will be shown in Sec. 4, the theoretical angular distribution of the bremsstrahlung γ quanta is such that most γ-quanta should be emitted forward, while the angular distribution of the γ quanta coming from the decay of π^0 mesons must be considerably more isotropic.

3. EXPERIMENTAL RESULTS

More than 7000 photographs obtained in three series of experiments with different initial π^+-meson energies beam have been analyzed. In these photographs there were observed 20 events of bremsstrahlung accompanying inelastic and elastic scattering, three events accompanying absorption, and two events which may be attributed either to bremsstrahlung accompanying charge exchange, or to the process $\pi^+ + A \rightarrow \pi^0 + \pi^0 + A'$.

Typical photographs of bremsstrahlung processes accompanying scattering and absorption are given in Figs. 1 to 3. The photograph shown in Fig. 2 can apparently be interpreted as bremsstrahlung accompanying elastic scattering, on the basis of the absence of a star at the point of interaction and of the small angle of scattering. Naturally these features are not sufficient to distinguish this event from bremsstrahlung accompanying inelastic scattering, since inelastic interaction might for one reason or another, not be accompanied by visible proton tracks in the photograph.

Since there exists no reliable criterion for distinguishing between eleastic and inelastic scattering, we have classified all the 20 observed events as bremsstrahlung accompanying scattering. These events are given in the table.

The values of the energies E_0 and E_p given in the table are obtained from measurements of the ranges of the particles. The precision with which the energies E_0 are determined is approximately 5%. The energy E_1 of events 9 and 12 has been determined from the energy of the prongs of the star in which the π^+-meson track ends after scattering. In two events (10 and 19) the energy E_1 is also found from the multiple scattering of the π^+ meson. The γ-quanta energy E_γ was determined from the ranges of the electron and positron of the pair.

As can be seen from the table, for the first 13 events the inequality $E_0 - (E_1 + E_p) < 140$ Mev holds, so that these events cannot be interpreted as the result of the creation of a π^0 meson in accordance with the reaction $\pi^+ + A \rightarrow \pi^+ + \pi^0 + A'$, and must definitely be attributed to bremsstrahlung. In the remaining seven events (14 to

Observed events of bremsstrahlung emitted by π^+-mesons during scattering (energies given in Mev)

No.	π^+-meson energy				Energy of star prongs E_p	Energy of γ quanta, E_γ	$E_0 - (E_1+E_p)$
	Before scattering, E_0	After scattering, based on					
		Range	Ionization	Other Considerations			
1	237	>60	>100		>120	~ 10	<17
2	276	>55	>70		173	>30	<33
3	237	>50	>100		100	>23	<37
4	170	>110			—	>37	<60
5	183	63			54	>23	66
6	239	>40			120	>29	<79
7	213	>60	>100		20	>22	<93
8	147	>54			—	>13	<93
9	262			>80	77	>26	<105
10	266	>54	>160	160 ± 80	—	>17	<106
11	279	>165			—	>28	<114
12	235			>69	36	>55	<130
13	250	>65	>100		18	>60	<132
14	265	>12	>25		35	~ 15	<205
15	152	<5			~ 7	>24	<145
16	256	65			40	>30	151
17	247	55			20	>70	<172
18	261	>40			46	>24	<175
19	249	>54		~ 60	—	>35	<195
20	259	>35			—	>20	<224

20) $E_0 - (E_1 + E_p)$ may exceed 140 Mev, which indicates the possibility of creation of a π^0 meson. The identification of these events as bremsstrahlung requires a separate investigation.

Event 14 should be attributed to bremsstrahlung, since the γ-quantum energy determined from the ranges of the electron and the positron of the pair, and also from the angle between their paths, is approximately 15 Mev. A γ-quantum of such energy cannot be the result of π^0-meson decay and must be interpreted as being due to bremsstrahlung.

In event 15 the initial energy of the π^+ meson is $E_0 = 152$ Mev, i.e., very close to the energy threshold of creation of a π meson by a π meson. In view of the very low probability of observing this process at such a value of E_0, this case must also be attributed to bremsstrahlung.

The last five events (16 to 20) should be ascribed, with a high degree of probability, to bremsstrahlung on the basis of the following two considerations. Firstly, not more than one out of the five events can be ascribed to the competing process $\pi^+ + A \rightarrow \pi^+ + \pi^0 + A'$, the cross section of which can be estimated with an accuracy sufficient for present purposes from the results of Blinov et al.[6] Secondly, measurements of the angles of emission of the γ quanta, have shown the radiation in all five events to be directed forward, principally within the 10 to 40° range, while in the case of the process $\pi^+ + A \rightarrow \pi^+ + \pi^0 + A'$ a more isotropic angular distribution of the γ quanta is expected.

On the basis of the 20 events given in the table, we computed the total cross section for bremsstrahlung accompanying scattering (elastic and inelastic) in the energy range from 80 to 300 Mev, and found it to be $\sigma_S^\gamma = (4.5^{+1.2}_{-2.1}) \times 10^{-27}$ cm^2 per fluorine nucleus.

As can be seen from the table we did not observe a single case of bremsstrahlung in the energy range from 80 to 150 Mev. This can be explained, first, by the experimental condition, since in the energy range indicated the number of π mesons passing through the chamber will be smaller by a factor of several fold than at higher energies. Second, theoretical estimates (Sec. 4) show that the cross section for bremsstrahlung accompanying scattering at a π-meson energy of 100 Mev must be approximately one-half that obtained at an energy of 250 Mev.

4. COMPARISON OF EXPERIMENTAL RESULTS WITH THEORY

A theoretical estimate of the bremsstrahlung from π mesons may be made with sufficient accuracy in the quasi-classical approximation. The quasi-classical formula is obtained if the exact expression for the differential bremsstrahlung cross section $d\sigma_\gamma(\omega, \beta)$ is expanded in terms of the energies $\hbar\omega$ of the γ quantum. In this expansion the first term has the quasi-classical form, i.e., it is the product of the cross section $d\sigma(\beta)$ of the corresponding nonradiative process by the probability dW_γ of radiation of a γ quantum for a given state of motion of the particles. We have denoted by β the complete set of initial and final velocities of the interacting particles. As shown by Low,[7] a general form of the second term in the expansion of the exact cross section $d\sigma_\gamma(\omega, \beta)$ can also be derived. However, in making estimates of the total radiation there is no point in using the second term of the expansion, since when $\hbar\omega/E \ll 1$, where E is the energy of the colliding particles, it gives rise to a correction of the order of $\hbar\omega/E$, which is of no significance to us, while in the case $\hbar\omega/E \sim 1$ the contribution of this term is of the same order of magnitude as that of subsequent terms in the expansion, and therefore we cannot be sure that the accuracy is improved by using the second term of the expansion in the upper part of the spectrum of the γ quanta. Moreover, this term also contains a derivative (with respect to energies and angles of the amplitude of the nonradiative process) which is difficult to determine with sufficient accuracy from the available experimental data. With these remarks in mind, we shall restrict the comparison of our results with theory only to the first term in the expansion of $d\sigma_\gamma(\omega, \beta)$.

The advantage of the quasi-classical estimate of bremsstrahlung is that in this estimate the formulas are expressed in terms of the exact nonradiative process $d\sigma(\beta)$ independently of the model used for the interaction of the π meson with the nucleus. This is a very important fact, since there exist no reliable methods of making calculations in the case of strong interaction. With respect to the high-energy part of the spectrum of the γ quanta, where the quasi-classical approximation is inapplicable, we can see that at our π-meson energies this part of the spectrum makes no significant contribution to the total bremsstrahlung cross section.

If we take the nucleus to be infinitely heavy and if we denote by β_0 and β_1 the initial and the final velocities of the π meson without taking into account the energy-momentum loss due to radiation, we obtain in the quasi-classical approximation:

$$\begin{aligned} d\sigma_\gamma(\omega, \beta_0, \beta_1) &\approx dW_\gamma d\sigma(\beta_0, \beta_1) \\ &= \frac{1}{137}\left[\left(\frac{\beta_0}{(1-\beta_0 \cdot n)} - \frac{\beta_1}{1-\beta_1 \cdot n}\right) n\right]^2 \frac{d\Omega_\gamma}{4\pi^2}\frac{d\omega}{\omega} d\sigma(\beta_0, \beta_1), \end{aligned} \tag{1}$$

where $\mathbf{n}$ is the unit vector in the direction of radiation of γ quanta, $d\Omega_\gamma$ is an element of solid angle of the γ quanta, and $d\sigma(\beta_0, \beta_1)$ is the cross section of some nonradiative process.

To compute the total cross section for any one of the classes of bremsstrahlung defined in Sec. 2, we should substitute into formula (1) the expression for the differential cross section of the corresponding nonradiative process and integrate over the energies and directions of the γ quanta and over the final velocities of the π meson. Assuming an isotropic angular dependence, we express the cross section for the inelastic scattering of a π meson by a nucleus in the form

$$d\sigma_i(\beta_0, \beta_1) = \frac{\sigma_i(\beta_0, \beta_1)}{4\pi}\, d\Omega, \tag{2}$$

where $\sigma_i(\beta_0, \beta_1)$ is the total cross section for inelastic scattering, for which the final velocity of the π meson is given by β_1.

To obtain the cross section for the elastic scattering of a π meson, we make use of the diffraction type of angular dependence and write

$$d\sigma_d(\beta_0, \beta_1) = \frac{\sigma_d(\beta_0)}{\pi} \left| \frac{I_1(R\theta/\lambda)}{\theta} \right|^2 d\Omega, \tag{3}$$

where R is the nuclear radius, $\cos\theta = \boldsymbol{\beta}_0\boldsymbol{\beta}_1/\beta_0\beta_1$, $\beta_0 = \beta_1$, λ is the wavelength of the π meson, and $\sigma_d(\beta_0)$ is the total cross section for elastic scattering.

We shall combine the cross sections for π-meson absorption and charge-exchange scattering into a total cross section for processes in which the π-meson charge comes to rest or, more accurately, the charge is transferred to nonrelativistic nucleons:

$$d\sigma_r(\beta_0) = d\sigma_a(\beta_0) + d\sigma_e(\beta_0). \tag{4}$$

Replacing $d\sigma(\beta_0, \beta_1)$ in formula (1) by one of the expressions (2), (3), or (4) and integrating, we obtain the required expressions for the total cross sections of radiative processes. For bremsstrahlung accompanying inelastic scattering we obtain:

$$\begin{aligned} \sigma_i^\gamma &= \frac{1}{137} \ln \frac{xE_0}{\hbar\omega_{\min}} \\ &\times \sum_{\beta_1} \left(\frac{1}{\beta_0} \ln \frac{1+\beta_0}{1-\beta_0} + \frac{1}{\beta_1} \ln \frac{1+\beta_1}{1-\beta_1} - 4 \right) \frac{\sigma_i(\beta_0, \beta_1)}{\pi} \qquad (5) \\ &= \frac{1}{137} \ln \frac{xE_0}{\hbar\omega_{\min}} \left(\frac{1}{\beta_0} \ln \frac{1+\beta_0}{1-\beta_0} + \frac{1}{\beta_1} \ln \frac{1+\beta'}{1-\beta'} - 4 \right) \frac{\sigma_i(\beta_0)}{\pi}. \end{aligned}$$

In this formula $\hbar\omega_{\min}$ is the minimum measured energy of the γ quanta; in our experiments $\hbar\omega_{\min} \approx 10$ Mev, as can be seen from the table; β' is some average π-meson velocity after scattering (in the calculations we assume that β' corresponds to the kinetic energy $E_0/2$); x is a certain parameter describing the cutting off of the spectrum of the γ-quanta. If we take $x = 1$, i.e., the spectrum is not cut off, the quasi-classical formulas gives too high a value for the total cross section, compared with the exact formula. A correct choice of x can make the quasi-classical formulas as accurate as $\int d\sigma_\gamma(\omega, \beta)\, d\omega$. At our π-meson energies it is best to take $x \approx 1/2$.

Similarly, we obtain the total cross section for bremsstrahlung accompanying elastic scattering:

$$\sigma_d^\gamma = \frac{1}{137} \ln \frac{xE_0}{\hbar\omega_{\min}} I(\beta_0, \mu cR/\hbar)\, \frac{\sigma_d(\beta_0)}{\pi}. \tag{6}$$

where the integral $I(\beta_0, \mu cR/\hbar)$ must in general be evaluated numerically, but in our case we can use the approximate value of this integral for $(1-\beta^2)^{-1} \gg 1$ and $2\mu cR/\hbar \gg 1$, which turns out to be equal to $2.3/(\mu cR/\hbar)$.

Finally, the total bremsstrahlung cross section in the case when the charge is "stopped" is given by:

$$\sigma_r^\gamma = \frac{1}{137} \ln \frac{xE_0}{\hbar\omega_{\min}} \left(\frac{1}{\beta_0} \ln \frac{1+\beta_0}{1-\beta_0} - 2 \right) \frac{\sigma_r(\beta_0)}{\pi}, \tag{7}$$

where $\sigma_r = \sigma_a + \sigma_e$, the sum of the cross sections for the absorption and for charge-exchange scattering of π mesons.

To compare our results with theory we take into account the fact that the average π^+-meson energy in the observed 20 events of bremsstrahlung accompanying scattering is 234 Mev. The cross sections σ_i, σ_d and σ_r required for our calculations have been measured by Dzhelepov et al.[8] for 230-Mev π^- mesons.

Calculations with formulas (5) and (6) yield, at 230 Mev, a cross section for bremsstrahlung accompanying scattering $\sigma_s^\gamma = \sigma_i^\gamma + \sigma_d^\gamma = 3.5 \times 10^{-27}$ cm^2 per fluorine nucleus, which agrees with our value $\sigma_s^\gamma = (4.7^{+1.2}_{-2.0}) \times 10^{-27}$ cm^2. The cross section for bremsstrahlung accompanying the stopping of the charge, calculated according to formula (7), is $\sigma_r^\gamma = 2.5 \times 10^{-27}$ cm^2 which is also in agreement with our results in the five observed events of this type of bremsstrahlung.

In conclusion, let us compare the theoretical and the experimentally-observed angular distributions of the bremsstrahlung γ quanta. We have measured the angles of emission of the γ quanta in all the 20 events listed in the table. Only in 2 events is the bremsstrahlung directed backwards, while in 18 events it is directed forwards. Such a distribution is in agreement with the one expected theoretically, since formulas (1) to (3) give a value

≈ 10 for the forward-backward ratio.

In conclusion, we express our deep gratitude to I. Ia. Pomeranchuk for his interest in our work.

---

[1] L. D. Landau and I. Ia. Pomeranchuk, J. Exptl. Theoret. Phys. (U.S.S.R.) **24**, 505 (1953).

[2] Iu. A. Vdovin, Dokl. Akad. Nauk S.S.S.R. **105**, 947 (1955).

[3] V. G. Solov'ev, J. Exptl. Theoret. Phys. (U.S.S.R.) **29**, 242 (1955), Soviet Phys. JETP **2**, 159 (1956).

[4] R. E. Cutkosky, Phys. Rev. **109**, 209 (1958).

[5] Blinov, Lomanov, Meshkovskii, Shalamov and Shebanov, **Приборы и техника эксперимента** (Instruments and Exptl. Engineering) **1**, 35 (1958).

[6] Blinov, Lomanov, Shalamov, Shebanov, and Shchegolev, J. Exptl. Theoret. Phys. (U.S.S.R.), **35**, 880 (1958), this issue, p. 609.

[7] F. Low, Phys. Rev. **110**, 974 (1958).

[8] Dzhelepov, Ivanov, Kozodaev, Osipenkov, Petrov and Rusakov, J. Exptl. Theoret. Phys. (U.S.S.R.) **31**, 923 (1956), Soviet Phys. JETP **4**, 864 (1957).

Translated by G. Volkoff
188

SOVIET PHYSICS JETP VOLUME 35(8), NUMBER 4 APRIL, 1959

INVESTIGATION OF THE DEPOLARIZATION OF NEGATIVE MUONS IN LIQUID HYDROGEN

A. E. IGNATENKO, L. B. EGOROV, B. KHALUPA, and D. CHULTEM

Joint Institute for Nuclear Research

Submitted to JETP editor May 5, 1958; resubmitted July 14, 1958

J. Exptl. Theoret. Phys. (U.S.S.R.) **35**, 894-898 (October, 1958)

The angular distribution of decay electrons from μ^- mesons was measured in liquid hydrogen with the aid of scintillation counters. The distribution was found to be isotropic within the limits of experimental error. The degree of polarization of μ^- mesons in mesic hydrogen was determined from the electron angular distribution to be less than 2.5%. The observed complete depolarization of μ^- mesons can evidently be explained essentially by the mechanism suggested by Zel'dovich and Gershtein, according to which the μ^- meson jumps from one proton to another simultaneously with a transition to the hyperfine-structure ground state. Due to this mechanism a transition between orthohydrogen and parahydrogen is possible. It is impossible to determine the form of the interaction between μ^- mesons and nucleons by measuring the angular distribution of neutrons from the $\mu^- + p \rightarrow n + \nu$ reaction in liquid hydrogen because of the complete depolarization of the μ^- mesons.

INVESTIGATION of the capture of polarized μ^- mesons in hydrogen makes it possible to obtain information on the nature of the weak interaction between muons and nucleons.[1-3] It is usually assumed that μ^- mesons are absorbed by protons in mesic hydrogen through the reaction $\mu^- + p \rightarrow n + \nu$. The angular distribution of neutrons from this reaction provides one method of determining the type of interaction. The neutron angular distribution is described by

$$w(\theta) = 1 + a\beta\cos\theta, \tag{1}$$

where β is the asymmetry parameter in the neutron angular distribution, the magnitude and sign of which depend on the type of interaction, θ is the angle between the neutron path and muon spin, and a is a parameter which takes into account the degree of polarization of μ^- mesons in mesic hydrogen.

It follows from Eq. (1) that the polarization of μ^- mesons in mesic hydrogen must be measured before the experimental determination of the neutron angular distribution. The present article is concerned with an experimental investigation of μ^--meson polarization in liquid hydrogen. The work was performed on the synchrocyclotron of the Joint Institute for Nuclear Research.

1. BASIC THEORETICAL CONCEPTS

We consider the possible depolarization mechanisms for μ^- mesons slowed down and stopped in liquid hydrogen. It was shown in references 4 and 5 that when muons are slowed down in matter to a velocity comparable with electron velocities in atoms, the muons are not depolarized. Depolarization evidently does not occur even while the velocity is subsequently being reduced to zero, i.e., until capture in mesic atomic orbits. When a mesic hydrogen atom is formed incomplete depolarization is possible as a result of the spin-orbit interaction.[6] The two hyperfine states of the mesic hydrogen atom are the singlet ground state (F = 0) and the first excited triplet state (F = 1). When F = 0 the meson "has forgotten" its initial spin direction (it is depolarized). In the state F = 1 the meson "remembers" its spin direction (it is not depolarized). It is easily seen that in an isolated mesic hydrogen atom the muon does not make a transition between levels of the hyperfine structure during its lifetime. Indeed, since the excited state is 0.2 ev above the ground state the probability of a radiative transition ($\tau_{rad} = 10^6$ sec) is many orders of magnitude smaller than the probability of meson decay ($\tau \sim 10^{-6}$ sec).[7] Let us now consider what happens to a mesic hydrogen atom which is formed in liquid hydrogen. The following processes are possible when such atoms are produced by the stopping of muons in liquid hydrogen:

(1) Muon capture by a deuteron present in the liquid hydrogen:

$$\mu^-H + D \rightarrow \mu^-D + H + 135 \text{ ev};$$

(2) Scattering:

$$\mu^-H + H \rightarrow \mu^-H + H, \ \mu^-D + H \rightarrow \mu^-D + H;$$

(3) Formation of mesic molecular ions:

$$\mu^-H + H \rightarrow \mu^-HH,\ \mu^-H + D \rightarrow \mu^-HD,\ \mu^-D + H \rightarrow \mu^-DH.$$

The probabilities of these processes have been considered theoretically in references 7 to 11. One interesting result of these studies is the fact that the cross section for process (2) is two orders of magnitude greater than the cross section for the other processes. Zel'dovich and Gershtein[7] have shown that, because of the neutrality of the mesic hydrogen atom, there exists in the scattering process a very effective mechanism of muon "jumps" from one proton to another with a simultaneous transition to the lower hyperfine level. Since the probability of these jumps ($\sim 10^9$ sec^{-1}) is three orders of magnitude greater than the probability of muon decay (0.5×10^6 sec^{-1}), all mesic hydrogen atoms are put into the ground state of the hyperfine structure within the muon lifetime. Complete depolarization of the μ^- mesons should result from these transitions.

2. EXPERIMENTAL PROCEDURE

The polarization of μ^- mesons stopping in liquid hydrogen was investigated by measuring the anisotropy of the angular distribution of the decay electrons.[6]

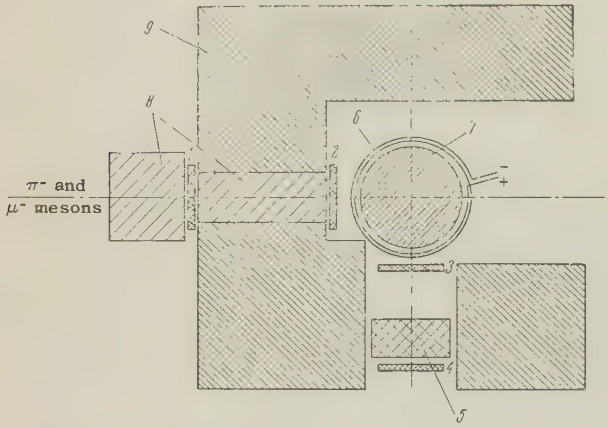

A negative pion beam of energy ~ 150 Mev and intensity ~ 900 π^-/cm^2-sec was directed at the experimental setup (see the figure). Aluminum absorbers with a total thickness of 32 cm were used to slow down the muons and to clear the pions from the beam. A fraction of the muons passed through the absorbers and were stopped in the target, which consisted of liquid hydrogen in an ordinary glass Dewar vessel. The Dewar had an inside diameter of 15 cm and length of 30 cm. The target was surrounded by a copper wire coil which generated the magnetic field required for muon precession. Two scintillation counters 1 and 2 connected in coincidence registered the muons which struck the target. Electrons from muon decay in the target were registered by counters 3 and 4, which were also connected in coincidence. The resolving time of the coincidence circuits was 5×10^{-8} sec. Plastic (polystyrene + 2% p-terphenyl + 0.1 α NPO) scintillators of 100 mm diameter and 6 mm thickness were used. A 6 g/cm^2 paraffin absorber was placed between counters 3 and 4. The electronic circuit functioned as follows. A (1 + 2)-coincidence pulse was delayed for 0.5 μ sec and initiated a gate of 1.5 μ sec duration for (3 + 4)-coincidence pulses, which reached a scaler and were registered by a mechanical counter. At the same time (1 + 2)-coincidence pulses reached their own scaler, which served as a monitor. Thus the circuit registered electrons with a range greater than 8 g/cm^2 produced during the time interval from 0.5 to 2 μ sec after the stopping of muons in the hydrogen. The angular distribution of the electrons was investigated by measuring the number of electrons as a function of the magnetizing current in the coil. The range of the magnetic field containing the target was in accordance with calculations for the precession of a mesic hydrogen atom in the triplet state. In this state the magnetic moment of the mesic hydrogen atom is approximately equal to the magnetic moment of the muon and the angular momentum is given by $F = \frac{1}{2} + \frac{1}{2} = 1$. It is easily shown that the precession frequency of mesic hydrogen atoms in a magnetic field is one half as great as the precession frequency of free muons. A 20-cm lead shield entirely surrounded the target and counters for the purpose of reducing the background. The electron counting rate was usually 20 per minute. The background level was 4 counts per minute and was independent of the magnetic field. The "low" background was attained because the target Dewar, shield, and magnetizing coil consisted of materials with relatively large Z, in which the probability of μ^--meson decay is small. The experiment revealed no dependence of the electron counting rate on the magnetizing current. The asymmetry parameter a in the angular distribution of decay electrons, $I(\theta) = 1 + a \cos\theta$, was found to be -0.01 ± 0.01.

$R = 1.00 \pm 0.01$ was found for the ratio of the number of electrons at the maximum and minimum of the expected precession curve, for which the best statistical results are obtained.

a and R were corrected for the delay time, gate width, μ^--meson decay and solid angle of the electron detector. The indicated errors are the standard deviations.

3. INTERPRETATION OF RESULTS

The values of a and R show that the angular distribution of electrons was isotropic within the limits of experimental error. These results made it possible to determine the degree of polarization P of muons in mesic hydrogen through use of the energy dependence of electron asymmetry in μ^+-e^+ decay. We shall assume that μ^+-meson beams from internal synchrocyclotron targets have approximately the same degree of polarization independently of the proton energy.[12] By assuming that our μ^--meson beam had the same degree of polarization as a μ^+-meson beam we can determine P from the inequality $3a_0 \leq P \leq 4a_0$ in reference 13, where a_0 is the asymmetry parameter for the integrated spectrum. From this inequality we obtain $P = 2.9 \pm 2.9\%$. The results for R indicate that any remaining polarization of muons in hydrogen does not exceed 2.5%.

It was pointed out at the beginning of this article that, because of the fine and hyperfine structures, meson depolarization is incomplete when mesic hydrogen atoms are produced. Our experiments[14] show that in mesic atoms of C, O, Mg and S the polarization amounts to 16 ± 4%. When μ^--mesons stop in matter with zero nuclear spin the principal depolarization mechanisms will be the spin-orbit interaction and the interaction between the magnetic fields of the atomic electron shell and of the μ^- meson during its lifetime in the K orbit. In matter with non-zero nuclear spin there will be an additional depolarization mechanism due to the hyperfine interaction. This last mechanism reduces the polarization of μ^- mesons in such substances. As mesic-hydrogen atoms are formed in hydrogen, meson depolarization results mainly from the fine and hyperfine structure interactions. The electron shells cause no depolarization. For this reason the expected polarization of μ^- mesons would be much higher than 6% immediately after the formation of mesic hydrogen. The polarization which we observed experimentally was below 2.5%. In addition to the mechanisms already mentioned, μ^--meson depolarization can accompany the scattering of mesic hydrogen atoms in atomic magnetic fields. However, this will be insignificant because of the small number of collisions required for the muon to drop to the lower hyperfine state.[14,15] It appears that the observed complete depolarization results mainly from the mechanism suggested by Zel'dovich and Gershtein, whereby a muon "jumps" from one proton to another and simultaneously drops to the lower state of the hyperfine structure. This result is of fundamental importance since it shows that complete meson depolarization prevents determination of the nature of muon-nucleon interaction through measurement of the neutron angular distribution from the $\mu^- + p \rightarrow n + \nu$ reaction in liquid hydrogen.

The question arises whether muon depolarization can be prevented in some way. It is quite evident that we cannot prevent the depolarization that results from the fine and hyperfine structure. It might appear that we could prevent depolarization by the "jump" mechanism through the use of gaseous hydrogen, where the number of collisions between mesic hydrogen atoms and ordinary hydrogen atoms would be smaller, with a resulting smaller number of "jumps." But this is not a likely method of preserving the polarization, since the probability of the indicated transitions is so large that jumps occur after the first few collisions.[7]

As has been pointed out to us by V. B. Beliaev and B. N. Zakhar'ev, muon depolarization resulting from the jump mechanism and the hyperfine structure can be prevented only if we can completely polarize the (hydrogen) medium in the direction of polarization of the muon beam.

We have been considering collisions between mesic hydrogen atoms and ordinary hydrogen atoms. Let us now consider collisions between hydrogen molecules and mesic hydrogen atoms. We know that ordinary hydrogen consists of 75% orthohydrogen molecules (with parallel nuclear spins) and 25% parahydrogen molecules (with antiparallel spins). Since spontaneous transitions between ortho- and paramolecules are impossible the ratio 3:1 is preserved in liquid hydrogen. Only in the presence of certain catalysts (such as activated charcoal) can orthomolecules be transformed into paramolecules. It is easily seen that the jump mechanism can lead to such a transformation in the presence of mesic hydrogen atoms. Therefore if hydrogen is bombarded with a sufficiently intense muon beam the 3:1 ratio will become nearly 1:1.

In conclusion, the authors thank Academician Ia. B. Zel'dovich and S. S. Gershtein for making their work available to us before publication, and for a discussion of our results. The authors also wish to thank V. B. Beliaev and B. N. Zakhar'ev for numerous discussions and for their continued interest.

---

[1] Shapiro, Dolinskii and Blokhintsev, Dokl. Akad. Nauk SSSR **116**, 946 (1957), Soviet Phys. "Doklady" **2**, 475 (1957).

[2] B. L. Ioffe, J. Exptl. Theoret. Phys. (U.S.S.R.) **33**, 308 (1957), Soviet Phys. JETP **6**, 240 (1958).

[3] Huang, Yang, and Lee, Phys. Rev. **108**, 1340 (1958).

[4] G. W. Ford and C. J. Mullin, Phys. Rev. **108**, 477 (1958).

[5] A. M. Bincer, Phys. Rev. **107**, 1434 (1957).

[6] Garwin, Lederman, and Weinrich, Phys. Rev. **105**, 1415 (1957).

[7] S. S. Gershtein, J. Exptl. Theoret. Phys. (U.S.S.R.) **34**, 463 (1958), Soviet Phys. JETP **7**, 318 (1958).

[8] Ia. B. Zel'dovich and A. D. Sakharov, J. Exptl. Theoret. Phys. (U.S.S.R.) **32**, 947 (1957), Soviet Phys. JETP **5**, 775 (1957).

[9] Ia. B. Zel'dovich, J. Exptl. Theoret. Phys. (U.S.S.R.) **33**, 310 (1957), Soviet Phys. JETP **6**, 242 (1958).

[10] J. D. Jackson, Phys. Rev. **106**, 330 (1957).

[11] Hayashi, Nakano, Nishida, Suekane, and Yamaguchi, Progr. Theoret. Phys. (Japan) **17**, 615 (1957).

[12] Mukhin, Ozerov, and Pontecorvo, J. Exptl. Theoret. Phys. (U.S.S.R.) **35**, 340 (1958).

[13] H. Uberall, Nuovo cimento **6**, 533 (1957).

[14] Ignatenko, Egorov, Khalupa, and Chultem, J. Exptl. Theoret. Phys. (U.S.S.R.) **35**, 1131 (1958), Soviet Phys. JETP **8** (in press).

[15] V. W. Hughes, Phys. Rev. **108**, 1106 (1958).

Translated by I. Emin
189

SOVIET PHYSICS JETP VOLUME 35(8), NUMBER 4 APRIL, 1959

AN INVESTIGATION OF THE INTERACTION BETWEEN 250–270 Mev π^+ MESONS AND CARBON NUCLEI WITH THE AID OF A PROPANE BUBBLE CHAMBER

WANG KAN-CHANG, WANG TSO-TSIANG, DING DA-TSAO, L. N. DUBROVSKII, E. N. KLADNITSKAIA, M. I. SOLOV' EV

Joint Institute for Nuclear Research

Submitted to JETP editor May 5, 1958

J. Exptl. Theoret. Phys. (U.S.S.R.) **35**, 899-906 (October, 1958)

The interaction between 250 to 270-Mev π^+ mesons and carbon nuclei was measured by means of a propane bubble chamber. The total and differential cross sections for elastic and inelastic scattering as well as the total cross section for absorption and charge exchange of the π^+ mesons were determined. The prong distributions were obtained both for stars containing mesons and for those without mesons. Within the experimental errors, elastic scattering can be described by diffractional scattering for a nucleus with $K = 0.54 \times 10^{13}$ cm^{-1}, $V = 30$ Mev, and $R = 3.2 \times 10^{-13}$ cm. The inelastic scattering data confirm the assumption that π mesons interact with separate nucleons in the nucleus and that the number of interactions in the carbon nucleus is not large. Analysis of stars not containing mesons permits one to assert that the absorption of a π^+ meson in the carbon nucleus and the subsequent decay of the π^+-C system cannot be explained on the basis of the evaporation model or the so-called cascade process.

1. INTRODUCTION

THERE have been many studies of π-meson interactions with nuclei, and in particular with carbon, for π meson energies below 200 Mev;[1-4] a few studies have dealt with energies greater than 200 Mev.[5-7] These studies were made with the aid of either Wilson chambers or scintillation counters.

In the present investigation a propane bubble chamber was used to study the interactions of π^+ mesons with carbon. The advantage of using a propane bubble chamber is that the carbon nuclei are in a working fluid (C_3H_8) and the point of the π^+-C interaction is plainly visible. The disadvantage is that the tracks left by low-energy particles are not visible. For example, elastic π^+-C scatterings (for $E_\pi = 270$ Mev) appear in a propane chamber as stars with a single prong.

2. EXPERIMENTAL ARRANGEMENT AND GEOMETRY

A propane bubble chamber with a diameter of 110 mm and a depth of 55 mm was used in the experiment. Its construction has already been described.[8]

The chamber was irradiated by π^+ mesons from the synchrocyclotron in the Laboratory for Nuclear Problems of the Joint Institute for Nuclear Research. Positive π mesons were generated in a polyethylene target. In our experiments we used targets 16, 20, and 30 cm thick placed in the path of a beam of 660-Mev protons extracted from the synchrocyclotron chamber. An analyzing magnet was used to isolate a monochromatic beam of π^+ mesons from the $p + p \rightarrow \pi^+ + d$ reaction. The mesons were emitted at an angle of 9° to the direction of the proton beam. After magnetic analysis, the meson beam was sent through a collimator in a concrete shield 4 meters thick into the room containing the bubble chamber. The beam entered the chamber through a thin wall 40 mm in diameter, having first passed through a lead collimator 20 cm long and a copper filter (18 g/cm^2), both placed directly before the chamber. The filter was used to rid the π^+-meson beam of protons with the same momentum as the mesons. The experimental set up is shown in Fig. 1. A total of 3500 photographs were obtained for π^+ mesons with an energy of 270 ± 10 Mev, and 400 photographs were obtained for an energy of 250 ± 10 Mev. A UIM-21 microscope[9] was used to process the photographs.

A special electronic radio circuit, fed with 80 to 100 cps pulses from the photo-transducer of a frequency variator, was used to synchronize the operation of the bubble chamber with that of the synchrocyclotron. Every 12 seconds the circuit was opened to admit 3 or 4 pulses from the photo-

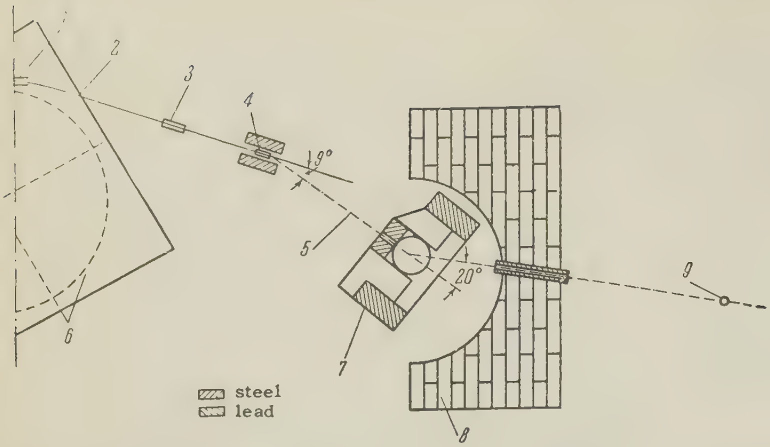

FIG. 1. The experimental setup. 1) magnetic channel, 2) proton beam with E = 660 Mev, 3) quadrupole lens, 4) polyethylene target, 5) π^+ meson beam, 6) synchrocyclotron chamber, 7) magnet, 8) cast-iron bricks, 9) propane bubble chamber.

transducer and accordingly to yield 3 or 4 pulses for switching on the high frequency to the control circuit. The initial triggering pulse could be regulated by a delay in such a way that the chamber would register the third or fourth pulse of the accelerated particles.

3. EXPERIMENTAL RESULTS

I. Elastic π^+-C Scattering

The reaction

$$\pi^+ + \mathrm{C} \rightarrow \pi^+ + \mathrm{C} \qquad (1)$$

must be distinguished from other reactions such as

$$\pi^+ + p \rightarrow \pi^+ + p \quad (\theta < 15°), \qquad (2)$$

$$\pi^+ + (n) \rightarrow \pi^+ + n, \qquad (3)$$

$$\pi^+ + (p) \rightarrow \pi^+ + p \quad (\theta < 15°), \qquad (4)$$

where (n) and (p) indicate that the reaction occurs because of a bound neutron or a bound proton respectively.

Our statistics did not include interactions by π^+ mesons with deviations larger than 10° from the beam trajectory or interactions with a scattering angle $\theta < 10°$ (θ being the scattering angle of the π^+ meson in the laboratory coordinate system) For angles up to 10° large contributions are made by Coulomb scattering, π-μ-e decay, and elastic π^+-p scattering, all of which are indistinguishable from reaction (1) in the propane chamber. Since the probability for elastic scattering of π^+ mesons by carbon for angles > 70° is very small, it was assumed that scattering into angles > 70° belonged to reaction (3).

Occurrences of elastic π^+-p scattering in the interval $10° < \theta < 15°$ were excluded from the statistics in accordance with the data of Pontecorvo et al.[10] Furthermore, occurrences belonging to reactions (3) and (4) for $10° < \theta < 70°$ (when $\theta >$ 15° reaction (4) appears as a two-pronged star) were excluded in accordance with the inelastic scattering distributions for carbon as obtained by Dzhelepov et al.[5]

The elastic scattering cross section for $10° \leq \theta \leq 70°$ was measured to be $\sigma_{\mathrm{elas}} = (170 \pm 16)$ millibarns.

Besides the total elastic cross section, the differential cross section (Fig. 2) was obtained. According to Watson et al.,[11] the real part of the nuclear potential well for carbon is 30 Mev deep for $E_\pi = 270$ Mev. On the basis of the "optical model"[12] for positive pion-carbon scattering we

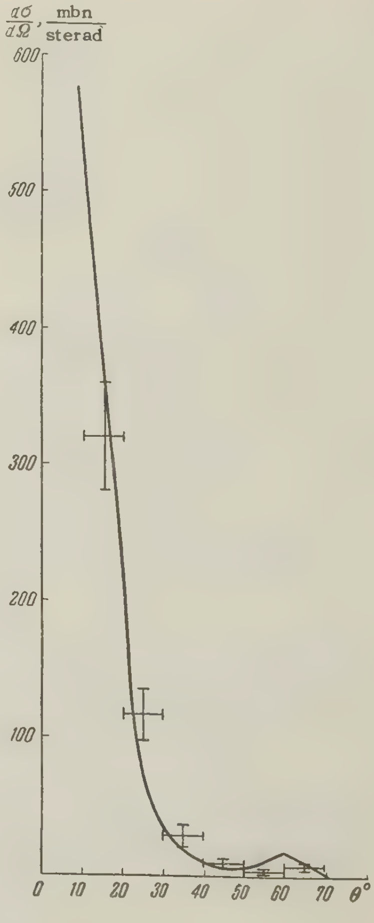

FIG. 2. Angular distribution of elastic scattering of 270-Mev π^+ mesons by carbon.

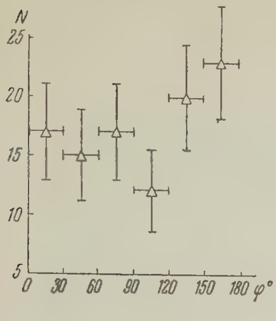

FIG. 3. The azimuthal distribution of elastic scattering of 270-Mev π^+ mesons by carbon.

computed the angular distribution for a hypothetical uniform distribution of nuclear material inside a sphere of radius $R = 1.4 A^{1/3} \times 10^{-13}$ cm $= 3.2 \times 10^{-13}$ cm, $K = 0.54 \times 10^{13}$ cm^{-1} and $V = 30$ Mev (solid curve in Fig. 2). Here K is the absorption coefficient for π^+ mesons in the nuclear material. This coefficient was determined (cf. Dzhelepov et al.[5]) from the equation

$$K = [(\sigma_{\pi^+-p} + \sigma_{\pi^+-n}) A/2]/(^4/_3\pi R^3),$$

where σ_{π^+-p} and σ_{π^+-n} are the total interaction cross sections for π^+ mesons with free protons and neutrons respectively for $E_\pi = 270$ Mev, as given by Barkov and Nikol'skii;[13] R is the radius of the carbon nucleus. The angular distribution for the elastically scattered π^+ mesons is seen to be in satisfactory agreement with the diffraction-scattering curve. The diffraction scattering cross section for $10° < \theta < 70°$, obtained by integrating over the theoretical curve, is 193 millibarns.

The azimuthal distribution for elastic scattering through an angle φ was also plotted for 104 cases with $15° < \theta < 70°$. It was found that 54 π^+ mesons were scattered into the upper hemisphere and 50 into the lower. 49 and 55 π^+ mesons were scattered respectively into the right and left hemispheres. Thus, within the limits of statistical error, the distribution in φ was symmetrical. To increase the statistics, the φ distribution was reflected about the 180° axis and folded together (Fig. 3) (i.e., points 0° and 360° coincided). It can be seen that the distribution is anisotropic. Such a distribution can be explained by the lower viewing efficiency for cases with an angle of φ near 90°, as well as by the lack of sufficient statistics.

If we add ~12 cases of elastic π^+-C scattering to the $45° < \varphi < 135°$ interval, so that the distribution becomes isotropic, the elastic scattering cross section will be (192.2 ± 18.5) millibarns, which is in very good agreement with the diffractional scattering cross section for $V = 30$ Mev with $K = 0.54 \times 10^{13}$ cm^{-1}

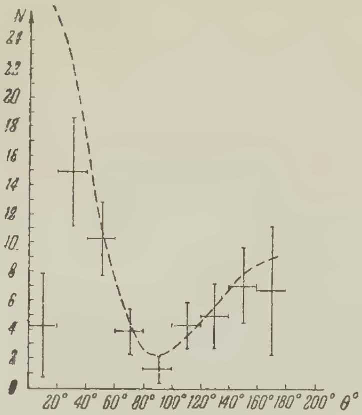

FIG. 4. The angular distribution for inelastic scattering of π mesons by carbon in the laboratory system.

II. Inelastic π^+-C scattering

The inelastic scattering of π^+ mesons by carbon occurs as follows

$$\pi^+ + \mathrm{C} \rightarrow \pi^+ + (N \text{ prongs}) \; (N = 0,\ 1,\ 2, \ldots.\ 6) \quad (5)$$

It is difficult to distinguish reaction (5) from interactions that accompany π^+ meson absorption or charge exchange if the energy of the secondary π^+ meson in reaction (5) is less than 60 Mev ($g/g_0 \geq 2$ or 2.5 for π^+ mesons with $E < 60$ Mev and for protons with $E \leq 250$ Mev[14]). Such ambiguous cases increased the experimental error of the measured cross section. Examples of elastic π^+-p scattering ($\theta > 15°$) are usually easily distinguished from examples of inelastic π^+-C scattering on account of the kinematics and coplanarity of the interaction. There were, however, four cases difficult to attribute to elastic or quasi-elastic π^+ meson-proton scattering because of a considerable error in the measurement of the angle φ.

To obtain the inelastic π^+-C cross section for $\theta > 70°$ we included in our statistics of stars containing a meson those stars as described by reaction (3) that had been singled out during our investigation of one-pronged stars. It is necessary to include cases of bound nucleon scattering in the interval $0° \leq \theta \leq 15°$ and bound neutron scattering in the interval $15° \leq \theta \leq 70°$. These were obtained by comparing the angular distribution for the inelastically scattered π mesons, produced in the course of our work, with the distribution reported by Dzhelepov et al.[5] The inelastic scattering cross section is

$$\sigma_{\text{inel}} = (120^{+38}_{-19}) \text{ millibarns.}$$

The angular distribution in the laboratory coordinate system for π^+ mesons inelastically scattered by carbon shown in Fig. 4, resembles the angular distribution for 270-Mev π^+ mesons scat-

TABLE I. Distribution of stars by prongs

Number of stars	Number of prongs						
	1*	2*	3	4	5	6	7
With a meson	46^{+9}	27_{-3}	5	1			
Without a meson	17	45^{+8}	35	14	2	1	1

*Error due to distribution.

tered by hydrogen as measured by us and shown dotted in the same figure. This experimentally-determined fact indicates that scattering in the nucleus involves separate nucleons and that the number of scatterings in the carbon nucleus is small. This view has been advanced before by several authors.[3,5,15-17] The discrepancy for $0° < \theta < 20°$ can be explained by assuming that when the scattering is through a small angle (in the case of a single collision), the π^+ meson loses but a small portion of its energy, while the low-energy recoil proton ($E_p < 10$ Mev) is invisible in propane. On the other hand, a careful scanning of some of the photographs failed to uncover any circumstance that would explain the reaction

$$\pi^+ + (n) \rightarrow \pi^0 + p \quad \text{for } \theta > 75°.$$

Consequently, one is led to think that more is involved than the invisibility of low-energy protons in propane; Pauli's principle must also play a role.

Table I illustrates the dependence of the number of stars on the prong count per star with no account being taken of the scattered π^+ meson. From these data it follows that for the majority of inelastic scatterings of π^+ mesons a single recoil particle is visible — probably a proton. Many of these examples are quasi-elastic collisions. This fact, serves as an additional confirmation of the view that in most cases of inelastic scattering the π^+-meson collides with an individual nucleon in the carbon nucleus and only once.

III. π^+-Meson Absorption in Carbon and Charge Exchange

Propane is a poor photon detector. In our chamber the probability of pair production by photons was less than 3%. Actually, not a single pair was observed. Therefore, it was not possible to obtain separate cross sections for absorption and charge exchange. The observed cross section for stars without mesons was $\sigma = \sigma_a + \sigma_c = (165^{+34}_{-22})$ millibarns, where σ_a is the absorption cross section and σ_c the charge-exchange cross section. The uncertainty includes the statistical and distribution correction error. The prong distribution for stars containing a meson and those lacking one is included in Table I.

For stars lacking a meson the angular distributions of secondary particles with a range of 16 mm or less and those with more than 16 mm were determined for a projection onto the photograph plane (16 mm is the range of a 30-Mev proton, 30 Mev being the upper limit of the evaporation spectrum[18] of evaporated particles for nuclei with $A = 100$). An anisotropic prong distribution was found. As expected, the angular distribution for long (> 16 mm) prongs tended more in the forward direction. The fact that the distribution for short (< 16 mm) prongs is anisotropic and that the number of the nucleons in the carbon nucleus is small suggests that evaporation is not the mechanism of particle emission when a 270 Mev π^+ meson is absorbed by carbon. Moreover, as Table I indicates, among all the stars lacking a meson, we observed one seven-pronged star, one six-pronged star, and two five-pronged stars. The prongs of each of these stars emerge from the nucleus more or less symmetrically. For example, in the case of the six-pronged star three of the prongs extend out for more than 5 cm, and form included angles of 110°, 123°, and 118°, whereas the other three prongs extend for several millimeters. The angle between the direction of one of the high-energy prongs and the plane containing the two other similar prongs is ~ 20°. The average number of visible ($E_p > 10$ Mev) prongs per star for all of the stars lacking a meson is 2.6. In view of the small charge of the carbon nucleus, it is possible to rule out as a mechanism the so-called cascade process, in which the number of prongs is normally much lower than the number of nuclear protons.

We propse that when π^+ mesons are absorbed by light nuclei, such as carbon, all of the energy (in our case 410 Mev) is distributed among all of the nucleons, and an "explosion" of the nucleus immediately ensues. The probability of a given number of charged particles is found in the following manner. Let us assume that upon absorption of a π^+ meson by a carbon nucleus the system formed consists of 7 protons and 5 neutrons with an excitation energy of 410 Mev. This system disintegrates very rapidly, explosively, into several free nucleons and one nuclear fragment.

All of the allowed transitions were considered. For example, a transition in which 7 protons are emitted leaving a nuclear fragment of 5 neutrons is prohibited, a transition in which two protons or two protons and one neutron are emitted with

TABLE II

Number of stars	No. of prongs for stars without a meson						
	1	2	3	4	5	6	7
Experimental data	17	45^{+8}	35	14	2	1	1
Computed data	25.2	44.5	24.7	14.3	6.1	1.6	0.4

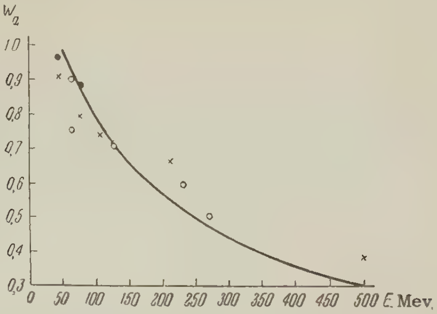

FIG. 5. The energy dependence of σ_a/σ_{total} for π mesons. ○ – interaction of π^+ mesons with carbon; ● – π^- meson absorption in the photographic emulsion; × – π^+ meson absorption in emulsions.

a fragment in the form of ${}_5B^{10}$ or ${}_5B^9$ is allowed, etc.

If the average energy carried off by the fragment nucleus and the binding energy of the nucleons in the nucleus are considered, one can compute the average momentum of a nucleon escaping from the system. We further propose that the probability of any allowed transition is proportional to the third power of this average momentum. By combining the probability of the allowed transitions with the corresponding number of protons we obtain the relative weights of these transitions and, for our statistics, the expected prong distribution shown in Table II.

A comparison of the experimental and computed data indicates that the absorption of π^+ mesons by carbon and the subsequent decay occurs via the proposed mechanism.

In Fig. 5, the black dots represent the energy dependence of the σ_a/σ_{total} ratio for the carbon nucleus. The data for $E_\pi = 62$ Mev were taken from Byfield et al.[1] for $E_\pi = 125$ Mev from Kessler and Lederman,[3] and for $E_\pi = 230$ Mev from Dzhelepov et al.[5] The decrease in σ_a/σ_{total} with an increase in energy is evidence of a decrease in the contribution of π^+-meson absorption to the nuclear interaction between mesons and carbon. The probability of $\pi^\pm$-meson absorption by two nucleons in a nucleus was computed on the assumption that a π meson with momentum $|\kappa|$ is absorbed only if the relative momentum of the two nucleons equals or exceeds $|\kappa|$ or, in other words, that the distance between the two nucleons is equal to or less than $1/|\kappa|$. For this purpose a two nucleon function $\psi_{1,2} = \sqrt{\alpha/2\pi}\, e^{-\alpha r}/r$ was assumed, in which case the momentum distribution is given by

$$N(\mathbf{k}) = \left| \int_0^\infty \psi_{1,2} e^{i\mathbf{k}\mathbf{r}}\, d\mathbf{r} \right|^2$$

The quantity α was determined from the expression $\alpha^2 h^2/M = 18$ Mev.[19] The meson absorption probability for the two nucleons is

$$W_a(\kappa) \sim 4\pi \int_\kappa^\infty N(\mathbf{k})\, k^2 dk,$$

where k is the wave number of the nucleons, and κ the wave number of the π mesons. The energy dependence of this probability is shown by the solid curve in Fig. 5. The curve is normalized to the experimental data at $E_\pi = 125$ Mev.[3] At $E_\pi = 230$ Mev[5] and 270 Mev (the present investigation) the cross section $\sigma = \sigma_a + \sigma_c$ is known. One can then deduct the charge exchange cross section as determined from data on the charge exchange between a free proton and π^- mesons. Of course, this is approximate. As can be seen from Fig. 5, the theoretical curve reproduces the energy dependence of σ_a/σ_{total} moderately well. Experimental data on the absorption of π^+ and π^- mesons in the nuclei of the photographic emulsion[20–23] were also included in Fig. 5. Consequently, one may conclude that the contribution of σ_a to σ_{total} decreases with an increase in energy for all the nuclei.

From Fig. 5 it can be seen that the discrepancy between the experimental and theoretical data increases as the energy of the incident π mesons increases. This can be explained by the fact that the greater the energy of the π mesons, the greater the absorption contribution from π mesons after a preliminary scattering in the nuclear matter.

4. TOTAL CROSS SECTION FOR THE INELASTIC INTERACTION OF MESONS WITH CARBON

The measured total inelastic cross section of 270-Mev π^+ mesons on carbon is

$$\sigma_{inel} = 296^{+35}_{-28} \text{ millibarns.}$$

A reduction in the distribution correction error has reduced the error here. Within the experimental error the measured cross section is in agreement with the value $\sigma_{in} = 272$ millibarns which, according to the optical model, is given by

$$\sigma_{inel} = \pi R^2 \{1 - [1 - (1 + 2KR) e^{-2KR}] / 2K^2R^2\},$$

where R is the radius of the carbon nucleus and is equal to 3.2×10^{-13} cm, and K is the absorption coefficient, equal to 0.54×10^{13} cm^{-1}. The measured cross section is also in agreement with the value of 300 millibarns as obtained from the "inelastic interaction cross section vs. energy" curve for carbon, based on the data given by Ignatenko et al.[7]

CONCLUSION

The results obtained in the present investigation of the interaction of π^+ mesons with carbon can be summarized as follows.

1. The total and differential cross sections obtained for the elastic scattering of π^+ mesons by carbon for energies from 250 to 270 Mev are in good agreement with the computations based on the optical model with an absorption coefficient $K = 0.54 \times 10^{13}$ cm^{-1} and with $V = 30$ Mev and $R = 3.2 \times 10^{-13}$ cm for the real part of the complex potential.

2. For the angular distribution in φ no asymmetry was observed to the right, while to the left it was the same as reported by Kozodaev et al.[24]

3. Within the limits of experimental error, the cross section for the inelastic interaction is in agreement with that computed from the optical model with $K = 0.54 \times 10^{-13}$ cm^{-1} and $R = 1.4 A^{1/3} \times 10^{-13}$ cm $= 3.2 \times 10^{-13}$ cm.

4. The angular distribution obtained for inelastic scattering of π^+ mesons by carbon confirms the assumption reported by other authors that the interaction of π^+ mesons with complex nuclei occurs through the interaction with separate nucleons in the nucleus and that the number of the interactions in the carbon nucleus is not large.

5. The prong distribution was obtained for stars lacking a meson. An attempt was made to explain this distribution.

6. The ratio σ_a/σ_{total} was plotted as a function of π meson energy. The decrease in the ratio with an increase in meson energy is in agreement with the decrease in the probability of π meson absorption by two nucleons in the nucleus as the energy of the meson increases.

The authors express their gratitude to Prof. V. P. Dzhelepov for making it possible for them to use the accelerator belonging to the Laboratory for Nuclear Problems, to R. M. Suliaev, Iu. A. Shcherbakov, A. I. Filippov, and L. B. Parfenov for their help in conducting the experiment, and to the group of laboratory technicians under the direction of I. A. Ivanovskaia for their help in evaluating the results.

[1] Byfield, Kessler, and Lederman, Phys. Rev. **86**, 17 (1952).

[2] Lederman, Byfield, Kessler and Rogers, Phys. Rev. **90**, 344 (A) (1953).

[3] J. Kessler and L. Lederman, Phys. Rev. **94**, 689 (1954).

[4] A. Shapiro, Phys. Rev. **84**, 1063 (1951).

[5] Dzhelepov, Ivanov, Kozodaev, Osipenkov, and Rusakov, J. Exptl. Theoret. Phys. (U.S.S.R.) **31**, 923 (1956), Soviet Phys. JETP **4**, 864 (1957).

[6] Ignatenko, Mukhin, Ozerov, and Pontecorvo, Dokl. Akad. Nauk SSSR, **103**, 395 (1955).

[7] Ignatenko, Mukhin, Ozerov, and Pontecorvo, J. Exptl. Theoret. Phys. (U.S.S.R.) **31**, 545 (1956), Soviet Phys. JETP **4**, 351 (1957).

[8] Solov'ev, Kladnitskaia, and Smirnov, High-Energy Lab. Report (1956).

[9] Kan-chang, Tso-tsiang, Da-tsao, Kladnitskaia, and Solov'ev, High-Energy Lab. Report, Joint Institute for Nuclear Research (November, 1957).

[10] Mukhin, Ozerov, and Pontecorvo, J. Exptl. Theoret. Phys. (U.S.S.R.) **31**, 371 (1956), Soviet Phys. JETP **4**, 237 (1957).

[11] Frank, Gammel, and Watson, Phys. Rev. **101**, 891 (1956).

[12] Fernback, Serber, and Taylor, Phys. Rev. **75**, 1352 (1949).

[13] L. M. Barkov and B. A. Nilol'skii, Usp. Fiz. Nauk. **61**, 341 (1957).

[14] Blinov, Krestnikov, and Lomanov, J. Exptl. Theoret. Phys. (U.S.S.R.) **31**, 762 (1956), Soviet Phys. JETP **4**, 661 (1957).

[15] M. Blau and M. Caulton, Phys. Rev. **96**, 150 (1954).

[16] Kozodaev, Suliaev, Filippov, and Shcherbakov, J. Exptl. Theoret. Phys. (U.S.S.R.) **31**, 701 (1956), Soviet Phys. JETP **4**, 580 (1957).

[17] N. A. Mitin and E. L. Grigor'ev, Dokl. Akad. Nauk. SSSR **103**, 219 (1955).

[18] E. Segre, Experimental Nuclear Physics, vol. II, (Wiley, 1953).

[19] Bruckner, Eden, and Francis, Phys. Rev. **98**, 1445 (1955).

[20] H. Bradner and B. Rankin, Phys. Rev. **87**, 547, 553 (1952).

[21] Bernardini, Booth and Lederman, Phys. Rev. **83**, 1075 (1951).

[22] A. H. Morrish, Phys. Rev. **90**, 674 (1953).

[23] G. Bernardini and F. Levy, Phys. Rev. **84**, 610 (1951).

[24] Kozodaev, Suliaev, Shcherbakov, and Filippov, J. Exptl. Theoret. Phys. (U.S.S.R.) **33**, 1047 (1957), Soviet Phys. JETP **6**, 806 (1958).

Translated by A. Skumanich
190

SOVIET PHYSICS JETP VOLUME 35(8), NUMBER 4 APRIL, 1959

X-RAY DIFFRACTION STUDY OF THE THERMAL EXPANSION OF ANTIFERROMAGNETIC MnTe

N. P. GRAZHDANKINA and D. I. GURFEL'

Institute of Metal Physics, Academy of Sciences, U.S.S.R.

Submitted to JETP editor May 10, 1958

J. Exptl. Theoret. Phys. (U.S.S.R.) **35**, 907-910 (October, 1958)

The variation of the critical lattice parameters of manganese telluride in the vicinity of the antiferromagnetic transition point was investigated by x-ray diffraction. A hypothesis concerning the magnetic structure of MnTe is advanced on the basis of the data obtained. The Néel point $T_N = 310°K$ was determined from the anomalous variation of the thermal expansion coefficient, and the dependence of T_N on hydrostatic pressure was determined.

An x-ray diffraction investigation of the thermal expansion coefficient of the antiferromagnetic compound MnTe is of interest for two reasons. A detailed study of the anomalous expansion or compression of the crystal along its principal crystallographic axes in the temperature region of the antiferromagnetic transition (T_N) leads to a hypothesis regarding the magnetic structure of this antiferromagnetic substance. X-ray diffraction studies of the antiferromagnetic oxides MnO, FeO, and NiO[1-3] have shown that the transition from the paramagnetic to the antiparamagnetic state of these compounds is accompanied by reduced symmetry of their lattices, which are of the cubic NaCl type. The definite magnetic structure of these compounds that was inferred from this result was confirmed by neutron-diffraction experiments.[4] Very few such investigations have thus far been made of substances with hexagonal lattices. A study of the antiferromagnetic compounds CrSb[5,6] and MnTe,[7] which possess a hexagonal lattice of the NiAs type, has shown that the change in the crystal lattice near the Néel temperature of these compounds consists only in a change of their axial dimensions without a transition to another symmetry class. It should be noted that the data for MnTe need verification, since the Néel temperature which was determined by Greenwald[7] from the anomalous variation of the thermal expansion coefficient ($T_N = +50°C$) differs markedly from the value of 35°C given by the same author in another article.[5]

Investigation of the anomalous thermal expansion around the Néel temperature makes it possible through the use of thermodynamical calculations to determine the variation of the antiferromagnetic transition temperature of manganese telluride under changing hydrostatic pressure. This is of interest for its own sake and for verification of the Néel-temperature shift under hydrostatic pressure which was measured by Grazhdankina.[8]

PREPARATION OF SAMPLE AND METHOD OF MEASUREMENT

Manganese telluride samples were prepared by fusing carefully mixed fine powders of manganese and tellurium in sealed evacuated quartz ampoules at $t = 800°C$. The raw material was electrolytic manganese of the following composition: 99.8% Mn, 0.07% S, 0.07% C, and 0.03% P. The manganese was remelted under a high vacuum for degassing. Chemical analysis of the tellurium showed the following: Te > 99.999%, 0.0001% Cu, 0.0002% Ag, Bi < 0.0001%, 0.0001% Sb, and As. Samples in the form of discs of 9 mm diameter and 1 mm thickness were prepared by pressing finely powdered manganese telluride in a special mold. This was followed by annealing at a low temperature. X-ray phase analysis showed the presence of traces of $MnTe_2$ in addition to the principal MnTe phase.

The thermal expansion coefficient of manganese telluride was determined by the x-ray diffraction method that was developed by Kosolapov and Trapeznikov,[9] which differs from the ordinary back-reflection method mainly by the possibility it affords of obtaining aluminum lines as a standard and lines of the test material on the same film. Errors due to film shrinkage during development can thus be avoided and the accuracy of the measurements is considerably enhanced. Using the aluminum lattice constant a (20°C) = 4.040 A and the linear thermal expansion coefficient $\alpha_{Al} = 25.5 \times 10^{-6}\ deg^{-1}$, we calculated the effective

Lattice constants and volume (V) of MnTe unit cell

T, °K	a, A	c, A	c/a	V, A^3	T, °K	a, A	c, A	c/a	V, A^3
253	4.083	6.696	1.639	96.66	320	4.091	6.716	1.642	97.34
286	4.086	6.700	1.639	96.90	334	4.093	6.719	1.642	97.46
293	4.087	6.701	1.639	96.93	347	4.093	6.723	1.642	97.52
306	4.088	6.708	1.640	97.08	358	4.094	6.724	1.642	97.59
313	4.089	6.716	1.642	97.24					

distance A between the sample and the film, which differed for different lines of the x-ray diffraction pattern. From a knowledge of A for the two extreme lines we could determine A for any intermediate line of MnTe (taking into account the thickness of the aluminum standard foil which was cemented to the surface of the sample). The constants of the MnTe lattice were calculated from the lines (135) α_1, (306) α_1 and (135) α_2, (306) α_2. The error in the constants a and c, defined as the mean deviation of individual values of a and c from the average of five values, amounted to 0.026%.

The photographs were taken with a KROS-1 camera using the x-ray lines $K\alpha_1 = 1.537\,\text{A}$ and $K\alpha_2 = 1.541\,\text{A}$ from a tube with a copper anticathode. The sample and cemented-on aluminum foil were clamped to a heater by means of a special band consisting of a hollow brass cylinder through which water flowed from a Hoeppler thermostatic bath thus maintaining the temperature of the sample constant to within 0.1°. For the production of low temperatures the thermostatic-bath liquid was ethylene glycol with dry ice as the refrigerant. Temperatures were measured by a potentiometer with the aid of a copper-constantan thermcouple clamped tightly to the sample.

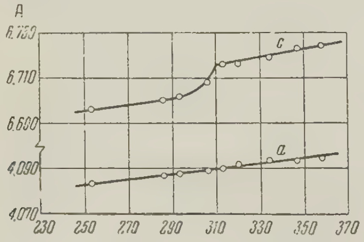

FIG. 1

RESULTS AND DISCUSSION

Thermal expansion of the manganese telluride lattice was investigated in the temperature range from 250 to 370°K. At room temperature (+20°C) the constants a and c had the following values: $a = 4.087 \pm 0.001\,\text{A}$ and $c = 6.701 \pm 0.002\,\text{A}$. These differ somewhat from the values given by Oftedal[10] (a = 4.132, c = 6.711), Greenwald[3] (a = 4.142, c = 6.703) and Furberg[11] (a = 4.146, c = 6.709). The parameters of the MnTe lattice at different temperatures are shown in the table and in Fig. 1.

The given temperature range includes the antiferromagnetic transition temperature $T_N = 310$°K, at which point our measurements show a kink in the temperature dependence curves of electrical resistance and magnetic susceptibility. Figure 1 shows a kink located at the same point on the temperature dependence curve of the thermal expansion of c, although there is no change of the linearity of the temperature dependence of a in the same range. The ratio c/a increases from 1.639 at room temperature to 1.642 at 350°K. This represents an increase of unit cell volume by 0.27% during the transition from the antiferromagnetic to the paramagnetic state. A calculation of the linear thermal expansion coefficients along the a and c axes of the crystal gave the following results: $\alpha_a = 2.79 \times 10^{-5}\ \text{deg}^{-1}$, $\alpha_c\ (T > T_N) = 2.68 \times 10^{-5}\ \text{deg}^{-1}$ and $\alpha_c\ (T < T_N) = 1.90 \times 10^{-5}\ \text{deg}^{-1}$. At the Néel temperature the jump of the linear expansion coefficient along the c axis is $\Delta\alpha_c = 12 \times 10^{-5}\ \text{deg}^{-1}$ (Fig. 2). The volume thermal expansion coefficient of manganese telluride at T = 300°K is $7.48 \times 10^{-5}\ \text{deg}^{-1}$, which is close to the value of α_V for aluminum.

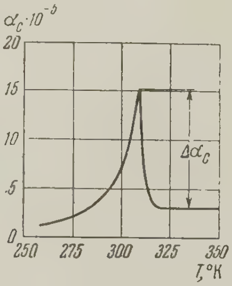

FIG. 2

As we compare our data with those of Greenwald[3] we must first note their qualitative agreement. In both instances we find that when manganese telluride is heated above T_N the anomalous expansion of the crystal occurs only along the c axis. The type of crystal structure was not observed to change within the investigated temperature range. However the temperature $T_N = 329$°K given by Greenwald and the anomalous change of the thermal expansion coefficient at the Néel temperature, $\Delta\alpha_c = 6 \times 10^{-5}$, are distinctly different from our results. We attribute this discrepancy to the fact that in the vicinity of T_N Greenwald measured the lattice parameters at large temperature intervals (20 to 30°), as a result of which it became very difficult to determine the exact position of T_N from a kink in the curve of $c(T)$. The absolute values of c at different temperatures are in good agreement with our results.

The structure of the magnetic sublattices of the antiferromagnetic compound MnTe is unknown because no neutron-diffraction studies have been made up to the present time. However, by using the relation which Smart and Greenwald[3] established between the magnetic structure of antiferromagnetics and variations of the lattice parameter around T_N, as well as experimental results of the neutron-diffraction and x-ray diffraction studies of CrSb,[5,6] which has the same crystal structure as MnTe, we can draw some inferences regarding the magnetic structure of manganese telluride. The sharp change of crystal dimension along the c axis, while the constant a varies linearly, around T_N supplies evidence that the magnetic moments of the Mn atoms are parallel to the c axis, that is, perpendicular to the (001) plane, with all moments in any single (001) plane lined up parallel but with opposite orientations in neighboring (001) planes. Thus the nearest neighbors of Mn atoms have antiparallel magnetic moments, whereas next nearest neighbors have parallel moments.* In such a structure of the magnetic lattice the manganese atoms must interact mainly directly without participation of the tellurium atoms. The established anisotropic change of the lattice indicates that in the present case, unlike that of ferromagnets, magnetic forces rather than exchange forces are important at the magnetic transition temperature. From the foregoing we infer the invalidity for manganese telluride of Li's[13] ideas regarding the dominant role of a superexchange interaction in anisotropic changes of antiferromagnetic lattices upon passing through the Néel temperature.

In conclusion we shall calculate the shift of the Néel point of manganese telluride under hydrostatic pressure. Our value for the jump of the thermal expansion coefficient, $\Delta\alpha = 12 \times 10^{-5}$ deg^{-1}: and Kelley's value[12] for the anomalous change of the specific heat, $\Delta C_p = 5$ cal/deg-mol, at $T_N = 310°K$ are inserted into Ehrenfest's equation for a second order phase transition, $dT_n/dp = VT_N \times \Delta\alpha/\Delta C_p$. In calculating the molar volume V the density of manganese telluride was taken from x-ray data to be 12.48 g/cm^3. Our result is $dT_N/dp = 2.6 \times 10^{-3}$ deg/kg/cm^2, which agrees within the limits of experimental error with the value for dT_N/dp obtained through an investigation of the variation of electrical properties in the same compound under hydrostatic pressure.[8]

In conclusion we wish to thank A. K. Varskaia for assistance and suggestions.

---

*In a lattice of the NiAs type the nearest neighbors of a given magnetic atom are located along the c axis at the distance $c/2$.

---

[1] H. P. Rooksby, Acta Cryst. **1**, 226 (1958).

[2] N. C. Tombs and H. P. Rooksby, Nature **165**, 442 (1950).

[3] J. S. Smart and S. Greenwald, Phys. Rev. **82**, 113 (1951).

[4] C. G. Shull and J. S. Smart, Phys. Rev. **76**, 1256 (1949).

[5] B. T. M. Willis, Acta Cryst. **6**, 425 (1953).

[6] A. I. Snow, Revs. Modern Phys. **25**, 127 (1953).

[7] S. Greenwald, Acta Cryst. **6**, 396 (1953).

[8] N. P. Grazhdankina, J. Exptl. Theoret. Phys. (U.S.S.R.) **33**, 1524 (1957), Soviet Phys. JETP **6**, 1178 (1958).

[9] G. F. Kosolapov and A. K. Trapeznikov, J. Exptl. Theoret. Phys. (U.S.S.R.) **5**, 729 (1935).

[10] I. Oftedal, Z. physik. Chem. **128**, 135 (1927).

[11] S. Furberg, Acta Chem. Scand. **7**, 693 (1953).

[12] K. K. Kelley, J. Am. Chem. Soc. **61**, 203 (1939).

[13] Yin-Yuan Li, Phys. Rev. **100**, 627 (1955).

Translated by I. Emin
191

SOVIET PHYSICS JETP VOLUME 35(8), NUMBER 4 APRIL, 1959

ELECTRIC EXPLOSION OF SPIRAL WIRES IN VACUUM

I. F. KVARTSKHAVA, V. V. BONDARENKO, P. D. MELADZE, and K. V. SULADZE

Submitted to JETP editor May 10, 1958

J. Exptl. Theoret. Phys. (U.S.S.R.) **35**, 911-916 (October, 1958)

When a bent wire is exploded in vacuo, the motion of the explosion products through the magnetic field of the current produces current tubes and also certain glow effects, due to the interaction of the streams of explosion products with each other. By scanning the explosion with a mirror, the stream fronts were found to have a speed of 10^6 cm/sec. A possibility of thermally insulating the plasma by means of the strong magnetic field that exists during a very short time of explosion is demonstrated. A qualitative explanation is proposed for the observed effect.

1. INTRODUCTION

THE authors[1] have previously reported on an experimental investigation of electric explosion of wires in vacuo. An examination of these data has led to the conclusion that in the case of straight wires the radial motion of the explosion products through the magnetic fields produces thin layered cylindrical channels, coaxial with the wire, through which most of the discharge current flows. To investigate this effect further, we experimented with electric explosions of wires curved in different manners (mostly in helical form).

In the investigations we used integral photography of the explosion, continuous photography of mirror scans and oscillography of the current and voltage, the setup being approximately as described in reference 2.

A capacitor bank with total capacity of 4.8 μf at 50 kv working voltage was used to explode the wires.

2. RESULTS OF THE EXPERIMENTS

Figures 1 and 2 show photographs of the explosion curves of copper wires in vacuo. Photograph 1 of Fig. 1 shows the characteristic explosion picture of helically-wound wires at relatively high explosion-circuit capacitor voltages. The photograph was taken at right angle to the axis of the helix. As in the case of all integral photographs of explosions, this picture shows the glowing wire at the initial stage of the discharge, during which it acquires the energy needed for the explosion. The glow of the wires is due to the presence of a thin brightly-glowing discharge layer, becoming coiled under the influence of the strong magnetic field of the current.[1] An examination of the current and voltage oscillograms shows that the explosion of the wire occurs at the end of this stage and the discharge is immediately followed by a second discharge in the vapor of the wire. The remaining portion of the picture, which obviously occurs after the start of the explosion of the wire, must be attributed to mutual collisions between the streams of explosion products and to their motion through the magnetic field of the current.

The mechanism of interaction between the moving explosion products and the magnetic field, with which we begin our examination of the results presented here, is described in detail in reference 1. It is based on the following two premises:

1. Regardless of the initial shape of the wire, the explosion products propagate in its immediate vicinity perpendicularly to the wire surface.

2. When the explosion products travel through the magnetic field **H** with a velocity **v**, an additional electric field $\mathbf{E} = (1/c)\mathbf{v} \times \mathbf{H}$ (c is the velocity of light in vacuo)[3] is produced in the discharge and causes a corresponding redistribution of the current density.

The first premise makes it easy to explain the inclined glowing strips of photograph 1, located midway between each pair of neighboring turns of the helix and parallel to the latter. Actually, when the streams move in directions normal to the wire, the only streams colliding are those beginning on sections of neighboring turns, which lie on one plane normal to the turns. If the rates of flow are equal, the streams will meet at points in space located on this plane and equidistant from the above mentioned cross sections. At different points of space, the collisions will occur at different angles and at different instants of time, depending on the positions of these points relative to the wire. At points opposite the streams, in view of the short duration of the processes (see

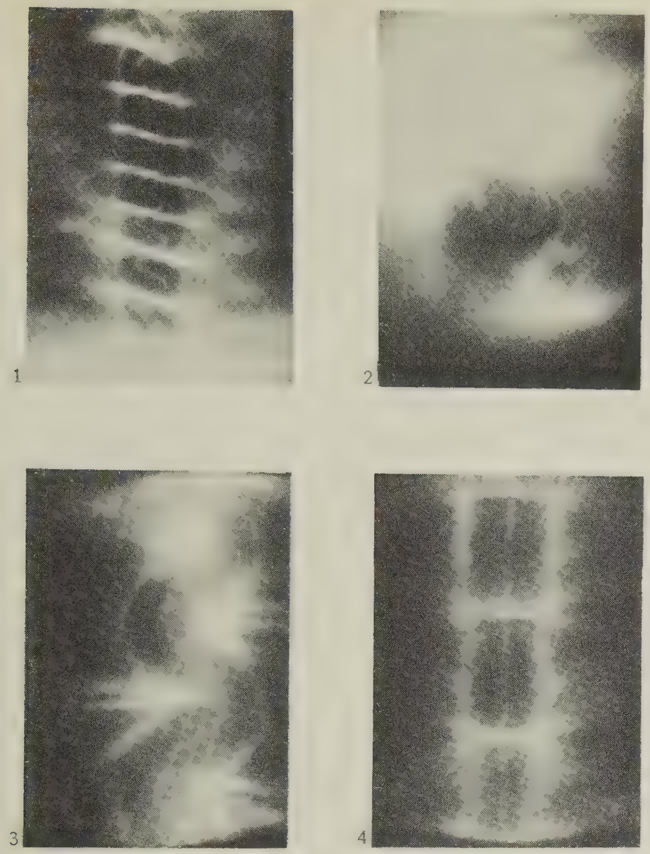

FIG. 1. Integral pictures of the explosion of copper wires: 1) helix of 3 mm diameter and 4 mm pitch, made of wire 0.15 mm in diameter and 80 mm long. Initial voltage on explosion-circuit capacitor U_0 = 30 kv; 2) helix of 8 mm diameter and 8 mm pitch, made of wire 0.2 mm diameter and 80 mm long, U_0 = 30 kv; 3) sinusoidal wire of 0.2 mm diameter and 70 mm length. U_0 = 30 kv; 4) the same picture in a different projection.

below), adiabatic compression will occur and produce a corresponding glow of the vapors. The bright strips represent the summary picture of all these glows. In the case of a cylindrical helix, the geometric locus of points with maximum glow intensity will be a helical surface having a common axis with the helix and passing midway between each pair of neighboring turns. For a given stream velocity, the visible radial extent of this surface should be limited by the fact that as the distance from the axis of the helix increases, the streams intersect at smaller angles and their density diminishes at the same time. The resultant reduced compression causes the glow of the vapor to cease at a certain distance from the axis of the helix. It is seen from this picture, however, that even before this takes place, the strongly compressed radial streams begin to branch axially, and it is there that the boundary of the glowing helical surface is located. As the helix is gradually stretched, the interaction between these streams becomes weaker, and the explosion takes on the appearance of that of a straight wire.[1]

It must be noted that the photographs of the explosion of a helix show one half of the glowing helical surface, that closest to the camera lens, since the light from the opposite half is fully screened by the explosion products that propagate in the direction of the lens. This is confirmed by photograph 2 of Fig. 1, taken at 45° to the axis of the helix, on which we see only the glow of the original helix. The image of the glowing helical surface is completely lacking here, since the glow of the explosion products is screened by the radial streams that move between neighboring portions of the helical surface. In the foreground of the picture we see a glowing plasma flowing along the axis of the spiral. This plasma is produced by the radial compression of the vapor inside the spiral.

Thus, part of the picture of the explosion of a helical wire can be adequately explained by the interaction between the streams of explosion products.

Photograph 1 and the other analogous photographs show an almost cylindrical glowing thin layer, coaxial with the helix and intersecting in sequence all the neighboring portions of the heli-

FIG. 2. Pictures of explosions of wires: 1) wire bent in circle of 50 mm diameter, wire of 0.2 mm diameter and 120 mm length, U_0 = 30 kv; 2) straight wires of aluminum and copper, joined at an angle of 45°, each wire 25 mm long, 0.15 mm in diameter, U_0 = 30 kv; 3) mirror scan of explosion of wire bent in circle of 25 mm diameter, wire of 0.2 mm diameter and 40 mm length, mirror speed ~60,000 rpm, U_0 = 30 kv.

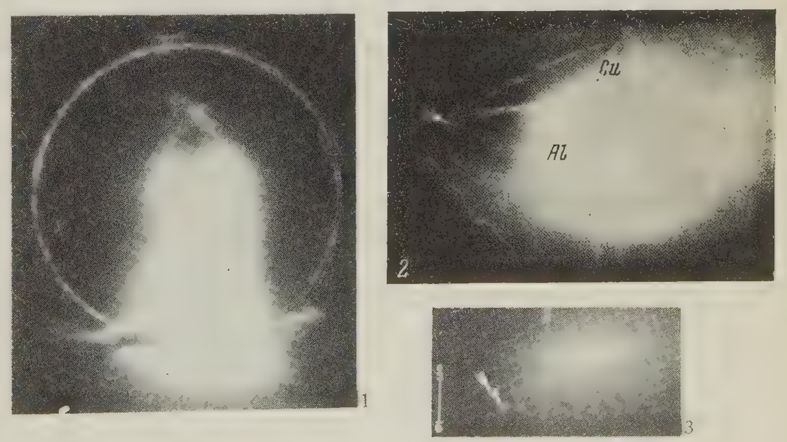

cal surface. The glow of this layer cannot be attributed to the interaction between the streams, for in these regions all the streams propagate mostly in the radial direction without any noticeable mutual interference. According to reference 1, the glow of a thin-wall cylinder can be attributed to the formation of suitable current channels (which we shall call current tubes), provided the magnetic field due to the current has a suitable configuration.

Let us trace the possible variations in the form of the current-induced magnetic field during the explosion of the helix. In the first stage, when the wire acquires the energy for the explosion, the current obviously retains its helical form, and the field inside the helix is determined by the number of ampere turns. After the start of the explosion, the streams move inside the helix transverse to this field and, according to the second premise, produce an additional electric field, which keeps the current helical until the encounter with the streams from the neighboring turns causes a breakdown between the streams, thus "straightening" the current. From this instant on the outward-directed streams from the helix penetrate the magnetic field due to the straight current. As a result, according to the mechanism indicated in reference 1, it is possible for a current tube to form.

Photograph 3 of Fig. 1 shows the explosion of a wire bent in sinusoidal form, photographed perpendicular to the plane of the wire. Photograph 4 of the same figure shows the explosion of a similar wire photographed parallel to this plane. Each of these photographs shows the glowing wire. Photograph 3 shows that the streams from each half wave of the sinusoidal wire converge to corresponding "foci" where adiabatic compression causes the vapor to glow bright. Upon leaving the region of maximum compression each stream clearly breaks up into two streams, which diverge in the direction of the axis of the sine wave. Sometimes the streams split into three parts, the central one remaining perpendicular to the axis of the sine wave. The same photograph shows the current tube, which has, in the projection used here, the same type of curvature as the wire, in accordance with the distribution of the streams and of the magnetic field due to the current. It must be noted that in this case, too, the current tube is better delineated in places where the stream flow is undisturbed. Photograph 4 shows all these phenomena in another projection.

Photograph 1 of Fig. 2 shows the explosion of a wire bent into a circle, taken perpendicular to the plane of the circle. In this case the radial streams that move in the plane of the circle or make small angles with this plane collide with each other at the center or near the center of the circle, causing adiabatic compression and glow of the vapor. What is remarkable here is the absence of a current tube around the wire. This is due to the small gap between the ends of the wire (~ 10 mm), which breaks down within a very short time ($\sim 0.5\ \mu$ sec) after the start of the discharge, so that the current stops flowing along the original position of the wire. We thus have here a positive confirmation of the direct connection between the glow of the tubes and the flow of the discharge current through the tubes. This experiment shows also that the glow of the vapor at the place where the streams converge is due to adiabatic compression and not to the current.

If wires bent in zigzag shape are exploded, the geometric loci of the points of convergence of the streams, in accordance with the first premise, should be planes perpendicular to the plane of the wire and passing through the corresponding zigzag vertices. The photographs show the projections of these glowing planes in the form of straight lines, coinciding with the diagonals of the corresponding zigzag angles, if the speeds of the streams are the same. If the zigzag angle is made up of wires of different material, say aluminum and copper, then, as can be seen from photograph 2 of Fig. 2, the projection of the glowing plane is nearer to the copper wire. This means that under identical explosion conditions, the explosion products of aluminum propagate faster than those of copper.

Photograph 3 of Fig. 2 shows a mirror scan of the explosion of a wire bent in a circle. The slit of the optical system was aligned with the vertical diameter of the circle. The scanning photograph shows first the image of a glowing wire (marked by an arrow) and then, following the explosion of the wire and the convergence of the stream to the center, the corresponding glow of the condensed vapor. Knowing the radius of the circle and the scanning rate, it is possible to calculate from this picture the velocity of the fronts of the explosion-product streams. Calculation yields a value of $\sim 10^6$ cm/sec. It is also seen from this photograph that the duration of the glow of the wire prior to the start of the explosion is $\sim 0.3\ \mu$ sec, and the glow of the vapor compressed at the center of the circle lasts $\sim 5\ \mu$ sec. Obviously, the scattering of the explosion products terminates within this time.

Figure 3 shows by way of an example an os-

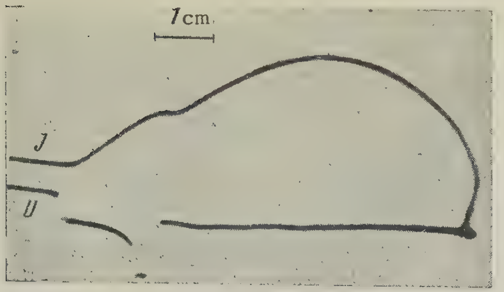

FIG. 3. Oscillogram of explosion of copper helix of 10 mm diameter and 10 mm pitch, wire of 0.2 mm diameter and 150 mm length, U_0 = 10 kv.

cillogram of the discharge, obtained during the explosion of a helical wire in vacuum. The current oscillogram (upper line) shows the characteristic "plateau" of the current, due to the fact that during this stage all the residual voltage across the capacitor is applied to the wire, and the current does not increase.[1] The voltage oscillogram (lower curve) confirms this fact. From similar oscillograms it is possible to calculate with sufficient accuracy the energy balance in the wire-explosion process.[4] Such calculations show that at relatively high capacitor voltages, the wire receives, during the time from the start of the discharge to the end of the "plateau" of the current, an energy equal to or perhaps greater than the total energy of evaporation.

3. DISCUSSION OF RESULTS. COMPARISON WITH RESULTS OF OTHER INVESTIGATIONS

The photographs discussed above demonstrate clearly the spatial distribution of the streams of the explosion products of the wires and indicate that the interactions between these streams exhibit certain peculiarities. For example, it turns out that in certain cases, after adiabatic compression, the streams are capable of branching into several independent streams. An explanation for this branching must be sought in the short duration of the compresssion process and in the high degree of this compression. From an examination of photograph 3 of Fig. 2 it follows that the duration of the compression process does not exceed several microseconds and since the velocity of the front of the streams reaches $\sim 10^6$ cm/sec, the degree of compression should be high.* From an examination of the integral explosion pictures it follows that the necessary condition for the branching of the streams is that the streams reach a region in space where the angle of convergence of the neighboring streams diminishes rapidly and where, at the same time, the stream density diminishes. As a result, conditions are produced for an almost explosive expansion of the previously compressed streams. The pictures cited show that the expansion is mostly in the direction of the symmetry axis of the wire. Consequently, this is the very direction in which the component parts of the stream effect the momentum exchange necessary for the branching. It can be assumed that the cause of the observed branching of the streams is the same factor that leads, in the case of a strong explosion with spherical or cylindrical symmetry, to the formation of regions of reduced density and pressure at the center or along the axis of the explosion (see, for example, reference 5).

When we recorded the results of the experiments, we became convinced that the occurrence of current tubes of different shapes can be qualitatively explained on the basis of the mechanism cited in reference 1. This again confirms the correctness of the aforementioned second premise.

The effect of the motion of the medium on the spatial distribution of the discharge-current density was also considered in references 6 to 8 in connection with an investigation of the compression of a plasma column (at low gas pressures) under the influence of a magnetic field due to a very intense pulsed current. There the plasma column has a chance to negotiate several transverse compressions and expansions. The added electric field produced during the compression is directed opposite to the external field, and in those regions of the plasma where the radial speed of the medium is maximum, it may even lead to reversal of the current.

In the explosion of wires, in view of the good condensibility of the metal vapor, the explosion-product streams are always directed away from the wire towards the cold walls of the chamber. The additional electric field in the regions of the radial stream motion has therefore the same direction as the external field. This indeed makes stable current tubes possible.

The mirror scan of the explosion shown in photograph 3 of Fig. 2 makes it possible to estimate with greater accuracy, than in reference 1, the connection between the duration of the scattering of the explosion products and the lifetime of the current tubes. According to this photograph, the scattering of the explosion products terminates after several (5 or 6) microseconds. Since, in accordance with our assumption, the existence of the current tubes is directly connected with the presence of corresponding radial streams, it is obvious that with the cessation of these streams the current tubes should also vanish. Thus, the lifetime of the current tubes for wires of usual dimensions (length ~ 10 cm, diameter ~ 0.1 to 0.2 mm) should not exceed several microseconds. This is well confirmed by the mirror scan of the explosion of both direct and curved wires.

---

*A picture of the explosion of a copper helix connected in series with a tungsten wire shows that the glow of the compressed vapor is considerably brighter than the surface glow of molten tungsten.

Certain data obtained during the explosion of wires in vacuo indicate apparently the existence of magnetic thermal insulation of the plasma during the stage of strong coiling of the discharge on the surface of the wire. In fact, many mirror-scan explosion pictures show that at relatively high discharge-capacitor voltages and at the usual wire dimensions, the duration of the strong discharge-coiling stage amounts to 0.3 sec. Comparison of the integral glow of the coiled discharge with the integral glow of the surface of molten tungsten wire (see reference 3) shows that the discharge glow is considerably brighter than the tungsten. Considering that the duration of the tungsten glow is at least one order of magnitude greater than the duration of the glow of the coiled discharge, we can conclude that the degree of ionization of the plasma in the coil should be higher. This is quite natural, for according to discharge oscillograms taken of coils of transverse dimension on the order of the radius of the wire (see integral photographs), the current density reaches $\sim 10^7$ amp/cm^2, and the field gradient reaches an order of 10^3 v/cm. In addition, calculation of the energy from the oscillograph data shows that in the cases considered here the energy supplied to the wire towards the end of the strong discharge-coiling stage is equal to or even greater than the total energy of evaporation. Under this condition, the wire would evaporate vigorously prior to the termination of the coiling stage and the integral photographs would not show a clear picture of the stabilized coil. Thus, the dense and highly-heated plasma turns out to be confined in the very narrow channel of the coil, which bounds with the high vacuum, showing unambiguously the existence of good magnetic thermal insulation for the plasma. This is readily understood if it is taken into account that according to the oscillographic data the magnetic field at the surface of the string reaches several times 10^5 Oe. The "magnetic wall" of the current channel can then withstand, from the plasma side, a maximum pressure of $\sim 10^4$ atmos, and the strong coiling of the current can exist until the thermal pressure of the plasma exceeds this value. As soon as the plasma pressure becomes greater, an explosive scattering of the vapor begins through the magnetic field of the current, and the effects described above take place.

---

[1] Kvartskhava, Bondarenko, Meladze, and Suladze, J. Exptl. Theoret. Phys. (U.S.S.R.) **31**, 737 (1956), Soviet Phys. JETP **4**, 637 (1957).

[2] Bondarenko, Kvartskhava, Pliutto, and Chernov, J. Exptl. Theoret. Phys. (U.S.S.R.) **28**, 191 (1955), Soviet Phys. JETP **1**, 221 (1955).

[3] H. Alfven, Cosmical Electrodynamics, Oxford, 1950 (Russ. Transl. M., 1952).

[4] Kvartskhava, Bondarenko, Pliutto, and Chernov, J. Exptl. Theoret. Phys. (U.S.S.R.) **31**, 745 (1956), Soviet Phys. JETP **4**, 623 (1957).

[5] A. I. Sedov, Методы подобия и размерности в механике (Methods of Similitude and Dimensionality in Mechanics), M., 1952.

[6] I. V. Kurchatov, Атомная энергия (Atomic Energy) No. 3, 65 (1956).

[7] Artsimovich, Anrianov, Dobrokhotov, Luk'ianov, and Pdogornyi, Атомная энергия (Atomic Energy) No. 3, 84 (1956).

[8] Bezbatchenko, Golovin, Ivanov, Kirillov, and Iavlinskii, Атомная энергия (Atomic Energy) No. 5, 20 (1956).

Translated by J. G. Adashko
192

SOVIET PHYSICS JETP VOLUME 35(8), NUMBER 4 APRIL, 1959

NUCLEAR BINDING ENERGIES IN THE REGION OF THE 82 PROTON AND 126 NEUTRON MAGIC NUMBERS

R. A. DEMIRKHANOV, T. I. GUTKIN and V. V. DOROKHOV

Submitted to JETP editor May 17, 1958

J. Exptl. Theoret. Phys. (U.S.S.R.) **35**, 917-925 (October, 1958)

The results of measurements of masses of isotopes of bismuth, lead, thallium, and mercury, which were made with a mass spectrograph having a resolving power of 60,000 to 80,000, are presented. The masses of the isotopes were determined by direct comparison with the masses of appropriate organic compounds. The values of the masses of the Pb^{206}, Pb^{207} and Pb^{208} isotopes found from different doublets are internally consistent. The nuclear binding energies computed from the measured isotopic masses confirm the presence of a shell structure with completion of a shell at 82 protons and 126 neutrons. The difference in binding energy for nuclei with odd and even numbers of nucleons and its smoothing out as the shell is filled can be seen clearly. After the filling of the shell at $Z = 82$ and $N = 126$, the binding energy of the next neutron is greater than that of the next proton. The binding energy for a pair of neutrons, which gives Hg^{204}, is greater than the binding energy for a pair of protons, which gives Pb^{204}.

INTRODUCTION

THE determination of binding energies of nucleons in nuclei in the region of the 82 proton and 126 neutron magic numbers is of fundamental importance for explaining the structure of nuclei. On the basis of the shell model, the jump in binding energy of the next nucleon after the filling of the shell should be of the order of 2 or 3 Mev. In order to determine the size of the discontinuity in the mass region $A \sim 200$ to an accuracy of 10%, the relative accuracy of the measurement of $\Delta M/M$ must be better than 10^{-6}. The data available at present on masses of isotopes and nuclear binding energies in the mass region $A \sim 200$ have errors exceeding the required figure given above.[1-3] The small error given in reference 2 for the measurements of masses of the Pb^{207}, Pb^{206}, Pb^{204}, Tl^{205}, Tl^{203}, Bi^{209}, and Hg^{202} isotopes is explained by the fact that in determining the masses of these isotopes from the energy balance of nuclear reactions the mass of Pb^{208} was taken as a standard and was assigned zero error. The mass of Pb^{208} was taken from the mass spectrograph measurements of Duckworth.[1] A precision measurement of the masses of the lead isotopes is therefore of interest not only from the point of view of explaining the structure of nuclei near $A \sim 200$, but also in order to get a more precise value of the mass of the Pb^{208} isotope to serve as a standard in calculating masses of heavy isotopes from the energy balance of nuclear reactions.

In addition, since Pb^{206}, Pb^{207}, Pb^{208}, and Bi^{209} are the final products in four of the radioactive series, their masses can be used as a base for calculating the masses of all the radioactive isotopes with $Z \geq 82$ from the energy balance of nuclear reactions. The masses of the Bi^{209}, Pb^{206}, Pb^{204}, Tl^{205}, Tl^{203}, Hg^{204}, Hg^{202}, Hg^{201}, Hg^{200}, Hg^{199}, and Hg^{198} isotopes have not been determined mass-spectrographically. The values calculated from energy balance of nuclear reactions for some of these isotopes contain a sizeable error ($\sim 3000\,\mu$MU). The value of the binding energy for an additional neutron or proton determined from these values does not allow us to get a clear picture of nuclear structure, because of the large error in the measurements.

In carrying out the present work we used various means for increasing the accuracy of measurement. The measurement of the masses of the lead, mercury, bismuth, and thallium isotopes was done on a mass spectrograph which has been described earlier.[4,5] The resolving power of the apparatus, as determined from doublet lines, was 60,000 to 80,000. To increase the accuracy of the measurements, the masses of the bismuth, lead, thallium, and mercury isotopes were determined by direct comparison with the masses of appropriate organic compounds containing H^1, C^{12}, N^{14}, and O^{16}. The masses of these isotopes had been measured previously[4,5] to sufficient accuracy. No

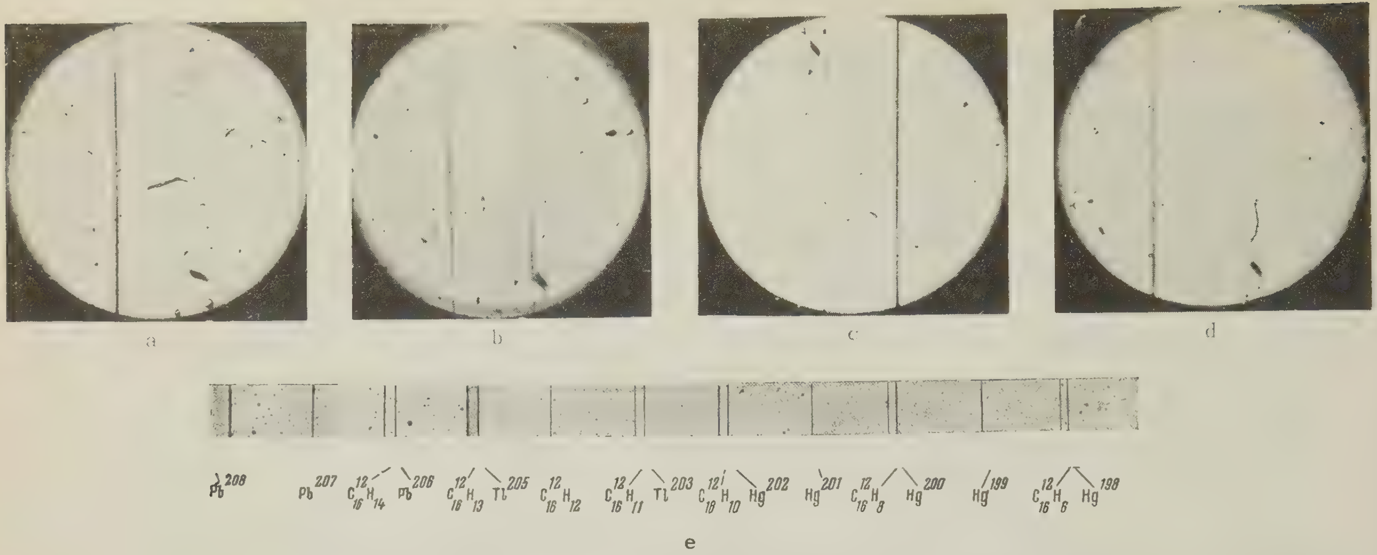

FIG. 1. Photographs of mass-spectrographic doublets and spectra of Pb, Tl, Hg and diphenylbutadiene: a) $C^{12}_{16}H_8$ – Hg^{200} doublet (× 37; M200); b) $C^{12}_{16}H_{10}$ – Hg^{202} doublet (× 37; M202); c) $C^{12}_{16}H_{12}$ – Pb^{204} doublet (× 37; M204); d) $C^{12}_{16}H_{15}$ – Pb^{207} doublet (× 37; M207); e) spectrum of Pb, Tl, Hg, and diphenylbutadiene (× 6; M206).

correction was made for content of rare isotopes in the hydrocarbons. The presence of a significant amount of C^{13} would have resulted in a marked broadening of the lines with a clearly visible asymmetry (a marked drop in intensity toward the low mass side). No such effect was noticed on the plates (cf. Fig. 1); this is even more correct for the rare isotopes D and N^{15}, which are less abundant. We can therefore state that errors due to the presence of rare isotopes are excluded.

MEASUREMENT OF MASSES OF ISOTOPES

Lead isotopes: Pb^{204}, Pb^{206}, Pb^{207}, and Pb^{208} To check internal consistency, the masses of the lead isotopes were determined from various doublets. The lead ions were obtained by introducing tetramethyl lead vapor in one case and metallic lead vapor in another into the gas discharge region of a plasma ion source, using an evaporator of special construction.

In the first case we observed on the screen of the mass spectrograph spectra of both the lead isotopes and their hydrocarbon compounds, such as $PbCH_3$, $Pb(CH_3)_2$, $Pb(CH_3)_3$, and $Pb(CH_3)_4$. In this case the main discharge was supported by helium. Appropriate organic compounds were introduced into the gas discharge region by means of a heater of approximately the same construction as that for metallic lead. The evaporator construction enabled us to produce quickly a filling with a new sample of material without dismounting the source and breaking the vacuum in the system. A check of internal consistency was made not only with lead ions but also by measuring the masses of the lead isotopes from doublets in various combinations with organic compounds, including the case where the molecular weight of the organic compound was equal to the atomic weight of lead. In this case we eliminate completely the phenomena that lead to the systematic measurement error due to the dissociation of the molecules both with respect to the hydrocarbons and with respect to the lead.[6]

In determining the mass of the Pb^{208} isotope, we used anthraquinone ($C_{14}H_8O_2$, M = 208) to form the doublet; this also gave us the doublet for Pb^{207} at mass 207. In another case the doublet line for Pb^{207} was obtained from the organic compound $C_{15}H_{12}O$. We used diphenylbutadiene ($C_{16}H_{14}$, M = 206) for the measurements of the masses of the Pb^{206} and Pb^{204} isotopes. The results of the measurements, obtained in each case from 18 to 20 mass-spectra, are given in Tables I and II.

The data of Tables I and II show that within the limits of error of the measurement there is internal consistency for the values of the doublets and the isotopic masses determined from different doublet combinations. The values of the masses of the isotopes were determined in the one case from metal vapor, in the other from the products of dissociation of tetramethyl lead. There was good agreement, within the statistical error of the measurement, when the doublet pair for a given lead isotope was formed by means of different organic compounds. This may serve as a confirmation of the absence of systematic errors in the measurement and of the reliability of the data.

TABLE I

Doublet	ΔM in 10^{-3} MU	Mass of lead isotope in MU	Average value of mass of lead isotope in MU	Product from which ions were obtained
$Pb^{204}-C_{16}H_{12}$	120,472 ± 44	204,038352 ± 48	204,038352 ± 48	$C_{16}H_{12}$ from $C_{16}H_{14}$ Pb^{204} from metal vapor
$Pb^{206}-C_{15}H_{14}$	134,849 ± 33	206,040259 ± 39	206,040184 ± 76	Pb^{206} from metal vapor
$Pb^{206}-C_{16}H_{14}$	135.000 ± 66	206.040108 ± 69		Pb^{206} from $Pb(CH_3)_4$
$Pb^{207}-C_{15}H_{11}O$	105.273 ± 35	207,041589 ± 40	207.041574 ± 35	$C_{15}H_{11}O$ from $C_{15}H_{12}O$ Pb^{207} from metal vapor
$Pb^{207}-C_{14}H_7O_2$	68.887 ± 50	207,041587 ± 54		$C_{14}H_7O_2$ from $C_{14}H_8O_2$ Pb^{207} from metal vapor
$Pb^{207}-C_{14}H_7O_2$	68.928 ± 110	207,041546 ± 112		$C_{14}H_7O_2$ from $C_{14}H_8O_2$ Pb^{207} from $Pb(CH_3)_4$
$Pb^{208}-C_{14}H_8O_2$	75.919 ± 47	208,042697 ± 51	208.042658 ± 35	Pb^{208} from metal vapor
$Pb^{208}-C_{14}H_8O_2$	75.998 ± 59	208.042618 ± 63		Pb^{208} from $Pb(Ch_3)_4$

TABLE II

Author	Mass of isotope in MU			
	Pb^{204}	Pb^{206}	Pb^{207}	Pb^{208}
Duckworth[1]	—	—	207,042900±1600	208,041600±1000
Huizenga[2]	204.036859±130*	206.038826±10*	207.040580±10*	208,041640±0*
Our data	204.038352±48	206.040184±76	207.041574±35	208.042658±35

*Errors marked with an asterisk should be increased by ± 1000μ MU because of the error in the determination of the mass of Pb^{208}, as given by mass-spectrographic measurements.[1]

TABLE III

Doublet	Value of ΔM in 10^{-3} MU	Masses of mercury isotopes in MU	
		from our data	from nuclear reactions*
$Hg^{198}-C_{16}H_6$	80,259±68	198.029713±71	198,029000±3000
$Hg^{199}-C_{13}H_{11}O$	107,674±38	199,031548±45	199,030550±3050
$Hg^{200}-C_{16}H_8$	94,354±43	200,031902±47	200,031910±3010
$Hg^{201}-Hg^{202}$	100.398±32	201.034564±62	201.034000±3000
$Hg^{202}-C_{16}H_{10}$	107.588±48	202.034952±52	202.035341±620**
$Hg^{204}-C_{16}H_{12}$	119.784±43	204.039040±47	204.037323±230**

*Huizenga[2] and Wapstra.[3]
**Data obtained using the mass of Pb^{208} as a standard.[1]

TABLE IV

Doublet	Value of ΔM in 10^{-3} MU	Masses of thallium isotopes in MU	
		from our data	from nuclear reactions*
$Tl^{203}-C_{16}H_{11}$	113.059±36	203.037623±41	203,035951±400*
$Tl^{205}-C_{16}H_{13}$	127.061±38	205.039905±43	205.038480±130*

*Huizenga.[2]

TABLE V

Doublet	Value of ΔM in 10^{-3} MU	Mass of bismuth isotope in MU	
		from our data	from nuclear reactions*
Bi^{209}—$C_{14}H_{13}N_2$	127.516±63	209.046864±71	209,045794±50*

*Huizenga[2].

TABLE VI

Isotope	M – Mass of isotope in MU from our data	M′ – mass of isotope in MU from nuclear reaction data. The mass of Pb^{208} from the present work is taken as standard	$\Delta = M - M'$ in 10^{-3} MU
Hg^{198}	198.029713 ± 71	198.029000 ± 3000*	+0.713
Hg^{199}	199.031548 ± 45	199.030550 ± 3050*	+0,998
Hg^{200}	200.031902 ± 47	200.031910 ± 3010*	—0,008
Hg^{201}	201.034564 ± 62	201.034000 ± 3000*	+0,564
Hg^{202}	202,034952 ± 52	202,036359 ± 620	—1,407
Hg^{204}	204,039040 ± 47	204.038341 ± 230	+0,699
Tl^{203}	203.037623 ± 41	203.036969 ± 400	+0,654
Tl^{205}	205.039905 ± 43	205.039498 ± 130	+0,407
Pb^{204}	204.038352 ± 48	204.037877 ± 130	+0,475
Pb^{206}	206.040184 ± 76	206.039844 ± 10	+0,340
Pb^{207}	207,041574 ± 35	207.041598 ± 10	—0,024
Pb^{208}	208.042658 ± 35	208.042658 ± 0	0,000
Bi^{209}	209,046864 ± 71	209.046812 ± 50	+0,052

*The mass of the O^{16} isotope[3] was used as a standard in the calculations. These values are given without correction.

Mercury isotopes: Hg^{198}, Hg^{199}, Hg^{200}, Hg^{201}, Hg^{202}, and Hg^{204}. The mercury ions were obtained by introducing mercury vapor into the gas-discharge region of the ion source. Diphenylbutadiene was used to form the doublet pairs. The values of the mass differences of these doublets and the masses of the mercury isotopes calculated from them are given in Table III. For comparison we give in the table the data obtained from nuclear reactions.

Thallium isotopes: Tl^{203} and Tl^{205}. The thallium ions were obtained from metallic thallium vapor. Diphenylbutadiene was used to form the doublet pair. The values of the mass differences of the doublets and the masses of the isotopes are given in Table IV. For comparison we also include data from nuclear reactions.

Bi^{209} isotope. Bismuth ions were obtained from vapors of metallic bismuth. Phenylhydrazone acetophenone ($C_{14}H_{13}N_2$, $M = 209$) was used to form the doublet pair. The mass difference of the doublet and the mass of the isotope calculated from these data are given in Table V.

Comparing the values of isotopic masses found in the present work with the corresponding data from nuclear reactions (cf. Tables II to V), we see that in general they agree with one another within the limits of error of the measurements. However, this agreement is achieved only as a result of the large errors in determination of the masses of isotopes from the Q values of nuclear reactions. For the Hg^{198}, Hg^{199}, Hg^{200}, and Hg^{201} isotopes, for which in the last analysis the mass of O^{16} is taken as a base, the large error in the measurement results from using a large number of intermediate steps with their corresponding Q values. For all those isotopes for which the mass of the Pb^{208} isotope is used as a standard, the magnitude of the error of the measurement is determined both by the errors of the corresponding Q values and by the accuracy of measurement of the mass of Pb^{208}. In his tables, Huizenga[2] used for the Pb^{208} isotope the value $M = 208.041640 \pm 1000\,\mu$MU* found by Duckworth.[1] For the whole set of isotopes presented here, the differences of the average values are sufficiently large ($\sim 1500\,\mu$ MU) as to be possibly due to the inaccuracy of the value of the mass of Pb^{208} which was taken as a standard.

In Table VI we give the masses of the isotopes calculated using Q-values with the value of the mass of the Pb^{208} isotope which was found in the present work as the standard. We then find agreement, within the limits of error of the measurements, between the present data and the calculated values for most of the isotopes, even though the

---

*The errors of measurements in the text and tables are given in μMU.

TABLE VII

Isotope	A	Z	N	Binding energy of nucleons in the nucleus in Mev	Binding energy per nucleon in Mev
Hg^{198}	198	80	118	1566.100±0.066	7.90960±0,00033
Hg^{199}	199	80	119	1572.758±0,043	7,90331±0,00021
Hg^{200}	200	80	120	1580,795±0.044	7,90397±0,00022
Hg^{201}	201	80	121	1586.682±0.057	7,89394±0,00034
Hg^{202}	202	80	122	1594.685±0,048	7,89450±0,00024
Hg^{204}	204	80	124	1607.614±0,044	7,88046±0,00022
Tl^{203}	203	81	122	1599,782±0.038	7,88070±0.00019
Tl^{205}	205	81	124	1614,390±0.040	7,87507±0,00020
Pb^{204}	204	82	122	1606.685±0,045	7.87590±0,00022
Pb^{206}	206	82	124	1621,712±0,071	7,87238±0,00034
Pb^{207}	207	82	125	1628.784±0,033	7,86852±0.00016
Pb^{208}	208	82	126	1636.141±0,033	7,86606±0,00016
Bi^{209}	209	83	126	1639,806±0.066	7,84596±0.00031

*1 MU = 931,162 ± 24 kev.

TABLE VIII

Isotope	A	Z	N	Mass of isotope in MU	Binding energy of nucleons in the nucleus, in Mev	Binding energy per nucleon, in Mev
Bi^{208}	208	83	125	208,045699±90	1632.524±0,084	7,84867±0.00041
Pb^{209}	209	82	127	209.047492±70	1640.006±0,065	7,84692±0.00031
Bi^{210}	210	83	127	210,051378±40	1643,969±0,037	7,82842±0.00018
Pb^{210}	210	82	128	210.051447±40	1644.690±0.037	7,83185±0.00018
Po^{210}	210	84	126	210.050115±40	1644.360±0.037	7.83028±0.00018

error in measurement of the mass of the standard Pb^{208} isotope is ~30 times smaller than the error in the determination of the Pb^{208} mass value used in the tabulated data.[1,2] However, as one sees from Table VI, the values of the isotopic masses obtained by calculation from nuclear reaction data (cf. column 3) are essentially lower by 0.3 to 0.5 m MU than the present data, except for the mass of Hg^{202}.

BINDING ENERGY OF NUCLEONS IN THE NUCLEUS

The values of the masses of the bismuth, lead, thallium, and mercury isotopes found in the present work enable us to determine more precisely the binding energy of nucleons in the nucleus in the region of the 82 proton and 126 neutron magic numbers. The values of the nuclear binding energies and the binding energies per nucleon are given in Table VII. In addition to this, by using Q values from nuclear reactions and β decay, the masses of the Bi^{208}, Pb^{209}, Pb^{210}, Bi^{210}, and Po^{210} isotopes were calculated (cf. Table VIII). In these calculations, the masses of Pb^{208} and Bi^{209} found in the present work were used as standards. The mass of the Pb^{209} isotope was calculated from the $Pb^{208}(d, p)Pb^{209}$ reaction with the value Q = 1.64 ± 0.05 Mev.[7] The value found for the mass of the Pb^{209} isotope is $M_{Pb^{209}} = 209.047492 \pm 70$ MU. The value for Pb^{209} was also calculated using the value Q = 0.63 ± 0.01 Mev[8] obtained from the $_{82}Pb_{127} \rightarrow {}_{83}Bi_{126}$ β decay. The value of the mass of the Pb^{209} isotope found from this reaction was $M_{Pb^{209}} = 209.047544 \pm 67$, which within the limits of error of the measurement is in satisfactory agreement with the value found from the $Pb^{208}(d, p)Pb^{209}$ reaction. The calculated values of nuclear binding energies are given in Table VIII. Figure 2 shows the curve for the binding energy per nucleon in the nucleus. The significant difference of the binding energies of the Bi^{208}, Pb^{209}, Bi^{209}, Pb^{210}, and Po^{210} compared with the Pb^{208} isotope is a confirmation of the existence of a nuclear shell structure with closing of shell at Z = 82 and N = 126. The difference in binding energy of nucleons in nuclei with even and odd

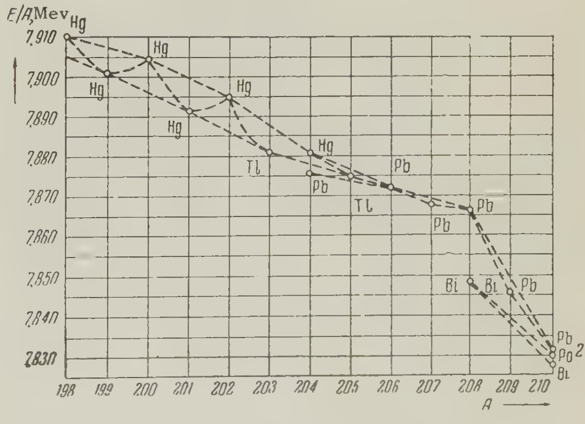

FIG. 2. Binding energy per nucleon in the region 198 ≤ A ≤ 210.

TABLE IX

Isotope	Z	N	Binding energy of the last neutron, in Mev	Isotope	Z	N	Binding energy of the last neutron, in Mev
Hg^{199} Hg^{198}	80 80	119 118	6,658	$Au^{197}*$ $Pt^{196}*$	79 78	118 118	6.105
Hg^{200} Hg^{199}	80 80	120 119	8,037	$Au^{198}*$ $Pt^{197}*$	79 78	119 119	6,467
Hg^{201} Hg^{200}	80 80	121 120	5.887	$Au^{199}*$ $Pt^{198}*$	79 78	120 120	5.691
Hg^{202} Hg^{201}	80 80	122 121	8,003	Hg^{201} $Au^{200}*$	80 79	121 121	6.395
$Hg^{203}*$ Hg^{202}	80 80	123 122	5,994	$Hg^{202}*$ $Au^{201}*$	80 79	122 122	7.826
$Tl^{204}*$ Tl^{203}	81 81	123 122	7.362	$Tl^{202}*$ Hg^{201}	81 80	121 121	6,322
Tl^{205} $Tl^{204}*$	81 81	124 123	7,246	Tl^{203} Hg^{202}	81 80	122 122	5.095
Pb^{207} Pb^{206}	82 82	125 124	7,072	$Tl^{204}*$ $Hg^{203}*$	81 80	123 123	6.463
Pb^{208} Pb^{207}	82 82	126 125	7,357	Tl^{205} Hg^{204}	81 80	124 124	6.776
Pb^{209} Pb^{208}	82 82	127 126	3.845	Pb^{206} Tl^{205}	82 81	124 124	7.322
Pb^{210} Pb^{209}	82 82	128 127	4.684	$Bi^{207}*$ Pb^{206}	83 82	124 124	3.866
$Pb^{211}*$ Pb^{210}	82 82	129 128	4,355	$Bi^{208}*$ Pb^{207}	83 82	125 125	3.644
Bi^{209} Bi^{208}	83 83	126 125	7,282	Bi^{209} Pb^{208}	83 82	126 126	3.665
Bi^{210} Bi^{209}	83 83	127 126	4.554	Bi^{210} Pb^{209}	83 82	127 127	4,354
$Bi^{211}*$ Bi^{210}	83 83	128 127	5.280	$Bi^{211}*$ Pb^{210}	83 82	128 128	4.390
$Po^{215}*$ $Po^{214}*$	84 84	131 130	4.087	$At^{215}*$ $Po^{214}*$	85 84	130 130	4.067
$Po^{216}*$ $Po^{215}*$	84 84	132 131	5,806	$At^{216}*$ $Po^{215}*$	85 84	131 131	4,568
$Po^{217}*$ $Po^{216}*$	84 84	133 132	4.088	$At^{217}*$ $Po^{216}*$	85 74	132 132	4.745
$Po^{218}*$ $Po^{217}*$	84 84	134 133	5.608	$At^{218}*$ $Po^{217}*$	85 84	133 133	5.175
$Po^{219}*$ $Po^{218}*$	84 84	135 134	3.628	$At^{219}*$ $Po^{218}*$	85 84	134 134	5,136

*Binding energies calculated from the data of references 2 and 3.

mass numbers[10] is seen very clearly on the curve. As we see from Fig. 2, as the shell is filled this difference decreases. The effect of the nuclear shell structure can also manifest itself in the energy for binding the (Z + 1)-th proton and the (N + 1)-th neutron. The values of these quantities are given in Table IX. The tables show that there is a sharp discontinuity in the binding energy at 83 protons and 126 neutrons. A characteristic feature in the filling of the shells is the fact that the binding energy for a neutron is greater than that for a proton. This can be seen directly from Fig. 2, by comparing the binding energies of Pb^{209} and Bi^{209} and Bi^{209} with those of Pb^{210} and Po^{210}, and also from Table IX. It can be seen especially clearly from a comparison of the binding energies of the Pb^{204} and Hg^{204} isotopes. The proton shell is filled at Pb^{204}, so that one would expect a maximum binding energy compared to other isotopes having A = 204. However, at the stable isotope Hg^{204}, the binding energy proved to be greater, because of the larger value of the binding energy of a pair of neutrons compared to the corresponding pair of protons in Pb^{204}. This effect is washed out in the packing fraction curve. Thus for very accurate measurements the use of the packing fraction curve is not suitable for analysis of dependences of nuclear binding energies. We see from Table IX that the binding energy of the last neutron or proton satisfies the odd-even rule, i.e., the energy for binding each odd proton or neutron is less than that for binding each even one.

In addition to the jump in binding energy at the closing of the shell (i.e., at $N = 127$ and $Z = 83$), we also noted a non-monotonic behavior of the curve of binding energy of the last proton or neutron for the nuclei with $N = 121$ and $Z = 81$ (cf. Table IX), i.e., 6 neutrons and 2 protons from the start of the filling of the new shell. In order to check whether there is any regularity in the jumps of binding energy in this region, we used, in addition to the measured values of the masses of 13 isotopes and the corresponding nuclear binding energies, the values of binding energies from references 2 and 3, even though the uncertainties of the tabulated data of reference 2 and especially of reference 3 are so great that it is impossible to speak of regularities with any certainty on the basis of these data. From examination of these data, one also sees a non-monotonic behavior of the curve of binding energy of the last neutron or proton for some other nuclei which are shifted by 6 neutrons and 2 protons, i.e., for which $Z' = Z + 2$ and $N' = N + 6$.

With respect to the neutrons, this non-monotonicity of the curve of binding energies for a shift of 2 protons and 6 neutrons appears in the fact that the binding energy of the 115-th neutron for $Z = 78$, of the 121-st neutron for $Z = 80$, of the 127-th neutron for $Z = 82$ and of the 133-rd neutron for $Z = 84$ is markedly low. For protons this non-monotonic behavior for a shift of 2 protons and 6 neutrons manifests itself in a more complicated way. After Bi^{209} with $Z = 83$ and $N = 126$, the jump in the binding energy for $Z = 81$ and $N = 120$ cannot be used, since no nucleus exists for $Z = 81$ and $N = 120$. The nearest nucleus with $Z = 81$ and an even number of neutrons, i.e., with $N = 122$, has a minimal binding energy compared to its neighbors, as we see from Table IX. A markedly reduced value of the binding energy of the last proton occurs at $Z = 79$ and $N = 120$, and at $Z = 77$ and $N = 114$. The uncertain drop in binding energy of the last proton at $Z = 85$ and $N = 132$ becomes completely clear on the curve of binding energy of the last proton as a function of neutron number in the region $130 \leq N \leq 134$.

The "anomaly" noted by Johnson and Nier[9] in the binding energy of nuclei in the region of $N = 90$ may possibly be of this same type. Small nuclear deformations are known to be unstable. A change in the shape of the nucleus and, consequently, of the size of its surface results in a discontinuity. A change of the surface of the nucleus may be one of the reasons for jumps in the binding energy of even-odd and odd-even nuclei.

For the majority of the isotopic masses found in the present work, the nuclear binding energies are raised by approximately 1500 kev compared with those calculated from nuclear reactions,[2] in which the value of the mass of Pb^{208} found in reference 1 is used as a standard value.

In conclusion the authors must express their thanks to E. E. Baron', T. N. Lebsadza, K. A. Kovyrzina, and V. M. Shoniia for the preparation of the metal-organic compounds and heavy hydrocarbons, and also to P. S. Brostiuk, M. I. Dzkuia, and G. A. Dorokhova for practical assistance in the work.

---

[1] H. E. Duckworth and R. S. Preston, Phys. Rev. **82**, 468 (1951). Stanford, Duckworth, Hogg and Geiger, Phys. Rev. **85**, 1039 (1952). B. G. Hogg and H. E. Duckworth, Can. J. Phys. **32**, 65 (1954).

[2] J. R. Huizenga, Physica **21**, 410 (1955).

[3] A. H. Wapstra, Physica **21**, 385 (1955).

[4] Demirkhanov, Gutkin, Dorokhov, and Rudenko, Атомная энергия (Atomic Energy) **1**, 21 (1956).

[5] Demirkhanov, Gutkin, and Dorokhov, Атомная энергия (Atomic Energy) **2**, 544 (1957).

[6] T. I. Gutkin, Приборы и техника эксперимента (Instr. and Meas. Engg.) No. 5, 46 (1957).

[7] D. M. Van Patter and W. Whaling, Revs. Modern Phys. **26**, 402 (1954).

[8] R. W. King, Revs. Modern Phys. **26**, 327 (1954).

[9] W. H. Johnson and A. O. Nier, Phys. Rev. **105**, 1014 (1957).

[10] V. A. Kravtsov, Usp. Fiz. Nauk **47**, 341 (1952).

Translated by M. Hamermesh
193

POSITRON SPECTRUM OF $Eu^{152,154}$

D. L. KAMINSKII and M. G. KAGANSKII

Leningrad Physico-Technical Institute, Academy of Sciences, U.S.S.R.

Submitted to JETP editor May 26, 1958

J. Exptl. Theoret. Phys. (U.S.S.R.) **35**, 926-931 (October, 1958)

The spectrum of positrons emitted in the decay of $Eu^{152,154}$ has been studied. The spectrum consists mainly of positrons due to pair conversion of 1410-kev γ quanta and of a β^+ spectrum with an end-point energy $E_0 = 700 \pm 20$ kev. The spectrum is identified as being due to positron decay of Eu^{152} ($T_{1/2} = 13$ years), with an intensity of 1.2×10^{-4} positrons per disintegration. The value of $\log(\tau f)$ for this transition is 12.1.

1. INTRODUCTION

MANY papers (references 1 to 4 and others) have been devoted to the study of the decay of Eu^{152} which has a half-period of 13 years. However, a number of important details of the disintegration scheme remains unclear. In particular, no positron decay of Eu^{152} has yet been observed. Yet an investigation of the positron spectrum of Eu^{152} would enable us to obtain new data on its decay scheme, to determine the energy difference for the transition $Eu^{152} \rightarrow Sm^{152}$ and, consequently, to obtain more precise data on electron capture. Attempts to observe positron emission from europium by means of a magnetic-lens spectrometer did not meet with success.[5] In this paper we describe the results of an investigation of the positron spectrum of $Eu^{152,154}$ by means of a spectrometer designed for the study of weak positron spectra.

2. DESCRIPTION OF THE APPARATUS

The experimental setup with which the positron spectrum was investigated is shown schematically in Fig. 1.

We used a magnetic spectrometer of the sector type with double focusing of the beam as described in our earlier paper.[6] The radius of its mean trajectory is 250 mm. Measurements of the positron spectrum were carried out with a spectrometer solid angle equal to 1% of 4π. The relative half-width of the instrumental line was 1.5% with a source width of 1 to 2 mm and with a detector entrance slit 12 mm wide.

The focusing magnetic field of the spectrometer had the following distribution in the median plane:

$$H = H_0\left[1 - \frac{1}{2}\left(\frac{r - r_0}{r_0}\right) + \frac{3}{8}\left(\frac{r - r_0}{r_0}\right)^2\right],$$

where r_0 is the radius of the mean trajectory. The focusing magnetic field, taking into account the stray field, gives an effective focusing angle equal to ~200°. The source 1 is situated in the magnetic field (Fig. 1), while the detector situated at the spectrometer focus is outside the magnetic field. The positrons were focused by the magnetic field and passed through the entrance slit of the detector 2, to the Geiger counter 3. They were then stopped in the aluminum target where they were annihilated. The annihilation γ radiation was recorded by two CsI(Tl) crystals. Thus, a positron was recorded by the coincidence of three pulses: a pulse in the Geiger counter and two pulses in the scintillation counters. The resolving time of the coincidence circuit was chosen equal to 2×10^{-6} sec. To reduce background, the only pulses recorded were those for which the scintillation pulse corresponded to γ-

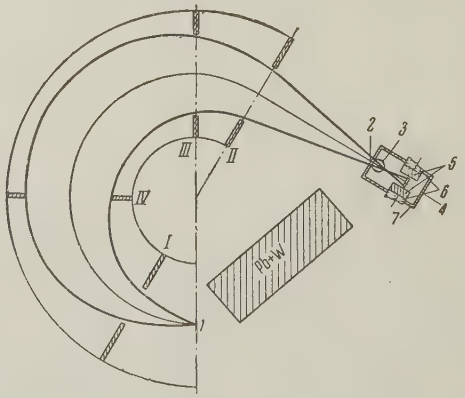

FIG. 1. The electron-optical diagram of the spectrometer. 1) source, 2) entrance slit of the detector, 3) Geiger counter, 4) aluminum target, 5) scintillators, 6) light guides, 7) detector chamber, I–IV) diaphragms.

radiation energy losses in the crystal between 100 and 600 kev.

To provide shielding from cosmic rays, a "blanket" consisting of two layers of type AMM-9 counter tubes was placed above the detector. Above the "blanket" there was a layer of lead (10 cm thick) to absorb the soft component of cosmic rays. The "blanket" was connected in anti-coincidence to the main triple-coincidence circuit, and cut off the part of the background due to showers produced by μ mesons in the neighborhood of the detector. The detector was shielded from the γ-radiation of the source by a lead-tungsten block placed between the two.

The circuit described above for recording positrons had, in the absence of the source, a background of 0.8 to 1.0 counts per hour, and the presence of even quite strong sources of $Eu^{152,154}$ did not appreciably alter the value of the background. One disadvantage of the circuit was the relatively small efficiency for the detection of positrons, defined in our case as the ratio of the number of triple coincidences to the number of pulses recorded by the Geiger counter (with the background subtracted). In our case the efficiency amounted to 4 or 5% for positrons of energy greater than 300 kev. Owing to scattering of positrons between the Geiger counter and the target, the efficiency of positron recording depended on their energy. This dependence is shown in Fig. 2.

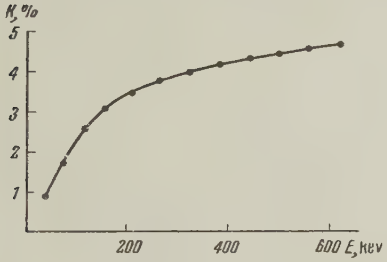

FIG. 2. Dependence of the efficiency K of the recording system on positron energy.

The source consisted of europium oxide of natural composition irradiated with neutrons. It was precipitated from an emulsion of carefully powdered europium oxide onto an aluminum foil 5 μ thick. The sources prepared in this manner had measured 4×20 mm^2 and their density did not exceed 2 mg/cm^2.

The spectrometer was calibrated against lines of conversion electrons from $Eu^{152,154}$, whose energies have been measured with sufficient accuracy.[1]

3. POSITRON SPECTRUM

To check the spectrometer we measured the well-known positron spectra of Cu^{64}, Zn^{65} and the internal-conversion positron spectrum of ThC[11]. The results obtained agree with data available in the literature. As an example, our positron spectrum and that of Owen and Primakoff[7] are compared in Fig. 3. The difference observed at $H\rho <$ 2000 Oe-cm is apparently due to the slowing down of β particles in the relatively thick sources used by us.

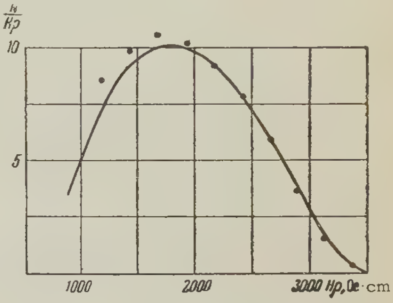

FIG. 3. The positron spectrum of Cu^{65}. Solid curve – according to Owen and Primakoff,[7] ● – our results.

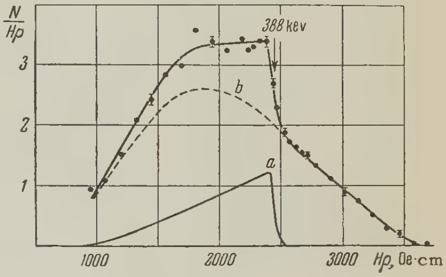

FIG. 4. The positron spectrum of $Eu^{152,154}$, a) pair conversion positrons for a 1410-kev γ quantum, b) β^+ spectrum.

The positron spectrum of $Eu^{152,154}$, reduced to equal interval widths, is shown in Fig. 4. Here a correction has already been introduced, in accordance with Fig. 2, to take into account the energy dependence of the efficiency of the recording system. The measured positron spectrum exceeds the background by 2 or 3 orders of magnitude. When the source was displaced relative to the diaphragm 1 (Fig. 1) in such a way that the β-particle beam did not pass through the spectrometer, the recorded intensity of radiation fell to background level. This shows that the observed positron spectrum is not due to the γ radiation from the source, since the conditions for irradiation of the spectrometer chamber and of the detector by γ rays practically do not change when the source is displaced. At the same time positrons production by γ quanta in the source itself (external pair production) is negligible.

A very important point is the possible presence in the composition of the source of radioactive contaminations which could give rise to emission of positrons. Some of the europium sources investigated were more than three years old, and therefore could not contain any short-lived activities. A careful study of the γ radiation from $Eu^{152,154}$ carried out by Bobykin and Novik[1] using sources prepared from the same material as used in our work, showed that this material contains insignifi-

		Results of calculations on the basis of data of references 10 to 12					Experimental results
		$E1$	$E2$	$E3$	$M1$	$M2$	
$\alpha_K \cdot 10^3$		0.48	1.05	2.15	1.55	3.65	
$\Gamma_p \cdot 10^4$	$Z=0$	2.2	0.63	0.21	0.28	0.08	$\Gamma_p/\alpha_K = (43 \pm 10) \times 10^{-2}$
	$Z=84$	1.2	0.42				
$(\Gamma_p/\alpha_K) \cdot 10^2$	$Z=0$	46	6	1	1.8	0.2	
	$Z=84$	25	4				

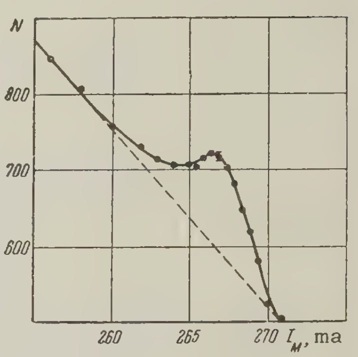

FIG. 5. Electron conversion line in the K shell for a 1410-kev γ quantum. N is the number of pulses per second recorded by the Geiger counter, I_M is the current in the winding of the spectrometer magnet.

cant amounts of Eu^{155} and Cd^{153}. Positron decay of these isotopes is apparently impossible,[8,9] and the observed spectrum should therefore be ascribed entirely to $Eu^{152,154}$.

As can be seen from Fig. 4, the positron spectrum is a complex one. The sharp falling-off of the spectrum at $H\rho \approx 2400$ Oe-cm is apparently due to the positron spectrum of the internal pair conversion of the 1410-kev γ line. The end point of this spectrum corresponds well to the energy $E_\gamma - 2mc^2 = 388$ kev. Since the energy distribution of positrons of pair conversion is known,[10] the whole pair-conversion positron spectrum can be reconstructed from the sharp discontinuity.* The spectrum constructed in this manner is shown in Fig. 4 (curve a).

The existence of this spectrum, as well as of an electron-conversion spectrum for the same transition, makes it possible to determine from the ratio of the coefficients of pair and electron conversion the multipole order of the transition. To do this, the same source was used to observe the positron spectrum and the part of the electron spectrum containing the K-conversion line for the 1410-kev transition. The results of measurements made on the electron spectrum are shown in Fig. 5. The ratio of the conversion coefficients was determined as the ratio of areas of the corresponding spectra,† the area of the conversion line being determined by interpolating the β spectrum under this line. The multipole order of the transition is determined by this method in a unique manner since, for example, in the K shell the ratio of the intensities of the internal conversion positron spectrum to that of the internal conversion electron spectrum, $I_p/I_e = \Gamma_p/\alpha_K$, falls off rapidly as the multipole order increases, since the pair-conversion coefficient Γ_p diminishes while the conversion coefficient in the K shell α_K increases. The table gives results of calculations for a number of different multipole orders, and also the value of Γ_p/α_K obtained in our experiment. The comparison of the calculated results with the experimental data gives for the multipole order of the transition the value E1, which corresponds to the data of Bobykin and Novik[1] and of Dzhelepov et al.[2] obtained from the electron-conversion coefficient in the K shell. For the pair-conversion coefficient we obtain the value $\Gamma_p = (2.0 \pm 0.5) \times 10^{-4}$ (for $\alpha_K = 0.48 \times 10^{-3}$).

After subtracting the pair-conversion positron spectrum belonging to the 1410 kev transition we are left with a positron spectrum (Fig. 4) that cannot be ascribed to pair conversion, both because of the shape of the spectrum (absence of a discontinuity on the high-energy side) and because of the absence of transitions with energies greater than 1410 kev in the γ spectrum of $Eu^{152,154}$. Figure 6 gives the Fermi plot for this

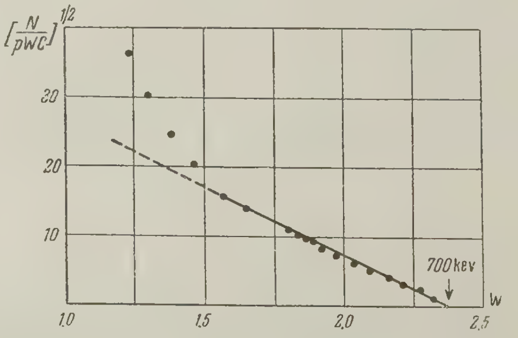

FIG. 6. Fermi plot for the β^+ spectrum. W – is the total positron energy in units of mc^2.

---

*The distribution of pair-conversion positrons in our case (Z = 62) was assumed to be the same as in the case Z = 84, calculations for which were made by Jaeger and Hulme.[10]

†In finding the above ratio, the difference in the efficiencies of the circuits for recording electrons and positrons was taken into account, since the electrons were recorded by a Geiger counter, while the positrons were recorded by a triple-coincidence circuit.

spectrum. It can be seen that the greater part of the spectrum lies on a straight line. This indicates that one of the europium isotopes undergoes positron β decay. The endpoint energy of the β spectrum is $E_0 = 700 \pm 20$ kev. Figure 6 shows that below 250 kev the experimental points deviate considerably from the Fermi straight line. This excess of positrons is probably due to the pair conversion of a number of weak γ lines accompanying the decay of $Eu^{152,154}$ ($E_\gamma = 1280$; 1110; 1086 kev[1,2]), and also to scattering in the source.

The observed β^+ spectrum should apparently be attributed to the decay of Eu^{152}. The following considerations are in favor of this hypothesis. No K capture was found in an investigation[13] of the decay of Eu^{154} free of Eu^{152}. At the same time, at $E_0 = 700$ kev the intensity of K capture exceeds the intensity of β^+ decay by approximately a factor of 100. On the other hand, when the natural mixture of europium isotopes (Eu^{151} — 47.8% and Eu^{153} — 52.2%) is irradiated with neutrons, the Eu^{152} content is considerably greater than the Eu^{154} content.* Therefore, the β^+-spectrum observed experimentally cannot be attributed to the decay of Eu^{154}.

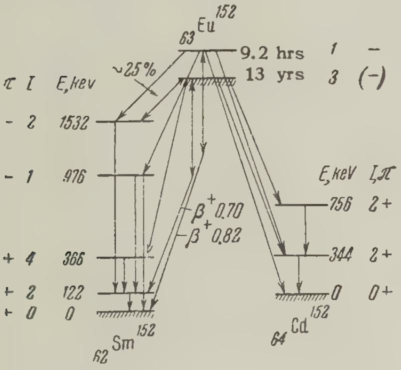

FIG. 7. The decay scheme for $Eu^{152,152m}$ with the positron decay branches according to the results of Grodzins[15] and to our data.

The intensity of the positron branch of the decay of Eu^{152} was calculated on the basis of the decay scheme shown in Fig. 7. This part of the decay scheme of Eu^{152} can at the present time be regarded as reliably established.

After having determined the intensity of the β^+ spectrum relative to the internal conversion positron spectrum (Fig. 4), we determined the intensity of the positron decay of Eu^{152}: $I = (1.2 \pm 0.2) \times 10^{-4}$ positron per decay. In this calculation the conversion coefficient for a 1410-kev γ quantum was taken to be 1.5×10^{-4} (an interpolation between the values $\Gamma_p = 2.2 \times 10^{-4}$ for $Z = 0$ and $\Gamma_p = 1.2 \times 10^{-4}$ for $Z = 84$) (cf. the table), and the intensity of electron capture into the 1532-kev level of Sm^{152} amounts to 25% of all the transitions of Eu^{152} (cf. Fig. 7). The area under the positron β spectrum was found by extrapolating the Fermi plot (Fig. 6) towards the lower energies.

As can be seen from Fig. 7, the observed β^+ decay agrees with the decay scheme of Eu^{152} confirmed by a number of workers.[1-4] The positron decay goes to the first excited state of Sm^{152}. According to the decay scheme this transition is first forbidden ($\Delta I = 1$, with a change of parity). This agrees with the experimentally-observed allowed shape of the β^+ spectrum. However, the observed value of $\log(\tau f) = 12.1$ is too large for a first forbidden transition. It should be noted that very large values of $\log(\tau f)$ are characteristic also for the other transitions in the decay of Eu^{152}, electron capture and β^- decay.

Grodzins and Kendall[15] have observed the β^+ decay of the Eu^{152m} isomer ($T_{1/2} = 9.2$ hours) to the ground state of Sm^{152}; the end-point energy of the spectrum was found to be 820 kev. The comparison of these data with those obtained in our work shows (cf. Fig. 7) that the energy interval between the ground and the isomeric states of europium is less than 20 kev.* This value differs appreciably from the value (80 ± 25 kev) obtained by Grodzins, but agrees with the value 30 ± 40 kev according to the data of Nathan and Waggoner.[4]

It should be noted that the data obtained by us on the total energy of the transition $Eu^{152} \rightarrow Sm^{152}$ do not agree with the results of the recently published paper by Bhattacherjee et al.[16]

In conclusion, the authors express their gratitude to V. M. Kel'man for his continued attention and interest in our work, and to L. A. Sliv for valuable remarks made in the course of discussing our results.

---

*According to reference 14 the capture cross section for Eu^{151} amounts to ~9000 barns with ≈1400 barns representing the cross section for the formation of the 9.2-hour isomer of Eu^{152}, while the capture cross section for Eu^{153} amounts to only ≈ 420 barns.

*The value quoted here does not take into account the error in the determination of the β^+-spectrum end-point energy by Grodzins and Kendall.[15]

[1] B. V. Bobykin and K. N. Novik, Izv. Akad. Nauk S.S.S.R. ser. fiz. 21, 1556 (1957) [Columbia Techn. Transl. 21, 1546 (1957)].

[2] Dzhelepov, Zhukovskii, and Nedovesov, Izv. Akad. Nauk S.S.S.R. ser. fiz. 19, 296 (1955) [Columbia Techn. Transl. 19, 269 (1955)].

[3] Cork, Brice, Helmer and Sarason, Bull. Am. Phys. Soc. 2, 316 (1957).

[4] O. Nathan and M. A. Waggoner, Nucl. Phys. 2, 548 (1957).

[5] J. M. Hill and L. R. Shepard, Proc. Phys. Soc. **A63**, 126 (1950).

[6] D. L. Kaminskii and M. G. Kaganskii, Приборы и техника эксперимента (Instruments and Meas. Engg.) (in press).

[7] G. E. Owen and H. Primakoff, Phys. Rev. **74**, 1406 (1948).

[8] Bisi, Germagnoli, and Zappa, Nucl. Phys. **1**, 593 (1956).

[9] A. Marty and M. Vergens, Compt. rend. **242**, 1438 (1956).

[10] J. C. Jaeger and H. R. Hulme, Proc. Roy. Soc. **A148**, 708 (1955).

[11] L. A. Sliv and I. M. Band, Таблицы коэффициентов внутренней конверсии (Tables of Internal Conversion Coefficients) Acad. Sci. Press, 1956.

[12] M. E. Rose, Phys. Rev. **78**, 184 (1950).

[13] J. O. Juliano and S. S. Stephens, Phys. Rev. **108**, 341 (1957).

[14] Атлас эффективных нейтронных сечений элементов (Atlas of Effective Neutron Cross Sections of the Elements), Acad. Sci. Press, 1955.

[15] L. Grodzins and H. Kendall, Nucl. Sci. Abstr. **10**, 12B, 254 (1956).

[16] Bhattacherjee, Nainan, Raman and Sahai, Nuovo cimento **7**, 501 (1958).

Translated by G. Volkoff
194

SOVIET PHYSICS JETP VOLUME 35(8), NUMBER 4 APRIL, 1959

TYPES OF INTERACTION IN BETA DECAY. THE DECAY OF Na^{24}

N. A. BURGOV and Iu. V. TEREKHOV

Submitted to JETP editor May 26, 1958

J. Exptl. Theoret. Phys. (U.S.S.R.) **35**, 932-939 (October, 1958)

The electron-neutrino correlation in the β decay of Na^{24} was investigated using nuclear resonance scattering of the Mg^{24} γ rays that accompany the β decay of Na^{24}. A gaseous Na^{24} source was employed. The most probable value of the correlation constant was found to be $\lambda = -0.23 \pm 0.19$. It follows from these data that in the β decay of Na^{24} only the axial vector interaction should be involved, which corresponds to $\lambda = -1/3$.

INTRODUCTION

AN important problem in the theory of weak interactions is the determination of the type of interaction in β^- decay. The discovery of parity nonconservation has increased the number of experiments which involve the interaction constants. Nevertheless at this time the question of determining the interaction types has not been solved.

Prior to the discovery of parity nonconservation the established belief was that β decay is due to tensor and scalar covariants in the interaction Hamiltonian. This view was based on the electron-neutrino correlation experiments in He^6 (references 1, 2) and Ne^{19} (references 3, 4) as well as on the absence of Fierz interferences in the experimental determinations of β-decay spectrum shapes.

However, as was shown by Lee and Yang,[5] the absence of Fierz terms does not prove that only one of the covariants is present in transitions governed by Fermi selection rules (scalar S and vector V covariants). Neither can it be concluded that only one of the axial vector or tensor covariants, which are responsible for β decays governed by Gamow-Teller selection rules, is present.

The absence of Fierz terms requires only that the following expression vanish*

$$\mathrm{Re}\{(C_V C_S^* + C_V' C_S^{*\prime}) |M_F|^2 + (C_T C_A^* + C_T' C_A^{*\prime}) |M_{GT}|^2\}, \quad (1)$$

which will happen if $C_S = -C_S'$, $C_V = C_V'$, $C_T = -C_T'$, $C_A = C_A'$. This follows from data on polarization of β electrons.[6] Furthermore, the angular correlation between the electron and neutrino in Ar^{35} was measured recently.[7] There are reasons to believe that the β^+ decay of Ar^{35} is mainly due to the Fermi type of interaction.

As a result of this experiment the correlation constant was found to be $\lambda = 0.70 \pm 0.17$, which means a substantial contribution from the vector interaction.

The results of the Ar^{35} experiment can be satisfactorily explained by a combination of either vector and axial vector, or vector and tensor interactions. Thus a contradiction resulted, and the necessity arose for further measurements of the interaction constants responsible for β decay.

1. EXPERIMENTAL PROCEDURE

In all experiments[1-4,7] mentioned previously the electron-neutrino correlation was determined from observations of the nuclear recoil. One of the authors[8] has proposed a different method for determining the correlation, utilizing the nuclear-resonance scattering effect of the γ-rays that accompany β decay. This method consists in the following:

Suppose that the radioactive substance has a decay scheme as shown in Fig. 1, i.e., the β decay is followed by two γ-rays in cascade, with energies $E_{\gamma 1}$ and $E_{\gamma 2}$.

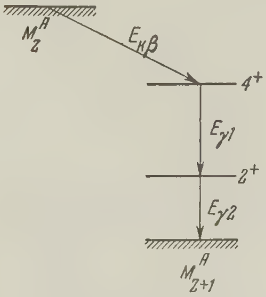

FIG. 1. Decay scheme.

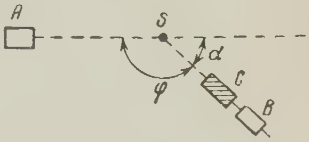

FIG. 2. Diagram of the setup.

In the experimental setup, shown schematically in Fig. 2, the detector A registers γ-rays of energy $E_{\gamma 1}$ and the detector B registers γ-rays of energy $E_{\gamma 2}$. A scatterer C is placed in the path of the γ-rays of energy $E_{\gamma 2}$, (corresponding to transitions to the ground state), consisting of M^A_{Z+1} nuclei resulting from the β^- decay of the M^A_Z nuclei of the source S. The detectors A and B are required to register in coincidence. The absorption of the γ-rays of energy $E_{\gamma 2}$ in the scatterer C is measured as a function of the angle φ between the directions of the observed γ-rays $E_{\gamma 1}$ and $E_{\gamma 2}$.

---

*We use the notation of reference 5.

Beside the usual absorption of γ-rays due to the photo-effect, Compton effect, and pair production there is the additional absorption in C due to resonance scattering of γ-rays by the nuclei of the scatterer.

As was shown in reference 8, the average resonance scattering cross section depends not only on the width Γ of the level in which the scattering takes place but also on the quantity λ which characterizes the interaction type in β decay. The average cross section equals

$$\bar{\sigma} = \sigma_0 \frac{\pi}{4} \frac{\Gamma}{E_{\gamma 2}} \int\limits_{p_0}^{p_{\mathrm{N\,max}}} \frac{m_1 c}{p_{\mathrm{N}}} f(p_{\mathrm{N}})\, dp_{\mathrm{N}}, \qquad (2)$$

where

$$p_0 = \left| \frac{E_{\gamma 1}}{c} \cos\alpha - \frac{E_{\gamma 2}}{c} \right|, \qquad \sigma_0 = 2\pi\lambda\!\!\!^{-}{}^2 (2j+1)/(2i+1), \qquad (3)$$

$\lambda\!\!\!^{-}$ is the wavelength of the γ-ray of energy $E_{\gamma 2}$, divided by 2π; j is the spin of the excited level; i is the spin of the ground level; Γ is the natural width of the excited level; m_1 is the nuclear mass; $p_{\mathrm{N\,max}}$ is the maximum momentum that the nucleus can receive in the process of β decay; $\alpha = \pi - \varphi$ (φ is the angle between the directions of emission of the two γ-rays); $f(p_{\mathrm{N}})$ is the distribution function of the recoil nuclei. This function $f(p_{\mathrm{N}})$ is normalized according to

$$\int\limits_0^{p_{\mathrm{N\,max}}} f(p_{\mathrm{N}})\, dp_{\mathrm{N}} = 1 \qquad (4)$$

and depends on the correlation constant λ of the β decay. In deriving Eq. (2) it was assumed that the recoil nuclei are free, i.e., that their motion during the lifetime of the excited states is not perturbed by collisions with other nuclei.

It was further assumed that no correlation exists between the directions of emission of the β- and γ-rays.

A numerical calculation was performed of the cross section for Na^{24} whose decay scheme is similar to that pictured in Fig. 1.

The energies of the β- and γ-rays were taken as follows:

$$E_{k\beta} = 1.4 \text{ Mev}, \quad E_{\gamma 1} = 2.76 \text{ Mev}, \quad E_{\gamma 2} = 1.38 \text{ Mev}.$$

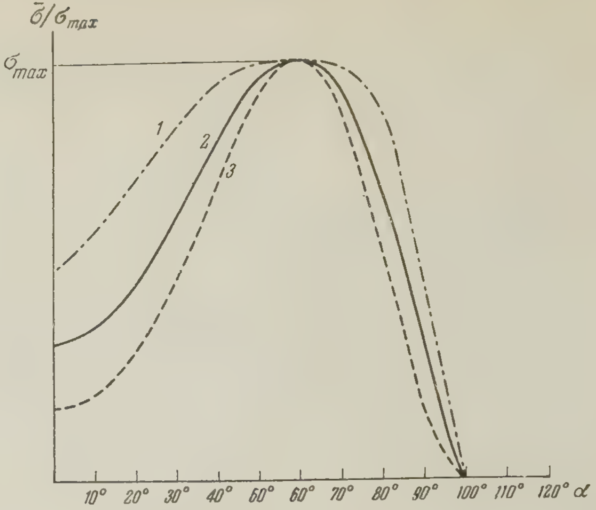

FIG. 3. Dependence of the cross section $\bar{\sigma}_r$ on the angle α: the curve labelled 1 corresponds to $\lambda = +1$, 2 – to $\lambda = 0$, 3 – to $\lambda = -1$.

The maximum of the cross section occurs for

$$\cos\alpha = E_{\gamma 2} / E_{\gamma 1}, \qquad (5)$$

i.e., for $\alpha = 60°$.

The dependence of the calculated cross section on the angle α is shown in Fig. 3 for the three values $\lambda = -1, 0, +1$. All curves are normalized to the same value at $\bar{\sigma} = \sigma_{\max}$. As can be seen, the angular dependence of the cross section varies noticeably with the values of the correlation constant λ.

2. DESCRIPTION OF THE SETUP AND EXPERIMENT

In this work the experiments on electron-neutrino correlation were performed with a gaseous source of Na^{24}.

The experimental setup, the block diagram of which is shown in Fig. 4, is essentially similar to the setup described previously.[9]

As is well known, metallic sodium in the gaseous state is monoatomic, consequently molecular binding did not have to be considered. To create a source of sufficient intensity it was necessary to keep it at a temperature of ~ 900°C, which corresponds to a vapor pressure of metallic sodium in a hermetic container of stainless steel of the order of one atmosphere. At this pressure the time between collisions should be longer than 10^{-11} sec.

Preliminary measurements[9] performed with a liquid-sodium source had shown that the lifetime of the level $E_{\gamma 2} = 1.38$ Mev was less than 2×10^{-12} sec. Therefore, in the gaseous source used, the recoil nuclei may be treated as free. Part of the metallic sodium remains in the liquid phase when the source is heated and the γ-rays from

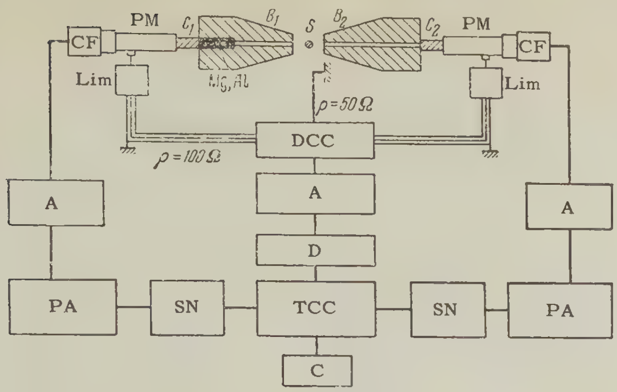

FIG. 4. Block diagram of the setup. S – γ-ray source, B_1 and B_2 – lead collimators, C_1 and C_2 – tolan crystals, PM – photomultiplier FEU-33, CF – cathode follower, Lim – limiters, DCC – double coincidence circuit ($2\tau = 2 \times 10^{-9}$ sec), A – amplifiers (K = 200, f = 3 Mc/sec), D – discriminator and tuning device to 10^{-6} sec, FU – shaping network for 10^{-6} sec, TCC – triple coincidence circuit ($2\tau = 10^{-6}$ sec), Ch – counter, PA – single channel pulse height analyzer.

the liquid phase were kept at < 1% of the γ-rays from the gaseous phase by blocking the lower part of the container with a lead shield.

The γ-rays were registered by scintillation counters consisting of FEU-33 photomultipliers and tolane crystals. The angle $\alpha = \pi - \varphi$ was varied by rotating one of the detectors around the axis of the source.

The pulse from each detector was fed into a "fast" coincidence circuit with a resolving time of 2×10^{-9} sec and, simultaneously, into a single-channel pulse-height analyzer so tuned as to pass only pulses from γ-rays of a single energy. From there the pulses were fed into a "slow" coincidence circuit of resolving time 10^{-6} sec and then were registered.

A scatterer composed of magnesium nuclei was placed in the path of the γ-rays headed for the counter registering γ-rays of energy $E_{\gamma 2} = 1.38$ Mev. Then α was varied from 0° to 100° and the additional absorption of γ-rays in magnesium due to resonant scattering was observed. In the aluminum scatterer no such resonant scattering should appear.

The magnesium scatterer was 80 mm long; the aluminum scatterer's length was so adjusted as to give the same absorption as magnesium in the absence of resonant scattering, i.e., at angles $\alpha > 100°$.

3. EXPERIMENTAL RESULTS AND ANALYSIS OF THE MEASUREMENTS

To exclude from the calculations the usual absorption of γ-rays due to the photoeffect, Compton effect, and pair production the ratio of the transparency of the magnesium and aluminum samples

$$A_k = \frac{T_{\mathrm{Mg}}}{T_{\mathrm{Al}}} = \frac{N_{\mathrm{Mg}}}{N} \bigg/ \frac{N_{\mathrm{Al}}}{N} = \frac{N_{\mathrm{Mg}}}{N_{\mathrm{Al}}} \qquad (6)$$

was measured for various angles α.

Here N_{Mg} is the number of true coincidences with the resonant scattering magnesium in place, N_{Al} is the number of true coincidences with the aluminum scatterer, N is the number of true coincidences without any scatterer, T_{Mg} and T_{Al} are the transparencies of the magnesium and aluminum absorbers.

However

$$T_{\mathrm{Mg}} = T_{\mathrm{Mg},a}\, T_{\mathrm{Mg},r}; \quad T_{\mathrm{Al}} = T_{\mathrm{Al},a}, \qquad (7)$$

where T_a is the transparency of the sample due to the usual absorption and scattering of γ-rays and T_r is the transparency due to the resonant scattering of γ-rays. Thus

$$\frac{N_{\mathrm{Mg}}}{N_{\mathrm{Al}}}(\alpha) = \frac{T_{\mathrm{Mg},a}}{T_{\mathrm{Al},a}}\, T_{\mathrm{Mg},r}(\alpha). \qquad (8)$$

The ratio $T_{Mg,a}/T_{Al,a}$ was determined experimentally without coincidences and found to be 1.0006 ± 0.0002, i.e., unity for all practical purposes. Therefore one may assume

$$T_{\mathrm{Mg},r}(\alpha) \approx N_{\mathrm{Mg}}(\alpha) / N_{\mathrm{Al}}. \qquad (9)$$

The experimentally determined absorption due to resonant scattering is shown in Table I for a few values of α.

TABLE I

α, °	$1-T_{Mg,r}(\alpha)$	α, °	$1-T_{Mg,r}(\alpha)$
0	0.011±0,004	40	0.036±0.007
10	0.015±0.006	60	0.052±0.004
15	0.017±0.004	85	0.026±0.009
30	0.032±0.005	120	0.001±0.004

Since the experimentally-determined transparency is near unity, one may write

$$1 - T_{\mathrm{Mg},r}(\alpha) = n_{\mathrm{Mg}}\bar{\sigma}_{\mathrm{Mg},r}\, d_{\mathrm{Mg}}, \qquad (10)$$

where $\bar{\sigma}_{Mg,r}$ is the resonant scattering cross section given by Eq. (2), n_{Mg} is the number of nuclei of the Mg^{24} isotope per unit volume of the scatterer, and d_{Mg} is the thickness of the magnesium scatterer.

From expression (10) we can calculate the maximum resonant scattering cross section. It is given by

$$\sigma_{\max} = (1.93 \pm 0.15) \cdot 10^{-25}\ \mathrm{cm}^2. \qquad (11)$$

If we denote by

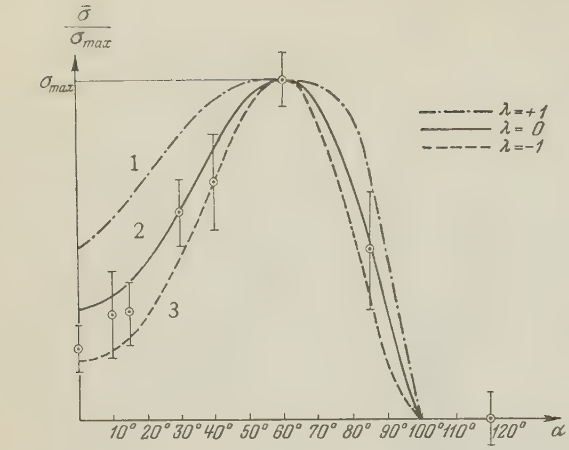

FIG. 5. Experimental results. 1 corresponds to λ = + 1, 2 to λ = 0, 3 to λ = – 1.

$$\overline{D} = \frac{\bar{\sigma}_{\mathrm{Mg},r}(\alpha)}{\sigma_{\max}(60^\circ)} = \frac{1 - T_{\mathrm{Mg},r}(\alpha)}{1 - T_{\mathrm{Mg},r}(60^\circ)} \qquad (12)$$

the quantities determined experimentally, and by D the ones calculated theoretically, we can obtain from Table I the ratios of the resonant scattering cross section to the maximum cross section for various angles α. The results are shown in Table II and plotted in Fig. 5.

TABLE II

α,°	$\overline{D} = \frac{\bar{\sigma}_{\mathrm{Mg},r}(\alpha)}{\sigma_{\max}(60^\circ)}$	α, °	$\overline{D} = \frac{\bar{\sigma}_{\mathrm{Mg},r}(\alpha)}{\sigma_{\max}(60^\circ)}$
0	0.21 ± 0.07	40	0.69 ± 0.14
10	0.29 ± 0.12	60	1.00
15	0.32 ± 0.09	85	0.50 ± 0.18
30	0.62 ± 0.10	120	0.00 ± 0.07

We included the root-mean-square errors in Table II and in Fig. 5. For each point the error $x = \overline{D} - D$, corresponding to a definite value of λ from +1 to –1, is characterized by the normal distribution law.

By multiplying the probabilities of all points referring to the same value of λ, we find the most probable distribution of $x = \overline{D} - D$ as a function of λ with the result

$$\lambda = -0.23 \pm 0.19. \qquad (13)$$

The error in measurement comes from the distribution of probabilities for λ, which lies in the indicated region with a probability of 67%.

From (2) and (11) we can determine the width, and therefore the lifetime of the excited level at 1.38 Mev. With λ = – 0.23 we find

$$\tau = (2.6 \pm 0.2) \cdot 10^{-13} \text{ sec.} \qquad (14)$$

Measurements were performed with a solid Na^{24} source. The technique used was the same as for the gaseous source. The results of the measurements are compiled in Table III.

TABLE III

α,°	$1 - T_{\mathrm{Mg},r}(\alpha)$
100	0.003 ± 0.008
90	0.000 ± 0.008
65	0.007 ± 0.008
62	0.010 ± 0.008
60	0.024 ± 0.006

TABLE IV

α,°	$1 - T_{\mathrm{Mg},r}(\alpha)$
0	0.001 ± 0.004
40	0.000 ± 0.005
50	0.003 ± 0.005
60	0.001 ± 0.004
100	0.001 ± 0.004

In this experiment, as in the liquid source experiment,[9] additional resonant absorption was observed only in a narrow region near the angle α = 60°.

The interpretation of the results for the solid source is analogous to that expounded in the paper dealing with the liquid source.[9]

The presence of the resonant scattering effect in a solid source indicates that the lifetime of the excited state with $E_{\gamma_2} = 1.38$ Mev is comparable to the time between collisions of the recoil nucleus in the solid (of the order 10^{-13} sec), which confirms the result (14).

In order to be assured that the measured resonant scattering effect was not due to some asymmetry in the apparatus we performed a control experiment using a Co^{60} source in place of Na^{24}. The decay scheme of Co^{60} is similar to that of Na^{24} except that the emitted γ-rays have energies $E_{\gamma_1} = 1.17$ Mev and $E_{\gamma_2} = 1.33$ Mev. The results of this experiment are shown in Table IV.

It is seen that there is no dependence of the absorption on the angle α, proving the absence of asymmetries in the apparatus.

4. DISCUSSION OF RESULTS AND CONCLUSIONS

In the process of β^- decay the Na^{24} nucleus of spin and parity 4^+ is transformed into the 4^+ level of the Mg^{24} nucleus. Thus, this is a $j \rightarrow j$ transition allowed by both the Fermi ($\Delta j = 0$, no) and the Gamow-Teller ($\Delta j = 0, \pm 1$, no, $0 \rightarrow 0$) selection rules.

However from a consideration of the isotopic spin T and the experiments on circular polarization of Na^{24} γ-rays* it will follow that the Fermi matrix element should be much smaller than the Gamow-Teller matrix element.

Experiments on the circular polarization of γ-rays from a number of emitters, including Na^{24}, are described in references 10 and 11. It is found that the polarization coefficient α is small, which allows the conclusion to be drawn that the β decay of Na^{24} is due to only Gamow-Teller or only Fermi interaction type. If both types were present simultaneously, the interference term would increase greatly and α would be large.

---

*We are grateful to A. I. Alikhanov, V. A. Liubimov, and K. A. Ter-Martirosian for calling these possibilities to our attention.

In view of the importance of the question, one more experiment[12] on the circular polarization of Na^{24} γ-rays was performed.

The circular polarization of γ-rays was detected by using the method of transmission of γ-rays through a ferromagnetic alloy whose thickness was several radiation lengths for 2.76-Mev γ-rays. As result the sensitivity was somewhat higher than in other experiments[10,11] where the circular polarization was deduced from the dependence of the intensity of the scattered γ-rays on the direction of the magnetic field. The results of this work again indicate no significant interference term within the limits of experimental errors.

Consider next the isotopic spin T. Fermi type transitions are governed by the selection rule $\Delta T = 0$, Gamow-Teller type by $\Delta T = 0, \pm 1$.

The ground state of Na^{24} has $T_\xi = -1$. If the rule is invoked that the ground state has the smallest possible isotopic spin, the isotopic spin of Na^{24} ground state is expected to be $T = 1$ and of Mg^{24} ground state $T = 0$.

It is known that excited states of Mg^{24} with $T = 1$ appear only for excitation energies ~ 10 Mev; all lower levels have $T = 0$.

It has been shown[13] that the β^+ transition $Al^{24} \rightarrow Mg^{24}$ to the 9.35 Mev excited state is a super allowed (log ft = 3.35) $\Delta j = 0$, $\Delta T = 0$, $T = 1$, $A = 4n$ type transition; consequently the 9.35-Mev level has $T = 1$.

Wilkinson calculated the first $T = 1$ level of Mg^{24}, excluding the Coulomb term from the binding energy, and found for its energy 9.45 Mev, which is in close agreement with experiment. Therefore the 4.14-Mev energy level will have isotopic spin $T = 0$. If that is the case, Fermi type transition can only amount to a small admixture to the Gamow-Teller type due to the inexactness of isotopic spin quantum numbers.

It may therefore be taken as established that the β decay of Na^{24} is due predominantly to the Gamow-Teller interaction type, i.e.,

$$|M_F|^2 \ll |M_{GT}|^2.$$

It then follows from the present work that in β-decay governed by Gamow-Teller selection rules the interaction type is axial vector, corresponding to the correlation constant $\lambda = -0.33$.

Taking into account the errors in the present experiment, the conclusion may be drawn that the tensor interaction is not the sole one, as would follow from the He^6 experiment,[2] but that it is present only as an admixture to the basic axial vector interaction.

The authors are grateful to Academician A. I. Alikhanov, K. A. Ter-Martirosian and V. A. Liubimov for numerous discussions and advice; and to A. I. Zubkov, V. G. Alpatov, and K. H. Rostovtsev for help in carrying out the experiment.

---

[1] B. M. Rustad and S. L. Ruby, Phys. Rev. **89**, 880 (1953).

[2] B. M. Rustad and S. L. Ruby, Phys. Rev. **97**, 991 (1955).

[3] W. P. Alford and D. R. Hamilton, Phys. Rev. **95**, 1351 (1954).

[4] Maxson, Allen, and Jentschke, Phys. Rev. **97**, 109 (1955).

[5] T. D. Lee and C. N. Yang, Phys. Rev. **104**, 254 (1956).

[6] Alikhanov, Eliseev, and Liubimov, J. Exptl. Theoret. Phys. (U.S.S.R.) **34**, 1045 (1958), Soviet Physics JETP **7**, 723 (1958).

[7] Herrmannsfeldt, Maxson, Stähelin, and Allen, Phys. Rev. **107**, 641 (1957).

[8] N. A. Burgov, J. Exptl. Theoret. Phys. (U.S.S.R.) **33**, 655 (1957), Soviet Phys. JETP **6**, 502 (1958).

[9] N. A. Burgov and Iu. V. Terekhov, **Атомная энергия** (Atomic Energy) **2**, 514 (1957).

[10] H. Schopper, Phil. Mag. **2**, 710 (1957).

[11] F. Boehm and A. H. Wapstra, Phys. Rev. **109**, 456 (1958).

[12] Alikhanov, Liubimov, Balats, Lebedev, and Obukhov, Report at Paris Conference, July, 1958.

[13] M. Bolsterli and E. Feenberg, Phys. Rev. **97**, 736 (1955).

[14] D. H. Wilkinson, Phil. Mag. **1**, 1031 (1956).

Translated by A. Bincer
195

SOVIET PHYSICS JETP VOLUME 35(8), NUMBER 4 APRIL, 1959

ENERGY OF THE X-RAYS EMITTED BY INTENSE PULSED DISCHARGES IN HYDROGEN

N. G. KOVAL' SKII, I. M. PODGORNYI, and S. KHVASHCHEVSKII

Submitted to JETP editor May 27, 1958

J. Exptl. Theoret. Phys. (U.S.S.R.) 35, 940-946 (October, 1958)

The maximum energy of the x-rays emitted by an intense pulsed hydrogen discharge has been determined. The energy values presented are obtained from an analysis of the recoil-electron energy spectrum measured in a cloud chamber.

1. INTRODUCTION

It has been reported[1] that strong x-rays are generated by intense pulsed discharges in light gases for certain values of the initial pressure. It has also been observed that under the same conditions the curves of discharge voltage and current exhibit characteristic discontinuities at well-defined instants of time. The appearance of the x-ray burst usually coincides with the appearance of the second break on the current curve. In discharges in heavy gases[2] the x-ray energy is found to be considerably smaller than in light gases. If the discharge takes place in deuterium, neutron bursts are observed in addition to the x-ray bursts.[3]

The neutron bursts from pulsed discharges in deuterium have been studied by a number of authors (cf., for example, references 4 to 6); on the other hand, since the appearance of the first papers in this field there has been practically no information concerning the properties of the hard x-rays produced by a gas discharge in a cylindrical chamber.

The present work describes measurements of the energy of the x-rays characteristic of a hydrogen discharge. These measurements were undertaken in order to obtain data which would serve as a basis for the analysis of the mechanisms which have been proposed to explain the acceleration of charged particles in pulsed high-current discharges.

2. METHOD OF MEASUREMENT

In 1953, when hard x-rays were first observed in intense discharges in hydrogen and deuterium, estimates were made of the upper energy limits of the x-ray spectrum. Various approaches were used in making these estimates: filter measurements, measurements of the length of recoil-electron tracks in nuclear emulsions, measurements with shielded scintillation detectors, and photoeffect measurements [the (γ, n) reaction in Be]. From an analysis of these measurements it was definitely established that the x-ray energies were of the order of hundreds of kev although the voltage across the discharge tube was 10 to 20 kv. However, because of the slope of the spectral distribution curve it was difficult to set an upper limit on the energy.

In the present work, in order to make a more precise determination of the x-ray energy the measurements have been carried out in a cloud chamber. The use of a cloud chamber makes it possible to avoid certain difficulties which are characteristic of the methods cited above. The basic advantage of the cloud chamber in studying short x-ray bursts is the relatively small time during which the instrument is sensitive. Nuclear emulsions record the cosmic-ray background throughout the entire experiment; the cloud chamber is sensitive for only a short period of time so that there is a considerable improvement in the signal-to-noise ratio. Moreover, the possibility of following tracks of recoil electrons or photoelectrons which are formed by single photons, without any interference due to the pulsed discharge, represents a considerable advantage for the cloud chamber as compared with a shielded scintillation detector.

The energy of the electrons was determined from measurements of track length in the chamber. The well-known method by which electron energy is determined from the curvature of the trajectory in a magnetic field could not be used in the present work, because at electron energies of 200 kev the mean scattering angle is considerably greater than the largest angle for which the track curvature can be measured.

To determine the energy of the x-ray photons from the electron energies, one must decide whether these electrons are formed as a result of the photoeffect or the Compton effect. At energies of 200 to 400 kev the probability for the photoeffect in air, with which the cloud chamber is filled, can be neglected as compared with the probability for the Compton effect. However, the production of photo-electrons in the glass walls of the cloud chamber can be important at these energies. The ratio σ_c/σ_{ph}, as a function of energy of the x-ray photons, was computed theoretically for glass; the results of the calculation are shown in Fig. 1. Inasmuch as the purpose of the work was a determination of the limiting energy of the x-ray photons, the Compton probability was computed for electrons acquiring energies from $0.9\,E_{max}$ to E_{max}, where E_{max} is the maximum energy transferred by the photon to the electron in the Compton process. As is apparent from Fig. 1, the predominance of Compton electrons in glass is insignificant in the photon-energy region around 200 kev. However, the probability of Compton formation can be greater for the entire cloud chamber. To verify this point we carried out calibration experiments in which the chamber was exposed to an x-ray flux of known energy from a pulsed x-ray tube.

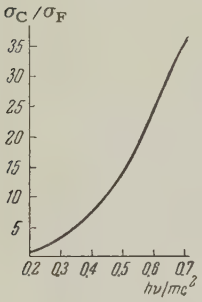

FIG. 1. Ratio for the probabilities of the Compton effect and photoeffect in glass.

3. EXPERIMENTAL SETUP

The pulsed discharges in hydrogen were produced with a bank of twelve capacitors (IM-3/50) totaling 36 μf. The discharges were excited in a porcelain tube 170 mm in diameter and 1000 mm long. In order to reduce the lead inductance of the circuit, the discharge tube was located in a coaxial line and placed directly above the capacitors. The stray inductance of the external circuit was 0.5 μh. The capacitor bank could be charged to 50 kv from a high-voltage supply. The external circuit was closed by triggering a thyratron (cf. Fig. 2). The triggering pulse was obtained from a special system which was controlled by a mechanical synchronizer. After each discharge the tube was evacuated and filled with a new charge of hydrogen gas. The hydrogen was admitted to the discharge tube from a measured volume which was first filled to a known pressure through a nickel filter. Under these conditions a controlled amount of gas could be admitted to the discharge tube regardless of the wall temperature.

The discharges were produced at hydrogen pressures of 6×10^{-2} mm Hg. The maximum x-ray intensity was found at this pressure for the experimental conditions described here. For a pressure of 6×10^{-2} mm Hg and a voltage of 40 kv the peak current was 200 kiloamperes.

The spectrum of the electrons produced by x-ray photons was measured with a cloud chamber with a rubber diaphragm. The chamber diameter was 280 mm and the depth was 80 mm. The chamber was charged with purified air and a water-alcohol mixture (66% alcohol and 33% water) to a pressure of 2 atmos (abs). Illumination was furnished by pulsed lamps (IPK-600). The pictures were taken with a camera with a "Jupiter 1.5" lens. The chamber was triggered simultaneously with the application of the voltage to the discharge tube. The light pulse was delayed with respect to the chamber expansion by means of a special mechanical synchronizing system (Fig. 2). An electronic synchronizing system could not be used because of the interference due to the discharge itself.

It is difficult to follow the tracks produced by high-energy electrons because of the large number of short tracks on the photographs. For this reason, the measurements in the high-energy re-

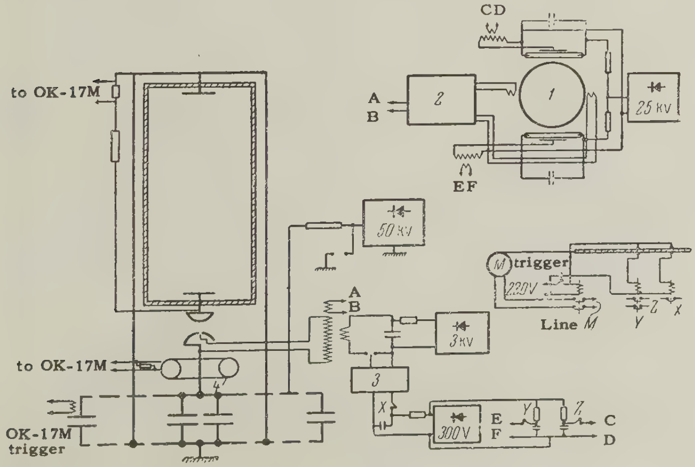

FIG. 2 Diagram of the apparatus. 1) Cloud chamber 2) Control system for the cloud chamber 3) Pulse transformer 4) Rogovskii loop.

gion were made with the cloud chamber shielded from the discharge tube by a thick layer of lead, which is a strong absorber for soft x-rays. The discharge tube was surrounded by lead shields 15 mm thick. Since the maximum x-ray intensity is found close to the electrode which is at the positive potential when the discharge is initiated ("anode"), the cloud chamber was mounted at the same height as the "anode" and at a distance of approximately 1 meter from the axis of the discharge tube.

The time behavior of the discharge was observed with a two-beam pulsed oscilloscope (OK-17M). The current flowing in the main circuit of the pulsed generator was measured with a Rogovskii loop and an RL integrating network. The Rogovskii loop was a toroidal coil which linked the conductor carrying the current. The winding was terminated by a small non-inductive resistance. The voltage across the resistance R is given by the simple formula $V = RI/n$ where I is the current and n is the number of turns in the coil. The voltage from the non-inductive resistance R was applied to one of the pairs of plates of the pulsed oscilloscope. The Rogovskii loop was characterized by the following parameters: $n = 300$ and $R = 0.256\,\Omega$.

The voltage was measured with a low-resistance divider, connected across the discharge tube. The total resistance of the divider was 100,000 ohns. The voltage was fed to the other pair of plates through a 100-ohm resistance. The relative x-ray intensity was measured with a scintillation detector consisting of a FEU-19M photomultiplier and an NaI crystal. The pulse from the multiplier was fed to an amplifier which was specially designed to operate in the presence of the strong interference due to the discharge. The amplifier output was applied to the plates of the oscilloscope; the discharge current or voltage pulse could be applied to the other pair of plates.

The voltage and current pulses and the pulses from the scintillation detector were fed to the oscilloscope through RK-2 cable. All cable connections were carefully shielded. The oscilloscope was triggered from a coil located at the high-voltage input of one of the condensers. A typical current oscillogram and detector pulse are shown in Fig. 3.

The calibration measurements were made with a pulse generator which supplied voltages up to 300 kv. The pulses from the generator were applied to a ZBPM-200 x-ray tube. This tube can be pulsed at 300 kv if it is oil-cooled and operated at reduced filament current (after a suitable period of processing). In order to be sure that the experimental conditions were the same in the discharge experiments and the calibration experiments, the pulsed x-ray tube was shielded by a lead sheet 15 mm thick.

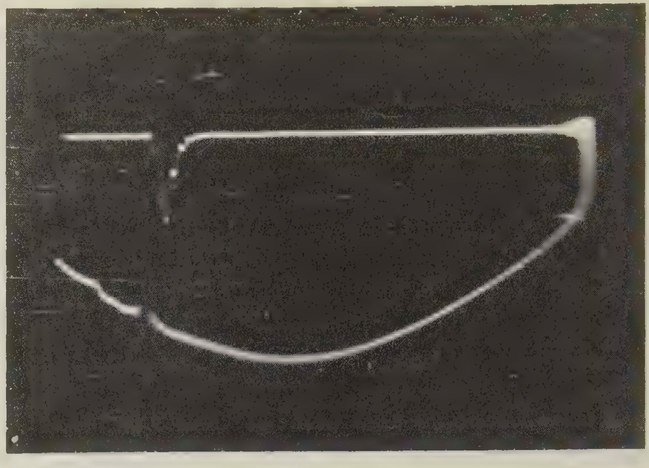

FIG. 3. Oscillogram of the discharge current and the x-ray burst. The total length of the sweep is 20 microseconds.

4. RESULTS OF THE MEASUREMENTS

It is well-known that the intensity of the x-ray bursts varies strongly from discharge to discharge. For this reason simultaneous observations were made of the tracks in the cloud chamber and the pulses from the scintillation detector. If no pulse was observed on the oscillogram the track picture was not used. Thus, in the analysis we excluded track photographs of discharges in which the x-ray yield was small. In some cases the x-ray bursts were so intense that it was difficult to follow individual tracks. Such photographs were also rejected.

Since the tracks were photographed with a single camera the photographs represent the projection of the electron tracks on the plane perpendicular to the optical axis of the camera. If the projected track is highly curved the projected length is $\pi/4$ of the actual length. Curved electron tracks have been studied in reference 7; in this work it has been shown that this correction factor yields a rather high degree of accuracy.

To analyze the experimental data the photographs were enlarged to natural size; the tracks were then traced carefully and the lengths were measured. In order to obtain the true range of the electrons in the chamber the measured track lengths were multiplied by $4/\pi$, as indicated above. The electron energies were determined from an energy-range curve which was plotted using well-known experimental values.

In order to measure the background, the

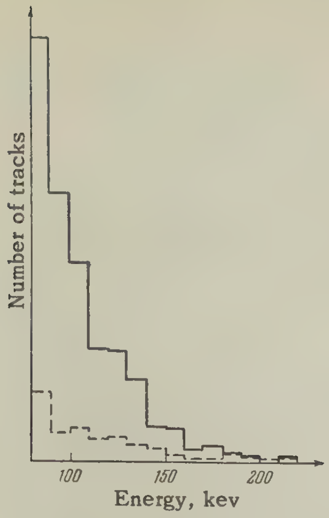

FIG. 4. Energy distribution for the recoil electrons formed by x-rays from a gas discharge.

chamber was operated again after taking each x-ray electron picture, and photographs were made of the tracks due to the cosmic-ray background and the residual radioactivity. A histogram of the energy spectrum of the x-ray electrons from a hydrogen discharge is shown in Fig. 4. The spectrum measured for the background electrons is shown in the same figure (dashed). The same number of x-ray electron track photographs and background photographs were analyzed in plotting these histograms. Of a total of 500 photographs, 189 were found suitable in accordance with the criteria given above.

In Figs. 5 and 6 are shown the calibration histograms for the electron spectra produced in the chamber by x-rays from the pulsed tube. The x-ray tube was pulsed at 240 and 285 kv. The upper limits for the electron energy in these histograms is 120 and 140 kev respectively.

It follows from the theory of the Compton effect that the maximum energy of Compton electrons produced by x-ray photons of 240 and 285 kev is 116 and 145 kev. Within the limits of the present accuracy, these values are in agreement with the experimental results. For these same x-ray energies the maximum energy for photoelectrons ejected from the glass (highest ionization potential approximately 20 kv) is 220 and 265 kev.

Thus, the experimental data indicate that at energies above 200 kev the probability of the Compton effect is considerably greater than the probability of the photoeffect.

An examination of the histogram in Fig. 4 indicates that the upper energy limit for electrons in the cloud chamber is 180 kev for discharges in hydrogen. If we assume that the limiting-energy electrons are Compton electrons, we can find the energy of the x-ray photons. The appropriate calculation indicates that an intense discharge in hydrogen with 40 kv across the capacitor produces x-ray photons with energies of 320 kev. These same experimental data show that the x-ray photons with energies greater than 320 kev represent, on the average, less than 0.1% of the total number of photons from the discharge.

The voltage across the discharge tube was measured by different methods and the results were consistent. The error in all measurements was less than 5%. It may be noted, however, that the upper energy limit was obtained by averaging over a large number of pulses; hence it is possible that the spectrum of an individual discharge may contain photons with higher energies.

5. CONCLUSIONS

A comparison of the experimental data pertaining to neutron and x-ray bursts in intense discharges in deuterium and hydrogen would seem to indicate that the mechanism is the same for both gases.

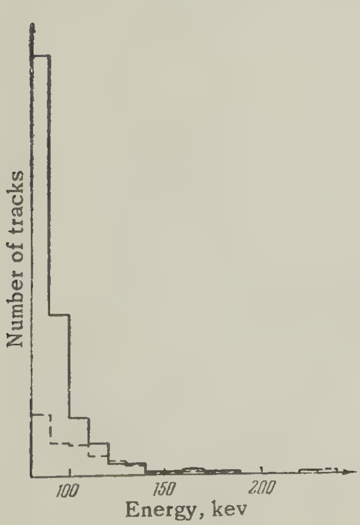

FIG. 5. Distribution of electrons formed by the x-rays from a pulsed x-ray tube.

FIG. 6. Distribution of electrons formed by the x-rays from a pulsed x-ray tube.

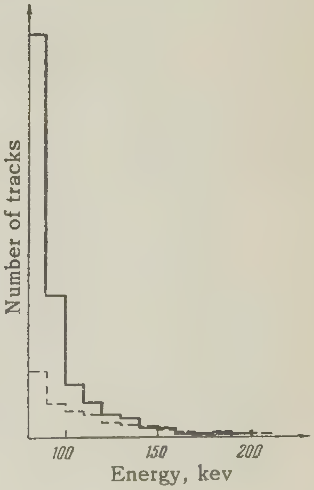

It may be of interest to list the presently available experimental facts pertaining to the hard radiation from a gas discharge.

1. The neutron and x-ray bursts are observed at the same time in the development of the discharge.
2. The deuterons associated with the neutrons in a deuterium discharge are accelerated toward the cathode, whereas the maximum x-ray intensity is found in the region of the anode.
3. The x-ray and neutron radiation are observed only for a well-defined region of initial pressures in the discharge tube; this region is the same for both types of radiation.
4. The maximum deuteron energy is estimated as 250 kev. Within the limits of the experimental errors this value is in good agreement with the upper limit of the x-ray spectrum (and consequently the electrons which are produced by x-ray photons) obtained in the present work, which is 320 kev.

All these factors indicate that the neutron and x-ray radiation can not be explained by some type of betatron acceleration mechanism;[8] this conclusion has already been indicated.[1]

The experimental facts indicate that there is a relation between the hard x-rays from intense pulsed discharges and the neutron radiation produced in deuterium discharges. These radiation effects result, apparently, from the production of electric fields along the axis of the discharge tube; these fields accelerate the charged particles (electrons and ions). As has been indicated in reference 1, these electric fields may be produced as a result of the redistribution of current which follows a change in the radius of the discharge column. When certain types of instabilities arise these fields can become very strong; in particular, strong fields can be produced as a result of constrictions in the discharge column.

The authors are indebted to L. A. Artsimovich and S. Iu. Luk'ainov for valuable discussions and to T. L. Asatiani for assistance in the construction of the cloud chamber.

---

[1] S. Iu. Luk'ianov and I. M. Podgornyi, Атомная энергия (Atomic Energy) 3, 97 (1956).

[2] I. M. Podgornyi and S. A. Chuvatin, Dokl. Akad. Nauk SSSR **117**, 795 (1957), Soviet Phys. "Doklady" **2**, 543 (1957).

[3] L. A. Artsimovich, Andrianov, Dobrokhotov, Luk'ianov, Podgornyi, Sinitsin, and Filippov, Атомная энергия (Atomic Energy) 3, 84 (1956).

[4] Anderson, Baker, Colgate, Ise, and Pyle, Report to the International Conference on Gaseous Discharges, Venice, June (1957).

[5] Berglund, Nilsson, Ohlin, Siegbahn, Sundström, and Svennerstedt, Nuclear Instruments **1**, 233 (1957).

[6] L. C. Burkhardt and R. H. Lovberg, Nature **181**, 228 (1958).

[7] San-Tsiang, Marty, and Dreyfus, J. phys. et radium **8**, 269 (1947).

[8] Ia. P. Terletzkii, J. Exptl. Theoret. Phys. (U.S.S.R.) **32**, 927 (1957), Soviet Phys. JETP **5**, 755 (1957).

Translated by H. Lashinsky
196

SOVIET PHYSICS JETP VOLUME 35(8), NUMBER 4 APRIL, 1959

ON THE THEORY OF LONGITUDINAL RELAXATION OF PARAMAGNETIC SALT SOLUTIONS

S. A. AL' TSHULER and K. A. VALIEV

Kazan' State University; Kazan' Pedagogical Institute

Submitted to JETP editor March 18, 1958

J. Exptl. Theoret. Phys. (U.S.S.R.) 35, 947-958 (October, 1958)

Paramagnetic longitudinal (spin-lattice) relaxation in solutions of salts of the iron group and rare earth elements is considered theoretically. The calculations are based on the assumption that, like ionic crystals, liquid solutions contain paramagnetic complexes. The normal vibrations of these complexes are perturbed by the Brownian motion of the surrounding particles; as a result, the electric field acting on the paramagnetic ions is changed and relaxation transitions are induced between different stationary states. It is shown that, when the interval between the two lower Stark sublevels of the ion is $\delta \sim 2kT$, two longitudinal relaxation times exist; one is due to transitions between various Stark (orbital) levels without spin flip, and the other is due to transitions within a Stark level with change of the spin direction. The paramagnetic resonance line width is due to transitions of the first type. The predictions of the theory are in good agreement with the experimental data referring on copper, chromium, and manganese salt solutions.

1. INTRODUCTION

THE current theories of longitudinal (spin-lattice) relaxation in liquid solutions of paramagnetic salts are in contradiction with many experimental facts. At the base of the theory of Bloembergen, Purcell, and Pound,[1] which finds wide application in the region of nuclear magnetic resonance, lies the assumption that the exchange of energies between the spin system and Brownian motion takes place through the fluctuations of the magnetic dipole-dipole interaction of the particles, brought about by this Brownian motion. In its application to solutions of paramagnetic salts, this theory gives values for the longitudinal relaxation times which are comparable to those observed by experiment only for very high concentrations of the magnetic particles.

McConnell[2] and McGarvey[3] have proposed another relaxation mechanism. They consider the paramagnetic ion, together with the solvate shell surrounding it, as a "micro-crystallite" which can rotate under the action of Brownian motion. The energy of the paramagnetic ion in the external magnetic field H, the Stark splitting of the spin levels in the crystalline field, and the hyperfine structure will depend on the direction of H relative to the axes of the crystallite. Therefore, rotations of the crystallite produces an exchange of energy between the paramagnetic ion and Brownian motion. The theoretical conclusions of McConnell and McGarvey confirm the experimental investigations of the paramagnetic-resonance line width in absorption, which unfortunately has been carried out only at a single frequency of the radiofrequency field and at one temperature. The many-sided experimental investigation of paramagnetic resonance in liquid solutions of salts, carried out by Kozyrev[4] at different temperatures and over a wide frequency range, has revealed that, in the majority of cases, the experimental dependence of the longitudinal relaxation time on temperature and direction of the applied magnetic field is completely at variance with the predictions of the theory.[2,3] Evidently, none of the different mechanisms which can guarantee spin-lattice interaction could be considered important in current theories. We shall show that the principal mechanism corresponding to paramagnetic relaxation in liquids of paramagnetic solutions is the following.

In solid paramagnetic ionic crystals, the paramagnetic particle m and with the adjacent diamagnetic particles X usually form a paramagnetic complex, for example, MX_6 (M is a metallic ion, X is a molecule of water or other diamagnetic particle), the internal interaction of which must be considered first in the explanation of magnetic properties of the material. In solutions, the presence of a solvate shell allows us to make a similar assumption. We can assume that, at least in the course of time larger than the correlation time of the spin-lattice interaction, the paramagnetic ion and the neighboring molecules of the solvent form a stable complex whose vibrations can be characterized by a set of normal coordinates Q_1. The Brownian motion of the molecule of the liquid excites vibrations of the paramagnetic complex, and the latter changes the electric field in which the paramagnetic particle finds itself. This change is shown in the spin-orbit interactions of the electrons of the paramagnetic ion, and consequently can bring about a re-orientation of its magnetic moment.

2. METHOD OF COMPUTATION

The Hamiltonian that takes into account both the internal interaction of the paramagnetic ion M and the effect on it of the surrounding diamagnetic particles X of the complex is of the form

$$\hat{\mathscr{H}} = \hat{\mathscr{H}}_0 + \hat{\mathscr{H}}'(t), \qquad (1)$$

where the main part $\hat{\mathscr{H}}_0$ contains the coordinates and the spin variables of the electrons of the ion M, while the perturbation $\hat{\mathscr{H}}'$ depends also on the normal coordinates Q_i of the complex, which are random functions of the time t. Let E_l and E_k be a pair of energy levels of the unperturbed system $\hat{\mathscr{H}}_0$. We shall be interested in transitions of E_l and E_k under the action of the perturbation $\hat{\mathscr{H}}'$, the probability of which is obviously proportional to the square of the modulus of the matrix element $\mathscr{H}'_{lk}(t)$. Since $\mathscr{H}'_{lk}$ depends on Q_i, we shall apply the method of correlations. If we introduce the correlation function $K_{lk}(\tau) = \overline{\mathscr{H}'_{lk}(t)\,\mathscr{H}'_{lk}(t+\tau)}$ in the usual way, then the average transition probability per second between the levels E_l and E_k will be equal to

$$A_{lk} = \hbar^{-2} J(\omega_{lk}), \qquad (2)$$

where $\omega_{lk} = (E_l - E_k)/\hbar$ while $J(\omega_{lk})$ is the Fourier component of the correlation function, equal to

$$J(\omega_{lk}) = \int_{-\infty}^{\infty} K_{lk}(\tau) \exp(i\omega_{lk}\tau)\, d\tau. \qquad (3)$$

If it is assumed that the dependence of the correlation function on τ is determined by a Markoff law:

$$K_{lk}(\tau) = K(0) \exp(-|\tau|/\tau_c), \qquad (4)$$

then the transition probability takes the form

$$A_{lk} = \hbar^{-2}\, \overline{|\mathscr{H}'_{lk}|^2}. \qquad (5)$$

The meaning of the correlation time τ_c will be explained below.

In what follows, we shall assume for definiteness that the paramagnetic complex contains six diamagnetic particles X, distributed at the vertices of an octahedron. The spin-lattice interactions that arise through the normal vibrations of the octahedral complex were considered by Van Vleck,[5] who found that

$$\hat{\mathscr{H}}' = \sum_{i=2}^{6} V^{(i)} Q_i, \qquad (6)$$

where

$$V^{(2)} = -18C(x^2 - y^2), \quad V^{(3)} = -18C(r^2 - 3z^2)/\sqrt{3},$$
$$V^{(4)} = 24Cxy, \quad V^{(5)} = 24Cxz, \quad V^{(6)} = 24Cyz, \quad C = e'\mu/R^5. \qquad (7)$$

here $\mathbf{r}(x, y, z)$ is the radius vector drawn from the nucleus to the electron of the unfilled shell M; R is the equilibrium distance between the particles M and X, e′ is the charge of the ion M, and μ is the dipole moment of the molecule X. In the expressions derived for the coefficients $V^{(i)}$, terms proportional to $(r/R)^4$ and $(r/R)^6$ are omitted.

Thus, if we substitute

$$\mathscr{H}'_{lk}(t) = \sum_i V^{(i)}_{lk} Q_i(t) \qquad (8)$$

in formula (5) and consider the orthogonality of the normal coordinates, we obtain

$$A_{lk} = (\overline{Q^2}/\hbar^2) \sum_i |V^{(i)}_{lk}|^2\, 2\tau_c/(1 + \omega^2_{lk}\tau^2_c). \qquad (9)$$

For all normal vibrations, we have introduced a certain average quantity $\overline{Q_i^2} = \overline{Q^2}$.

It is known from optical[6] that the eigenfrequencies of the normal vibrations of the octahedral complexes of ions of the transition group lie within the range 4×10^{13} to 16×10^{13} sec^{-1} (200 to 800 cm^{-1}). The quantum mechanical mean square of the amplitude of the oscillator is equal to

$$\overline{Q^2} = (\hbar/2m\omega_0) \coth(\hbar\omega_0/2kT). \qquad (10)$$

For all normal coordinates Q_i of the complex, we have introduced a certain average frequency ω_0 and mass m (close to the mass of the complex).

The correlation time τ_c of the oscillators Q_i, brought about by the action of the dissipative forces, is naturally determined as the reciprocal value of the damping coefficient γ which can be compared with the width of the satellite lines in the Raman spectra of paramagnetic ions: $\gamma \sim 10$ cm^{-1} and $\tau_c \approx 1/\gamma \sim 10^{-12}$ sec. From experimental data (see reference 8) on the temperature dependence of the line width of the vibrational structure of optical spectra of the ions in crystals, it follows that the width increase upon heating is proportional to $\sqrt{T}$. We can reach this conclusion also by starting from theoretical considerations.[8,9] Thus the temperature dependence of the transition probability (9) will be given by the formula

$$A_{lk} \sim T^{-1/2} \coth (\hbar\omega_0 / 2kT) \qquad (11)$$

for $\tau_c^2 \omega_{lk}^2 \ll 1$, and

$$A_{lk} \sim T^{1/2} \coth (\hbar\omega_0 / 2kT) \qquad (12)$$

for $\tau_c^2 \omega_{lk}^2 \gg 1$.

Finally, we shall establish a simple connection which exists between the probabilities of relaxation transitions in liquid solutions and the probabilities of single phonon processes in crystals. For crystals, the transition probability is computed from the formula (see reference 10):

$$A_{lk}^{(k)} = 2\pi\hbar^{-2} \rho_{\omega_{lk}} \overline{|\mathscr{H}'_{lk}|^2}, \qquad (13)$$

where $\rho_\omega = 3V\omega^2/2\pi v^3$ is the spectral density of vibrations of the lattice of frequency ω, v is the average sound velocity, V is the volume of the crystal. If we denote the mass of the crystal by M_0, and the temperature by T_0, then the mean square of the matrix element of the energy of spin-lattice coupling will have the form:

$$\overline{|\mathscr{H}'_{lk}|^2} = \sum_i |V_{lk}^{(i)}|^2 \frac{\hbar}{2M_0\omega_{lk}} \frac{2R^2\omega_{lk}^2}{15 v^2} \frac{\exp (\hbar\omega_{lk} / kT_0)}{\exp (h\omega_{lk} / kT_0) - 1} . \qquad (14)$$

Assuming $\hbar\omega_{lk} = g\beta H \ll kT_0$, we obtain

$$A_{lk}^{(k)} = (1/5\,\pi\hbar^2) \sum_i |V_{lk}^{(i)}|^2 (R^2\omega_{lk}^2 / \rho v^5)\, kT_0, \qquad (15)$$

where ρ is the density of the crystal. Comparing (15) and (9), we readily obtain

$$A_{lk} = \frac{5\pi\rho v^5}{\omega_{lk}^2 (kT_0)} \frac{\overline{Q^2}}{R^2} \frac{2\tau_c}{1 + \omega_{lk}^2 \tau_c^2} A_{lk}^{(k)}. \qquad (16)$$

Taking for the constants the values $\rho = 2$ gm/cm^3, $v = 2 \times 10^5$ cm/sec, $T = 300°K$, $T_0 = 1°K$, $\overline{Q^2}/R^2 = 10^{-4}$, $\omega_{lk} = 10^{10}$ cps, and $\tau_c = 10^{-12}$ sec we obtain

$$A_{lk} = 10^8 A_{lk}^{(k)}. \qquad (17)$$

Thus, in measurements in crystals at low temperatures, the relaxation time in liquid solutions can be estimated from the spin-lattice relaxation time. In many salts of elements of the iron group, the relaxation time at helium temperatures is of the order of 10^{-2} to 10^{-1} sec. Therefore, for longitudinal relaxation times in liquid solutions of these salts at room temperature, we obtain $T_1 \sim 10^{-9}$ sec, which is of the same order as quantities obtained experimentally.

Let us turn our attention to a detailed consideration of the most typical paramagnetic salts. We shall consider, successively, solutions containing ions of elements of the iron group, ions of rare earth elements and, as a separate class, ions found in S-states.

3. IONS OF ELEMENTS OF THE IRON GROUP; CASE OF S = ½

Among the ions of elements of the iron group we must single out those for which the spin $S = \frac{1}{2}$ because in this case, according to Kramers' theorem,[11] Stark splitting of the spin energy levels is absent. We shall first consider doubly ionized copper atoms (ground state ^2D). Six molecules of water form a distorted octahedron around the copper ion, creating a strong electric field of cubic symmetry and a weak tetragonal field. We can characterize the system of orbital energy levels of Cu^{+2} (Fig. 1), which are formed in these electric fields, by the following wave functions:[12]

$$\psi_a = (\psi_2 + \psi_{-2}) / \sqrt{2},\ \psi_b = \psi_0,\ \psi_c = (\psi_2 - \psi_{-2}) / \sqrt{2},$$
$$\psi_d = (\psi_1 + \psi_{-1}) / \sqrt{2}, \quad \psi_e = (\psi_1 - \psi_{-1}) / \sqrt{2}. \qquad (18)$$

The double spin degeneracy of each of the simple orbital levels is removed in the magnetic field; the magnetic sublevels can be characterized by the quantum numbers $M = \pm\frac{1}{2}$. The width $\Delta\nu$ of the resonance line $(a;\ M = -\frac{1}{2} \rightarrow \frac{1}{2})$ is equal to the sum of the transition probabilities from each of the sublevels $(a;\ M = \pm\frac{1}{2})$ to all the remaining. Since the transition probabilities from the lower levels to the upper are proportional to the corresponding Boltzmann factors, we obviously cannot consider transitions to the levels c, d and e. Of the remaining transitions; the only important ones are those completed between different orbital levels without a change in the spin direction. The matrix elements of the perturbation $\mathcal{H}'$ for these transitions are equal to

$$\mathscr{H}'_{a,-1/2;\,b,-1/2} = \mathscr{H}'_{a,1/2;\,b,1/2} = \mathscr{H}'_{ab}$$
$$= 16\sqrt{3}\, e'\mu\bar{r}^2 Q_4 / 7R^5, \qquad (19)$$

while for a transition between the magnetic sublevels of the lower orbital state, a matrix element differing from zero appears only in the third approximation, and is equal to

$$\mathscr{H}'_{a,-1/2;\,a,+1/2} \approx \lambda g\beta H \Delta^{-2} \mathscr{H}'_{ab}. \qquad (20)$$

Here λ is the spin-orbit coupling constant. Finally, with the help of (19) and (9), we get the following expression for the half-width of the resonance line:

$$\Delta\nu = 6\left(\frac{16\, e'\mu\bar{r}^2}{7R^5}\right)^2 \frac{\overline{Q^2}}{\hbar^2} \frac{2\tau_c}{1 + \tau_c\omega_{ab}^2} \exp(-\delta / 2kT). \qquad (21)$$

This equation gives a good account of all the experimental facts established by Kozyrev[13] for several copper salts. It follows from (21) that the width of the paramagnetic resonance line $\Delta\nu$ ought not to depend upon the direction of the magnetic field H. Actually, experiments carried out at different frequencies of the oscillating magnetic field (which differ over a range of one hundred) have not revealed any notable change in the width $\Delta\nu$. If the relaxation were determined by a McConnell mechanism,[2] then the width ought to change by $\sim 10^4$ times. We note that the mechanism assumed by us also would give such a strong dependence on the field H if the relaxation transitions with change of spin orientation played the dominant role, as is evident from (20).

It has been established from experiments on aqueous solutions of $Cu(NO_3)_2$ that, heating from $\sim 300°$ to 400°K increases the width by a factor of 1.8.[14] In crystals, the interval $\delta = \hbar\omega_{ab} \sim 1000$ cm^{-1}. It is natural to assume that in aqueous solutions, too, the value of δ has this same order of magnitude. In this case, $\omega_{ab}^2\tau_c^2 \gg 1$, and therefore the temperature dependence of the width will be given by the formula

$$\Delta\nu \sim \sqrt{T}\coth(\hbar\omega_0/2kT)\exp(-\delta/2kT). \qquad (22)$$

We assume the frequency ω_0 to be 500 cm^{-1}, Hence, to explain the increased width observed in the heating from $\sim 300°$ to 400°K, it is necessary to set $\delta \approx 750$ cm^{-1}. A certain decrease in the value of δ in the transition from the crystal to the liquid solution is possibly connected with the fact that the distortion of the regular octahedral form of the paramagnetic complex in the solutions is connected only with the effect of Yang and Teller.

To estimate the order of magnitude of the quantity $\Delta\nu$, we transform (21) into

$$\Delta\nu = 12\left(\frac{16}{7}\frac{e'\mu}{R^2\delta}\frac{\overline{r^2}}{R^2}\right)^2\frac{\overline{Q^2}}{R^2}\frac{\exp(-\delta/2kT)}{\tau_c}. \qquad (23)$$

We assume the dimensionless quantity in the parentheses to be equal to unity. It is uncertain whether an estimate obtained by direct calculation is more accurate, because the substitution of the paramagnetic complex for a point charge and six dipoles in the calculation of the energy of spin-lattice interaction is obtained only in very rough approximation. If we assume that $\overline{Q^2}/R^2 \sim 10^{-4}$, we obtain $\Delta\nu \sim 10^9$ cps, which agrees well with the experimental value.

FIG. 1. Successive splitting of the ground energy level of Cu^{+2} under the action of a strong cubic field, a weak tetragonal field, and a magnetic field.

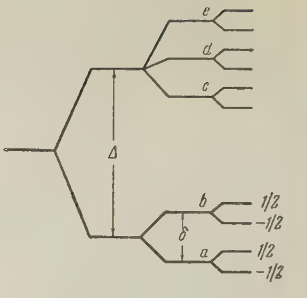

Measurement of paramagnetic resonance in different copper-salt solutions permits us to establish an interesting fact:[4] the closer the g-factor is to the pure spin value, the greater will be the width of the absorption line. In first approximation,[15] $g = 2 - 4\lambda/\Delta$. The increase in the width $\Delta\nu$ with decrease in the ratio $|\lambda/\Delta|$ follows directly from (21). A decrease in $|\lambda/\Delta|$ can be a consequence only of the preservation of the equilibrium distance R between the Cu^{++} ion and the water molecules; in this case, the energy interval δ is probably preserved, too.

Hitherto we could recognize "spin-lattice" interactions in paramagnetic solutions only from experimental data on the width of the paramagnetic resonance line. However, we shall employ an entirely different method of investigation — measurement of the paramagnetic absorption in parallel fields in which we can determine the longitudinal (spin-lattice) relaxation time T_1. In the case of copper salts (since the interval between two lowest orbital levels is comparatively small) there is a large difference between the values of $\Delta\nu$ and $1/T_1$. In the computation of T_1 for Cu^{++}, we make use of the equation:[16]

$$1/T_1 = \alpha/C, \qquad (24)$$

where α is the coefficient of thermal conductivity between the spin system and the lattice, while C is the specific heat of the spin system. With sufficient accuracy we can regard as possible relaxation transitions only those between the levels a and b (Fig. 1) which takes place without a change in spin. Let the lattice temperature be equal to T and let $T_s = T + \Theta$ be the temperature of the spin system. The excess of the number transitions per second from level b to level a over the inverse transitions will be equal to

$$\Delta N = N_b A_{ba} - N_a A_{ab} = N_a A_{ab} \times [\exp(-\delta/k(T+\Theta) + \delta/kT) - 1] = N_a A_{ab}\delta\Theta/kT^2. \qquad (25)$$

Here N_a and N_b are the numbers of particles in levels a and b, respectively. The coefficient α (the energy given up by the lattice per second if $\Theta = 1°$) will be equal to

$$\alpha = N_a A_{ab}\delta^2/kT^2. \qquad (26)$$

For calculation of the specific heat C, we make use of the equation (see reference 17):

$$C = \overline{(\Delta E)^2}/kT^2. \qquad (27)$$

Here $\overline{(\Delta E)^2}$ is the mean-square energy fluctuation, which can easily be calculated by taking into account the population of levels a and b. As a result we obtain

$$\overline{(\Delta E)^2} = N_a \delta^2 (e^{-\delta / kT} - e^{-2\delta / kT}). \tag{28}$$

If we take into consideration that $\Delta \nu = 2A_{ab}$, we easily obtain with the aid of (24), (26), (27), and (23)

$$\frac{1}{T_1} = 6\left(\frac{16}{7}\,\frac{e'\mu}{R^2\delta}\,\frac{\overline{r^2}}{R^2}\right)^2 \frac{\overline{Q^2}}{R^2\tau_c}\,\frac{\exp(\delta / 2kT)}{(1 - e^{-\delta / kT})}.$$

$$\approx \frac{\Delta\nu}{2}\,\frac{e^{\delta / kT}}{(1 - e^{-\delta / kT})}. \tag{29}$$

It is interesting to note that, in contrast to the width $\Delta\nu$, the quantity $1/T_1$ decreases with increasing temperature. This unusual temperature dependence of the relaxation time is explained by the fact that in our case the specific heat of the spin system will increase upon heating more rapidly than the probability of relaxation transitions.

It should be kept in mind that the nonequilibrium distribution of particles between the levels $a, -\frac{1}{2}$ and $a, \frac{1}{2}$ (or the levels $b, -\frac{1}{2}$ and $b, \frac{1}{2}$) cannot be cancelled out with the help of the relaxation transitions $a, -\frac{1}{2} \rightarrow b, -\frac{1}{2}$ and $a, \frac{1}{2} \rightarrow b, \frac{1}{2}$. Therefore, there will be another relaxation time T_1' in addition to the time T_1. The value of T_1' can be estimated, according to (9), (19), and (20), by the formula:

$$\frac{1}{T_1'} \approx 6\,\frac{\overline{Q^2}}{\hbar^2 R^2}\left(\frac{\lambda g\beta H}{\Delta^2}\right)^2\left(\frac{16}{7}\,\frac{e'\mu}{R^2}\,\frac{\overline{r^2}}{R^2}\right)^2 2\tau_c. \tag{30}$$

At $H \sim 10^4$ Oe and room temperature, we have $1/T_1' \sim 10^8\ \text{sec}^{-1}$.

There is also a third way of measuring quantities which depend on the probabilities of relaxation transition. According to reference 18, the changes in the magnetic field of paramagnetic ions in a solution, which take place during relaxation processes, determine the value of the longitudinal relaxation time of the nuclei of the solvent. Changes of the magnetic field in the transitions $a, \frac{1}{2} \rightarrow b, \frac{1}{2}$ and $a, -\frac{1}{2} \rightarrow b, -\frac{1}{2}$ take place only as a result of the small difference in the values of the g-factors of the levels a and b. Therefore, special consideration is required for the solution of the problem as to whether these transitions or the transitions in the change in the spin direction play the dominant role in processes of nuclear relaxation.

In addition to the Cu^{++} ion, the case $S = \frac{1}{2}$ also applies to the triply-charged titanium ion and the quadruply-charged vanadium ion. (solutions of vanadium require special consideration because the linear molecule V — 0 and the ion V^{+4} have completely different systems of energy levels. The orders of the orbital levels will be reversed in these ions. The width of the resonance line will be determined by relaxation transitions between the levels $e \rightarrow d$ and $e \rightarrow c$ (the e level is now the ground level). It was shown in reference 10 that

$$\mathcal{H}'_{ed} = -\frac{12\sqrt{3}}{7} C\left(\sqrt{2}\,Q_3 - \frac{2}{3}\,Q_6\right),$$

$$\mathcal{H}'_{ec} = \frac{12\sqrt{3}}{7} C\left(\sqrt{2}\,Q_2 + \frac{2}{3}\,Q_5\right). \tag{31}$$

Thence, with the help of (9) we obtain an equation similar to (21), namely:

$$\Delta\nu = \frac{528\,\overline{Q^2}}{\hbar^2}\left(\frac{e'\mu\overline{r^2}}{R^5}\right)^2\left[\frac{2\tau_c e^{-\delta_{ed}/kT}}{1 + \tau_c^2\,\omega_{ed}^2} + \frac{2\tau_c e^{-\delta_{ec}/kT}}{1 + \tau_c^2\,\omega_{ec}^2}\right]. \tag{32}$$

In solutions containing the ions Ti^{+3} and V^{+4}, the resonance lines will be 1 to 2 orders of magnitude wider than for Cu^{+2} for the following reasons: (1) the intervals δ_{ed} and δ_{ec} here are less than the interval δ for Cu^{+2}; (2) the splitting in a cubic field, and consequently the effective charge e', is larger here than for Cu^{+2}; (3) two orbital levels are located close to the ground level.

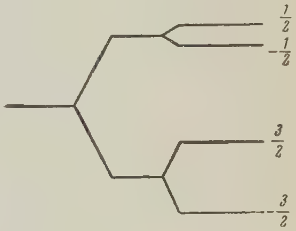

FIG. 2. Splitting of the spin quadruplet of the Cr^{+3} ion, which is located in the ground orbital energy level in electric and magnetic fields.

4. IONS OF THE IRON GROUP; THE CASE $S > \frac{1}{2}$

Let us first consider the Cr^{+3} ion. The ground term of the free ion Cr^{+3} in a cubic field created by the six particles X is so split that the lowest orbital level is simple. The "crystalline" field splits the spin-quadruplet into two doublets, (Fig. 2) the interval between which is equal to $\sim 0.1\ \text{cm}^{-1}$. We shall assume that the magnetic field is directed along the axis of symmetry of the weak trigonal electric field. It is easy to establish that a change in the direction of H relative to the axes of symmetry of the paramagnetic complex has little effect on the relaxation mechanism that we have considered. We shall enumerate the spin levels by the value of the paramagnetic quantum number M. The matrix element of the perturbation $\mathcal{H}'$ which connects the spin levels M and M′, differs from zero only in the third approximation, and has the form:[10]

$$\begin{aligned}\mathscr{H}'_{M,M'} = \{\varepsilon_1[\sqrt{3}(\hat{S}_y^2-\hat{S}_x^2)Q_2+(3\hat{S}_z^2-{}^{15}/_4)Q_3] \\ +\varepsilon_2[(\hat{S}_x\hat{S}_y+\hat{S}_y\hat{S}_x)Q_4 \\ +(\hat{S}_z\hat{S}_x+\hat{S}_x\hat{S}_z)Q_5+(\hat{S}_z\hat{S}_y+\hat{S}_y\hat{S}_z)Q_6]\}_{M,M'},\end{aligned} \qquad (33)$$

where

$$\varepsilon_1 = 54\sqrt{3}\,\frac{\lambda^2}{\Delta^2}\left(\frac{e'\mu}{R^3}\right)\frac{\overline{r^4}}{R^4},$$

$$\varepsilon_2 = \frac{12{,}324}{175}\,\frac{\lambda^2}{\Delta^2}\left(\frac{e'\mu}{R^3}\right)\left(\frac{\overline{r^2}}{R^2}-\frac{55}{36}\,\frac{\overline{r^4}}{R^4}\right).$$

Here $\hat{S}$ is the spin operator; $M, M' = \pm 1/2, \pm 3/2$. Substituting (33) in (9), we obtain for relaxations transitions:

$$\begin{aligned}A_{M,M+1} &= 4\hbar^{-2}\varepsilon_2^2\overline{Q^2}\tau_c(S_xS_z+S_zS_x)^2_{M,M+1}, \\ A_{M,M+2} &= 2\hbar^{-2}(\varepsilon_2^2+3\varepsilon_1^2)\overline{Q^2}\tau_c(S_x^2-S_y^2)^2_{M,M+2}.\end{aligned} \qquad (34)$$

Here we have assumed that $\tau_c\omega_{M,M'} \ll 1$. Calculation of the longitudinal relaxation time is carried out by using the expression:[16]

$$\frac{1}{T_1} = (2S+1)\sum_{l>k} A_{lk}(E_l-E_k)^2 \Big/ \sum_{l>k}(E_l-E_k)^2, \qquad (35)$$

which is valid if $E_l - E_k \ll kT$ for all values of l and k. We shall carry out calculations for two limiting cases of strong and weak magnetic fields. If the field H is strong and the spin levels are equidistant, then

$$\frac{1}{T_1} = (96\,\overline{Q^2}/20\,\hbar^2)(3\varepsilon_1^2+2\varepsilon_2^2)\tau_c. \qquad (36)$$

If $H = 0$, then

$$1/T_1 = (36\,\overline{Q^2}/\hbar^2)(\varepsilon_1^2+\varepsilon_2^2)\tau_c. \qquad (37)$$

Taking $\lambda/\Delta \sim 0.01$, and assigning to the remaining constants in (36) and (37) the values assumed in the previous section, we obtain $1/T_1 \sim 10^9 - 10^{10}\ \mathrm{sec}^{-1}$. The line width observed[14] in measurements of paramagnetic resonance in solutions containing Cr^{+3} has the same order of magnitude and falls off slowly with increasing temperature. Equations (36) and (37) predict a temperature dependence for the width of the form

$$1/T_1 \sim T^{-1/2}\coth(\hbar\omega_0/2kT). \qquad (11')$$

It is well known from chemical and optical investigations that complexes of the Cr^{+3} ion in solutions are very stable. The stability of the complex characterizes the value of the binding energy in the complex, and consequently the frequency of the normal vibrations of the complex, which in this case[6] reaches ~800 cm^{-1}. It then follows that in the temperature range 300° – 400° K the change in the line width should be given by the relation $1/T_1 \sim T^{1/2}$, which explains the results of experiments sufficiently accurately.

For all ions for which the lowest orbital level in the octahedral field is a singlet, we obtain Eqs. (36) and (37). The ions Ni^{+2} and V^{+2} belong to this group. For the remaining ions of the iron group, with the exception of Mn^{+2} and Fe^{+3} considered below, we can assume that the width of the resonant line will, as for Cu^{+2}, be determined by relaxation transitions between different orbital levels.

5. IONS IN S-STATES

Crystals of the ions Mn^{+2}, Fe^{+3}, Gd^{+3}, Eu^{+4}, and Cm^{+3} make up a special place among the paramagnets. These ions are in S states, as a consequence of which the electric field of the crystal (acting by means of the very distance perturbation terms of the ion) bring about a very small (less than 1 cm^{-1}) splitting of the ground energy level. For this same reason, the spin-lattice relaxation time in crystals containing these ions is comparatively long. The behavior of liquid solutions containing ions in the S states is quite similar. We shall carry out a calculation of the longitudinal relaxation for the Mn^{+2} ion, (ground state ^6S). As in the calculations for the relaxation times in crystals,[19] we shall calculate the matrix elements by the method equivalent operators; we shall estimate the factor α arising here from the value of the fine structure of the spin levels. The matrix elements of $\mathcal{H}'$ that differ from 0 are:

$$\begin{aligned}\mathscr{H}'_{M,M+1} &= (12\,e'\mu\alpha\overline{r^2}/R^4) \\ &\times(S_xS_z+S_zS_x)_{M,M+1}(Q_5+iQ_6)/R.\end{aligned} \qquad (38)$$

$$\begin{aligned}\mathscr{H}'_{M,M+2} &= (12\,e'\mu\alpha\overline{r^2}/R^4) \\ &\times(S_x^2-S_y^2)_{M,M+2}(3Q_2+iQ_4)/R.\end{aligned} \qquad (39)$$

The value of $e'\mu\alpha\overline{r^2}/R^4$ has the order of magnitude of the Stark splitting of the ground state. In view of this fact, we replace it by the fine-structure constant which for Mn^{+2}, in particular, is equal to $D = 0.025$ cm^{-1}.[20] We can then represent the transition probabilities in the following from:

$$A_{M,M+1} = \frac{36\cdot 16\,D^2\overline{Q^2}}{\hbar^2R^2}\tau_c(S_xS_z+S_zS_x)^2_{M,M+1}, \qquad (40)$$

$$A_{M,M+2} = \frac{36\cdot 80\,D^2\overline{Q^2}}{\hbar^2R^2}\tau_c(S_x^2-S_y^2)_{M,M+2}. \qquad (41)$$

We compute the relaxation time with the help of (35). For strong magnetic fields,

$$\frac{1}{T_1} = \frac{274\cdot 64\cdot 36}{105}\,\frac{D^2\overline{Q^2}}{\hbar^2R^2}\tau_c. \qquad (42)$$

If $H = 0$, however, then

$$\frac{1}{T_1} = \frac{36 \cdot 16 \cdot 157}{7} \frac{D^2}{\hbar^2} \frac{\overline{Q^2}}{R^2} \tau_c. \qquad (43)$$

A numerical estimate yields $T_1 \sim 10^{-7}$ sec.

Experiments[14] show that the line width in solutions of Mn^{+2} at first decreases upon heating and then, beginning at temperatures $T_0 \sim 350°K$, increases. Equation (11) explains such a change if it is assumed that $\hbar\omega_0 \approx kT_0 \approx 250\ cm^{-1}$.

6. IONS OF THE RARE EARTH ELEMENTS

Judging from the vibrational structure of the optical absorption lines of the rare earth ions, the solvate complexes formed in solutions of salts of rare earth elements are as stable as those in solutions of salts of the iron group. In the case of aqueous solutions, we can assume that the metallic ion is surrounded by six water molecules located at the vertices of an octahedron, and that the fundamental component of the electric field has a cubic symmetry while the weak component is rhombic. Of those ions with an odd number of electrons, we consider Ce^{+3} (ground state $^2F_{5/2}$). The diagram of the successive splitting of the levels of $^2F_{5/2}$ in cubic, rhombic, and magnetic fields is drawn in Fig. 3; the magnetic sublevels are characterized by the following wave functions:[20]

$$\psi_a = (\sqrt{5}\Phi_{-5/2} + \Phi_{3/2}) / \sqrt{6}, \quad \psi_b = (\sqrt{5}\Phi_{5/2} + \Phi_{-3/2}) / \sqrt{6},$$

$$\psi_c = \Phi_{1/2}, \quad \psi_d = \Phi_{-1/2}, \qquad (44)$$

$$\psi_f = (\Phi_{-5/2} - \sqrt{5}\,\Phi_{3/2}) / \sqrt{6}, \quad \psi_g = (\Phi_{5/2} - \sqrt{5}\Phi_{-3/2}) / \sqrt{6}.$$

The width of the resonance line due to transitions between the sublevels of the lowest Kramers' doublet is

$$\Delta\nu_{fg} = A_{fg} + \sum_i A_{fi} + \sum_i A_{gi}; \quad i = a, b, c, d. \qquad (45)$$

The greatest matrix element of the perturbation $\mathcal{H}'_{fg}$ arises in the second approximation upon consideration of the non-diagonal matrix elements of the Zeeman energy of the ion:

$$\hat{\mathscr{H}}_z = {}^6/_7\, \beta\, (\mathscr{H}\mathbf{J}), \qquad \mathscr{H}_z(f, a)$$

$$= -\mathscr{H}_z(b, g) = -(4\sqrt{5}/7)\,\beta H.$$

The matrix elements of $\mathcal{H}'$, which connect the different Stark sublevels, differ from zero in the first approximation. Some of these are:[21]

$$\mathscr{H}'(f, b) = -\mathscr{H}'(a, g) = -\left(\sqrt{5}\,\frac{e'\mu}{R^5}\right)\overline{r^2}\,(Q_5 + iQ_6). \qquad (46)$$

Now we can compute the matrix element

$$\mathscr{H}'_{fg} = \mathscr{H}_z(f, a)\,\mathscr{H}'(a, g) / (-\Delta)$$

$$+ \mathscr{H}'(f, b)\,\mathscr{H}_z(b, g) / (-\Delta) \qquad (47)$$

$$= ({}^{40}/_7)\,(\beta H / \Delta)\,(e'\mu\overline{r^2} / R^5)\,(Q_5 + iQ_6).$$

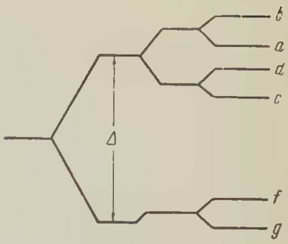

FIG. 3. Successive splitting of the ground energy level of the Ce^{+3} ion under the action of a strong cubic field, a weak rhombic field, and a magnetic field.

In addition to those in (46), matrix elements of the following transitions also differ from zero: f → a, f → c, f → d, g → b, g → c; in magnitude, these are close to (46). Therefore, in the calculation of transition probabilities to the upper Stark level we multiply the matrix element of (46) by $\sqrt{8}$. After calculation of the transition probabilities in accord with Eqs. (9), (46), and (47), we obtain

$$A_{fg} = \frac{800}{49\,\hbar^2}\left(\frac{\beta\mathscr{H}}{\Delta}\right)^2\left(\frac{e'\mu\overline{r^2}}{R^5}\right)^2 \overline{Q^2}\,\frac{2\tau_c}{1 + \tau_c^2\omega_{fg}^2}; \qquad (48)$$

$$\sum_i A_{fi} \approx \frac{180}{\hbar^2}\left(\frac{e'\mu\overline{r^2}}{R^5}\right)^2 \overline{Q^2}\,\frac{2\tau_c}{1 + \tau_c^2\omega_{fi}^2}\exp(-\hbar\omega_{fi}/2kT). \qquad (49)$$

Here $\hbar\omega_{fi}$ is the mean interval between Stark sublevels and has a value of $\sim 100\ cm^{-1}$. Comparison of (48) and (49) shows that transitions to the higher Stark levels make the chief contribution to the line width. This conclusion obviously applies to all ions in which the lower Stark level is a Kramers' doublet and the energy interval up to the next sublevel is $\hbar\omega_{fi} \sim kT$, i.e., in all rare earth ions with an odd number of electrons. An estimate of the width $\Delta\nu_{fg}$ will be most accurate if we equate (49) and (21). For Ce^{+3}, the resonance line is one or two orders of magnitude wider than for Cu^{+2}, owing to the smaller value of the intervals between the lower Stark sublevels and the large number of the sublevels.

In the case of ions with an even number of electrons, the Stark sublevels preserve a non-Kramers degeneracy. Therefore, the matrix elements of the perturbations between the Zeeman sublevels are different from zero in first approximation and have the order of (46). Moreover, there are the same effective relaxation transitions between different Stark levels for ions with a different number of electrons. Thus, if the number of electrons is even, the width of resonance lines ought to be larger (all the conditions being equal) than for ions with an odd number of electrons.

CONCLUSION

Let us consider briefly the effects shown by the hyperfine interactions on the intensity of relaxation transitions. The simplest spin-Hamiltonian, for an ion whose nucleus has a spin I not equal to zero, is of the form:

$$\hat{\mathcal{H}}_S = 2\beta H S_z + (g-2)\beta H S_z + ASI. \qquad (50)$$

The vibrations of particles surrounding a paramagnetic ion lead to a change in the quantities $(g-2)$ and A. If the changes are comparable, the hyperfine interactions can markedly change the probability of relaxation transitions. It is easy to represent the width of the individual hyperfine components of the resonance line as

$$\Delta\nu_{I_z} = (p + qI_z)^2. \qquad (51)$$

Here p^2 is the width at $I = 0$, and detailed calculations are required for each ion separately in the determination of the constant q.

Finally, we note that Eq. (16), which connects the probabilities of relaxation transitions in liquid solutions and in crystals, is not always valid. In liquids, if the interval δ between the lowest Stark sublevels does not exceed approximately $5kT$, the width of resonance line is determined by relaxation transitions between the sublevels. In crystals, if the quantity δ/k is greater than the Debye temperature, relaxation transitions between different Stark sublevels are scarcely probable. Equation (16) can be used to establish differences in the origin of relaxations in crystals and in the liquid solutions.

In conclusion, the authors express their sincere gratitude to B. M. Kozyrev for criticisms on the results obtained.

---

[1] Bloembergen, Purcell, and Pound, Phys. Rev. **73**, 679 (1948).

[2] H. J. McConnell, J. Chem. Phys. **25**, 709 (1956).

[3] B. R. McGarvey, J. Phys. Chem. **61**, 1232 (1957).

[4] B. M. Kozyrev, Doctoral Dissertation, Phys. Inst. Acad. Sci., Moscow, 1957.

[5] J. H. Van Vleck, J. Chem. Phys. **7**, 72 (1939).

[6] M. L. Schultz, J. Chem. Phys. **10**, 194 (1942). S. Freed and S. I. Weissman, J. Chem. Phys., **8**, 840 (1940). M. Kobayashi and J. Fujita, J. Chem. Phys. **23**, 1354 (1955).

[7] L. D. Landau and E. M. Lifshitz, **Статистическая физика** (*Statistical Physics*) GITTL, Moscow (1951), p. 107.

[8] M. A. El'iashevich, **Спектры редких земель** (*Rare Earth Spectra*) GITTL, 1953, p. 183.

[9] Ia. I. Frenkel', **Электродинамика** (*Electrodynamics*) Vol. 2, ONTI 1937 p. 167.

[10] J. H. Van Vleck, Phys. Rev. **57**, 436 (1940).

[11] H. A. Kramers, Proc. Amsterdam **33**, 959 (1930)

[12] B. Bleaney and K. W. H. Stevens, Repts. Progr. Phys. **16**, 108 (1953).

[13] B. M. Kozyrev, Faraday Soc. Discussions, **19**, 135 (1955).

[14] B. M. Kozyrev, Izv. Akad. Nauk SSSR **21**, 828 (1957) [Columbia Techn. Transl. **21**, 828 (1957)].

[15] A. Abragam and M. H. L. Pryce, Proc. Roy. Soc., London **A206**, 164 (1952).

[16] C. Gorter, *Paramagnetic Relaxation*, IIL, Moscow, 1949, pp. 105-107 (Russian Translation). [Amsterdam, 1947].

[17] A. Sommerfeld, *Thermodynamics and Statistical Physics*, IIL, Moscow, 1955, pp. 351 (Russian Translation).

[18] A. I. Rivkind, Dokl. Akad. Nauk SSSR **102**, 1107 (1955). N. Bloembergen, J. Chem. Phys. **37**, 572 (1957).

[19] Sh. Sh. Bashkirov, **Физика металлов и металловедение** (Physics of Metals and Metal Research) **6**, 2 (1958).

[20] B. Bleaney, Proc. Roy. Soc. (London) **A205**, 336 (1951).

[21] S. A. Al'tshuler, J. Exptl. Theoret. Phys. (U.S.S.R.) **24**, 681 (1953).

Translated by R. T. Beyer
197

ON FINDING THE MATRIX OF THE $a + a' \to b + b'$ REACTION

S. M. BILEN'KII, L. I. LAPIDUS, L. D. PUZIKOV, and R. M. RYNDIN

Joint Institute for Nuclear Research

Submitted to JETP editor April 23, 1958

J. Exptl. Theoret. Phys. (U.S.S.R.) **35**, 959-961 (October, 1958)

We consider the conditions necessary for finding the matrix of the $a + a' \to b + b'$ reaction from experimental data. Invariance under rotation and reflection in space is used to find the number of complex scalar functions that define the reaction matrix M. Invariance of the reaction under time reversal gives relations between the polarization effects in the direct and inverse reactions. We find the number of experiments necessary for the complete determination of the reaction matrix.

WOLFENSTEIN and Ashkin[1] have used invariance under rotation and reflection in space and under time reversal to obtain general expressions for the scattering amplitudes of particles with spin 0 and $\frac{1}{2}$ on particles with spin $\frac{1}{2}$. These expressions have been used[2] together with the fact that the S matrix is unitary to discuss the problem of how many experiments are necessary to completely determine the scattering amplitudes for these cases.

In the present note we perform a similar analysis for the general case of the $a + a' \to b + b'$ reaction. We first construct the amplitude for the process, and then find a relation between the direct and inverse reaction matrices which follows from invariance under time reflection. The two possible directions of the reaction are then used as an example to establish the number of experiments necessary to find the amplitude of the process in general.

We introduce the complete set of matrices

$$T^{JM}(j_b, j_a) = A(j_b, j_a, J) \sum_{m_a, m_b} (j_a J m_a M \mid j_a J j_b m_b) \chi_{j_b m_b} \overset{+}{\chi}_{j_a m_a}. \tag{1}$$

Here $\chi_{j_a m_a}$ and $\chi_{j_b m_b}$ are the spin functions of the initial and final states, and j_a, j_b, m_a, and m_b are the total spins and their z-components. The T^{JM} operators satisfy the condition

$$\overset{+}{T}{}^{JM}(j_b, j_a) = (-1)^M T^{J,-M}(j_a, j_b).$$

From this we obtain

$$A^*(j_b, j_a, J)\sqrt{2j_b+1} = (-1)^{j_a - j_b}\sqrt{2j_a+1}\,A(j_a, j_b, J).$$

Let us expand the reaction matrix in terms of the complete set of T^{JM} operators. We have

$$M_{b_a}(\mathbf{n}_b, \mathbf{n}_a) = \sum_{JMj_aj_b} \Phi^{JM}_{j_b j_a}(\mathbf{n}_b, \mathbf{n}_a) T^{JM}(j_b, j_a), \tag{2}$$

where $\mathbf{n}_a$ and $\mathbf{n}_b$ are unit vectors in the directions of the relative momenta. From invariance under rotation we may conclude that the $\Phi^{JM}_{j_b j_a}$ functions are of the form

$$\Phi^{JM}_{j_b j_a}(\mathbf{n}_b, \mathbf{n}_a) = \sum_{\lambda} a^{\lambda}_{j_b j_a J} \psi^{\lambda *}_{JM}(\mathbf{n}_b, \mathbf{n}_a), \tag{3}$$

where $a^{\lambda}_{j_b j_a J}$ are arbitrary complex scalar functions of the energy and the angle between $\mathbf{n}_a$ and $\mathbf{n}_b$, and

$$\psi^{\lambda}_{JM}(\mathbf{n}_b, \mathbf{n}_a) = \sum_{\mu, \mu'} (r-\lambda, r+\lambda, \mu, \mu' \mid r-\lambda, r+\lambda, J, M) Y_{r-\lambda, \mu}(\mathbf{n}_a) Y_{r+\lambda, \mu'}(\mathbf{n}_b). \tag{4}$$

Thus the amplitude is entirely determined by the $a^{\lambda}_{j_b j_a J}$ functions. The number of such functions can be found from Eqs. (1) to (4). If all the particles involved in the reaction have integral spin, this number is

$$N_0(i_1, i_2, I_1, I_2) = {}^1/_2(2i_1+1)(2i_2+1)(2I_1+1)(2I_2+1) \pm {}^1/_2(-1)^{i_1+i_2+I_1+I_2}, \tag{5}$$

where i_1, i_2, I_1, and I_2 are the spins of the particles (the minus sign refers to the case in which internal parity changes, and the plus sign to the case in which there is no change of internal parity). In other cases N_0 is given by Eq. (5) without the last term.

Invariance of the theory under time reversal gives the relation

$$k_a M^{+}_{ba}(\mathbf{n}_b, \mathbf{n}_a) = k_b T M_{ab}(-\mathbf{n}_a, -\mathbf{n}_b) T. \tag{6}$$

Here T is the time reversal operator, whose action on the simultaneous eigenfunction of the angular momentum and its z-component is given by

$$T\psi_{JM} = (-1)^{J-M}\psi_{J,-M}.$$

If $b^{\lambda}_{j_a j_b J}$ are scalar functions in the expansion of the inverse reaction matrix $M_{ab}(\mathbf{n}_a, \mathbf{n}_b)$ in a form analogous to (2), Eq. (6) gives

$$k_a a^{\lambda}_{j_b j_a J} = k_b b^{-\lambda}_{j_a j_b J}. \tag{7}$$

Equation (6) can also be used for a general reaction to establish the relation between the quantities observed in the direct and inverse reactions. Assume the operators $T^{q_a \kappa_a}$, $T^{q'_a \kappa'_a}$, . . . to act on the spin variables of particles a, a′, . . . , respectively. We then have

$$\begin{gathered} \sigma_{ba} \langle T^{q_b \varkappa_b} T^{q'_b \varkappa'_b} \rangle = \sum_{q_a q'_a \varkappa_a \varkappa'_a} \langle T^{q_a \varkappa_a} T^{q'_a \varkappa'_a} \rangle \\ \times \operatorname{Sp} T^{q_b \varkappa_b} T^{q'_b \varkappa'_b} M_{ba}(\mathbf{n}_b, \mathbf{n}_a) \overset{+}{T}{}^{q_a \varkappa_a} \overset{+}{T}{}^{q'_a \varkappa'_a} M^{+}_{ba}(\mathbf{n}_b, \mathbf{n}_a) \end{gathered} \tag{8}$$

and a similar expression for the inverse reaction with an interchange of a and b. Condition (6) then gives[3]

$$\begin{gathered} k_a^2 \operatorname{Sp} T^{q_b \varkappa_b} T^{q'_b \varkappa'_b} M_{ba}(\mathbf{n}_b, \mathbf{n}_a) \overset{+}{T}{}^{q_a \varkappa_a} \overset{+}{T}{}^{q'_a \varkappa'_a} M^{+}_{ba}(\mathbf{n}_b, \mathbf{n}_a) \\ = (-1)^{q_a + q'_a + q_b + q'_b + \varkappa_a + \varkappa'_a + \varkappa_b + \varkappa'_b} k_b^2 \operatorname{Sp} T^{q_a, -\varkappa_a} T^{q'_a, -\varkappa'_a} \\ \times M_{ab}(-\mathbf{n}_a, -\mathbf{n}_b) \overset{+}{T}{}^{q_b, -\varkappa_b} \overset{+}{T}{}^{q'_b, -\varkappa'_b} M^{+}_{ab}(-\mathbf{n}_a, -\mathbf{n}_b). \end{gathered} \tag{9}$$

Let us now use two directions of a reaction as an example to analyze the conditions necessary to determine a reaction matrix from experimental data. The number of independent real functions entering into $M_{ba}(\mathbf{n}_b, \mathbf{n}_a)$ (or $M_{ab}(\mathbf{n}_a, \mathbf{n}_b)$) is $2N_0(i_1, i_2, I_1, I_2)$. The number of functions which determine the scattering matrix $M_{aa}(\mathbf{n}_a, \mathbf{n}'_a)$ (or $M_{bb}(\mathbf{n}_b, \mathbf{n}'_b)$) is reduced, as a result of time reversal invariance, from $2N_0(i_1, i_2, i_1, i_2)$ to $N(i_1, i_2) = N_0(i_1, i_2, i_1, i_2) + (2i_1 + 1)(2i_2 + 1)$. Therefore the total number of real functions entering into the matrix of these reactions is

$$N(i_1, i_2) + N(I_1, I_2) + 2N_0(i_1, i_2, I_1, I_2). \tag{10}$$

It can be shown further that considerations based on the fact that the S matrix is unitary further reduces by a factor of 2 the number of independent functions which must be determined from experiment.

The authors thank Ia. A. Smorodinskii for interesting discussions of the questions considered here.

---

[1] L. Wolfenstein and J. Ashkin, Phys. Rev. **85**, 947 (1952).

[2] Puzikov, Ryndin, and Smorodinskii, J. Exptl. Theoret. Phys. (U.S.S.R.) **32**, 592 (1957), Soviet Phys. JETP **5**, 489 (1957).

[3] M. I. Shirokov, J. Exptl. Theoret. Phys. (U.S.S.R.) **33**, 975 (1957), Soviet Phys. JETP **6**, 748 (1958).

Translated by E. J. Saletan
198

SOVIET PHYSICS JETP VOLUME 35(8), NUMBER 4 APRIL, 1959

ON SOME PECULARITIES OF CYCLOTRON RESONANCE IN METALS WITH NON-CONVEX FERMI SURFACES

E. A. KANER

Institute of Radio Physics and Electronics, Academy of Sciences, Ukrainian S.S.R.

Submitted to JETP editor April 27, 1958

J. Exptl. Theoret. Phys. (U.S.S.R.) **35**, 962-964 (October, 1958)

It is shown that "logarithmic" cyclotron resonance should take place at Larmor frequencies near the hyperbolic limiting points of a non-convex Fermi surface.

In previous papers[15] it was shown that cyclotron resonance takes place in metals with an arbitrary non-quadratic dispersion law $\epsilon(p)$[*] at Larmor frequencies that are extremal in p_H:

$$\Omega_{\text{ext}} = eH/cm_{\text{ext}} = 2\pi eH/c\,(\partial S/\partial\varepsilon)_{\text{ext}}$$

and at values of Ω at elliptic limiting points.[†]

However, in the investigation of Larmor resonant frequencies in the case of non-convex Fermi surface, resonance was not observed at Larmor frequencies that correspond to hyperbolic limiting points.

It is clear that for certain directions of the constant magnetic field **H**, besides the elliptic limiting points (B, B′, C, C′ — see drawing), limiting points of the hyperbolic type A and A′ (saddle points) are present on a non-convex surface. Near these points, the effective mass M as a function of p_x ($Ox \parallel \mathbf{H}$) experiences discontinuities, since $m = (1/2\pi)\,\partial S/\partial\epsilon$ is determined in region 1 ($|p_x| < p_x^A$) by the areas $S(\zeta_0, p_x)$ of the cross section of the entire Fermi surface, while in region 5, for example, the effective mass is determined by the area $S(\zeta_0, p_x)$ only in this same region. Therefore, the Larmor frequency $\Omega(p_x) \sim 1/m(p_x)$ also points to a discontinuity of the function at $p_x = p_x^A$, $p_x^{A'}$, which reduces to cyclotron resonance for $\omega = q\,\Omega(p_x^A)$ (q = integer) and $\ln(\omega/\nu_0) \gg 1$. The present communication is devoted to a clarification of the properties of resonance at the hyperbolic limiting points.

Resonance at hyperbolic limiting points is logarithmic and for $\omega \gg \nu_0$ [$\nu_0 = \bar{\nu}(p_x^A)$], "sharpness" of the resonance is determined by $\ln(\omega/\nu_0)$. If the frequency ω and the magnetic field H satisfy the condition $\omega = q\,\Omega_4(p_x^{A'} - 0)$ (Ω_4 is determined by the cross-sectional area only in region 4) then, with logarithmic accuracy, the principal values of the tensor of the surface impedance $Z_{\mu\nu}$ are equal to

$$Z_\alpha = \sqrt{3}h\left(\frac{\pi\omega^2 q}{e^2c^4}\right)^{1/3}\left[\frac{\ln(\omega/\nu_0) + id}{a_\alpha}\right]^{1/3}, \qquad (1)$$

where

$$a_\alpha = \left.\frac{n_\alpha^2}{K\partial\ln m/\partial\varphi}\right|_{\varphi_2-0} - \left.\frac{n_\alpha^2}{K\partial\ln m/\partial\varphi}\right|_{\varphi_1+0} \qquad (2)$$

($0 < d \sim 1$). For $a_\alpha < 0$:

$$\operatorname{Re} Z_\alpha \sim \left(\ln\frac{\omega}{\nu_0}\right)^{-4/3}, \quad \operatorname{Im} Z_\alpha \sim \left(\ln\frac{\omega}{\nu_0}\right)^{-1/3}. \qquad (2a)$$

If $a_\alpha > 0$,

$$Z_\alpha \sim \left(\ln\frac{\omega}{\nu_0}\right)^{-1/3}. \qquad (2b)$$

There are similar formulas for resonance (per effective mass) from the other side of the intersection $p_x = p_x^{A'} + 0$. In this case there remains in the expression (2) for a_α only the one term (one of the principal values of a_α is equal to 0; consequently, the resonance takes place at the chosen polarization of the external electromagnetic field along the direction of the velocity at the point $p_x = p_x^{A'}$; $\varphi = \varphi_2$, $\epsilon = \zeta_0$ (for details see references 3 and 5).

Cyclotron resonance at the remaining (extremal) Larmor frequencies in the case of a non-convex Fermi surface obviously possesses the same pecularities as for the convex surfaces (see references 1 to 5).

Calculations confirm the assertions made without proof in references 2 and 5 that, for a non-convex surface, not all curves $\nu_z \equiv -m^{-1} \times dp_y/d\tau = 0$ on the Fermi surface give a resonance contribution, but only those which correspond to

---

[*] We follow the notation of reference 2.

[†] At the limiting point, the velocity of the electrons (normal to the Fermi surface) is parallel to the magnetic field H.

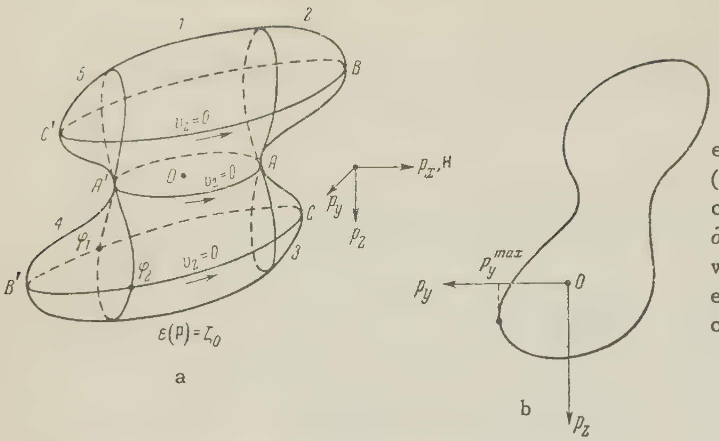

a

b

a) non-convex Fermi surface $\varepsilon(p) = \zeta_0$; B, B′, C, C′ – elliptic limiting points; A, A′ – hyperbolic limiting points (saddle points). The regions 1 to 5 correspond to the regions of discontinuity of the effective mass $m(p_x) = 1/2\pi\, \partial S(\varepsilon, p_x)/\partial\varepsilon$; b) the intersection of the non-convex surface $\varepsilon(p) = \zeta_0$ with the plane $p_x = \text{const}$ for $|{}^{*}p_x| < p_x^{(A)}$ (the trajectory of the electron in momentum space or the projection of the trajectory of the electron in the metal on the zy plane: $z \to -p_y$, $y \to p_z$).

a real minimum in the quantity $z = \Omega^{-1} \int \nu_z d\tau = -p_y/m\Omega$, i.e., a maximum $p_y(\tau)$ (τ/Ω is the period of rotation of the electron in its orbit). This condition guarantees a multiple hit of the electron in the skin depth and physically corresponds to a situation in which the highest point of the trajectory of the electron in the metal is located in this layer. The remaining extrema of $p_y(\tau)$ do not lead to resonance, inasmuch as the corresponding points of the trajectory of the electron in the metal lie outside of the skin layer, where the electron undergoes virtually no interactions with the high frequency field.

Equation (1) for Z_α is valid with logarithmic accuracy, inasmuch as there is no small parameter close to resonance. If $\ln(\omega/\nu_0) \sim 1$, Eq. (1) no longer holds, but it allows us to judge the qualitative picture of resonance at hyperbolic limiting points. Admitting all the difficulties associated with achieving large values of $\ln(\omega/\nu_0)$, we point out that for very pure specimens even at the present time, the values of $\omega/\nu_0 \sim 400$-600 [$\ln(\omega/\nu_0) \sim 5$-6] have been obtained. For example, for the samples of tin investigated in the research of Kip and others[6] at $\omega = 2\pi \cdot 24{,}000$ Mcs the value of ω/ν_0 was greater than 200.

In connection with the effect pointed out here, there are definite possibilities for determining the structure of the Fermi surface.

---

[1] M. Ia. Azbel' and E. A. Kaner, J. Exptl. Theoret. Phys. (U.S.S.R.) **30**, 811 (1956), Soviet Phys. JETP **3**, 772 (1956).

[2] M. Ia. Azbel' and E. A. Kaner, J. Exptl. Theoret. Phys. (U.S.S.R.) **32**, 896 (1957), Soviet Phys. JETP **5**, 730 (1957).

[3] E. A. Kaner and M. Ia. Azbel', J. Exptl. Theoret. Phys. (U.S.S.R.) **33**, 1461 (1957), Soviet Phys. JETP **6**, 1126 (1958).

[4] E. A. Kaner, J. Exptl. Theoret. Phys. (U.S.S.R.) **33**, 1472 (1957), Soviet Phys. JETP **6**, 1135 (1958).

[5] M. Ia. Azbel' and E. A. Kaner, J. Phys. Chem. Solids, **6** (1958).

[6] Kip, Landenberg, Rosenblum, and Wagoner, Phys. Rev. **108**, 494 (1957).

Translated by R. T. Beyer.
199

SOVIET PHYSICS JETP VOLUME 35(8), NUMBER 4 APRIL, 1959

MUTUAL ELECTRON CORRELATIONS IN METAL OPTICS

R. N. GURZHI

Physico-Technical Institute, Academy of Sciences, Ukrainian S.S.R.

Submitted to JETP editor April 27, 1958

J. Exptl. Theoret. Phys. (U.S.S.R.) **35**, 965-969 (October, 1958)

The absorption of infrared electromagnetic waves in metals is considered on the basis of Landau's Fermi-liquid theory,[1] with the quantum properties of the electromagnetic field taken into account.

THE present paper is devoted to an investigation of the absorption in metals of electromagnetic waves in the infrared region of the spectrum from the point of view of the Fermi-liquid theory developed by Landau.[1] This problem has already been considered by Silin.[2]* However, in his paper the classical transport equation was used to describe the Fermi liquid, whereas in the infrared region of the spectrum the quantum properties of the electromagnetic field (see references 3 to 5) are essential for an evaluation of the volume absorption (due to the collisions of the electrons with one another and with the lattice phonons).

If the system is in a state close to equilibrium, the energy of the quasi-particles is of the form

$$\varepsilon(\mathbf{p}, \mathbf{r}, t) = \varepsilon^{(0)}(\mathbf{p}) + \delta\varepsilon(\mathbf{p}, \mathbf{r}, t) \tag{1}$$

where $\epsilon^{(0)}(\mathbf{p})$ is the dispersion law of the quasi-particles when there is no external field, and

$$\delta\varepsilon(\mathbf{p}, \mathbf{r}, t) = \int d\mathbf{p}' \cdot \Phi(\mathbf{p}, \mathbf{p}')\, \delta f(\mathbf{p}', \mathbf{r}, t).$$

In the last formula $\delta f(\mathbf{p}, \mathbf{r}, t)$ is the non-equilibrium correction to the distribution function,

$$f(\mathbf{p}, \mathbf{r}, t) = f_0(\mathbf{p}) + \delta f(\mathbf{p}, \mathbf{r}, t),$$

$$f_0(\mathbf{p}) = \left[1 + \exp\left(\frac{\varepsilon^{(0)}(\mathbf{p}) - \varepsilon_0}{kT}\right)\right]^{-1};$$

the function $\Phi(\mathbf{p}, \mathbf{p}')$ characterizes the interelectron correlation.

In correspondence with (1) it is natural to write the "electron" Hamiltonian in an external electromagnetic field in the form

$$\hat{H}(1) = \hat{H}^{(0)}(1) + \delta\hat{H}(1),$$

where

$$\hat{H}^{(0)} = \varepsilon^{(0)}\left(-i\hbar\nabla + \frac{e}{c}\mathbf{A}(\mathbf{r}, t)\right),$$

$$\mathbf{A}(\mathbf{r}, t) = \mathbf{A}(\mathbf{r})\, e^{i\omega t} + \mathbf{A}^*(\mathbf{r})\, e^{-i\omega t}.$$

Using the calculations performed in references 3 and 5 we easily obtain a quantum transport equation for the system of such electron quasi-particles interacting with the lattice vibrations and colliding one with another. In the linear approximation this equation is of the form

$$i\omega\delta f + \mathbf{v}\frac{\partial}{\partial \mathbf{r}}\left(\delta f - \delta\varepsilon\frac{\partial f_0}{\partial\varepsilon^{(0)}}\right) - e\mathbf{E}\cdot\mathbf{v}\frac{\partial f_0}{\partial\varepsilon^{(0)}}$$
$$= (\hat{J}_{ep} + \hat{J}_{ee})\left(\delta f - \frac{e}{i\omega}\mathbf{E}\cdot\mathbf{v}\frac{\partial f_0}{\partial\varepsilon^{(0)}}\right) \tag{2}$$
$$- (\hat{K}_{ep} + \hat{K}_{ee})\left(\frac{e}{i\omega}\mathbf{E}\cdot\mathbf{v} - \delta\varepsilon\right).$$

Here the indices ep and ee denote terms arising respectively due to electron-phonon and electron-electron collisions; $\mathbf{E}(\mathbf{r}) = -(i\omega/c)\mathbf{A}(\mathbf{r})$ is the electrical field strength. $\hat{J}_{ep}$ and $\hat{J}_{ee}$ can be obtained from the corresponding classical collision operators by substituting for $\delta(a)$ (the δ-function that describes the conservation of energy during a collision) the average[3,5] $\frac{1}{2}[\delta(a + \hbar\omega) + \delta(a - \hbar\omega)]$ (we have denoted by a the difference between the energies of the colliding particles before and after the collision). Furthermore,

$$\hat{K}_{ep}\delta\varepsilon(\mathbf{p}) = -\frac{\Delta}{(2\pi\hbar)^3}\frac{\pi}{Mu\hbar}C^2\int_{|\mathbf{q}| \leqslant q_0} d\mathbf{q}\cdot q\,(\delta\varepsilon(\mathbf{p} + \mathbf{q}) - \delta\varepsilon(\mathbf{p}))\frac{1}{2\hbar\omega}$$
$$\times \{[\delta(a + \hbar\omega) - \delta(a - \hbar\omega)]$$
$$\times [-(\bar{N}_q + 1) f_0(\mathbf{p})(1 - f_0(\mathbf{p} + \mathbf{q})) + \bar{N}_q f_0(\mathbf{p} + \mathbf{q})$$
$$\times (1 - f_0(\mathbf{p}))] + [\delta(b + \hbar\omega) - \delta(b - \hbar\omega)]$$
$$\times [-\bar{N}_q f_0(\mathbf{p})(1 - f_0(\mathbf{p} + \mathbf{q}))$$
$$+ (\bar{N}_q + 1) f_0(\mathbf{p} + \mathbf{q})(1 - f_0(\mathbf{p}))]\};$$
$$a = \varepsilon(\mathbf{p}) - \varepsilon(\mathbf{p} + \mathbf{q}) - h\nu_q, \quad b = \varepsilon(\mathbf{p}) - \varepsilon(\mathbf{p} + \mathbf{q}) + h\nu_q,$$
$$\bar{N}_q = \left[\exp\left(\frac{h\nu_q}{kT}\right) - 1\right]^{-1}$$

For the sake of simplicity we have here assumed that the phonons possess a very simple dispersion law: $h\nu_{\mathbf{q}} = u|\mathbf{q}|$, where $\mathbf{q}$ is the phonon momentum, u the sound velocity in the metal, $q_0 = k\Theta/u$

---

*The author is deeply grateful to V. P. Silin for making his paper available in advance of publication.

the limiting phonon momentum, Θ the Debye temperature, M the mass of an atom in the lattice, Δ the volume of an elementary cell in the crystal, and C a constant of the same order of magnitude as the average energy of an electron in the metal.

$$\hat{K}_{ee}\,\delta\varepsilon(\mathbf{p}) = -\frac{\pi e^4}{\hbar(2\pi\hbar)^6}\sum_g\iiint d\mathbf{p}'\,d\mathbf{p}_1\,d\mathbf{p}_1'$$

$$\times[\nu(|\mathbf{p}-\mathbf{p}_1|)-\nu(|\mathbf{p}-\mathbf{p}_1'|)]^2\,\delta(\mathbf{p}+\mathbf{p}'-\mathbf{p}_1-\mathbf{p}_1'+2\pi\hbar\,\mathbf{g})$$

$$\times(\delta\varepsilon+\delta\varepsilon'-\delta\varepsilon_1-\delta\varepsilon_1')\,\frac{1}{2\hbar\omega}\,[\delta(\varepsilon+\varepsilon'-\varepsilon_1$$

$$-\varepsilon_1'+\hbar\omega)-\delta(\varepsilon+\varepsilon'-\varepsilon_1-\varepsilon_1'-\hbar\omega)]\,\{f_0(\mathbf{p})\,f_0(\mathbf{p}')\,[1-f_0(\mathbf{p}_1)]$$

$$\times[1-f_0(\mathbf{p}_1')]-f_0(\mathbf{p}_1)f_0(\mathbf{p}_1')[1-f_0(\mathbf{p})]\,[1-f_0(\mathbf{p}')]\},$$

where the summation extends over all reciprocal lattice vectors **g**.

$$\nu(|\mathbf{p}|) = \int d\mathbf{r}\,e^{i\,\mathbf{p}\cdot\mathbf{r}/\hbar}\varphi(|\mathbf{r}|),$$

$\varphi(|\mathbf{r}|)$ is the interaction potential of two electrons.

One can easily verify that in the classical limiting case $(\hbar\omega/kT \to 0)$

$$\hat{K}_{ep}\delta\varepsilon = -\hat{J}^{(cl)}_{ep}\delta\varepsilon\partial f_0/\partial\varepsilon^{(0)},\quad \hat{K}_{ee}\,\delta\varepsilon = -\hat{J}^{(cl)}_{ee}\delta\varepsilon\partial f_0/\partial\varepsilon^{(0)}.$$

The dependence of the field and the electron distribution on the coordinates does not affect the volume absorption, i.e., (2) we can drop terms containing spatial derivatives in Eq. 2, which can then be easily solved by successive approximations (since the terms on the right hand side of the transport equation are small in the infrared region of the spectrum),

$$\delta f^{(I)}(\mathbf{p}) = \frac{e}{i\omega}\,(\mathbf{E}\cdot\mathbf{v})\,\frac{\partial f_0}{\partial\varepsilon^{(0)}},\quad \delta f^{(II)} = \frac{e}{\omega^2}(\hat{K}_{ep}+\hat{K}_{ee})\,\mathbf{E}\cdot\mathbf{V}(\mathbf{p}),$$

$$\mathbf{V}(\mathbf{p}) = \mathbf{v}(\mathbf{p}) + \int\frac{dS_{p'}}{v(\mathbf{p}')}\,\Phi(\mathbf{p},\mathbf{p}')\,\mathbf{v}(\mathbf{p}'), \tag{3}$$

where the integration extends over the surface $\epsilon(\mathbf{p}) = \epsilon_0$ in momentum space.

The electrical current density is of the form[2]

$$\mathbf{j} = -\frac{2e}{(2\pi\hbar)^3}\int d\mathbf{p}\cdot\mathbf{v}(\mathbf{p})\,f(\mathbf{p})$$

$$\simeq -\frac{2e}{(2\pi\hbar)^3}\int d\mathbf{p}\cdot\mathbf{v}(\mathbf{p})\left[\delta f(\mathbf{p}) - \delta\varepsilon\,\frac{\partial f_0}{\partial\varepsilon^{(0)}}\right].$$

If we substitute the function of the first approximation into this equation we are led to the following dielectric-constant tensor,[2]

$$\varepsilon_{\alpha\beta} = -(4\pi e^2/\omega^2)(N/m)_{\alpha\beta},\quad(\alpha,\beta = x, y),$$

where

$$(N/m)_{\alpha\beta} = a_{\alpha\beta} + a_{\alpha z}\,a_{z\beta}/a_{zz},\quad a_{ik} = \frac{2}{(2\pi\hbar)^3}\int\frac{dS_{\mathbf{p}}}{v(\mathbf{p})}v_i(\mathbf{p})V_k(\mathbf{p}).$$

We have chosen here a Cartesian coordinate system with a z axis directed out of the metal perpendicularly to its boundary.

The function $\delta f^{(II)}$ gives the conduction current, which can in a natural way be written in the form

$$j_i = [\sigma^{(ep)}_{ik}(\omega) + \sigma^{(ee)}_{ik}(\omega)]\,E_k.$$

Let the incoming wave be polarized along one of the principal directions of the symmetrical tensor $(N/m)_{\alpha\beta}$. We shall take the x and y axes along the principal directions of this tensor. The corresponding volume absorption has then the form

$$A^{(\alpha)} = \frac{8\pi\omega^2}{c^3}\,\delta^3_\alpha\left[\sigma_{\alpha\alpha} - 2\,\frac{a_{\alpha z}}{a_{zz}}\,\sigma_{\alpha z} + \left(\frac{a_{\alpha z}}{a_{zz}}\right)^2\sigma_{zz}\right],$$

where

$$\delta_\alpha^{-2} = (4\pi e^2/c^2)\,(N/m)_{\alpha\alpha}.$$

If the metal surface is oriented in such a way that all three axes x, y, and z can be directed along principal axes of the a_{ik} tensor then

$$A^{(\alpha)} = (8\pi\omega^2/c^3)\,\delta^3_\alpha\sigma_{\alpha\alpha}.$$

The phonon-conductivity tensor $\sigma^{(ep)}_{ik}$ depends in general in rather a complicated fashion on T and ω. If ħω ≫ kT, which is practically always satisfied in the near infrared region of the spectrum, we have*

$$\sigma^{(ep)}_{ik}(\omega) = \frac{e^2}{\omega^2}\int_0^{q_0} dqq^3\coth\left(\frac{h\nu_q}{2kT}\right)B_{ik}(q),$$

$$B_{ik}(q) = \frac{\Delta}{(2\pi\hbar)^6}\,\frac{2\pi}{Mu\hbar}\,C^2$$

$$\times\int d\Omega_{\mathbf{q}}\int\frac{dS_{\mathbf{p}}}{v(\mathbf{p})}V_i(\mathbf{p})\,[\mathbf{V}(\mathbf{p}+\mathbf{q})-\mathbf{V}(\mathbf{p})]_k\,\delta(\varepsilon(\mathbf{p}+\mathbf{q})-\varepsilon_0),$$

where $d\Omega_{\mathbf{q}}$ is an element of solid angle in momentum space. In the low temperature region (T ≪ Θ) it follows from this formula that

$$\sigma^{(ep)}_{ik}(\omega)\,\frac{\omega^2}{e^2} \approx \int_0^{q_0} dq\cdot q^3B_{ik}(q) + \left(\frac{T}{\Theta}\right)^5 48q_0^5B'_{ik}(0) + \ldots.$$

At high temperatures (T ≫ Θ) we have

$$\sigma^{(ep)}_{ik}(\omega)\,\frac{\omega^2}{e^2} \approx \frac{T}{\Theta}\,2q_0\int_0^{q_0} dqq^2B_{ik}(q)$$

$$+\frac{\Theta}{T}\,\frac{1}{6q_0}\int_0^{q_0} dq\cdot q^4B_{ik}(q) + \ldots.$$

Taking the correlation between electrons into account does therefore in both limiting cases not lead to a qualitative change in the temperature dependence of the conductivity and only influences the numerical values of the coefficients of the corresponding powers of T/Θ.

A simple calculation shows (cf. reference 5) that

---

*Here and henceforth we have assumed that the quantities ħω, kT, and kΘ are small compared to the Fermi energy ε_0.

$$\sigma_{ik}^{(ee)}(\omega) = (e/\omega)^2 [(kT)^2 + (\hbar\omega/2\pi)^2]\, b_{ik}\,,$$

where b_{ik} are the constant coefficients

$$b_{ik} = \frac{4e^4\pi^3}{3\hbar(2\pi\hbar)^9} \sum_{g} \iiiint \frac{dS_{\mathbf{p}}}{v(\mathbf{p})} \frac{dS_{\mathbf{p}'}}{v(\mathbf{p}')} \frac{dS_{\mathbf{p}_1}}{v(\mathbf{p}_1)} \frac{dS_{\mathbf{p}_1'}}{v(\mathbf{p}_1')}$$

$$\times [\nu(|\mathbf{p} - \mathbf{p}_1|) - \nu(|\mathbf{p} - \mathbf{p}'_1|)]^2$$

$$\times V_i(\mathbf{p})\, [\mathbf{V}(\mathbf{p}) + \mathbf{V}(\mathbf{p}') + \mathbf{V}(\mathbf{p}_1) - \mathbf{V}(\mathbf{p}_1')]_k$$

$$\times \delta(\mathbf{p} + \mathbf{p}' - \mathbf{p}_1 - \mathbf{p}_1' + 2\pi\hbar\mathbf{g}).$$

In this way, the absorption due to interelectronic collisions changes only in absolute magnitude. However, this fact can apparently be observed experimentally, if we compare the results obtained in the near infrared region of the spectrum with the results of measurements of the static electrical conductivity of the metal. In the latter case the measurements must be performed in the very low temperature range ($T \lesssim 10°K$) so that collisions with the phonons can be neglected. At such temperatures the resistivity of even very pure specimens is mainly caused by impurities. Using this fact, we can easily show that in our case the static electrical conductivity is

$$\sigma_{ik} \approx e^2 a_{ik}^{(0)}/\nu^{(en)} - e^2 (kT)^2 b_{ik}^{(0)} / (\nu^{(en)})^2,$$

where the quantities $a_{ik}^{(0)}$ and $b_{ik}^{(0)}$ are the same respectively as a_{ik} and b_{ik} for $\mathbf{V}(\mathbf{p}) = \mathbf{v}(\mathbf{p})$; for the sake of simplicity we have assumed that frequency $\nu^{(en)}$ of collisions with the impurities is isotropic.

If the interelectronic correlation is essential, the quantities $a_{ik}^{(0)}$ and $b_{ik}^{(0)}$ are, generally speaking, different from a_{ik} and b_{ik}. The quantities a_{ik} and b_{ik} can be determined from measurements in the near-infrared region of the spectrum (1 to $10\,\mu$): a_{ik} from the polarization of the wave, reflected from the metal surface, and b_{ik} from the frequency dependence of the absorption.

In the case of an isotropic Fermi surface, we can easily show that

$$\mathbf{V}(\mathbf{p}) = \mathbf{v}(\mathbf{p})(1 + \gamma(p)),\quad \gamma(p) = \int \frac{dS_{\mathbf{p}'}}{v(\mathbf{p}')} \Phi(\mathbf{p}, \mathbf{p}') \cos\chi,$$

where χ is the angle between the vectors $\mathbf{p}$ and $\mathbf{p}'$. For an isotropic metal accounting for the mutual electron correlation thus reduces to multiplying the earlier expression for the volume absorption by a factor $[1 + \gamma(p_0)]^2$

$$A = A_0 (1 + \gamma(p_0))^2,$$

where

$$A_0 = (2\delta/c)(\nu^{(ep)} + \nu^{(ee)}),\quad \delta = (4\pi N e^2/mc^2)^{-1/2},$$

$\nu^{(ep)}$ and $\nu^{(ee)}$ are the respective effective collision frequencies. According to reference 4 we have in the near-infrared region of the spectrum

$$\nu^{(ep)}(T, \omega) = 2\nu_0^{(ep)}(\Theta) \left(\frac{T}{\Theta}\right)^5 \int_0^{\Theta/T} dx \cdot x^4 \coth\frac{x}{2}\,,$$

where $\nu_0^{(ep)}(T)$ is the classical high-temperature collision frequency (which is proportional to T).

The interelectronic collision frequency is of the form[5]

$$\nu^{(ee)}(T, \omega) = \nu_0^{(ee)}(T)\, [1 + (\hbar\omega/2\pi kT)^2],$$

where $\nu_0^{(ee)}(T)$ is the corresponding classical collision frequency which is well known to be proportional to T^2.

As was noted in reference 5, $\nu_0^{(ee)}(T) \neq 0$ only when Umklapp processes are possible. This statement is justified also in the case of an arbitrary quadratic dispersion law $\epsilon(\mathbf{p}) = \frac{1}{2}\alpha_{ik} p_i p_k$. It is of interest that when there are correlations between the electrons the absorption is, generally speaking, different from zero also when there are no Umpklapp processes in the case of an anisotropic quadratic dispersion law. Indeed, from the fact that $\mathbf{v}(\mathbf{p})$ is a linear function of the components of the vector $\mathbf{p}$ ($v_i = \alpha_{ik} p_k$), it does not follow that the vector $\mathbf{V}(\mathbf{p})$ must possess the same property (see reference 3).

In conclusion the author expresses his gratitude to M. I. Kaganov and M. Ia. Azbel' for discussions of the results of the present paper.

---

[1] L. D. Landau, J. Exptl. Theoret. Phys. (U.S.S.R.) **30**, 1058 (1956), Soviet Phys. JETP **3**, 920 (1956).

[2] V. P. Silin, J. Exptl. Theoret. Phys. (U.S.S.R.) **34**, 707 (1958), Soviet Phys. JETP **7**, 486 (1958).

[3] R. N. Gurzhi, J. Exptl. Theoret. Phys. (U.S.S.R.) **33**, 451 (1957), Soviet Phys. JETP **6**, 352 (1958).

[4] R. N. Gurzhi, J. Exptl. Theoret. Phys. (U.S.S.R.) **33**, 660 (1957), Soviet Phys. JETP **6**, 506 (1958).

[5] R. N. Gurzhi, Thesis, Physico-Techn. Inst. Acad. Sci. Ukrain. S.S.R., 1958.

Translated by D. ter Haar
200

DEPOLARIZATION OF μ^+ MESONS IN METALS

I. V. IAKOVLEVA

Moscow Engineering Physics Institute

Submitted to JETP editor May 5, 1958

J. Exptl. Theoret. Phys. (U.S.S.R.) 35, 970-973 (October, 1958)

The problem of the depolarization of μ^+ mesons in metals is treated on the assumption that mesonium is formed. It is shown that the exchange interaction of the electron in mesonium with the electron fluid of the metal decidedly diminishes the depolarization of μ^+ mesons. On reasonable assumptions about the dimensions of mesonium in a metal, estimates are obtained that are in good agreement with the experimental data.

THE problem of the depolarization of μ^+ mesons in condensed media has taken on importance in connection with the discovery of the nonconservation of parity in weak interactions.[1-3]

As a consequence of the nonconservation of parity in the $\pi^+ \to \mu^+$ decay, the μ^+ mesons are produced polarized along the direction of their motion, and in the two-component theory of the neutrino[2-4] this polarization is complete. To determine the polarization of the μ^+ mesons one can use the nonconservation of parity in the subsequent $\mu^+ \to e^+$ decay.

When integrated over the energy, the angular distribution of the decay positrons has the form[2] $1 + a \cos\theta$. Here θ is the angle between the momentum of the μ^+ meson and the direction of emission of the positron, and $a = Pa_0$, where P is the polarization of the μ^+ meson and a_0 depends on the type of interaction chosen in the theory.

It is possible, however, that during the time elapsing from the production of the μ^+ meson until its decay there can be appreciable depolarization owing to the interaction of the μ^+ meson with the medium.

The experimental data show that the angular anisotropy of the positrons depends strongly on the substance in which the μ^+ mesons are stopped.[5] In particular, in metals the anisotropy is larger than in many other substances. The lifetime of the μ^+ meson ($\tau_0^+ \approx 2 \times 10^{-6}$ sec) is evidently not long enough for any appreciable depolarization to occur in metals.

One of the possible mechanisms for the depolarization of μ^+ mesons is the formation of mesonium — the bound system of a μ^+ meson and an electron.

It is readily verified that owing to the hyperfine structure of the ground state of mesonium the formation of this system $(\mu^+ + e^-)$ leads, in the absence of a surrounding medium, to depolarization of the μ^+ meson by an average factor of two. This value of the depolarization is obtained on the assumption that both directions of the spin of the captured electron are equally probable.

In the case of formation of mesonium in condensed media one must also take into account irreversible processes of interaction with the medium. This means that the behavior of the density matrix ρ of the system of the spins of the μ^+ meson and electron is described by the Wangsness-Bloch equation:[6,7]

$$\frac{\partial\rho}{\partial t} = -\frac{i}{\hbar}[\hat{H},\rho] - \frac{\pi}{\hbar}\,\mathrm{Sp}_b\,[\hat{\bar{V}},\,[\hat{\bar{V}},\rho\rho^{(b)}]], \tag{1}$$

where the index (b) refers to the medium and $\rho^{(b)}$ is the equilibrium density matrix of the medium. Here we have: $\hat{H} = (\epsilon/2)\,\sigma_k^{(\mu)}\sigma_k^{(e)}$, with $\epsilon = 16\mu_e\mu_\mu/3r_0^2$ in vacuum, where $r_0 = \hbar^2/m_e e^2$ is the Bohr radius; $\sigma_k^{(\mu)}$, $\sigma_k^{(e)}$ are the Pauli spin matrices of the μ^+ meson and the electron, respectively; and $\hat{\bar{V}}$ is the part of the operator $\hat{V}$ for the interaction of mesonium with the medium which is diagonal in the energy. ($\bar{V}_{nk} = V_{nk}[\delta(E_n^{(b)} - E_k^{(b)})]^{1/2}$; $E_n^{(b)}$ and $E_k^{(b)}$ are energy levels of the medium.)

The density matrix ρ can be represented as a linear combination of operators:

$$\rho = \sum_{\varkappa k}\rho_{\varkappa k}U_\varkappa^{(\mu)}U_k^{(e)}, \tag{2}$$

$$U_0^{(\mu)} = \chi^{(\mu)}/\sqrt{2};\; U_0^{(e)} = \chi^{(e)}/\sqrt{2};$$

$$U_j^{(\mu)} = \sigma_j^{(\mu)}/\sqrt{2};\; U_i^{(e)} = \sigma_i^{(e)}/\sqrt{2},$$

normalized by the condition

$$\mathrm{Sp}\,(U_i U_k) = \delta_{ik}\,,$$

where $\chi^{(\mu)}$, $\chi^{(e)}$ are unit operators. The coefficients $\rho_{\varkappa k}$ are the average values of the corresponding operators:

$$\rho_{\varkappa k} = \langle U_{\varkappa}^{(\mu)} U_{k}^{(e)} \rangle. \tag{3}$$

As the medium to be considered we take a metal in which all the valence electrons take part in the conductivity. In such a metal the centers of the crystal lattice do not produce any magnetic fields with which the spin of the μ^+ meson could interact, and we neglect the direct interaction of the μ^+ meson with the conduction electrons. Therefore in our case $\hat{V}$ is the operator for the interaction of the spin of the captured electron with the conduction electrons:

Assuming that the relaxation times of the electron spin in the three independent directions are the same, we find without difficulty:

$$\begin{gathered}\frac{\partial \rho_{0i}}{\partial t} = \frac{\varepsilon}{\hbar}\sum_{\varkappa k} e_{ki\varkappa}\,\rho_{\varkappa k} - \frac{W}{\hbar}\rho_{0i}\,,\\ \frac{\partial \rho_{j0}}{\partial t} = \frac{\varepsilon}{\hbar}\sum_{\varkappa k} e_{\varkappa jk}\,\rho_{\varkappa k}\,,\\ \frac{\partial \rho_{ji}}{\partial t} = \frac{\varepsilon}{\hbar}\sum_{\varkappa k} (e_{kij}\,\rho_{0k} + e_{\varkappa ji}\,\rho_{\varkappa 0}) - \frac{W}{\hbar}\rho_{ji}\,;\end{gathered} \tag{4}$$

$\hbar/W$ is the relaxation time of the spin of the captured electron in the metal; $e_{i\kappa k}$ is the antisymmetric unit tensor.

The general solution of the system (4) has the form:

$$\begin{gathered}\rho_{0i} = a_{0i}\exp\{-\gamma_0 t\} + b_{0i}\exp\{-(\gamma_r - i\gamma_i)\,t\}\\ + b^*_{0i}\exp\{-(\gamma_r + i\gamma_i)\,t\},\\ \rho_{j0} = a_{j0}\exp\{-\gamma_0 t\} + b_{j0}\exp\{-(\gamma_r - i\gamma_i)\,t\}\\ + b^*_{j0}\exp\{-(\gamma_r + i\gamma_i)\,t\},\\ \rho_{ji} = a_{ji}\exp\{-\gamma_0 t\} + b_{ji}\exp\{(\gamma_r - i\gamma_i)\,t\}\\ + b^*_{ji}\exp\{-(\gamma_r + i\gamma_i)\,t\}.\end{gathered} \tag{5}$$

Using Eqs. (4) and (5) we get the following system of algebraic equations:

$$\begin{aligned}&-\gamma_0 a_{0i} = (\varepsilon/\hbar)e_{ki\varkappa}\,a_{\varkappa k} - (W/\hbar)\,a_{0i}\,,\\ &-(\gamma_r - i\gamma_i)b_{0i} = (\varepsilon/\hbar)\,e_{\varkappa ki}\,b_{\varkappa k} - (W/\hbar)\,b_{0i}\,,\\ &-\gamma_0 a_{j0} = (\varepsilon/\hbar)\,e_{\varkappa jk}\,a_{\varkappa k},\\ &-(\gamma_r - i\gamma_i)\,b_{j0} = (\varepsilon/\hbar)\,e_{\varkappa jk}\,b_{\varkappa k},\\ &-\gamma_0 a_{ji} = (\varepsilon/\hbar)\,(e_{kij}\,a_{0k} + e_{kji}\,a_{k0}) - (W/\hbar)\,a_{ji}\,,\\ &-(\gamma_r - i\gamma_i)\,b_{ij} = (\varepsilon/\hbar)\,(e_{kji}\,b_{k0} + e_{kij}\,b_{0k}) - (W/\hbar)\,b_{ji}\,.\end{aligned} \tag{6}$$

On the assumption that at the instant of its capture the electron is unpolarized and that there is no polarization correlation ρ_{ji}, we have for the initial conditions:

$$\begin{gathered}a_{0i} + b_{0i} + b^*_{0i} = 0,\\ a_{j0} + b_{j0} + b^*_{j0} = \rho^{(0)}_{j0}, \quad a_{ji} + b_{ji} + b^*_{ji} = 0,\end{gathered} \tag{7}$$

where $\rho^{(0)}_{j0}$ is the value of the polarization vector ρ_{j0} of the μ^+ meson at the initial time.

As will become evident later, in metals $W \gg \epsilon$. Keeping the first few terms of the expansion in the small parameter ϵ/W, we readily obtain the relations

$$\begin{gathered}\rho_{j0} = \rho^{(0)}_{j0}\left\{\left[1 + 2\left(\frac{\varepsilon}{W}\right)^2\right]e^{-2\varepsilon^2 t/\hbar W}\right.\\ \left. - 2\left(\frac{\varepsilon}{W}\right)^2\cos\left(\sqrt{2}\,\frac{\varepsilon}{\hbar}\,t\right)e^{-Wt/\hbar}\right\},\\ \rho_{0i} = \rho^{(0)}_{i0}\left\{2\left(\frac{\varepsilon}{W}\right)^2 e^{-2\varepsilon^2 t/\hbar W} - \sqrt{2}\left(\frac{\varepsilon}{W}\right)\sin\left(\sqrt{2}\,\frac{\varepsilon}{\hbar}\,t\right)e^{-Wt/\hbar}\right\},\\ \rho_{ji} = \rho^{(0)}_{k0}\left\{\left(\frac{\varepsilon}{W}\right)e^{-2\varepsilon^2 t/\hbar W} - \left(\frac{\varepsilon}{W}\right)\cos\left(\sqrt{2}\,\frac{\varepsilon}{\hbar}\,t\right)e^{-Wt/\hbar}\right\}e_{jik}.\end{gathered}$$

Thus the relaxation time of the μ^+ meson spin turns out to be given by $\hbar W/\epsilon^2 \gg \hbar/\epsilon$, and thus during times of the order of $\hbar/\epsilon$, which are characteristic of the hyperfine splitting of mesonium, there is no halving of the polarization. Physically this means that the strong interaction with the conduction electrons breaks the coupling of the captured electron to the spin of the μ^+ meson, so that the depolarization of the μ^+ meson is slowed down.*

To obtain an estimate of the relaxation time of the electron spin in the metal we note the fact that the interaction of the electron in the mesonium atom with the conduction electrons is mainly an exchange interaction. When the mesonium atom collides with an electron with its spin opposite to that of the electron in the mesonium atom, the electrons can change places. Since such exchange collisions are due to Coulomb forces they are predominant over the magnetic interactions, which are relativistic effects.

For the number of exchange collisions in unit time we get:

$$\frac{W}{\hbar} = \frac{m}{\pi^2\hbar^3}\int_0^\infty \bar{n}(E)\,\sigma(E)\,(1 - \bar{n}(E))\,E\,dE,\ . \tag{8}$$

where $\sigma(E)$ is the cross section of the exchange interaction, which depends on the energy E of the conduction electron, and

$$\bar{n}(E) = (e^{(E-\mu)/kT} + 1)^{-1}$$

is the Fermi distribution. Computing the expression (8) under the conditions $kT \ll \mu$, $\mu = E$. (μ is the chemical potential, and E_0 is the Fermi limit energy) and with the approximation $\sigma(E_0) \sim r_0^2$, we readily find:

---

*Similar considerations have been given earlier in a qualitative form by Ia. B. Zel'dovich.

$$W = \frac{mE_0 kT}{\pi^2 \hbar^2} \cdot \sigma(E_0) \sim \frac{mE_0 r_0^2}{\pi^2 \hbar^2} kT;$$

here $\hbar^2/mr_0^2 = me^4/\hbar^2$ is the atomic unit of energy, and E_0 is also of the order of an atomic energy. Thus

$$W \sim kT \approx 300°.$$

Since $\epsilon = 16\mu_e\mu_\mu/3r_0^3 \approx 0.1°$, $W \gg \epsilon$, as was assumed above.

For the relaxation time of the μ^+ meson spin we get: $\tau_{\text{rel}} = \hbar W/2\epsilon^2 \sim 10^{-7}$ sec, i.e., $\tau_{\text{rel}} < \tau_0^+$. With such a ratio of the times some depolarization should occur. It must be noted, however, that in the calculations the radius of mesonium was taken to be the Bohr radius. In actual fact, in condensed media it can be somewhat larger. If we note further that the relaxation time of the μ^+ meson spin is very sensitive to the value assumed for the radius r_0 ($\tau_{\text{rel}} \sim r_0^6$, since $\tau_{\text{rel}} \sim \epsilon^{-2}$ and $\epsilon \sim r_0^{-3}$), when with reasonable assumptions regarding the radius of mesonium in metals we can get satisfactory agreement with experiment. Verification of the assumed depolarization mechanism could be obtained by experiments to determine the angular anisotropy of the positrons from $\pi^+ \rightarrow \mu^+ \rightarrow e$ decay at low temperatures.

The depolarization caused by the formation of mesonium in metals should increase with decrease of the temperature (since $W \sim kT$), whereas with other depolarization mechanisms the behavior will evidently be the opposite of this.

The writer expresses his deep gratitude to V. G. Nosov for directing this work and to S. T. Beliaev for suggesting the topic.

---

[1] T. D. Lee and C. N. Yang, Phys. Rev. **104**, 254 (1956).

[2] L. D. Landau, J. Exptl. Theoret. Phys. (U.S.S.R.) **32**, 405 (1957), Soviet Phys. JETP **5**, 336 (1957).

[3] T. D. Lee and C. N. Yang, Phys. Rev. **105**, 1671 (1957).

[4] A. Salam, Nuovo cimento **5**, 299 (1957).

[5] Garwin, Lederman, and Weinrich, Phys. Rev. **105**, 1415 (1957).

[6] U. Fano, Revs. Modern Phys. **29**, 74 (1957).

[7] R. K. Wangsness and F. Bloch, Phys. Rev. **89**, 728 (1953).

Translated by W. H. Furry
201

SOVIET PHYSICS JETP VOLUME 35 (8), NUMBER 4 APRIL, 1959

ON THE MECHANISM OF STRIPPING IN REACTIONS INVOLVING THE CAPTURE OF TWO NUCLEONS

V. V. KOMAROV, V. G. NEUDACHIN, A. M. POPOVA, and I. B. TEPLOV

Moscow State University

Submitted to JETP editor May 9, 1958

J. Exptl. Theoret. Phys. (U.S.S.R.) **35**, 974-977 (October, 1958)

Reactions of the (n, t) type are examined qualitatively. Two competing processes are discussed: (a) the process of "successive stripping" (n-d-t), and (b) the process of simultaneous capture of two nucleons.

As is known, a characteristic peculiarity of the angular distributions in the stripping reactions (d, p) and (d, n) and in the pick-up reactions (p, d) and (n, d) is the presence of a maximum in the region of small angles whose position permits the determination of the orbital angular momentum l of the captured nucleon.[1] The experimental data (e.g., references 2 to 4) show that a pick-up process may also occur in the reactions (n, t), (d, t), (d, α), and similar ones. In this connection attempts[5-7] were made to give a theoretical foundation for the stripping mechanism in a more general form, as an extension of the direct interaction process.

In the present paper we give a qualitative discussion of the reactions of the type (n, t), (p, t), (n, He^3), and (p, He^3).*

We consider the expression for the amplitude of the reverse reaction (t, n). In analogy to the usual stripping theory,[8] the amplitude is determined by the integral equation

$$\psi = \psi_0 - G\,(V_{01} + V_{02})\,\psi. \tag{1}$$

Here 0 is the index referring to the emitted neutron, 1, 2 are the indices of the nucleons captured by the nucleus, ψ_0 is the wave function of the initial system (nucleus A + triton), G is the Green's function for the Schrödinger equation of the final system (nucleus (A + 2) + neutron), and V_{ij} is the interaction potential of the two nucleons. In Born approximation the ψ on the right hand side is changed to ψ_0. In calculations using the method of distorted waves the Schrödinger equation contains the interaction between the neutron with the nucleus (A + 2), for example, in the form of the optical potential.

Generally speaking, two processes contribute to the amplitude of the reaction: (a) a transition of type (n-d-t) with the formation of a deuteron in the intermediary stage, and (b) a direct transition (n-t), made possible by the fact that the nucleons in the triton, as well as (on account of pair interactions) the nucleons in the nucleus, do not have a definite energy, so that the initial and final states of the nucleons are not orthogonal.

In general the angular distributions of the particles emitted in processes (a) and (b) may be different. We consider these distributions on the basis of the shell model of the nucleus. In this case the reaction cross section is determined, in the Born approximation, by the square of the matrix element

$$\begin{gathered} I = 2\left(\frac{n\,(n-1)}{2}\right)^{1/2} \langle l^{n-2}\,\alpha_2 L_2 S_2 J_2 T_2; \\ \mathbf{k}_t S_t \,|\, V_{01} \,|\, l^n\,\alpha_1 L_1 S_1 J_1 T_1;\ \mathbf{k}_n S_n \rangle, \end{gathered} \tag{2}$$

where we assume LS coupling, having in view the application of this formula to the lightest nuclei with a p shell.*

After summing the square of the matrix element over the magnetic quantum numbers of the initial and final states by the method of Levinson,[9] we obtain the following expression:

$$\begin{gathered} I^2 = 2n\,(n-1)\,(2L_1+1)\,(2S_1+1) \\ \times (2J_1+1)\,(2J_2+1)\,(2S_t+1) \\ \times \sum (2S+1)^{-1}\,(-1)^{\rho}\,(l^n\,\alpha_1\,L_1\,S_1\,T_1 \,|\, l^{n-2}\,\alpha_2\,L_2\,S_2\,T_2;\ l^2\,LST)^2 \\ \times C^2_{T_2T}\,(T_1\,M_{T_1};\ M_{T_2}\,0)\,C^2_{T^1/_2}\,(^1/_2 - {}^1/_2;\ 0 - {}^1/_2)\,D^2_{\mathbf{k}_n,\,\mathbf{k}_t}\,(l^2,\,L) \\ \times \sum_{\lambda} (2\lambda+1)\,(-1)^{\mu}\,W\,(S_1\,S_1\,L_1\,L_1,\ \lambda J_1)\,W\,(S_2\,S_2\,S_1\,S_1;\ \lambda S_1) \\ \times W\,(L_1\,L_1\,L_2\,L_2;\ \lambda L)\,W\,(L_2\,L_2\,S_2\,S_2;\ \lambda J_2); \\ \rho = J_2 - J_1 + S + 2S_2; \end{gathered}$$

---

*The reaction (p, t) for Li^7 was considered by A. I. Baz' (Paper delivered by A. A. Ogloblin at the Conference on Nuclear Reactions in Moscow, 1957).

*The qualitative conclusions are the same for jj coupling.

$$\mu = J_1 + J_2 + L + 2(S_1 + S_2 + L_1 + L_2);$$

$$D^2_{\mathrm{k}_n,\,\mathrm{k}_t}(l^2, L) = (2L+1)^{-1} \sum_{M_L} |\langle \mathrm{k}_t(0, 1, 2)| V_{01} | l^2 L M_L (1, 2);$$

$$\mathrm{k}_n(0)\rangle|^2. \qquad (3)$$

C and W denote, respectively, the Clebsch-Gordan and Racah coefficients; $(l^n\alpha_1 | l^{n-2}\alpha_2;\ l^2)$ is the parentage coefficient.[10,11] The wave functions of the free particles are normalized to unit amplitude. L is the total orbital angular momentum of the two nucleons escaping from the nucleus. A non-zero contribution to expression (3) comes only from those values of L which satisfy the condition

$$L = 0,\ 2,\ \ldots,\ 2l; \quad \mathrm{S}_t + \mathrm{J}_2 = \mathrm{L} + \mathrm{J}_1 + \mathrm{S}_n.$$

The expression for the differential cross section has the usual form:

$$\frac{d\sigma}{d\Omega} = \frac{M_n M_t}{4\pi^2\hbar^4}\,\frac{k_t}{k_n}\,\frac{1}{(2S_n+1)(2J_1+1)}\,I^2. \qquad (4)$$

In either process (a) or (b), the angular distributions are very similar in form to the somewhat smeared curves characteristic for the usual stripping process.[1] The difference between the processes (a) and (b) is that the value of the orbital angular momentum of the captured nucleon in the usual stripping theory is replaced by l in case (a), and by L in case (b). The interference term has, of course, a more complicated form. As in the usual stripping theory (for neutrons of energy ~ 15 to 20 Mev), the cross section for the transition (b) with L = 2 will, other conditions being equal, be one order of magnitude smaller than the cross section for the transition (b) with L = 0.

Figure 1 shows the angular distribution for the process (a) with $l = 1$ (nucleus with a p shell) obtained by an approximate treatment of the "successive stripping" (p-d-t). It was assumed that the energy of the system is conserved in the intermediate stage. The calculation was made for the reaction $\mathrm{Li}^7(\mathrm{p, t})\mathrm{Li}^6$ with E_p = 12 Mev, since experimental data are available for this case.[2]

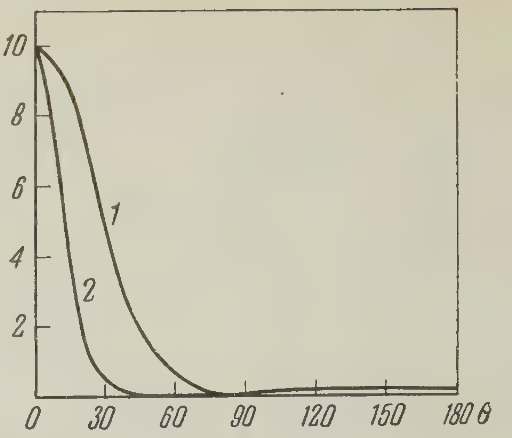

FIG. 2. Angular distribution for process (b); reaction $\mathrm{Li}^7(\mathrm{p, t})\mathrm{Li}^5$, L = 0. Curve 1) E_p = 12 Mev, curve 2) E_p = 35 Mev.

Figure 2 shows the angular distributions for the process (b) with L = 0 at E_p = 12 and 35 Mev. Figure 3 shows the case L = 2 at the same energies. The angular distributions for process (b) are also calculated approximately. In the computation, oscillator wave functions were used for the nucleons bound in the nucleus. This permits the use of a representation that separates the center-of-mass motion of the two nucleons from their relative motion;[12] in the result, the integration in the matrix element becomes much simpler, as it is extended over the whole range of the argument. (This procedure affects the angular distribution very little[13]). Furthermore, the interaction between the nucleons was assumed to have the form of a delta function. The internal wave function of the triton was taken from the paper of Newns.[15] In the general case, when several values L contribute to expression (3), and when the intermediary deuterons in process (a) have sufficient energy, the angular distribution will be the sum of several contributions, and its analysis will be more difficult. An example for this case is the reaction $\mathrm{Li}^7(\mathrm{p, t})\mathrm{Li}^5$, where the sum over L in formula (3) comprises two values, L = 0 and L = 2, with approximately equal parentage coefficients.[10,11] We do not know the ratio of the amplitudes for processes (a) and (b). The experimental angular distributions[2] indicate the presence of two peaks: one with a maximum at 0°, and another, with half the amplitude, at ~ 55°. It may be assumed that the second peak is caused by

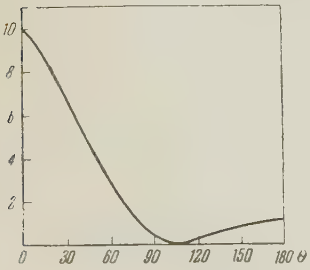

FIG. 1. Angular distribution for process (a); reaction $\mathrm{Li}^7(\mathrm{p, t})\mathrm{Li}^5$, E_p = 12 Mev, l = 1. Abscissa: angles in the center-of-mass system; ordinate: differential cross sections in arbitrary units.

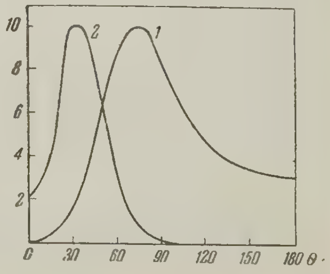

FIG. 3. Angular distribution for process (b); reaction $\mathrm{Li}^7(\mathrm{p, t})\mathrm{Li}^5$, L=2. Curve 1) Ep= 12 Mev, curve 2) Ep= 35 Mev.

either the interference of processes (a) and (b) for $L = 2$, or by process (b) with $L = 2$.

A whole series of cases exists where the situation is less complicated, and where the analysis is less ambiguous. In particular, we have such a case when the sum over L in expression (3) contains only one term, as, for example, in the reaction $Li^6(n, t)He^4$, where $L = 0$. The experimental angular distribution[4] is in qualitative agreement with the theory (Figs. 1 and 2). However, in this case the angular distributions for processes (a) and (b) are similar, which makes their separation impossible. A separation may be possible if the expression (3) contains only the term $L = 2$, for example (Fig. 3). This may be the case if the initial value of J is significantly different from the final value, as, for example, in the reactions $B^{10}(n, t)Be^8$ and $C^{12}(n, t)B^{10}$ with formation of the final nuclei in the ground state. However, experimental data for these reactions are missing up to now.

Processes (a) and (b) may also be separated in the reactions (n, t), (p, t), etc. for which the threshold for deuteron formation E_d^0 is above the threshold for triton formation E_t^0, where $E_d^0 - E_t^0$ is sufficiently large. It is of interest here to compare the angular distributions of the tritons for incident particles of energies below the threshold E_d^0, when only process (b) is possible, and for those of energies above the threshold E_d^0, when both processes are possible. If the probability of process (a) is comparable with the probability of process (b), some changes can be expected in the behavior of the excitation curve in the region of incident energies corresponding to the threshold for process (a). Thus, for the reaction $Be^9(n, t)Li^7$ the thresholds E_t^0 and E_d^0 are respectively equal to 11.5 and 16.2 Mev, while the corresponding values for the reaction $C^{12}(p, t)C^{10}$ are 5.8 and 17.9 Mev. At present, experimental data have only been published for the reaction $Be^9(n, t)Li^7$ at incident energies between E_d^0 and E_t^0.[3] The measured angular distribution has one maximum at 40°. The interpretation of this result is not clear, since expression (3) should get the largest contribution from $L = 0$.

We can also hope for a separation of the processes (a) and (b) if $l > L$. Examples for this may be found among the reactions with nuclei with the shell $1f_{7/2}$. For example, we can expect that in the reaction $Ca^{42}(p, t)Ca^{40}$ ($l = 3$, $L = 0, 1$) the angular distribution for the process (b) has a peak around 0°, while the maximum of the differential cross section for the process (a) will supposedly lie in the region of large angles.

In conclusion, the authors express their gratitude to S. S. Vasil'ev for a discussion of this paper and to A. S. Davydov for a discussion of the formulation of the problem.

---

[1] S. T. Butler, Proc. Roy. Soc. **A208**, 559 (1951).

[2] N. A. Vlasov and A. A. Ogloblin, **Тезисы докладов на Всесоюзной конференции по ядерным реакциям при малых и средних энергиях** (Abstracts of the proceedings of the All-Union Conference on Nuclear Reactions at Small and Intermediate Energies, Academy of Sciences, U.S.S.R.), 1957.

[3] Vasil'ev, Komarov, and Popova, Doklady Akad. Nauk SSSR **119**, 914 (1958), Soviet Phys. "Doklady" **3**, 354 (1958).

[4] G. M. Frye,Jr., Phys. Rev. **93**, 1086 (1954).

[5] J. Dabrowski and J. Sawicki, Phys. Rev. **97**, 1002 (1955).

[6] S. T. Butler, Phys. Rev. **106**, 272 (1957).

[7] Mohamed El Nadi, Proc. Phys. Soc. **70A**, 62 (1957).

[8] E. Gerjuoy, Phys. Rev. **91**, 645 (1953).

[9] I. B. Levinson and V. V. Vanagas, **Оптика и спектроскопия** (Optics and Spectroscopy) **2**, 10 (1957).

[10] I. B. Levinson, Тр. **Физ.-техн. ин-та** АН Лит. ССР (Proc. Phys.-Techn. Inst., Acad. of Sciences, Lithuanian S.S.R.) **2**, 17 and 36 (1957); Тр. АН Лит. ССР (Proc. Acad. of Sciences, Lithuanian S.S.R.) **B4**, 3 (1957).

[11] H. Jahn and M. Vanwieringen, Proc. Roy. Soc. **A209**, 502 (1951).

[12] R. Edmonds and B. Flowers, Proc. Roy. Soc. **A214**, 515 (1952).

[13] J. Talmi, Helv. Phys. Acta **25**, 185 (1952).

[14] T. I. Kopaleishvili, Тр. **Тбилисского гос.** ун-та (Proc. Tbilissi State University) **62**, 83 (1957).

[15] H. C. Newns, Proc. Phys. Soc. **A65**, 916 (1952).

Translated by R. Lipperheide
202

SOVIET PHYSICS JETP VOLUME 35(8), NUMBER 4 APRIL, 1959

ON THE HYDRODYNAMIC THEORY OF MULTIPLE PRODUCTION OF PARTICLES

G. A. MILEKHIN

P. N. Lebedev Physics Institute, Academy of Sciences, U.S.S.R.

Submitted to JETP editor May 9, 1958

J. Exptl. Theoret. Phys. (U.S.S.R.) **35**, 978-981 (October, 1958)

The problem of symmetries in the angular and energy distributions of secondary particles produced in nucleon-nucleus collisions or in collisions of two nuclei is considered on the basis of the hydrodynamic theory of multiple production of particles. It is shown that such symmetry appears in a certain special system of coordinates which is close to the center-of-mass system.

A hydrodynamic theory of multiple production of particles in the collision of two identical particles has been developed in a paper by Landau.[1] In this case it is obvious that the angular and energy distribution of the particles produced by the collision will be symmetrical in the center-of-mass system with respect to the plane perpendicular to the direction of motion of the colliding particles. In the present paper we shall show that in the collision of a nucleon with a nucleus the angular and energy distributions will also be approximately symmetrical in a certain system of coordinates which is close to the center-of-mass system.

It is convenient to conduct the calculations in the reference system in which the colliding particles have equal and opposite velocities. Because of the strong Lorentz contraction of the nucleon and nucleus the disturbance produced in the nucleus by the nucleon cannot spread far in the transverse direction during the time of the collision; we can therefore assume that the nucleon interacts only with a tube of nuclear matter lying directly in front of it.[2] Also because of the Lorentz contraction the motion of the system in the first moments after the collision will be in only one dimension. In proving the symmetry we need consider only the one-dimensional stage of the motion of the nuclear matter.

As has been shown by Khalatnikov,[3] an arbitrary one-dimensional motion of a medium in the extreme relativistic case is described by a potential χ which satisfies the equation

$$3\frac{\partial^2\chi}{\partial\eta^2} - \frac{\partial^2\chi}{\partial y^2} - 2\frac{\partial\chi}{\partial y} = 0, \tag{1}$$

where $y = \ln(T/T_0)$, $\eta = \tanh^{-1} v$, T and v are the temperature and speed of the medium, and T_0 is the initial temperature.* The coordinate x and the time t are expressed in terms of the potential χ in the following way:

$$x = e^{-y}\left(\frac{\partial\chi}{\partial y}\sinh\eta - \frac{\partial\chi}{\partial\eta}\coth\eta\right), \tag{2}$$

$$t = e^{-y}\left(\frac{\partial\chi}{\partial y}\coth\eta - \frac{\partial\chi}{\partial\eta}\sinh\eta\right). \tag{3}$$

Thus if the function $\chi(\eta, y)$ has been found, Eqs. (2) and (3) can be used to find the quantities $\eta(x, t)$ and $y(x, t)$, provided that

$$\partial(\eta, y)/\partial(x, t) \neq 0.$$

In the present paper we confine ourselves to the case in which the ratio n of the length of the tube to the dimensions of a nucleon, which is approximately the same as the number of nucleons in the tube, does not exceed 3.7. In this case (see reference 4), after passage of the shock waves beyond the boundaries of the system, a flow of the matter into empty space begins, in the form of running waves of rarefaction. This motion is described by the formulas:[3]

$$\eta = \pm\sqrt{3}\,y, \tag{4}$$

$$(x - x_1)/(t - t_1) = (v \pm c)/(1 \pm vc). \tag{5}$$

Here $c = 3^{-1/2}$ is the speed of sound; the sign + refers to the wave propagated in the positive x direction, and the sign − refers to the wave propagated in the opposite direction. The instant t_1 is that of the start of the efflux of the matter, and x_1 is the coordinate of the edge of the system at this instant. We choose the origin of our system in such a way that for the wave travelling to the right we have $x_1 = t_1 = 0$. We denote the corresponding quantities for the wave going to the left by l and t_0. As can easily be shown, $l = \frac{1}{4}(n+1)d$, $t_0 = \frac{3}{4}(n-1)d$, where d is the thickness of the relativistically contracted nucleon.

---

*The speed of light is set equal to unity.

According to Eq. (4) $\partial(\eta, y)/\partial(x, t) = 0$ in the region of the running wave, so that the running wave is just that particular solution that is not contained in the general solution of Eq. (1).

After the encounter of the two running waves a region comes into existence in which the variables η and y are independent, and which is accordingly described by Eq. (1). At the boundaries of this region and the running waves the conditions (4) and (5) must be fulfilled; using Eqs. (2) and (3), we get from these the following boundary conditions for χ:

$$\chi = 0 \text{ for } \eta = \sqrt{3}y, \tag{6}$$

$$\chi = -le^{y}\sinh\eta + t_0(e^{y}\cosh\eta - 1) \quad \text{for } \eta = -\sqrt{3}y. \tag{7}$$

The solution of (1) with the boundary conditions (6) and (7) can be obtained in the most convenient form by the following approach. We shall seek the solution in the regions $\eta > 0$ and $\eta < 0$ separately, and require that the two solutions agree for $\eta = 0$. Let us first find the solution for $\eta < 0$. To do this we introduce the new variables

$$\alpha = -\eta, \quad \beta = \eta - \sqrt{3}y, \quad u = \chi e^{y}.$$

After this Eq. (1) and the boundary condition (6) take the forms:

$$u_{\alpha\alpha} - 2u_{\alpha\beta} + u/3 = 0, \tag{8}$$

$$u = 0 \quad \text{for} \quad \beta = 0. \tag{9}$$

We carry out a Laplace transformation on the variable β and seek the solution in the form $U = a(p)e^{k\alpha}$. The quantity k is found from the conditions (8) and (9):

$$k = p - \sqrt{p^2 - {}^1/_3},$$

where we must take the minus sign for the square root. Making the inverse Laplace transformation, we get the solution in the form

$$u = \frac{1}{2\pi i}\int \exp\{-\sqrt{3}yp + \eta\sqrt{p^2 - {}^1/_3}\}\, a(p)\, dp. \tag{10}$$

Let us now consider the region $\eta > 0$. After the replacements

$$\eta' = -\eta,$$

$$u' = u + l\sinh\eta e^{2y} - t_0 e^{y}(\cosh\eta e^{y} - 1),$$

the problem reduces to the previous one, so that for $\eta > 0$

$$u_1 = \frac{1}{2\pi i}\int \exp\{-\sqrt{3}yp - \eta\sqrt{p^2 - {}^1/_3}\}\, a_1(p)\, dp - l\sinh\eta e^{2y} + t_0 e^{y}(\cosh\eta e^{y} - 1). \tag{11}$$

The unknown functions $a(p)$ and $a_1(p)$ are found from the conditions that $u = u_1$ and $\partial u/\partial\eta = \partial u_1/\partial\eta$ for $\eta = 0$. Simple calulations give:

$$a(p) = -\frac{l}{2}\frac{1}{(p + 2/\sqrt{3})\sqrt{p^2 - {}^1/_3}} + \frac{t_0}{2}\left(\frac{1}{p + 2/\sqrt{3}} - \frac{1}{p + 1/\sqrt{3}}\right), \tag{12}$$

$$a_1(p) = -\frac{l}{2}\frac{1}{(p + 2/\sqrt{3})\sqrt{p^2 - {}^1/_3}} - \frac{t_0}{2}\left(\frac{1}{p + 2/\sqrt{3}} - \frac{1}{p + 1/\sqrt{3}}\right). \tag{13}$$

After this, by means of Eqs. (10) and (12) or (11) and (13) we get the solution:*

$$\chi = \frac{\sqrt{3}}{2}\left(l - t_0\frac{\partial}{\partial\eta}\right)e^{y}\int_{\eta/\sqrt{3}}^{y} e^{-2y'} I_0\left(\sqrt{y'^2 - \eta^2/3}\right)dy' + \frac{\sqrt{3}}{2}t_0\frac{\partial}{\partial\eta}\int_{\eta/\sqrt{3}}^{y} e^{-y'} I_0\left(\sqrt{y'^2 - \eta^2/3}\right)dy'. \tag{14}$$

For the collision of identical particles it is obvious that $t_0 = 0$, and the solution found here is the same as that obtained by Khalatnikov.

By means of Eqs. (1) to (3) we can easily obtain the expressions for the derivatives of t and x with respect to y and η:

$$\begin{aligned} \frac{\partial t}{\partial y} &= e^{-y}\left(\frac{\partial\psi}{\partial y}\cosh\eta - \frac{\partial\psi}{\partial\eta}\sinh\eta\right), & \frac{\partial t}{\partial\eta} &= e^{-y}\left(\frac{\partial\psi}{\partial\eta}\cosh\eta - \frac{1}{3}\frac{\partial\psi}{\partial y}\sinh\eta\right), \\ \frac{\partial x}{\partial y} &= e^{-y}\left(\frac{\partial\psi}{\partial y}\sinh\eta - \frac{\partial\psi}{\partial\eta}\cosh\eta\right), & \frac{\partial x}{\partial\eta} &= e^{-y}\left(\frac{\partial\psi}{\partial\eta}\sinh\eta - \frac{1}{3}\frac{\partial\psi}{\partial y}\cosh\eta\right). \end{aligned} \tag{15}$$

Here $\psi = \partial\chi/\partial y - \chi$. The calculation of $\partial\psi/\partial y$ and $\partial\psi/\partial\eta$ gives:

$$\frac{\partial\psi}{\partial y} = \frac{\sqrt{3}}{2}e^{-y}\left(l\frac{\partial}{\partial y} - t_0\frac{\partial}{\partial\eta} - l\right)I_0(z), \tag{16}$$

$$\frac{\partial\psi}{\partial\eta} = \frac{\sqrt{3}}{2}e^{-y}\left(l\frac{\partial}{\partial\eta} - \frac{1}{3}t_0\frac{\partial}{\partial y} - \frac{1}{3}t_0\right)I_0(z); \tag{17}$$

$$z = \sqrt{y^2 - \eta^2/3}.$$

For an overwhelming majority of the particles z is large at the end of the one-dimensional state. It we use the first two terms of the asymptotic expansion of the Bessel function, Eqs. (16) and (17) can be written

---

*The solution of the one-dimensional problem for $n \leq 3.7$ has also been obtained in somewhat different form in reference 5. It is not difficult to reduce the solution there obtained to the form (14), which is convenient for our purposes.

$$\frac{\partial\psi}{\partial y} = \frac{\sqrt{3}}{2}\, le^{-y}\left(\frac{\partial}{\partial y} - 1\right) I_0(z') - \frac{t_0^2}{8\sqrt{3}l}\, e^{-y}\, \frac{I_1(z')}{z'}, \qquad (18)$$

$$\frac{\partial\psi}{\partial\eta} = \frac{\sqrt{3}}{2}\, le^{-y}\, \frac{\partial}{\partial\eta'}\, I_0(z'), \qquad (19)$$

where we have introduced the new variables

$$\eta' = \eta + t_0/2l, \quad z' = \sqrt{y^2 - \eta'^2/3}.$$

For our proof we must expand the right members of Eqs. (18) and (19) in Taylor's series in the differences $\eta' - \eta = \eta_0$.

The choice of the variable η' means that we go over into a new coordinate system moving relative to the original system with the speed $V = \tanh\ \eta_0$. In fact,

$$v' = \tanh\ \eta' = (v + V)/(1 + vV).$$

To sufficient accuracy for practical purposes this new coordinate system coincides with the center-of-mass system (the relative velocity of these systems is given by

$$\tanh\left[\frac{3}{2}\,\frac{n-1}{n+1} - \tanh^{-1}\frac{n-1}{n+1}\right] \leqslant 0.2,$$

since we are considering tubes that are not very long, $n \leq 3.7$).

It can be seen from Eqs. (18) and (19) that $\partial\psi/\partial y$ is an even function of η' and $\partial\psi/\partial\eta'$ is an odd function. From this and Eq. (15) one easily obtains the relations $x'(-\eta', y) = -x'(\eta', y)$, $t'(-\eta', y) = t'(\eta', y)$, from which our assertion about the symmetry of the emission of the particles in this system follows. The deviation from this symmetry in the region described by the solution (14) is of the same order asymptotically as the third term in the asymptotic expansion of the Bessel function, i.e., extremely small at the end of the one-dimensional stage. The running waves are practically entirely responsible for the disturbance of the symmetry. This disturbance is also small, since in the region of the running waves there are very few particles (of the order of one[5,6]). It can be seen from Eqs. (18) and (19) that if we confine ourselves to the first term of the asymptotic expansion of the Bessel function the one-dimensional stage will be described by the same formulas as in the case of the collision of identical particles (i.e., when $t_0 = 0$). Therefore to this accuracy the angular and energy distributions of the particles will be the same as in the collision of identical particles.

---

[1] L. D. Landau, Izv. Akad. Nauk SSSR, Ser. Fiz. **17**, 51 (1953).

[2] I. L. Rozental' and D. S. Chernavskii, Usp. Fiz. Nauk **52**, 185 (1954).

[3] I. M. Khalatnikov, J. Exptl. Theoret. Phys. (U.S.S.R.) **27**, 529 (1954).

[4] S. Z. Belen'kii and G. A. Milekhin, J. Exptl. Theoret. Phys. (U.S.S.R.) **29**, 20 (1955), Soviet Phys. JETP **2**, 14 (1956).

[5] Amai, Fukuda, Iso, and Mato, Progr. Theoret. Phys. **17**, 241 (1957).

[6] N. M. Gerasimova and D. S. Chernavskii, J. Exptl. Theoret. Phys. (U.S.S.R.) **29**, 372 (1955), Soviet Phys. JETP **2**, 344 (1956).

Translated by W. H. Furry
203

SOVIET PHYSICS JETP VOLUME 35(8), NUMBER 4 APRIL, 1959

ON THE PROPAGATION OF ELECTROMAGNETIC WAVES IN A MEDIUM WITH APPRECIABLE SPATIAL DISPERSION

V. M. AGRANOVICH and A. A. RUKHADZE

Submitted to JETP editor May 9, 1958

J. Exptl. Theoret. Phys. (U.S.S.R.) **35**, 982-984 (October, 1958)

A method for dealing with electromagnetic waves in a medium with spatial dispersion is presented which is more detailed than that given by Ginzburg. Expansions are obtained for the "direct" and the "inverse" spatial dispersions.

In recent papers by Pekar[1] and Ginzburg[2] treatments have been given of certain effects that appear in the propagation of electromagnetic waves in media with appreciable spatial dispersion of the dielectric constant. In determining the relation between the polarization **P** and the electric field intensity **E**, Pekar has at certain points used a microscopic approach. On the other hand, Ginzburg's treatment was phenomenological. These papers differed in many of their essential conclusions. Thus it is of interest to examine once more the question of including effects of spatial dispersion.

The microscopic approach is not indispensable for the determination of the connection between the macroscopic quantities **P** and **E**. If we confine ourselves hereafter to a range of frequencies close to one of the resonance frequencies,* a sufficiently general relation between **P** and **E** can be established easily. In fact, with accuracy up to terms of order $(a/\lambda)^2$ inclusive,† the energy of the polarized medium, including effects of spatial dispersion, has the form:

$$H = \delta\int_V \left[\dot{P}_i\dot{P}_i + \beta_{ik}P_iP_k + \gamma_{ikl}P_i\frac{\partial P_k}{\partial x_l} + \alpha_{iklm}\frac{\partial P_i}{\partial x_l}\frac{\partial P_k}{\partial x_m}\right]dV + \frac{1}{8\pi}\int(\mathbf{E}\cdot\mathbf{D} + \mathbf{H}\cdot\mathbf{B})\,dV, \qquad (1)$$

where β_{ik}, γ_{ikl}, α_{iklm} are components of tensors characterizing the medium. The tensor γ_{ikl} corresponds to the optical activity, and vanishes if the substance has a center of inversion. If we go over from the quantities **P**, **E**, and **D** to their Fourier components, the relation (1) leads to the following equations of motion:

$$-\omega^2 P_{\mathbf{q}i} + \beta_{ik}P_{\mathbf{q}k} + i\gamma_{ikl}q_lP_{\mathbf{q}k} + \alpha_{iklm}q_lq_mP_{\mathbf{q}k} - (\omega_0^2/4\pi)D_{\mathbf{q}i} = 0, \qquad (2)$$

where **q** is the wave vector, and $\omega_0 = (2\pi/\delta)^{1/2}$ is the plasma frequency corresponding to the dispersion electrons. If there are no free charges in the medium, Maxwell's equations give an additional relation connecting the quantities $P_{\mathbf{q}i}$ and $D_{\mathbf{q}i}$:

$$-\omega^2\mathbf{D}_\mathbf{q} + c^2q^2\mathbf{D}_\mathbf{q} + 4\pi c^2\{\mathbf{q}(\mathbf{q}\cdot\mathbf{P}_\mathbf{q}) - q^2\mathbf{P}_\mathbf{q}\} = 0. \qquad (3)$$

Equations (2) and (3) completely solve the problem of the characteristic vibrations of the polarized medium.

For isotropic and, generally speaking, for gyrotropic media $\beta = \beta$, $\alpha = \alpha_{1,2}$, $\gamma = \gamma e$, where e is the completely antisymmetric unit tensor of the third rank. Then the system of equations (2) and (3) takes the following form:

$$\begin{gathered}(\beta + \alpha_1q^2 - \omega^2)\mathbf{P}_\mathbf{q} + i\gamma[\mathbf{P}_\mathbf{q}\times\mathbf{q}] + \alpha_2\mathbf{q}(\mathbf{p}_\mathbf{q}\cdot\mathbf{q}) - (\omega_0^2/4\pi)\mathbf{D}_\mathbf{q} = 0,\\ 4\pi c^2\{\mathbf{q}(\mathbf{q}\cdot\mathbf{P}_\mathbf{q}) - q^2\mathbf{P}_\mathbf{q}\} + (c^2q^2 - \omega^2)\mathbf{D}_\mathbf{q} = 0.\end{gathered} \qquad (4)$$

For longitudinal waves $\mathbf{D}_\mathbf{q} = 0$, $\omega^2 = \beta + \alpha q^2$, where $\alpha = \alpha_1 + \alpha_2$. If we introduce the index of refraction n, we find that for longitudinal waves

$$n_\parallel^2 = (c^2/\alpha\omega^2)(\omega^2 - \beta). \qquad (5)$$

For the index of refraction of the transverse waves the system (4) gives an equation of the second degree in the variable n^2.

If the medium is inactive, the equation has the following form:

$$(n_\perp^2\alpha_1\omega^2/c^2 - \omega^2 + \beta)(n_\perp^2 - 1) - n_\perp^2\omega_0^2 = 0. \qquad (6)$$

If we set $\alpha_1 = 0$, then

$$n_0^2 = (\omega^2 - \beta)/(\omega^2 - \beta + \omega_0^2) \equiv \varepsilon_0(\omega), \qquad (7)$$

where n_0 is the index of refraction of the medium with neglect of spatial dispersion. From the relations (5) and (7) it follows that at resonance, where

---

*Just this frequency region is sensitive for the effects of spatial dispersion.

†For crystals a is of the order of the lattice constant, for a plasma it is the Debye screening radius, and so on.

$\epsilon_0 \to \infty$, $n_{\|} \neq 0$. This conclusion agrees with Ginzburg's work and contradicts that of Pekar. In the general case of an anisotropic medium one gets from Eqs. (2) and (3) a complicated equation for the determination of $n(\omega)$:

$$\left\| \left(\omega^2 + \frac{n^2\omega_0^2}{n^2-1}\right)\delta_{ik} - \beta_{ik} - in\frac{\omega}{c}\gamma_{ikl}s_l - n^2\frac{\omega^2}{c^2}\alpha_{iklm}s_l s_m - \frac{n^2\omega_0^2}{n^2-1}s_i s_k \right\| = 0 \tag{8}$$

($\mathbf{q} = n\omega\mathbf{s}/c$). In particular there follows from Eq. (8) the conclusion of Ginzburg, that in cubic crystals inclusion of the spatial dispersion leads to a weak anisotropy of the index of refraction.*

If in Eq. (2) we introduce instead of the quantities $\mathbf{P_q}$ quantities $\mathbf{E_q}$ and $\mathbf{D_q} = \mathbf{E_q} + 4\pi\mathbf{P_q}$, we get the relation

$$(\hat{A} + \omega_0^2)\,\mathbf{D_q} = \hat{A}\mathbf{E_q}, \tag{9}$$

where

$$A_{ik} = \omega^2\delta_{ik} - \beta_{ik} - i\gamma_{ikl}q_l - \alpha_{iklm}q_l q_m.$$

We introduce two matrices $\hat{a}$ and $\hat{b}$ $(\hat{a} + \hat{b} = A)$:

$$a_{ik} = \omega^2\delta_{ik} - \beta_{ik}, \quad b_{ik} = -i\gamma_{ikl}q_l - \alpha_{iklm}q_l q_m.$$

Let us suppose that the coordinate axes coincide with the principal axes of the tensor β_{ik} $(\beta_{ik} = \beta_i\delta_{ik})$. Then the expansions of the direct and inverse dispersion give as expressions for the quantities $\mathbf{D_q}$ and $\mathbf{E_q}$ as power series in the small matrix $\hat{b}$ the following:

$$\mathbf{D_q} = \mathbf{E_q} - \omega_0^2[(\hat{a}+\omega_0^2)^{-1} - (\hat{a}+\omega_0^2)^{-1}\hat{b}(\hat{a}+\omega_0^2)^{-1} + (\hat{a}+\omega_0^2)^{-1}\hat{b}(\hat{a}+\omega_0^2)^{-1}\hat{b}(\hat{a}+\omega_0^2)^{-1} - \ldots]\,\mathbf{E_q}, \tag{10}$$

$$\mathbf{E_q} = \mathbf{D_q} + \omega_0^2[\hat{a}^{-1} - \hat{a}^{-1}\hat{b}\hat{a}^{\;1} + \hat{a}^{-1}\hat{b}\hat{a}^{-1}\hat{b}\hat{a}^{-1} - \ldots]\,\mathbf{D_q}. \tag{11}$$

The expansion (10) is valid in the range of frequencies in which $|\omega^2 - \beta_i + \omega_0^2| \gg |b_{ik}|$, and the expansion (11) in the range in which $|\omega^2 - \beta_i| \gg |b_{ik}|$. From the expansion (10) one can determine the "gyration vector" $\mathbf{f}$ (cf. reference 3). For isotropic media and cubic crystals $\mathbf{f} = f\mathbf{s}$, where

$$f = (\omega/c)\,\omega_0^2\gamma/(\omega^2 + \omega_0^2 - \beta)^2. \tag{12}$$

Since the amount of rotation of the plane of polarization is proportional to ωf, far from resonance the relation (12) leads to Chandrasekhar's empirical formula,[4] which describes the dispersion of the optical activity in certain crystals consisting of inactive molecules. For molecular crystals of arbitrary symmetry the Chandrasekhar formula has been obtained previously by one of the present writers.[5] It is easy to show that the results of reference 5 also follow from the treatment that has been carried through above.

In conclusion the writers express their sincere gratitude to V. L. Ginzburg for valuable discussions, which were of very considerable help in the carrying out of this work.

---

*This anisotropy is absent in Pekar's work.

[1] S. I. Pekar, J. Exptl. Theoret. Phys. (U.S.S.R.) **33**, 1022 (1957), Soviet Phys. JETP **6**, 785 (1958).

[2] V. L. Ginzburg, J. Exptl. Theoret. Phys. (U.S.S.R.) **34**, 1593 (1958), Soviet Phys. JETP **7**, 1096 (1958).

[3] L. D. Landau and E. M. Lifshitz, Электродинамика сплошных сред (Electrodynamics of Continuous Media), Moscow 1957.

[4] S. Chandrasekhar, Proc. Ind. Acad. Sci. **A36**, 118 (1952).

[5] V. M. Agranovich, Оптика и спектроскопия (Optics and Spectroscopy) **1**, 338 (1956).

Translated by W. H. Furry
204

SOVIET PHYSICS JETP VOLUME 35(8), NUMBER 4 APRIL, 1959

THE BEHAVIOR OF A PARTICLE OF ARBITRARY SPIN IN AN EXTERNAL MAGNETIC FIELD

V. S. POPOV

Moscow State University

Submitted to JETP editor May 13, 1958

J. Exptl. Theoret. Phys. (U.S.S.R.) **35**, 985-988 (October, 1958)

A method of disentangling given by Feynman is used to solve the problem of the way the polarization of a particle possessing a magnetic moment changes in an external magnetic field.

In the present paper we treat the problem of the change of the polarization of a particle possessing a magnetic moment under the action of an external magnetic field of arbitrary time dependence. The solution is obtained by means of a method given by Feynman[1] for disentangling operator expressions containing noncommutating operators. This method has hitherto not been widely applied. It has been used to solve only one problem — that of the harmonic oscillator subjected to the action of an arbitrary external force (cf. reference 1, Sec. 5, and reference 4). Therefore it is of interest to solve other quantum-mechanical problems by the Feynman method, in order to elucidate the properties of this method and the difficulties that arise in applying it to concrete problems. One such problem, which can be solved completely by the Feynman method, is considered below. The results themselves are not new, and are for the most part contained in a paper by Majorana,[2] where they were obtained by a different method.

Let us consider a particle with magnetic moment $\mathbf{M} = \gamma\hbar\mathbf{I}$. Here γ is the gyromagnetic ratio and $\mathbf{I}$ is the spin angular momentum of the particle. The transformation of the wave function $\psi(t)$ from the time t to the infinitesimally different time $t + \Delta t$ is accomplished by means of the unitary operator

$$S(t, t+\Delta t) = 1 + i\gamma\mathbf{H}(t)\,\mathbf{I}\,\Delta t = \exp(i\gamma\mathbf{H}(t)\,\mathbf{I}\,\Delta t),$$

where $\mathbf{H}(t)$ is the external magnetic field. From this we get for a finite time interval:

$$\psi(t_2) = S(t_2, t_1)\,\psi(t_1),$$
$$S(t_2, t_1) = \lim_{N\to\infty}\prod_{i=1}^{N}\exp(i\gamma\mathbf{H}(t_i)\,\mathbf{I}\,\Delta t_i) = \exp\left[i\gamma\int_{t_1}^{t_2}\mathbf{H}(t)\,\mathbf{I}\,dt\right], \tag{1}$$

where in this formula t is an ordering parameter and indicates the order of action of the infinitesimal operators $1 + i\gamma\mathbf{H}(t)\mathbf{I}\Delta t$. Because of the fact that the components of the vector $\mathbf{I}$ do not commute with the exponent in Eq. (1) we cannot proceed with the usual rules familiar in analysis.

We shall try to represent $S(t_2, t_1)$ in a "disentangled" form:

$$S(t_2, t_1) = \exp(a\hat{I}_1)\exp(b\hat{I}_0)\exp(c\hat{I}_{-1}),$$
$$I_{\pm 1} = (\mp\hat{I}_x - i\hat{I}_y)/\sqrt{2},\quad \hat{I}_0 = \hat{I}_z, \tag{2}$$

where a, b, c are for the present unknown functions of the time.

By means of Eq. (2) one can easily find the probability amplitude of a transition from the state $|jm\rangle$ at the time t_1 to the state $|jm'\rangle$ at the time t_2, since on using for the right-hand exponent the series expansion

$$\exp(c\hat{I}_{-1}) = \sum_{k=0}^{\infty}\frac{c^k}{k!}\hat{I}_{-1}^{k}$$

we see that when it acts on ψ_{jm} only a finite number of terms of this series remain. Similarly, $\psi^{*}_{jm'}\exp(a\hat{I}_1)$ reduces to a finite sum, and consequently the transition amplitude $\langle jm'|S(t_2, t_1)|jm\rangle$ also contains only a finite number of terms.

To disentangle the operators $\hat{I}_1$, $\hat{I}_0$, $\hat{I}_{-1}$ we use the following artifice: we break up H_1I_1 into a sum of two terms:

$$\mathbf{HI} = xI_1 + (H_1 - x)I_1 + H_0I_0 + H_{-1}I_{-1},$$
$$H_{\pm 1} = (\mp H_x + iH_y)/\sqrt{2},\quad H_0 = H_z \tag{3}$$

and apply to the first term the theorem on the disentangling of an exponential factor proved by Feynman (cf. reference 1, Sec. 3):

$$S(t_2, t_1) = \exp\left[i\gamma\hat{I}_1\int_{t_1}^{t_2}x(t')\,dt'\right]$$
$$\times\exp\left\{i\gamma\int_{t_1}^{t_2}[(H_1 - x)I_1' + H_0I_0' + H_{-1}I_{-1}']\,dt'\right\}, \tag{4}$$
$$I_\mu'(t) = \exp\left[-i\gamma\hat{I}_1\int_{t_1}^{t_2}x(t')\,dt'\right]I_\mu\exp\left[i\gamma\hat{I}_1\int_{t_1}^{t_2}x(t')\,dt'\right].$$

We set

$$a(t) = i\gamma \int_{t_1}^{t_2} x(t')\,dt' \qquad (5)$$

and determine $a(t)$ in such a way that the operator I_1 in Eq. (4) may be completely disentangled. To do this we first find the explicit form of the operators $I'_\mu(t)$. Let $I_\mu(\alpha) = e^{\alpha I_1} I_\mu e^{-\alpha I_1}$; differentiating with respect to α, we obtain the system of equations

$$dI_1(\alpha)/d\alpha = 0, \; dI_0(\alpha)/d\alpha = -I_1(\alpha),$$

$$dI_{-1}(\alpha)/d\alpha = -I_0(\alpha)$$

with the initial conditions $I_\mu(0) = \hat{I}_\mu$. The solution of these equations is

$$I_1(\alpha) = \hat{I}_1, \; I_0(\alpha) = \hat{I}_0 - \alpha\hat{I}_1, \; \hat{I}_{-1}(\alpha) = \hat{I}_{-1} - \alpha\hat{I}_0 + \frac{\alpha^2}{2}\hat{I}_1. \qquad (6)$$

In an analogous way we get

$$e^{\alpha I_0} I_1 e^{-\alpha I_0} = I_1 e^{\alpha}, \; e^{\alpha I_0} I_{-1} e^{-\alpha I_0} = I_{-1} e^{-\alpha}. \qquad (7)$$

Now substituting the operators I'_μ from Eq. (6) into Eq. (4) and equating the coefficient of I_1 to zero, we get the equation for the determination of $a(t)$

$$da/dt = i\gamma(H_1 + H_0 a + {}^1/_2 H_{-1} a^2), \; a(t_1) = 0. \qquad (8)$$

Hereafter we shall everywhere set $t_1 = 0$.

We now have only to disentagle I_0 by means of a transformation of the type (7), and $S(t, 0)$ is then reduced to the form (2), where $a(t)$ is determined from Eq. (8) and the determination of $b(t)$ and $c(t)$ reduces to quadratures:

$$b(t) = i\gamma \int_0^t [H_0(t') + H_{-1}(t')\,a(t')]\,dt',$$
$$c(t) = i\gamma \int_0^t H_{-1}(t')\,e^{b(t')}\,dt'. \qquad (9)$$

An essential point is that a, b, c depend on the gyromagnetic ratio γ, but do not depend on the value of the spin j. Therefore the solution is obtained all at once for particles of arbitrary spin with the same value of γ.

Let us consider an example: a constant field, and perpendicular to it a uniformly rotating alternating field

$$H_z = H_0, \; H_x = H_1 \cos\omega t, \; H_y = H_1 \sin\omega t. \qquad (10)$$

Such a magnetic field is used in experiments on the measurement of the magnetic moments of atomic nuclei, and in this connection was first considered by Rabi.[3] Equation (8) takes the form:

$$-i\frac{da}{d\tau} = \frac{\sin\theta}{\sqrt{2}}(e^{-i\lambda\tau} - {}^1/_2 e^{i\lambda\tau} a^2) - a\cos\theta,$$

where

$$\tau = \omega_0 t, \; \omega_0 = -\gamma\sqrt{H_0^2 + H_1^2}, \; \tan\theta = H_1/H_0, \; \lambda = \omega/\omega_0.$$

Solving the equation with the boundary condition $a(0) = 0$, we find

$$\begin{gathered} a(\tau) = 2(e^{-i\lambda\tau} - e^{-i\mu\tau})/(n_1 e^{i(\lambda-\mu)\tau} - n_2), \\ e^{b(\tau)} = (n_1 - n_2)^2 e^{-i\mu\tau}/(n_1 e^{i(\lambda-\mu)\tau} - n_2)^2, \\ c(\tau) = 2(e^{i(\lambda-\mu)\tau} - 1)/(n_1 e^{i(\lambda-\mu)\tau} - n_2), \\ \mu = \cos\theta + n_1 \sin\theta/\sqrt{2}, \end{gathered} \qquad (11)$$

where n_1, n_2 are the roots of the equation

$$x^2 + 2\sqrt{2}x(\cos\theta - \lambda)/\sin\theta - 2 = 0.$$

Suppose the particle has spin $\frac{1}{2}$ and that at the initial time the z component of the spin is $\frac{1}{2}$. By means of Eq. (2) we find that the probability of reversal of the spin during the time t is given by

$$\underset{{}^1/_2 \to -{}^1/_2}{P(t)} = {}^1/_2 |c(t)\,e^{-b(t)/2}|^2 = \frac{q^2\sin^2\theta}{1 + q^2 - 2q\cos\theta}\sin^2\left(\frac{\omega t}{2}\sqrt{1 + q^2 - 2q\cos\theta}\right), \qquad (12)$$

$$q = \omega_0/\omega = 1/\lambda,$$

which agrees with the result of Rabi.[3]

Let us consider another representation of the S matrix, which is more convenient for particles with larger spin j; we try to represent $S(t, 0)$ in the form

$$S(t, 0) = \exp(i\alpha\hat{I}_x)\exp(i\beta\hat{I}_y)\exp(i\gamma\hat{I}_z), \qquad (13)$$

where α, β, γ are real functions of t (the reality follows from the unitary character of the S matrix; for the representation (2) a, b, c do not have to be real). Carrying out calculations analogous to those performed above, we find that the disentangling of $\hat{I}_x$, $\hat{I}_y$, $\hat{I}_z$ is possible and α, β, γ are determined by a system of equations of the type of Eq. (8), but more complicated. An important fact is that these equations involve only the gyromagnetic ratio γ, and not the spin j itself. Consequently, α, β, and γ do not depend on j and can be expressed uniquely in terms of the a, b, c determined from Eqs. (8) and (9). But each factor in Eq. (13) is the operator for a finite rotation around one of the coordinate axes, and therefore

$$S(t, 0) = D^{(j)}(\varphi, \vartheta, \psi), \qquad (14)$$

and furthermore the Eulerian angles φ, ϑ, ψ that define the resultant rotation are uniquely related to a, b, c and do not depend on j. To express φ, ϑ, ψ in terms of a, b c it suffices to examine the S matrix for a particle with spin $\frac{1}{2}$ situated in the same magnetic field. From Eq. (2)

we find the form of the S matrix in the system of functions $|\frac{1}{2}m>$, $m = \pm\frac{1}{2}$:

$$S^{(1/2)}(t,0) = \begin{pmatrix} e^{b/2} - (ac/2)\,e^{-b/2} & (c/\sqrt{2})\,e^{-b/2} \\ -(a/\sqrt{2})\,e^{-b/2} & e^{-b/2} \end{pmatrix} = D^{(1/2)}(\varphi, \vartheta, \psi), \tag{15}$$

from which we have

$$\sin\frac{\vartheta}{2} = \left(\frac{ac}{2}e^{-b}\right)^{1/2},\ e^{2i\varphi} = \frac{a}{c\,(e^{b} - ac/2)},\ e^{2i\psi} = \frac{c}{a\,(e^{b} - ac/2)}. \tag{16}$$

For the example (10) discussed above we have

$$\sin\frac{\vartheta}{2} = \frac{q\sin\theta}{\sqrt{1+q^2-2q\cos\theta}}\sin\left(\frac{\omega t}{2}\sqrt{1+q^2-2q\cos\theta}\right). \tag{17}$$

The probability of a transition during the time t from the state $|jm>$ into the state $|jm'>$, for a particle with spin j, is given by

$$P_{m\to m'}(t) = |D^{(j)}_{mm'}(\varphi, \vartheta, \psi)|^2$$

$$= [(j+m)!\,(j-m)!\,(j+m')!\,(j-m')!]\cos^{4j}\left(\frac{\vartheta}{2}\right) \tag{18}$$

$$\times\left[\sum_{\nu}(-1)^{\nu}\frac{\left(\tan\frac{\vartheta}{2}\right)^{2\nu-m+m'}}{\nu!\,(\nu-m+m')!\,(j+m-\nu)!\,(j-m'-\nu)!}\right]^2.$$

If we take here $j = \frac{1}{2}$, $m = \frac{1}{2}$, $m' = -\frac{1}{2}$ and substitute the value (17), we get the result (12).

In the general case the polarization state of a particle is characterized by a density matrix ρ. Expanding it in terms of the tensor operators T_{IM}, we find the way the polarization changes with time:

$$\rho = \sum_{0\leqslant I\leqslant 2j}\rho_{IM}T_{IM};\ \rho_{IM}(t) = \sum_{M'}\rho_{IM'}(0)\,D^{(I)}_{M'M}(\varphi, \vartheta, \psi). \tag{19}$$

If the particle has not only a magnetic dipole moment but also higher multipole moments, a complete disentangling of the S matrix cannot be carried through. This is due to the fact that for $I > 1$ the commutator $[T_{IM}, T_{IM'}]_-$ of two tensor operators of the same rank I cannot be expressed in terms of tensor operators of this same rank. It is always possible however, to separate out from the S matrix the part corresponding to the magnetic-dipole part of the Hamiltonian, $-\gamma(\mathrm{HI})$. A meaning can be given to this if it is permissible to regard the rest of the Hamiltonian as a perturbation.

I am sincerely grateful to I. S. Shapiro for his interest in this work and a number of valuable suggestions.

---

[1] R. P. Feynman, Phys. Rev. **84**, 108 (1951).
[2] E. Majorana, Nuovo cimento **9**, 43 (1937).
[3] I. I. Rabi, Phys. Rev. **51**, 652 (1937).
[4] I. Fujiwara, Prog. Theoret. Phys. **7**, 433 (1952).

Translated by W. H. Furry
205

SOVIET PHYSICS JETP VOLUME 35(8), NUMBER 4 APRIL, 1959

ON AXIALLY ASYMMETRIC NUCLEI

B. T. GEILIKMAN

Moscow State Pedagogic Institute

Submitted to JETP editor May 14, 1958

J. Exptl. Theoret. Phys. (U.S.S.R.) **35**, 989-991 (October, 1958)

The possibility of the existence of nuclei lacking axial symmetry is demonstrated within the framework of the generalized model.

DAVYDOV and Filippov[1] have assumed that medium and heavy nuclei may possess axial asymmetry and have calculated the energy levels of the nucleus and the probabilities of radiative transitions on the basis of this assumption. However, the theoretical possibility of the existence of axially-asymmetric nuclei is doubtful, since in A. Bohr's model the equilibrium value for the axial asymmetry of nuclei turns out to be equal to zero.[2*] It will be shown below that a consistent investigation within the framework of the generalized model leads to the result that in the general case the axial asymmetry of nuclei differs from zero.

We consider several nucleons outside a filled shell, which move within the field of the core and which do not interact with each other. The field of the core can be represented by an oscillator field which at a certain energy U_0 goes over into a horizontal straight line (if U_0 is significantly greater than the energy of the nucleon the horizontal part of the curve need not be taken into account). In the adiabatic approximation we neglect at first the kinetic energies of the "slow" collective degrees of freedom that determine the shape of the nucleus and evaluate the energies of the "fast" nucleon degrees of freedom corresponding to arbitrary values of the parameters that describe the shape of the nucleus. Therefore all three oscillator frequencies must at first be taken as arbitrary. Then the energy E_{nuc} of m nucleons is given by:

$$E_{\text{nuc}} = \hbar \sum_{s=1}^{m} \left[\left(n_{xs} + \frac{1}{2}\right)\omega_1 + \left(n_{ys} + \frac{1}{2}\right)\omega_2 + \left(n_{zs} + \frac{1}{2}\right)\omega_3\right];$$
$$n_{xs} + n_{ys} + n_{zs} = n. \qquad (1)$$

Since each frequency ω_i is inversely proportional[3] to the square of the corresponding semi-axis of the ellipsoid R_i we can assume that:

$$(\omega/\omega_1)^{1/2} = R_1/R = 1 + b_{00} - b_0 + b_2\sqrt{6};$$
$$(\omega/\omega_2)^{1/2} = R_2/R = 1 + b_{00} - b_0 - b_2\sqrt{6}; \qquad (2)$$
$$(\omega/\omega_3)^{1/2} = R_3/R = 1 + b_{00} + 2b_0.$$

We find b_{00} from the condition that the nuclear volume remains constant $\omega_1\omega_2\omega_3 = \omega^3 =$ const $(R_1R_2R_3 = R^3)$: $b_{00} \approx b_0^2 + 2b_2^2$, while the parameters $a_0 = 4(\pi/5)^{1/2}b_0 = \beta\cos\gamma$ and $a_2 = 4(\pi/5)^{1/2}b_2 = \beta\sin\gamma/\sqrt{2}$ have for small β the same meaning as in Bohr's paper;[2] β is the parameter describing the deviation of the nucleus from spherical shape, while γ is the axial asymmetry parameter (in the case of $\gamma = n\pi/3$; $n = 0, \mp 1, \ldots$ the nucleus is axially symmetric). To E_{nuc} we should add the energy of the core which depends on b_0 and b_2: $E_{core} = c_n\hbar\omega(b_0^2 + 2b_2^2)/2 = 5c_n\hbar\omega\beta^2/32\pi$. We substitute (2) into (1) and keep only terms linear in b_0 and b_2; the quadratic terms can be neglected in comparison with E_{core}, since their ratio to E_{core} is, evidently, of the order of $\sim m/(A-m) \ll 1$ (A is the nuclear mass number). In order to find the equilibrium shape of the nucleus we shall find the minimum with respect to b_0 and b_2 of the energy $E = E_{nuc} + E_{core} = m(n + 3/2)\hbar\omega + \Delta E$;

$$\Delta E/\hbar\omega = \sum_s^m [n_{xs}(b_0 - b_2\sqrt{6})/2 + n_{ys}(b_0 + b_2\sqrt{6})/2 - n_{zs}b_0] + c_n(b_0^2/2 + b_2^2). \qquad (3)$$

We then obtain

$$b_0 = \frac{1}{2c_n}\sum_s(2n_{zs} - n_{xs} - n_{ys}); \quad b_2 = \frac{1}{c_n}\sqrt{\frac{3}{8}}\sum_s(n_{xs} - n_{ys});$$
$$\beta = \frac{1}{c_n}\sqrt{\frac{\pi}{5}}\left\{3\left[\sum_s(n_{xs} - n_{ys})\right]^2 + \left[\sum_s(2n - 3n_{xs} - 3n_{ys})\right]^2\right\}^{1/2};$$
$$\gamma = \tan^{-1}\left\{\sum_s(n_{xs} - n_{ys})\left[\sum_s(2n - 3n_{xs} - 3n_{ys})\right]^{-1}\right\}. \qquad (4)$$

On substituting (4) into (3) we obtain

$$\frac{\Delta E}{\hbar\omega} = -\frac{1}{8c_n}\left\{3\left[\sum_s(n_{xs} - n_{ys})\right]^2 + \left[\sum_s(2n - 3n_{xs} - 3n_{ys})\right]^2\right\}.$$

---

[*] Brief indications of the possibility of the existence of axially asymmetric nuclei can be found only in unpublished numerical calculations of Gursky.[4]

It is easily seen that for a given principal quantum number n the lowest value of ΔE for one nucleon, equal to $\Delta E_{\min} = -n^2\hbar\omega/2c_n$, is given in three cases by:

$$1)\ n_x = n,\ n_y = n_z = 0;\ 2)\ n_y = n,\ n_z = n_x = 0;$$
$$3)\ n_z = n,\ n_x = n_y = 0.$$

Here $\gamma = 0$ or $\mp\pi/3$, i.e., the nucleus is axially symmetric; $\beta = (2/c_n)\sqrt{\pi/5}\ n$.

We can show that $\beta > 0$, i.e., that the nucleus is elongated, by calculating R_i from (2). As a result of this calculation we find that two of the ratios R_i/R are equal to $1 - n/2c_n$, while the third ratio is equal to $1 + n/c_n$. The second nucleon may have the same quantum numbers but for the third nucleon only the following values of n_x, n_y, n_z are possible as a result of Pauli's exclusion principle: $n_x = n-1$, $n_y = 1$, $n_z = 0$ or $n_y = 0$, $n_z = 1$ (if for the first pair of nucleons $n_x = n$) and two similar combinations involving $n_y = n-1$ and $n_z = n-1$, if $n_y = n$ or $n_z = n$ for the first pair. At the same time $\gamma = \tan^{-1}[\sqrt{3}/(6n-3)]$ (if we measure γ from zero) i.e., the nucleus turns out to be axially asymmetric. As further nucleons are added γ increases (cf. below; here $m \ll (n+1)(n+2)$ and $n > 1$, for $n = 1$, $\gamma = 0$).

Number of nucleons, m	$\leqslant 2$	3	4	5	6
$\tan\gamma$	0	$\frac{\sqrt{3}}{6n-3}$	$\frac{\sqrt{3}}{4n-3}$	$\frac{\sqrt{3}}{2.5n-3}$	$\frac{\sqrt{3}}{2n-3}$

We now consider an almost completely filled shell. In this case the energy is given by

$$\frac{\Delta E}{\hbar\omega} = c_{n+1}(b_0^2/2 + b_2^2) - \sum_s^m [n_{xs}(b_0 - b_2\sqrt{6})/2$$
$$+ n_{ys}(b_0 + b_2\sqrt{6})/2 - n_{zs}b_0],$$

m is the number of holes. The minimum in ΔE corresponds to

$$b_0 = \frac{1}{2c_{n+1}}\sum(n_{xs} + n_{ys} - 2n_{zs});$$

$$b_2 = \frac{1}{c_{n+1}}\sqrt{\frac{3}{8}}\sum_s(n_{ys} - n_{xs}).$$

As in a previous case the lowest value of ΔE for one hole is obtained for $n_x = n$, or $n_y = n$ or $n_z = n$, but $\beta = -(2/c_{n+1})\sqrt{\pi/5}\ n$ (two of the ratios R_i/R are equal to $1 + n/2c_{n+1}$, while the third is equal to $1 - n/c_{n+1}$), i.e., the nucleus is flattened. The values of γ are the same ones as in the first case (cf. above). Thus, γ reaches its greatest values in the middle of the shell. The average value of γ for a given shell decreases as the shell number n increases.

In Bohr's paper[2] the equilibrium value of γ was zero because the existence of axial symmetry was assumed from the outset in the expression for E_n.

The model in which the shells are filled in succession, starting with the first one, reduces to the model discussed above, which has several nucleons outside a filled shell. Indeed, if we use oscillator functions, we can easily show that the energy of each filled shell is equal to:

$$E_n/\hbar = {}^1/_3(n+1)(n+2)(n+{}^3/_2)(\omega_1+\omega_2+\omega_3)$$
$$\approx (n+1)(n+2)(n+{}^3/_2)\,\omega(1 + 5\beta^2/64\pi). \tag{5}$$

There are no terms linear in β in this expression. Thus, the filled shells, just as in the liquid drop model, determine only the value of the stiffness for the parameter β. We note that in the shell model we can determine the shape of the nucleus exactly, without having to restrict ourselves to small values of β. In order to do this it is necessary only, as was done earlier, to assume that levels with different values of n do not cross. The energy of a nucleus having m nucleons outside a filled shell is given by: $E = E_{\text{nuc}} + E_{\text{core}}$; E_{nuc} is determined for formula (1) as before; E_{core}, as is seen from (5), is of the form: $E_{\text{core}}/\hbar = c_n'(\omega_1+\omega_2+\omega_3 - 3\omega)$. The value of c_n' is smaller than the value given by (5), owing to Coulomb repulsion.

By finding directly the minimum of E with respect to ω_1, ω_2, ω_3, subject to the condition $\omega_1\omega_2\omega_3 = \text{const}$, we obtain:

$$\omega_i = \omega(\varepsilon_{i+1}\varepsilon_{i+2}\varepsilon_i^{-2})^{1/3};\ E_{\min}/\hbar = 3\omega[(\varepsilon_1\varepsilon_2\varepsilon_3)^{1/3} - c_n'];$$

here $\varepsilon_\alpha = \sum_s^m (n_{\alpha s} + {}^1/_2) + c_n'$.

For $m = 1$ or $m = 2$ the lowest value $E_{\min}$ is obtained, as before, for $n_x = n$, or $n_y = n$, or $n_z = n$; in the case of $m = 1$ two of the frequencies are equal to $\omega(n + c_n' + \frac{1}{2})^{1/3}/(c_n' + \frac{1}{2})^{1/3}$, while the third is equal to $\omega(c_n' + \frac{1}{2})^{2/3}/(n + c_n' + \frac{1}{2})^{2/3}$ and the nucleus is axially symmetric (small values of β correspond to $mn \ll c_n'$). For the third nucleon $n_x = n-1$ (if for the first pair $n_x = n$) etc. In this case

$$\omega_1/\omega = (c_n' + {}^5/_2)^{1/3}(c_n' + {}^3/_2)^{1/3}(3n + c_n' + {}^1/_2)^{-2/3};$$

$$\omega_2/\omega = (c_n' + {}^3/_2)^{1/3}(3n + c_n' + {}^1/_2)^{1/3}(c_n' + {}^5/_2)^{-2/3};$$

$$\omega_3/\omega = (3n + c_n' + {}^1/_2)^{1/3}(c_n' + {}^5/_2)^{1/3}(c_n' + {}^3/_2)^{-2/3},$$

i.e., the nucleus is asymmetric.

The model considered by us is too crude and simple to permit us on its basis to draw any quantitative conclusions with respect to real nuclei, but it is quite sufficient to establish the possibility in principle of the existence of axially asymmetric nuclei.

I wish to express my gratitude to A. S. Davydov for providing the possibility of studying his paper[1] prior to its publication and for interesting discussions.

---

[1] A. S. Davydov and G. F. Filippov, J. Exptl. Theoret. Phys. (U.S.S.R.) **35**, 440 (1958), Soviet Phys. JETP **8**, 303 (1959).

[2] A. Bohr, Kong. Dansk. Vid. Selsk. Mat.-fys. Medd., **26**, 14 (1952); **Проблемы современной физики** (Problems of Modern Physics) No. 9 (1955).

[3] W. Heisenberg, The Physics of Atomic Nuclei (Russian transl.) IIL, 1953.

[4] L. Wilets and M. Jean, Phys. Rev. **102**, 788 (1956); M. Gursky, Phys. Rev. **98**, 1205 (1955).

Translated by G. Volkoff
206

SOVIET PHYSICS JETP VOLUME 35(8), NUMBER 4 APRIL, 1959

ISOTOPIC EFFECT IN THE RESIDUAL ELECTRICAL RESISTANCE OF METALS

I. Ia. POMERANCHUK

Submitted to JETP editor May 20, 1958

J. Exptl. Theoret. Phys. (U.S.S.R.) 35, 992-995 (October, 1958)

The existence of various isotopes in a metal leads to a difference in the zero vibrations, depending on the different masses of these isotopes. This in turn leads to the appearance of a non-regular perturbing field which is capable of scattering the conduction electrons. Thus, even in crystals without physical defects or chemical impurities, a residual electrical resistance may arise. The magnitude of this resistance is estimated.

IF several different isotopes are found in the lattice of a metal, scattering of the conduction electrons is brought about by deviation of the zero vibrations of a given isotope from their average value. This effect leads to a finite residual electrical resistance in the metal at absolute zero, under conditions in which the resistance due to chemical and physical impurities is absent. In other words, in the purification of the metal, its residual resistance ought to decrease at first and then approach a constant limit. The scattering of interest to us is a result of the combined action of the following terms in the Hamiltonian, which we shall regard as a perturbation:

(1) The additional kinetic energy of the isotope contributes a term to the Hamiltonian (the origin of the coordinates coincides with the atom of the isotope at its equilibrium position)

$$-\frac{M-\overline{M}}{2}\dot{\mathbf{u}}(0)^2$$
$$= -\sum_{f_1 f_2 j_1 j_2}\frac{M-\overline{M}}{2}\left(a_{f_1 j_1}-a^{+}_{f_1 j_1}\right)\left(a_{f_2 j_2}-a^{+}_{f_2 j_2}\right)(\mathbf{j}_1\cdot\mathbf{j}_2)\frac{\hbar\sqrt{\omega_1\omega_2}}{2\,\overline{M}N}; \tag{1}$$

M is the mass of the isotopic atom, $\overline{M}$ the average mass of the atoms of the metal:

$$\overline{M}=\sum_s c_s M_s,\quad \sum_s c_s = 1, \tag{2}$$

c_s is the concentration of the isotope with mass M_s, $\mathbf{u}(0)$ the vector of the displacement of the isotopic atom from its equilibrium position, and $\mathbf{j}$ the polarization vector.

(2) We express the interaction of the electron with the vibrations of the lattice V (considering an idealized isotopic model of the metal without sound dispersion) in the usual way:

$$V(\mathbf{x}) = V_0\sum_{fj}\sqrt{\frac{\hbar\omega}{2\,\overline{M}s^2N}}\left(a_{fj}e^{i\mathbf{f}\mathbf{x}/\hbar}+a^{+}_{fj}e^{-i\mathbf{f}\mathbf{x}/\hbar}\right); \tag{3}$$

V_0 is the energy of atomic order, and s the speed of sound. Equations (1) and (3) give the scattering of the electrons in the third approximation of perturbation theory. Equation (1) contains matrix elements of three types: (a) those corresponding to phonon scattering $(\sim a_{\mathbf{f}_1},\ a^{+}_{\mathbf{f}_2})$, (b) those corresponding to the emission of two phonons $(\sim a^{+}_{\mathbf{f}_1},\ a^{+}_{\mathbf{f}_2})$, and (c) those corresponding to the absorption of two phonons $(\sim a_{\mathbf{f}_1},\ a_{\mathbf{f}_2})$. The process of scattering under the action of (1) and (3) is therefore obtained from the summation of three chains of processes which are graphically illustrated in the drawing (the initial and final states of the electron are characterized by the momenta $\mathbf{p}_0$ and $\mathbf{p}$ respectively).

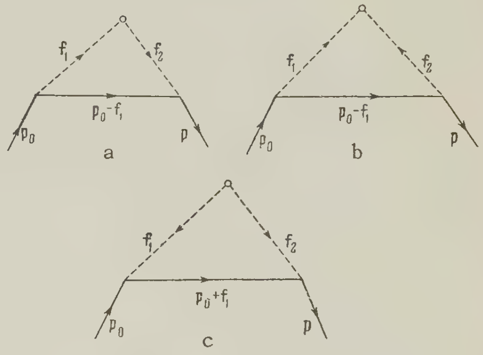

The matrix element arising under the action of the chain (b) has the form

$$-\sum_{j_1 j_2}\int V_0^2\frac{\hbar^2\omega_1\omega_2}{4\,\overline{M}^2s^2N^2}(M-\overline{M})(\mathbf{j}_1\cdot\mathbf{j}_2)$$
$$\times\left\{\frac{1}{[E(\mathbf{p}_0)-E(\mathbf{p}_0-\mathbf{f}_1)-sf_1][-sf_1-s\,|\,\mathbf{f}_1-\mathbf{q}\,|]}\right\}\frac{\Omega\,d^3f_1}{(2\pi\hbar)^3}. \tag{4}$$

Here $\hbar\omega_1 = sf_1$ and $\hbar\omega_2 = sf_2 = s\,|\mathbf{q}-\mathbf{f}_1|$, where $\mathbf{q}=\mathbf{p}_0-\mathbf{p}$ is the change in the momentum of the electron. Since only the order of magnitude of the effect is of interest, we shall not consider the difference in the velocities of longitudinal and transverse sound. In the case of chain (c) we obtain a matrix element that differs from (4) only in that, instead of the expression which appears in the curly brackets, we have

$$\left\{\frac{1}{[E(\mathbf{p}_0) - E(\mathbf{p}_0 + \mathbf{f}_1) - s\,|\mathbf{f}_1 + \mathbf{q}|]\,[-sf_1 - s\,|\mathbf{f}_1 + \mathbf{q}|]}\right\}. \tag{5}$$

In the integration of (4) and (5), the first factor can pass through zero. It is necessary to get around the singularity in a way as corresponds to the function $\delta_+(x)$. In this case, two terms arise — an integral in the sense of the principal value, and a term containing $i\delta[E(\mathbf{p}_0) - E(\mathbf{p}_0 - \mathbf{f}_1) - sf_1]$ in case (4), and $i\delta[E(\mathbf{p}_0) - E(\mathbf{p}_0 + \mathbf{f}_1) - s\,|\mathbf{f}_1 + \mathbf{q}|]$ in case (5). The part containing the principal value corresponds to $|E(\mathbf{p}_0) - E(\mathbf{p}_0 \mp \mathbf{f}_1)|$ a value on the order of atomic energies, which is significantly greater than sf_1 or $s\,|\mathbf{f}_1 + \mathbf{q}|$. Therefore, the principal value due to the chain (2) and (3) is the same in each case. Since the function $\delta[E(\mathbf{p}_0) - E(\mathbf{p}_0 - \mathbf{f}_1) - sf_1]$ appears with the factor i, it makes a contribution to the imaginary part of the transition matrix element. However, the sum of the imaginary parts entering from all the chains must vanish, since the matrix element itself must be real. Electrons are scattered by an isotopic atom by the presence of a small perturbing field close to the isotope. This field is produced by the deviations of the zero-point vibrations of the given isotope from their mean amplitude, taking into account the fact that the mean of the zero-point vibrations is small in comparison with the lattice constant a and, moreover, that the difference of the zero-point vibrations of the isotope is doubly small because of the smallness of $(M - \overline{M})/\overline{M}$, and because the perturbing field acting on the electron is very small. The scattering in such a field $V_{\text{eff}}(\mathbf{x})$ must be described by the Born approximation. The scattering matrix element with transfer of momentum $\mathbf{q}$ is expressed by the integral

$$\int V_{\text{eff}}(\mathbf{x})\, e^{i\mathbf{q}\mathbf{x}/\hbar}\, d^3x,$$

which is a real number, since $V_{\text{eff}}(\mathbf{x}) = V_{\text{eff}}(-\mathbf{x})$.

Thus there remains in (4) only the principal value of the integral, which is the same for the chains (b) and (c). The matrix element corresponding to the chain (a) has the form

$$-\sum V_0^2 \int \frac{\hbar^2\omega_1\omega_2}{4\,\overline{M}^2 s^2 N^2}\,\frac{\Omega\, d^3f_1}{(2\pi\hbar)^3}$$
$$\times\left\{\frac{1}{[E(p_0) - E(\mathbf{p}_0 - \mathbf{f}_1) - sf_1]\,[E(p_0) - E(\mathbf{p}_0 - \mathbf{f}_1) - s\,|\mathbf{f}_1 - \mathbf{q}|]}\right\}$$
$$\times(\mathbf{j}_1\cdot\mathbf{j}_2). \tag{6}$$

In the integral here, both factors in the curly brackets must vanish; therefore, we have, first, an integral in the sense of the principal value, and second, two terms proportional to

$$i\delta[E(p_0) - E(\mathbf{p}_0 - \mathbf{f}_1) - sf_1]$$
$$\text{or}\quad i\delta[E(p_0) - E(\mathbf{p}_0 - \mathbf{f}_1) - s\,|\mathbf{f}_1 - \mathbf{q}|].$$

In accord with what was said above, we shall omit these.

For an estimate of the order of magnitude, we can also discard the principal value of the integral in chain (a), since the energy differences in the curly brackets of (6) correspond to energies of atomic magnitudes. One of the differences in (4) and (5) was $\hbar\omega_1 + \hbar\omega_2 \sim \Theta \ll V_0$ (V_0 is of the order of several electron volts). We therefore have, in order of magnitude, the following matrix element (neglecting the chain (a) and assuming $E = p^2/2m$, m = effective mass of the electron) at $\mathbf{q} = 0$:

$$\mathscr{M} = -\frac{3}{2}V_0^2a^3\,\frac{M - \overline{M}}{(2\pi\hbar)^3 N\overline{M}^2 s}\int \frac{f\,|\mathbf{f} - \mathbf{q}|}{f + |\mathbf{f} - \mathbf{q}|}\,\frac{d^3f}{E(p_0) - E(\mathbf{p}_0 - \mathbf{f})}$$
$$= -\frac{3}{2}V_0^2a^3\,\frac{M - \overline{M}}{(2\pi\hbar)^3 N\overline{M}s}\,\frac{\pi m f_0^3}{3p_0}\,F\left(\frac{f_0}{2p_0}\right);$$

$$F\left(\frac{f_0}{2p_0}\right) = \ln\frac{2p_0 - f_0}{2p_0 + f_0} - \frac{2p_0}{f_0} - \frac{8p_0^3}{f_0^3}\ln\frac{4p_0^2 - f_0^2}{4p_0^2}; \tag{7}$$

f_0 is the maximum momentum of the phonon, p_0 is the momentum of the electron on the Fermi surface. We assume that $2p_0 > f_0$. Substituting $(2\pi^2)^{1/3}\hbar/a$ in (7) in place of f_0, we find

$$\mathscr{M} = -\frac{V_0^2(M - \overline{M})m}{8\,\overline{M}^2 s p_0 N}\,F\left(\frac{f_0}{2p_0}\right). \tag{8}$$

We thus find the total probability of scattering W in a medium consisting of s isotopes with concentration c_s, neglecting the dependence of $\mathscr{M}$ on q:

$$W \approx \frac{F^2}{64\pi}\,\frac{a^3V_0^4\,\overline{(M - \overline{M})^2}\,m^2}{\overline{M}^4 s^2\hbar^4}\,\frac{dp_0}{dE} = \frac{V_0^4F^2(\overline{M^2} - \overline{M}^2)\,a^3m^3}{64\pi\overline{M}^4 s^2\hbar^4 p_0}; \tag{9}$$

$$\overline{M^2} - \overline{M}^2 = \sum_s c_sM_s^2 - \Big(\sum_s c_sM_s\Big)^2.$$

The corresponding free path l is equal to:

$$l = \frac{dE}{dp}\,\frac{1}{W} \approx \frac{64\pi\overline{M}^4 s^2\hbar^4 p_0^2}{(\overline{M^2} - \overline{M})^2\,V_0^4F^2m^4a^3}. \tag{10}$$

Frequently, the quantities that enter here can be expressed in terms of the electrical conductivity σ at high temperatures ($T \gg \Theta$), which in our model is equal to

$$\sigma = 4\,(4\pi)^{1/3}e^2n_e^2\hbar^3a\overline{M}s^2/m^2V_0^2T \tag{11}$$

(T in energy units, n_e is the number of conduction electrons in 1 cm^3). Substituting $m^2V_0^2/\overline{M}s^2$ from (11) in (10), we find:

$$l \approx (36)^{1/3}\pi^{5/3}\frac{\overline{M}^2}{\overline{M^2}-\overline{M}^2}\,\frac{\sigma^2T^2}{n_e^2\nu_e^{4/3}as^2F^2e^4}\,; \qquad (12)$$

$$(\nu_e = n_e a^3).$$

For $\frac{\overline{M^2}-\overline{M}^2}{\overline{M}^2} \sim 10^{-4}$, which corresponds to natural tin, we obtain l of the order of several millimeters. If we introduce the path brought about by the impurities as

$$l_i = a/\varepsilon \qquad (13)$$

(ϵ is the concentration of impurities) then (12) corresponds to the following effective concentration ϵ_0:

$$\varepsilon_0 \approx \frac{1}{(36)^{1/3}\pi^{5/3}}\,\frac{\overline{M^2}-\overline{M}^2}{\overline{M}^2}\,\frac{n_e^2\nu_e^{4/3}a^2s^2F^2e^4}{\sigma^2T^2}\,. \qquad (14)$$

For $\epsilon \gg \epsilon_0$, the residual resistance is proportional to ϵ. For $\epsilon < \epsilon_0$, it no longer depends on ϵ.

We can improve the estimate of l if we introduce data on the electronic specific heat.

In conclusion, I express my gratitude to Academician L. D. Landau and to Iu. V. Sharvin for discussions in connection with this paper.

Translated by R. T. Beyer
207

SOVIET PHYSICS JETP VOLUME 35(8), NUMBER 4 APRIL, 1959

DEPOLARIZATION OF μ^--MESONS IN HYDROGEN, DEUTERIUM, AND TRITIUM

V. B. BELIAEV and B. N. ZAKHAR'EV

Joint Institute for Nuclear Research

Submitted to JETP editor May 19, 1958; resubmitted June 9, 1958

J. Exptl. Theoret. Phys. (U.S.S.R.) 35, 996-1000 (October, 1958).

A number of effects that depolarize μ^--mesons in hydrogen, deuterium and tritium, are considered. Complete depolarization in hydrogen and tritium occurs before the mesic atom is slowed down to thermal energies. Depolarization probabilities are given for the case of capture of the mesic atom by the K-orbit and in the case of formation of mesic molecules. A correction $\sim \mu/M$ was included in the calculations to allow for the motion of the nuclei. An approximate allowance is made for the difference in the hyperfine structure levels.

THE capture of polarized μ^- mesons is of interest in the investigation of the nature of the interaction between μ^- mesons and protons. However, the situation is made complicated by the fact that the mesons may be depolarized by the medium. In this paper this question is investigated for the cases of hydrogen, deuterium, and tritium.*

Partial depolarization of the meson occurs when it is captured by the K-orbit of the hydrogen mesic atom. A polarized meson with $s_z = 1/2$ can form together with a proton a system having a total spin either $F = 1$, or $F = 0$. The component F_z takes on the values 1 and 0 with equal probability. (In an unpolarized medium a polarized meson has equal probability of encountering a proton with its spin parallel or antiparallel to the z axis.) In the case $F_z = 0$ the meson "forgets" the initial direction of its spin (it becomes depolarized). However, the state $F_z = 1$ "remembers" the direction of the μ^- spin (depolarization does not occur). Thus, the probability of depolarization during the formation of mesic hydrogen is equal to $1/2$.

Similar arguments in the case of tritium and deuterium lead respectively to the values $1/2$ and $2/3$.

The main effect that depolarizes μ^--mesons which enter liquid hydrogen is the so-called "charge exchange" of the mesic atoms — the transfer of μ^- from the orbit of one atom to the orbit of another atom (this was pointed out to us by Zel'dovich). The probability of such processes

$$(p_1)_\mu + p_2 \to p_1 + (p_2)_\mu; \quad (d_1)_\mu + d_2 \to d_1 + (d_2)_\mu;$$
$$(t_1)_\mu + t_2 \to (t_2)_\mu + t_1 \tag{1}$$

can be computed by the method proposed by Zel'dovich and Sakharov.[2]

A system consisting of two identical nuclei and a meson can exist either in a symmetric Σ_g or an antisymmetric Σ_u state* with respect to a reversal of sign of the meson coordinates (inversion). By utilizing the fact that there are no transitions between the states Σ_u and Σ_g, we regard any state of our system as a superposition of these two noncoherent waves (Σ_u and Σ_g form a complete set of eigenfunctions of the interaction Hamiltonian).

Consider a mesic atom $(p_1)_\mu$ incident on a proton p_2. If we denote the state of the three particles in the case when μ^- is in the orbit of the first (second) proton by Φ_{p_1} (Φ_{p_2}), then

$$\Sigma_u = (\Phi_{p1} - \Phi_{p2}) / \sqrt{2}, \quad \Sigma_g = (\Phi_{p1} + \Phi_{p2}) / \sqrt{2}. \tag{2}$$

For large distances between $(p_1)_\mu$ and p_2 we can take the wave function Φ_{p_1} in the form of a converging wave:

$$\Psi_{\text{init}} = \Phi_{p1} = (e^{-ipr}/r)(\Sigma_u + \Sigma_g)/\sqrt{2}. \tag{3}$$

After scattering, the waves Σ_u and Σ_g will be shifted in phase by α_u and α_g respectively:

$$\Psi_{\text{final}} = (e^{ipr+i\alpha_u}/r)\Sigma_u/\sqrt{2} + (e^{ipr+i\alpha_g}/r)\Sigma_g/\sqrt{2} \tag{4}$$

or alternatively:

$$\Psi_{\text{final}} = (e^{ipr}/2r)\left[\Phi_{p1}(e^{i\alpha_u} + e^{i\alpha_g}) + \Phi_{p2}(e^{i\alpha_g} - e^{i\alpha_u})\right]. \tag{5}$$

The square of the absolute value of the coefficient of Φ_{p_2} determines the probability of charge exchange:

$$W = 1/2\left[1 - \cos(\alpha_u - \alpha_g)\right]. \tag{6}$$

We now determine α_u and α_g. They are equal

---

*An estimate of the charge-exchange cross section at thermal energies of the mesic atom has been made by Gershtein[1] for the case $(p_1)_\mu + p_2 \to p_1 + (p_2)_\mu$.

*We have in mind the ground states of the system.

TABLE I. Phases for the scattering of mesic atoms by nuclei

Energy E (ev), c.m.s.	In state Σ_u			In state Σ_g		
	Medium					
	Hydrogen	Deuterium	Tritium	Hydrogen	Deuterium	Tritium
100	—1.890	—2.936	—3.740	2.389	3.182	3.662
10	—0.646	—1.042	—1.360	3.173	5.104	5.749
1	—0.211	—0.343	—0.450	3.192	5.888	6.207
0.5	—0.145	—0.238	—0.313	3.186	6.011	6.248
0.1	—0.065	—0.106	—0.140	3.160	6.160	6.267
0.05	—0.047	—0.077	—0.101	3.157	6.195	6.276
0.01	—0.021	—0.034	—0.045	3.147	6.243	6.278

TABLE II. Cross sections for the scattering of mesic atoms by nuclei in 10^{-19} cm^2

Energy E(ev), c.m.s.	In state Σ_u			In state Σ_g		
	Medium					
	Hydrogen	Deuterium	Tritium	Hydrogen	Deuterium	Tritium
100	0.466		0.0545	0.242	0.421	
10	1,874	1.925	1.645		2.208	0,447
1	2.268	2.874	3.26	0.131	3.831	0.0998
0.5	2.130	2.830	3.225	0.1834	3.686	0.0421
0.1	2,178	2,890	3.35	0.156	3.900	0.0423
0.05	2.250	3.020	3.46	0.242	3.960	0.0176
0.01	2,280	2.990	3.48	0.151	4.160	0.0463

to twice the scattering phases δ_u and δ_g. Indeed, the asymptotic expression for the s component of the plane incident plus the spherical diverging waves $e^{ikz} + f(\theta)e^{ikr}/r$ will be given by:[3]

$$\frac{e^{i\delta}\sin(kr+\delta)}{kr} = \frac{1}{2ikr}\left[e^{2i\delta+ikr} - e^{-ikr}\right].$$

To find the scattering phases it is more convenient to solve, instead of the Schrödinger equation, the equivalent nonlinear first-order equation, obtained from the Schrödinger equation

$$u'' + (k^2 - V)u = 0 \tag{7}$$

by the substitution $u = \exp\left(\int \varphi\, dr\right)$, where[6] $\varphi = k\cot[kr + y(r)]$.

We thus have

$$y'(r) = -\alpha V(r)\sin^2(\beta r + y(r)) \tag{8}$$

together with the boundary condition $y(0) = 0$, where $\alpha = 2me^2/k\hbar^2$, $\beta = ka_0$, m is the reduced mass of the two heavy particles, a_0 is the Bohr radius of the mesic atom, $y(r)$ is a function that approaches the scattering phase $\delta(k)$ as $r \to \infty$, $V(r)$ is the effective interaction potential between the nuclei. We shall denote the latter by $V_1(r)$ when the three particles are in the Σ_u state, and by $V_2(r)$ when they are in the Σ_g state. Within the region of attraction, the potential $V_2(r)$ was chosen in the form of Morse's function with parameters taken[4,5] in agreement with spectroscopic data for the molecular ion H_2^+.

$V_1(r)$ is a repulsive potential and $V_2(r)$ is an attractive potential. Both potentials satisfy the conditions

$$\lim_{r\to 0} r^2 V(r) = 0; \quad \lim_{r\to\infty} rV(r) = 0,$$

imposed on $V(r)$ in Drukarev's paper.[6] Since V_1 and V_2 become infinite at $r = 0$ the boundary condition was taken in somewhat altered form: $y(\epsilon) = 0$, where ϵ is a very small quantity. The phases are stable with respect to small changes in ϵ.

Since the ratio μ/M of the meson mass to the nuclear mass is not negligible, appropriate corrections must be introduced into the potentials given above. The values of such corrections for the molecular ion H_2^+ are given by Dalgarno.[7] By means of a simple recalculation we obtain them for the case $(H_2)_\mu^+$ of interest to us. The results of numerical calculations carried out by S. Lomnev are given in Table I.

The values of the cross sections for processes (1) are given in Table II.

The scattering cross section in the case of deuterium in the state Σ_g is considerably larger than the cross section in hydrogen and in tritium. This is explained by the fact that in the mesic molecular ion $(d_2^+)_\mu$ there is a level close to 0, which produces a resonance. At the same time in the case

TABLE III

Energy E(ev), c.m.s.	Probability of charge exchange			Charge exchange cross sections, 10^{-19} cm²		
	Medium					
	Hydrogen	Deuterium	Tritium	Hydrogen	Deuterium	Tritium
100	0.824	0.027	0.809	0.426	0.007	0.139
10	0.393	0.019	0.541	2.032	0.049	0.932
1	0.067	0.003	0.133	3.464	0.0776	2.292
0.5	0.035	0.0012	0.075	3.570	0.061	2.550
0.1	0.007	0.0003	0.015	3.619	0.067	2.585
0.05	0.004	0.00013	0.0088	3.978	0.066	2.992
0.01	0.0005	0.00003	0.0016	2.585	0.0776	2.757

of the repulsive potential we obtain a smooth dependence of the cross section on the nuclear masses, as expected in view of the absence of bound states in the case of Σ_u.

The probabilities and the cross sections for charge exchange are given in Table III. The probabilities of charge exchange W are given in Table III in dimensionless units; the charge exchange cross sections are $\sigma = 4\pi k^{-2}W$.

In the case of deuterium the probability of losing the polarization as a result of one charge exchange is equal to ⅔, just as in the case of capture into the K orbit of the mesic atom.

It should be noted that during the collision time $\tau < 10^{-16}$ sec at energies $E > 0.01$ ev the interaction between the spins does not have time to flip them over, and therefore the "forgetting" occurs in the interval between transfers. The energy of interaction of the μ^--meson spin with the nuclear spin is given by $E \sim 0.2$ ev. The characteristic time of the spin-spin interaction (the time for depolarization in states with $F_z = 0$) is of order $\hbar/E \sim 10^{-15}$ sec. The time which the μ^- spends in the orbit of a mesic atom between successive charge exchanges is greater than 10^{-11} sec, as may be seen from Table III. From this it follows that in the state $F = 1$, $F_2 = 0$ the μ^- has time to become completely depolarized.

The phenomenon of charge exchange is possible only if the nuclear charge is $Z = 1$, otherwise the mesic atom will not be neutral and because of the Coulomb barrier the nuclei will be unable to approach each other to a distance $\sim 10^{-11}$ cm at which a transfer of the μ^- meson can occur. For this reason one of the effects mentioned by Day and Morrison[8] will not occur.

So far we have not taken into account the difference between the hyperfine structure levels of the mesic atom. At energies > 0.2 ev its effect on the scattering process can be neglected. At lower energies one should introduce into the charge exchange cross section a correction factor v_f/v_i where v_f is the velocity after the collision, while v_i is the velocity before the collision.[2,3] An exact calculation to take into account the energy of the hyperfine structure has been carried out by Gershtein.[1]

When the energy of the mesic atom is comparable with the binding energy of the hydrogen molecule, we must take into account the fact that the mesic atom is scattered not by free protons but by protons bound in the H_2 molecule. Owing to the very small size of the mesic atom in comparison with the hydrogen molecule, this is carried out in a manner similar to that in which binding is taken into account in the scattering of slow neutrons in hydrogen.[9,10] For the case of mesic atoms of thermal energy such a calculation has been made by Gershtein.[11]

After slowing down, the μ^- are captured into the orbit of one of the nuclei. The binding energy released goes into electron conversion (Auger effect) and into the breaking up of the hydrogen molecule. The mesic atom formed in this process receives a recoil energy on the order of several tens of electron volts.

In each collision of the mesic atom with nuclei it will lose on the average half its energy until it slows down to thermal velocities. By making use of such an outline of the various processes it is not difficult to follow the process of depolarization of the μ^- meson. From Table III it may be seen that in hydrogen and in tritium the complete depolarization of the μ^- meson due to charge exchange occurs before the mesic atom is slowed down to energies of several electron volts. In deuterium depolarization due to charge exchange practically does not occur at energies above thermal. One may hope that because of the level close to zero in the mesic molecular ion $(d_2^+)_\mu$ the latter will be formed prior to the complete depolarization of the muon. After the $(d_2^+)_\mu$ ion has been formed the process of "forgetting" the spin orientation will cease.

If the deuterium contains a small number of tritium nuclei the meson will soon transfer to one of them, and since such a process is irreversible further charge exchange processes will not occur. Such an effect can also prevent the complete loss of polarization.* It would be very interesting to check this experimentally. It should also be noted that if hydrogen nuclei could be polarized, the depolarization of the μ^- due to charge exchange and to the formation of molecules could be avoided. However, at the present time this cannot be accomplished.

Shmushkevich has called attention to the depolarization effect due to the spin-orbit coupling during the successive transitions of the meson between the levels of the mesic atom. Results of the experimental work carried out by Ignatenko et al.[12] indicate that the depolarization in such a case does not exceed 80%.

We take pleasure in expressing our gratitude to Academician Ia. B. Zel'dovich for directing this work, to S. S. Gershtein for very useful discussions, and also to Prof. Ia. A. Smorodinskii and A. E. Ignatenko for their interest in this work.

The authors are indebted to S. Lomnev for carrying out the numerical calculations on an electronic computer.

---

*A similar effect in hydrogen in the presence of a small admixture of deuterium does not affect the depolarization, since $W_{\text{depol}} > W_{\text{charge exch}}$ (pd).

[1] S. S. Gershtein, J. Exptl. Theoret. Phys. (U.S.S.R.) **34**, 463 (1958), Soviet Phys. JETP **7**, 318 (1958).

[2] Ia. B. Zel'dovich and A. D. Sakharov, J. Exptl. Theoret. Phys. (U.S.S.R.), **32**, 947 (1957), Soviet Phys. JETP **5**, 775 (1957).

[3] L. D. Landau and E. M. Lifshitz, **Квантовая механика** (Quantum Mechanics) Moscow, 1948 [Engl. Transl. Pergamon, 1958].

[4] P. Gombas, (The Many-Particle Problem in Quantum Mechanics) [Russian Transl., IIL, 1953].

[5] P. M. Morse, Phys. Rev. **34**, 57 (1929).

[6] G. F. Drukarev, J. Exptl. Theoret. Phys. (U.S.S.R.) **19**, 247 (1949).

[7] A. Dalgarno, Proc. Roy. Soc. **A237**, 383 (1956).

[8] T. B. Day and P. Morrison, Phys. Rev. **107**, 912 (1957).

[9] H. Bethe, Nuclear Physics (Russ. Transl.) part 2, p. 112, 1948.

[10] M. Hammermesh and J. Schwinger, Phys. Rev. **69**, 145 (1946).

[11] S. S. Gershtein, J. Exptl. Theoret. Phys. (U.S.S.R.) **34**, 993 (1958), Soviet Phys. JETP **7**, 685 (1958).

[12] Ignatenko, Egorov, Khalupa, and Chultem, J. Exptl. Theoret. Phys. (U.S.S.R.) **35**, 894 (1958), Soviet Phys. JETP **8**, this issue, p. 621.

Translated by G. Volkoff
208

SOVIET PHYSICS JETP VOLUME 35(8), NUMBER 4 APRIL, 1959

ON THE THEORY OF THE OPTICAL PROPERTIES OF CONDUCTORS IN THE CASE OF OBLIQUE INCIDENCE OF THE RADIATION

V. P. SILIN

P. N. Lebedev Physics Institute, Academy of Sciences, U.S.S.R.

Submitted to JETP editor May 21, 1958

J. Exptl. Theoret. Phys. (U.S.S.R.) 35, 1001-1004 (October, 1958)

A macroscopic theory of the optical properties of conductors is given for the case in which the mean free path of the electrons is not small in comparison with the characteristic distance for damping of the electromagnetic field. The difference from the usual optics of conductors comes from the inclusion of the surface current caused by the scattering of the electrons at the surface of the specimen. The case considered is that of incidence of radiation at an arbitrary angle with the surface of a massive conductor. It is shown that the effective complex indices of refraction depend on the angle of incidence, and also that the indices for different polarizations of the radiation differ from each other by a quantity of the order of the ratio of the speed of an electron to the speed of light.

THE theory of the optical properties of conductors with neglect of the anomalous skin effect is a problem of macroscopic electrodynamics. For an isotropic substance one can use as the constitutive equation of the material the relation

$$\mathbf{D} = \varepsilon(\omega)\mathbf{E}, \tag{1}$$

which connects the amplitude of the electric displacement with that of the electric field strength in the case in which the time dependence has the form $e^{i\omega t}$. In Eq. (1) $\epsilon(\omega) = \epsilon_1(\omega) + i\epsilon_2(\omega)$ is the complex dielectric permeability (our $\mathbf{D}$ is often written $\mathbf{D} - i(4\pi/\omega)\mathbf{j}$). On the other hand, it is often necessary to take into account the anomalous character of the skin effect, which is caused by the fact that in the optical region the depth of penetration of the electromagnetic field into a conductor is often comparable with, or even much smaller than, the mean free path of the electrons. Ordinarily the treatment of the optical properties of conductors in the region of the anomalous skin effect is based on a microscopic theory.[1-7] In the present note we shall give a macroscopic theory of the optics of conductors which is valid for the case in which the mean free path of the electrons is not small in comparison with the characteristic distance for damping of the electromagnetic field.

For the applicability of the macroscopic description it is essentially sufficient that during a single period of the field an electron traverses a distance much smaller than the skin depth, and in the optical region this condition is always fulfilled. The distance traversed by an electron during one vibration of the field is of the order of magnitude v/ω, where v is the speed of the electrons. Therefore we assume that

$$v/\omega \ll \delta \sim c/\sqrt{|\varepsilon(\omega)|}\,\omega \quad \text{or} \quad v/c \ll 1/\sqrt{|\varepsilon(\omega)|}. \tag{2}$$

For ordinary metals in the optical region this is equivalent to the condition $|\epsilon(\omega)| \ll 10^5$. Owing to this we can assume that during a period of the field a conduction electron is not displaced; therefore the connection of the current and the field is a local one, and in particular we can use the relation (1). At the surface of the conductor, however, owing to the diffuse scattering of the electrons, an additional effect arises which produces a surface resistance. Since such an effect of scattering at the surface is important only for electrons that lie within a depth below the surface of the metal of the order of magnitude of the distance traversed by an electron during one vibration of the field, it is clear that because of the smallness of this distance in comparison with the skin depth in the optical region we can assume that the diffuse scattering at the surface leads to a surface current*

$$\mathbf{i} = \gamma(\omega)\{\mathbf{E} - \mathbf{n}(\mathbf{n}\,\mathbf{E})\}. \tag{3}$$

Here $\mathbf{n}$ is the normal to the surface of the conductor and $\gamma(\omega)$ is the surface conductivity. An elementary estimate based on the theory of free electrons gives in the optical region $\gamma \sim (e^2 n_0/m)v(2\pi/\omega)^2$, where n_0 is the density of the conduction electrons, m is the mass and v the speed of an electron, and ω is the frequency of the alternating field. It is assumed moreover that the fraction of the electrons that undergoes diffuse scattering at the surface of the conductor is not small compared with unity. This value of γ agrees in order of magnitude with the value that can be deduced from the papers devoted to the microscopic optics of conductors.[1-6]

---

*It follows Onsager's general principle of the symmetry of the kinetic coefficients[8] that for an anisotropic crystal γ is a symmetric surface tensor, $\gamma_{ik} = \gamma_{ki}$. Furthermore in the case of no losses γ_{ik} is pure imaginary, and losses are due to the real part of γ_{ik}.

By means of Maxwell's equations and the material equations (1) and (3), one can determine the complex reflection coefficients. For a plane semi-infinite conductor the ratio of the amplitudes of the reflected wave (**R**) and the incident wave (**A**), in the case in which the electric vector is perpendicular to the plane of incidence, is given by

$$r_s = \frac{\cos\theta - \sqrt{\varepsilon(\omega) - \sin^2\theta} - 4\pi\gamma/c}{\cos\theta + \sqrt{\varepsilon(\omega) - \sin^2\theta} + 4\pi\gamma/c} = \frac{\cos\theta - \sqrt{n_s^2 - \sin^2\theta}}{\cos\theta + \sqrt{n_s^2 - \sin^2\theta}}. \tag{4}$$

Here θ is the angle of incidence (the angle between the direction of the wave vector of the incident wave and the normal to the surface of the conductor), and $n_s(\theta)$ is the effective complex index of refraction, given by the expression (cf. reference 7)

$$n_s^2(\theta) = \varepsilon(\omega) + (8\pi\gamma/c)\sqrt{\varepsilon(\omega) - \sin^2\theta} + (4\pi\gamma/c)^2 \tag{5}$$

One takes everywhere the value of the square root that has a negative imaginary part. The effective index of refraction is introduced in such a way that Eq. (4) agrees in form with the usual equation, the only difference being that n_s is now a function of the angle of incidence θ.

For the case of a wave with the electric vector lying in the plane of incidence we have the following expression for the ratio of the components of the respective amplitudes along the normal to the surface of the conductor:

$$r_p = \frac{\cos\theta\,[\sqrt{\varepsilon - \sin^2\theta} + 4\pi\gamma/c + \sin^2\theta/\sqrt{\varepsilon - \sin^2\theta}] - 1}{\cos\theta\,[\sqrt{\varepsilon - \sin^2\theta} + 4\pi\gamma/c + \sin^2\theta/\sqrt{\varepsilon - \sin^2\theta}] + 1}$$

$$= \frac{n_p^2\cos\theta - \sqrt{n_s^2 - \sin^2\theta}}{n_p^2\cos\theta + \sqrt{n_s^2 - \sin^2\theta}}, \tag{6}$$

where $n_p(\theta)$ is defined by the relation

$$n_p^2(\theta) = \varepsilon(\omega) + \frac{8\pi\gamma}{c}\sqrt{\varepsilon - \sin^2\theta} + \left(\frac{4\pi\gamma}{c}\right)^2 + \frac{4\pi\gamma}{c}\,\frac{\sin^2\theta}{\sqrt{\varepsilon(\omega) - \sin^2\theta}}. \tag{7}$$

From a comparison of the formulas (5) and (7) we see that $n_s(\theta)$ and $n_p(\theta)$ are the same, and we can speak of the existence of a single complex index of refraction, only under the condition that $\epsilon(\omega) \gg 1$, so that we can neglect the last term of the right member of Eq. (7), or else under the condition that we can neglect $\gamma(\omega)$. The latter condition corresponds to the normal skin effect.

In the limiting case $\epsilon(\omega) \gg 1$ the complex indices of refraction are not only equal, but also are independent of the angle of incidence. Therefore under these conditions the existence of the surface current (3) can be taken into account by the introduction of the effective dielectric permittivity

$$\varepsilon_{\mathrm{eff}}(\omega) = \varepsilon(\omega) + (8\pi\gamma/c)\sqrt{\varepsilon(\omega)} + (4\pi\gamma/c)^2.$$

In the short-wave region $\epsilon(\omega)$ is not large in comparison with unity, so that in taking the anomalous skin effect into account in this region it is necessary to use different complex indices of refraction for waves with different polarizations. Such an assertion is already made in the paper of Collins[7] on the microscopic theory of the anomalous skin effect for oblique incidence of the radiation on the surface of the metal. Quantitatively, however, there is an important difference here. Namely, in our treatment it turns out that n_p and n_s differ by a quantity $\sim 4\pi\gamma/c$, which is of the order v/c in the region $\epsilon(\omega) \sim 1$. In Collins' work, on the other hand, the two indices of refraction differ in this region by a quantity of the order of unity. This difference is due to the fact that in reference 7 the equation $\operatorname{div} \mathbf{E} = 0$ is assumed for the microscopic field, and this is approximately legitimate only in the region $|\epsilon| \gg 1$.

We write out below the formulas that determine the principal angle of incidence Θ and the principal azimuth Ψ; the former is given by the equation

$$(\operatorname{Re}\Xi)^2 + (\operatorname{Im}\Xi)^2 = 1, \tag{8}$$

and for the latter we have

$$\cot 2\Psi = -\operatorname{Re}\Xi/\operatorname{Im}\Xi, \tag{9}$$

where

$$\Xi = \frac{\cos\Theta}{\sin^2\Theta}\left\{\sqrt{\varepsilon - \sin^2\Theta} - \frac{4\pi\gamma}{c}\left[\frac{1}{1 - \varepsilon - (4\pi\gamma/c)\sqrt{\varepsilon - \sin^2\Theta}} - 1\right]\right\}. \tag{10}$$

In the particular case in which we can neglect the imaginary part of $\epsilon(\omega)$ and the real part of $\epsilon(\omega)$ is negative, we have in place of Eqs. (8) and (9):

$$\sin^4\Theta - \sin^2\Theta\cos^2\Theta + \varepsilon(\omega)\cos^2\Theta \approx 0, \tag{8'}$$

$$\cot 2\Psi = \frac{4\pi\gamma'}{c\sqrt{|\varepsilon - \sin^2\Theta|}}\,\frac{\varepsilon(\omega)}{\varepsilon(\omega)-1}. \tag{9'}$$

In this same case we have for the reflection coefficients:

$$R_s = |r_s|^2 = 1 - \frac{16\pi\gamma\cos\theta}{c(1-\varepsilon(\omega))}, \tag{11}$$

$$R_p = |r_p|^2 = 1 - \frac{16\pi\gamma\cos\theta}{c(1-\varepsilon(\omega))}\,\frac{\sin^2\theta - \varepsilon(\omega)}{\sin^2\theta - \cos^2\theta\varepsilon(\omega)}. \tag{12}$$

According to Eq. (10) the terms containing $\gamma(\omega)$ can also play a very important part in the case in which the imaginary part of $\epsilon(\omega)$ is small and the real part is positive and close to unity.

We note finally that our formula (6) has been obtained under the condition that the inequality $|\epsilon(\omega)| \ll 1$ does not hold. In the opposite case it is necessary to consider the excitation of plasma waves, and to do this the material equations (1) must be generalized to include spatial derivatives of the electric field.

[1] G. E. H. Reuter and E. H. Sondheimer, Proc. Roy. Soc. **A195**, 336 (1948).

[2] R. B. Dingle, Physica **19**, 311, 729, 1187 (1953); Appl. Sci. Res. **B3**, 69 (1953).

[3] V. L. Ginzburg and G. P. Motulevich, Usp. Fiz. Nauk **55**, 469 (1955); Fortschr. Physik **3**, 309 (1955).

[4] M. I. Kaganov and V. V. Slezov, J. Exptl. Theoret. Phys. (U.S.S.R.) **32**, 1496 (1957), Soviet Phys. JETP **5**, 1216 (1957).

[5] V. P. Silin, J. Exptl. Theoret. Phys. (U.S.S.R.) **34**, 707 (1958), Soviet Phys. JETP **7**, 486 (1958).

[6] L. P. Pitaevskii, J. Exptl. Theoret. Phys. (U.S.S.R.) **34**, 942 (1958), Soviet Phys. JETP **7**, 652 (1958).

[7] J. G. Collins, Appl. Sci. Res. **B7**, 1 (1958).

[8] L. D. Landau and E. M. Lifshitz, Электродинамика сплошных сред (Electrodynamics of Continuous Media), Moscow 1957.

[9] V. L. Ginzburg, J. Exptl. Theoret. Phys. (U.S.S.R.) **34**, 1593 (1958), Soviet Phys. JETP **7**, 1096 (1958).

Translated by W. H. Furry
209

SOVIET PHYSICS JETP VOLUME 35(8), NUMBER 4 APRIL, 1959

RELATIVISTIC THEORY OF POLARIZATION EFFECTS

Iu. M. SHIROKOV

P. N. Lebedev Physics Institute, Academy of Sciences, U.S.S.R.

Submitted to JETP editor May 21, 1958

J. Exptl. Theoret. Phys. (U.S.S.R.) 35, 1005-1012 (October, 1958)

A relation is obtained which connects the product of the wave functions of two free relativistic particles of given masses and spins with the wave function which describes the free motion of the system as a whole. This relation is the analogue of the Clebsch-Gordan relation for the composition of angular momenta. By means of this relation one can obtain formulas for relativistic polarization and correlation effects. Lorentz transformations are obtained for arbitrary tensor moments.*

1. In recent years a number of papers (for example references 2 and 3) have given general formulas expressing the cross section, the polarization, and other quantities characterizing the scattering of spinning particles, in terms of the matrix elements of the S matrix. Analogous formulas also exist for the correlation effects. The purpose of the present paper is to give the relativistic generalization of these results to the case of arbitrary spins of the colliding (or correlated) particles.

In the theory of angular momenta a large part is played by the Clebsch-Gordan expansion, which connects the product of the wave functions of two physical systems (with given angular momenta) with the wave function relating to the total angular momentum of the system as a whole. In dealing with collisions of two relativistic particles one has also to compound four-momenta and four-dimensional angular momenta. We shall show that a relation analogous to the Clebsch-Gordan expansion can be derived for the simultaneous composition of these quantities. For this we require the wave functions describing the free motion of relativistic particles, and the Lorentz transformation of these functions.

2. A nonrelativistic particle of mass κ and spin i is described by a wave function

$$\psi^{\varkappa i\alpha}_{m_i}(\mathbf{p}), \tag{1}$$

in which the arguments are the momentum $\mathbf{p}$ $(-\infty < p_1, p_2, p_3 < \infty)$ and the spin component m_i $(m_i = -i, -i+1, \ldots i)$. Besides its mass and spin, the particle can possess other invariant characteristics (for example charge), which we shall identify by the index α. On going over to the relativistic case we first have the question of what variables must serve as the arguments of the wave function of the particle. A unique answer (apart from the possibility of a similarity transformation) to this question is found in the theory of the representations of the inhomogeneous Lorentz group: the free motion of a particle of mass κ and spin i is described by a wave function (1) that depends on the same kinematic variables $\mathbf{p}$, m_i as in the nonrelativistic case. The transformations for space and time displacements and for spatial and Lorentz rotations are given by the infinitesimal transformations with the respective operators $\hat{\mathbf{p}}$, $\hat{p}_0$, $\hat{\mathbf{M}}$, $\hat{\mathbf{N}}$. For the wave function (1), according to references 4 and 5, these operators have the forms

$$\hat{\mathbf{p}} = \mathbf{p}, \qquad \hat{p}_0 = e_p \equiv \sqrt{p^2 + \varkappa^2}, \tag{2}$$

$$\mathbf{M} = i\left[\mathbf{p}\frac{\partial}{\partial \mathbf{p}}\right] + \mathbf{i}, \qquad \mathbf{N} = i\sqrt{e_p}\,\frac{\partial}{\partial \mathbf{p}}\sqrt{e_p} - \frac{[\mathbf{i}\times\mathbf{p}]}{e_p + \varkappa}, \tag{3}$$

where

$$[\mathbf{i}_1\mathbf{i}_2]_- = i\mathbf{i}_3, \; \ldots\ldots \; \mathbf{i}^2 = i(i+1). \tag{4}$$

Square brackets denote the vector product, and square brackets with minus sign as subscript denote the commutator. The slight difference between the forms of the operator $\mathbf{N}$ in Eq. (3) and in Eq. (11) of reference 5 comes from the fact that the corresponding wave functions differ by a factor $e_{\mathbf{p}}^{1/2}$. In the present paper the wave functions $\psi^{\mathrm{i}}_{\mathrm{m_i}}(\mathbf{p})$ are so chosen that the invariant normalization integral has the form

$$\sum_{m_i}\int d^3p\,\psi^{*\varkappa i}_{m_i}(\mathbf{p})\,\psi^{\varkappa i}_{m_i}(\mathbf{p}).$$

The operators defined in Eqs. (2) and (3) satisfy the well known commutation relations, which secure relativistic invariance,[6] and this proves the correctness of the choice of the wave functions (1). The uniqueness and completeness of the treatment is assured by the fact that the operators (2) and (3), taken for $0 < \kappa < \infty$ and for all integral and half-integral non-negative i, exhaust all the possible irreducible representations of the Lorentz group that are suitable for the description of free particles[7] (expect particles with zero rest mass, which require some special consideration).

---

*The formula for the relativistic polarization effects has also been obtained independently by Chou Kuang Chao and M. I. Shirokov at the Joint Institute for Nuclear Research.[1]

3. Let us construct for the wave function (1) the operator of a finite Lorentz transformation to a system moving with the four-velocity $u_\mu = (\mathbf{u}, iu_0)$ relative to the initial system. This transformation has the form:

$$\mathbf{x} = \mathbf{x}' + \frac{\mathbf{u}(\mathbf{u}\cdot\mathbf{x}')}{u_0+1} + \mathbf{u}t', \qquad t = \mathbf{u}\mathbf{x}' + u_0 t'. \tag{5}$$

To the transformation (5) there will correspond a transformation U of the wave function,

$$\psi = U(u)\psi'. \tag{6}$$

The explicit form of the transformation (6) is uniquely determined by the relations (2), (3) and can be found, for example, by the method indicated in reference 8, which gives

$$\psi_{m_i}(\mathbf{p}) = \int d^3p'\delta\{\mathbf{p}' - \mathbf{p}'(\mathbf{p})\}\sqrt{e_{p'}/e_p}D^i_{m_i m_i'}(\mathbf{p},\ \mathbf{u})\psi_{m_i}(\mathbf{p}')$$
$$= \sqrt{e_{p'}/e_p}D^i_{m_i m_i'}(\mathbf{p}\cdot\mathbf{u})\psi'_{m_i'}\{\mathbf{p}'(\mathbf{p})\}, \tag{7}$$

where

$$\mathbf{p}'(\mathbf{p}) = \mathbf{p} + \frac{\mathbf{u}(\mathbf{u}\cdot\mathbf{p})}{u_0+1} - \mathbf{u}e_p \tag{8}$$

is the transformation for the four-momentum, inverse to the transformation (5), and $D^i_{m_i m_i'}(\mathbf{p}, \mathbf{u})$ is the matrix of the three-dimensional rotation for the spin. (We remark that the indices $m_i m_i'$ of this D^i are transposed as compared with the corresponding indices in reference 9). This rotation can be specified by an orthogonal matrix a_{ij} which defines a rotation for an arbitrary three-vector b_i:

$$b_i = a_{ij}b_j';$$

the matrix a_{ij} turns out to be given by

$$a_{ij} = \delta_{ij} + \frac{p_i p_j(u_0-1)}{e_p + \varkappa(e_p u_0 - \mathbf{pu} + \varkappa)} + \frac{u_i p_j}{e_p u_0 - \mathbf{pu} + \varkappa}$$
$$+ \frac{p_i u_j(-e_p u_0 + 2\mathbf{up} - u_0\varkappa - e_p - \varkappa)}{(e_p+\varkappa)(e_p u_0 - \mathbf{pu} + \varkappa)(u_0+1)} - \frac{u_i u_j(e_p - \varkappa)}{(u_0+1)(e_p u_0 - \mathbf{pu} + \varkappa)} \tag{9}$$

It is obvious that the rotation is around the axis perpendicular to the vectors $\mathbf{p}$, $\mathbf{u}$. From the matrix a_{ij} one can determine the matrix $D^i_{m_i m_i'}$ for an arbitrary spin by the well-known relation

$$i_j = a_{jk}(D^i)^{-1}i_k D^i. \tag{10}$$

For spin ½ the matrix $D^{1/2}$ has been determined in reference 8 and is given by

$$D^{1/2} = \frac{(e_p+\varkappa)(u_0+1) - (\mathbf{u}\cdot\boldsymbol{\sigma})(\mathbf{p}\cdot\boldsymbol{\sigma})}{\sqrt{2(u_0+1)(e_p+\varkappa)(u_0 e_p - \mathbf{up} + \varkappa)}}\cdot \tag{11}$$

For spin 1 the matrix D^1 differs from a_{ij} only by the similarity transformation W:

$$W = \begin{pmatrix} 1/\sqrt{2} & -i/\sqrt{2} & 0 \\ 0 & 0 & 1 \\ -1/\sqrt{2} & -i/\sqrt{2} & 0 \end{pmatrix}, \tag{12}$$

$$D^1 = WaW^{-1}. \tag{13}$$

For higher spins (for example 3/2) it is convenient to calculate the matrix D^i not from the relation (10) but from the matrices D^j for lower spins:

$$\sum_{Jm_J}(iIm_i m_I \mid iIJm_J')D^J_{m'_J m_J}$$
$$= \sum_{m'_i m'_I} D^i_{m'_i m_i}D^I_{m'_I m_I}(iIm'_i m'_I \mid iIJm_J), \tag{14}$$

where $(iIm_i m_I \mid iIJm_J')$ are the vector-composition coefficients.

The above-described matrix D^i for the rotation of the spin in a Lorentz transformation is a purely relativistic effect (Thomas precession) without any nonrelativistic analogue.

4. The Lorentz transformation (7) for the wave function (1), as developed in the preceding section, provides a possibility for obtaining the basic formula of the present paper, the transformation from the wave functions of two free particles to the wave function of the system as a whole.

The wave function describing a system of two particles with masses κ_1 and κ_2 and spins i and I has the form

$$\psi^{\varkappa_1\varkappa_2 iI}_{m_i m_I}(\mathbf{p}_1,\ \mathbf{p}_2). \tag{15}$$

The wave function Φ of the system as a whole must depend on the total mass κ, the total intrinsic angular momentum J, the component of the total intrinsic angular momentum, m_J, and the total momentum $\mathbf{K}$; these quantities are defined by the relations:

$$\mathbf{K} = \mathbf{p}_1 + \mathbf{p}_2, \qquad \varkappa^2 = (e_{p_1} + E_{p_2})^2 - \mathbf{K}^2, \tag{16}$$

$$e_p = \sqrt{p^2 + \varkappa_1^2}, \quad E_p = \sqrt{p^2 + \varkappa_2^2}, \tag{17}$$

$$\mathbf{J} = \mathbf{M}_1 + \mathbf{M}_2, \qquad \mathbf{J}^2\Phi = J(J+1)\Phi. \tag{18}$$

The relations (18) are prescribed in the center-of-mass system (c.m.s.), in which $\mathbf{p}_1 + \mathbf{p}_2 = 0$.

The six variables κ, $\mathbf{K}$, J, m_J are not, however, sufficient for the description of the system (15), since the wave function (15) depends on the eight variables $\mathbf{p}_1$, $\mathbf{p}_2$, m_i, m_I. The two missing variables can of course be chosen to be invariants. For these two variables it is convenient to choose the orbital angular momentum l and the sum of spins $\mathbf{s}$, taken in the c.m.s.

$$\mathbf{J} = \mathbf{l} + \mathbf{s}, \tag{19}$$

$$\mathbf{l} = \mathbf{l}_1 + \mathbf{l}_2, \qquad \mathbf{l}^2\Phi = l\,(l+1)\,\Phi, \tag{20}$$

$$\mathbf{s} = \mathbf{i} + \mathbf{I}, \qquad \mathbf{s}^2\Phi = s\,(s+1)\,\Phi. \tag{21}$$

All the quantities in Eqs. (19) to (21) are also taken in the c.m.s. We now have everything required to obtain the transition from the two-particle function $\psi_{m_i m_I}(\mathbf{p}_1, \mathbf{p}_2)$ to the function $\Phi^{\kappa J l s}_{m_J}(\mathbf{K})$ describing the system as a whole. This transition will consist of the following transformations: By means of the respective transformations D^i, D^I defined in Eqs. (9) and (10) one translates the two spins into the c.m.s.; one then has further to go over from the momenta $\mathbf{p}_1$, $\mathbf{p}_2$ to the total momentum $\mathbf{K}$ and the half-difference of momenta $\mathbf{p}$ in the c.m.s. Since in this system the momenta of the particles are equal in magnitude and opposite in direction, the momentum $\mathbf{p}$ is equal to the momentum of the first particle transformed to the c.m.s. by means of Eq. (8):

$$\mathbf{p} = \mathbf{p}_1 + \frac{\mathbf{K}(\mathbf{K}\cdot\mathbf{p}_1)}{e_p + \varkappa} - \frac{\mathbf{K}}{\varkappa}\,e_{p_1}, \tag{22}$$

where the quantities $\mathbf{K}$, e_{p_1}, κ are determined in accordance with Eqs. (16) and (17). The matrix of this transformation is

$$\langle \mathbf{p}_1 | \mathbf{p} \rangle = \sqrt{e_{p_1} / e_p} \tag{23}$$

in consequence of the well known relation

$$d^3p_1 / e_{p_1} = d^3p / e_p = \text{inv}. \tag{24}$$

If we write the momentum $\mathbf{p}$ in spherical coordinates p, ϑ, φ, then the angular variables will describe the relative orbital motion and will be related to the angular momentum l defined in Eq. (20) and its component m_l,

$$(\vartheta\varphi \mid l m_l) = Y_{l m_l}(\vartheta\varphi), \tag{25}$$

while the absolute value p can be related to the total mass κ:

$$\varkappa = e_p + E_p. \tag{26}$$

From Eq. (26) it follows that

$$p^2 dp = d\varkappa\, p e_p E_p / (e_p + E_p), \tag{27}$$

so that

$$(\mathbf{p} \mid \varkappa l m_l) = \sqrt{\frac{p e_p E_p}{e_p + E_p}}\; Y_{l m_l}(\vartheta\varphi). \tag{28}$$

Now the spins i, I and the orbital angular momentum l have been transformed to the c.m.s. We must compound these three angular momenta according to the relation

$$\mathbf{J} = (\mathbf{i} + \mathbf{I}) + \mathbf{l} \tag{29}$$

by means of the proper Clebsch-Gordan coefficients. On combining the transformations calculated above, we can write the desired relation for the transition from ψ to Φ:

$$\begin{aligned} \psi^{\varkappa_1\varkappa_2 iI}_{m_i m_I}(\mathbf{p}_1,\ \mathbf{p}_2) &= \sum D^{i}_{m_i m_i'}(\mathbf{p}_1,\ \mathbf{K})\, D^{I}_{m_I m_I'}(\mathbf{p}_2\mathbf{K})\, Y_{l m_l}(\vartheta,\ \varphi) \\ &\quad \times (iIm_i'm_I' \mid iIsm_s)\,(lsm_lm_s \mid lsJm_J) \\ &\quad \times \sqrt{pe_{p_1}E_p / (e_p + E_p)}\; \Phi^{\varkappa J l s \varkappa_1 \varkappa_2 i I'}_{m_J}(\mathbf{K}) \\ &\equiv (\mathbf{p}_1\mathbf{p}_2 m_i m_I \mid V(\varkappa_1\varkappa_2 iI) \mid \varkappa J l s\, \mathbf{K}\, m_J)\, \Phi^{\varkappa J l s \varkappa_1 \varkappa_2 i I}_{m_J}(\mathbf{K}). \end{aligned} \tag{30}$$

The summation is taken over the indices m_i', m_I', m_l, m_s, m_J, l, s, J. The law of conservation of the four-momentum is taken into account by the relations (16) and (20). Mathematically the relation (30) is the expansion of the direct product of two irreducible representations of class P^{s}_{+m} (cf. reference 5) of the inhomogeneous Lorentz group in terms of irreducible representations. It is entirely analogous to the Clebsch-Gordan expansion for the three-dimensional rotation group. By means of the expansion (30) the angular distributions for arbitrary polarization and correlation effects can be expressed in terms of the S matrix parametrized in an invariant way.

5. As an example let us consider the case in which a particle of mass κ_1 and spin i is incident on a particle of mass κ_2 and spin I, and the result is the emergence of particles with masses κ_1', κ_2' and spins i′, I′. It is obvious that the wave function $\psi^{\kappa_1\kappa_2 iI}_{m_i m_I}(\mathbf{p}_1, \mathbf{p}_2)$ of the initial state will be related to the wave function $\chi^{\kappa_1\kappa_2 i'I'}_{m_i'm_I'}(\mathbf{p}_1', \mathbf{p}_2')$ of the final state in the following way:

$$\begin{aligned} \chi^{\varkappa_1'\varkappa_2' i'I'\alpha'}_{m_i' m_I'}(\mathbf{p}_1'\cdot\mathbf{p}_2') &= (\mathbf{p}_1'\cdot\mathbf{p}_2' m_i' m_I' \mid V(\varkappa_1'\varkappa_2' i'I') \mid \varkappa J l' s'\, \mathbf{K}\, m_J) \\ &\quad \times (\alpha' l' s' \varkappa_1' \varkappa_2' i' I' \mid S(\varkappa J) \mid \alpha l s \varkappa_1 \varkappa_2 i I) \\ &\quad (\varkappa J l s\, \mathbf{K}\, m_J \mid V^{-1}(\varkappa_1\varkappa_2 iI) \mid \mathbf{p}_1\mathbf{p}_2 m_i m_I)\, \psi^{\varkappa_1\varkappa_2 iI\alpha}_{m_i m_I}(\mathbf{p}_1\mathbf{p}_2), \end{aligned} \tag{31}$$

where α, α' are indices for the channels, $(\ldots\ldots V^{-1}\ldots\ldots)$ is the matrix inverse to the corresponding matrix in Eq. (30), and $(\alpha' l' s' \kappa_1' \kappa_2' i' I' \mid S(\kappa J) \mid \alpha l s \kappa_1 \kappa_2 i I)$ is the S matrix in invariant form. In virtue of the conservation laws the S matrix does not depend on K, m_J and is diagonal in the total mass κ and the total intrinsic angular momentum J. In practice it is of course more convenient to consider instead of the variable κ the energy of the incident particle, and this changes the normalization factor. The formula (28) differs in the following essential ways from the corresponding nonrelativistic expression: firstly, in the transformations V, V^{-1} the momenta are changed according to the relativistic relation (22), which is different from the nonrelativistic relation

$$\mathbf{p} = \mathbf{p}_1 - (\mathbf{K}/\varkappa)\varkappa_1 \quad \text{(nonrel.)} \tag{32}$$

and secondly, the transformation V contains the matrices D^i, D^I of the relativistic spin rotations. Finally, in Eq. (31) all the energy dependences are expressed in terms of masses.

According to Eq. (9) the rotation D^i (or D^I) becomes a unit matrix if the three-momentum of the particle is parallel to the three-momentum of the system as a whole. Therefore, in particular, the rotations D^i, D^I are absent from the matrix V^{-1} in Eq. (31) if in the initial state one of the particles is at rest, or if the momenta of the two particles are parallel.

Let us now go over from the wave function $\psi^{\kappa_1\kappa_2 iI}_{m_i m_I}(\mathbf{p}_1, \mathbf{p}_2)$ to the corresponding density matrix $(m_i' m_I' | \rho^{\kappa_1\kappa_2 iI}(\mathbf{p}_1, \mathbf{p}_2) | m_i m_I)$. For simplicity we give the further developments in symbolic form, without writing out the indices of the matrices. The relation (31) thus takes the form

$$\chi = VSV^{-1}\psi. \tag{33}$$

Corresponding to this the relation between the density matrices ρ of the incident wave and ρ_{sc} of the scattered wave is written in the form

$$\rho_{sc} = V(S-1)V^{-1}\rho V(S^{+}-1)V^{-1}. \tag{34}$$

As is well known,[3] the relation (34) contains a complete description of the scattering of polarized particles. For example, the angular distribution, with a suitable normalization, is given by

$$d\sigma/d\Omega = \operatorname{Sp}\rho_{sc} = \operatorname{Sp}\{V(S-I)V^{-1}\rho V(S^{+}-I)V^{-1}\}. \tag{35}$$

The polarization P is given by

$$\mathbf{P} = \operatorname{Sp}\{\mathbf{i}\rho_{sc}\}/i\operatorname{Sp}\rho_{sc}. \tag{36}$$

It can be seen from (34) that the relativistic effect of rotation of the spin does not appear in the scattering of unpolarized particles. In fact, in this case the matrix ρ of the initial state is a unit matrix with respect to the spin indices, so that the matrices D and D^{-1} acting on it from the left and the right cancel each other, and the matrices D and D^{-1} occurring in the V and V^{-1} at the beginning and end of the product in Eq. (35) cancel, because the trace is not affected by cyclic permutation of the factors. Nor does the use of a polarized target lead to the appearance of the relativistic effect, since the matrix D^I is unity for a particle at rest in the laboratory system. The relativistic spin effects can influence the cross section only in multiple scattering, for which the spin state obtained in the c.m.s. of the incident particle and the scatterer has to be transformed to the c.m.s. of the scattered particle and the next scatterer. Only in this case is the momentum of the particle not parallel to the relative velocity of the reference system, so that the corresponding spin rotation matrix D^I can be different from unity. We emphasize that all the above considerations relate to effects connected with the spin rotation.

The relativistic effects connected with the transformation of the momenta (forward bias of the cross section) occur in any scattering at sufficiently high energy.

6. For the study of the effect of the relativistic corrections on the polarization effects it is helpful to obtain a general formula for the transformation of the density matrix (i.e., the cross-section and all the tensor moments) in the passage from one Lorentz frame to another. The density matrix $\rho^{\kappa i}_{m_i m_i'}(\mathbf{p})$ for the scattered particle transforms like the outer product of a wave function by its conjugate, taken for the same value of the momentum:

$$\rho^{\varkappa i}_{m_i m_i'}(\mathbf{p}) \sim (-1)^{i-m}\,\psi^{\varkappa i}_{m_i}(\mathbf{p})\,\psi^{*\varkappa i}_{-m_i'}(\mathbf{p}). \tag{37}$$

The factor $(-1)^{i-m_i'}$ and the minus sign on the m_i' in $\psi^{*\kappa i}_{-m_i}(\mathbf{p})$ are introduced so that the spin matrices can act on $\rho_{m_i m_i'}$ from the left not only for the index m_i but also for the index m_i'. From this we can get the transformation for $\rho_{m_i m_i'}$ from the known transformations (2) and (3) for ψ_{m_i} and $\psi_{m_i'}$.

By simple calculations one can show that the operators of infinitesimal transformations given by Eq. (37) for the function ρ have the forms

$$\mathbf{p} = 0, \qquad p_0 = 0, \tag{38}$$

$$\mathbf{M} = -i\left[\mathbf{p}\times\frac{\partial}{\partial\mathbf{p}}\right] + \mathbf{i} + \mathbf{i}' \tag{39}$$

$$\mathbf{N} = i\sqrt{e_p}\,\frac{\partial}{\partial\mathbf{p}}\sqrt{e_p} - \frac{[(\mathbf{i}+\mathbf{i}')\times\mathbf{p}]}{e_p+\varkappa}. \tag{40}$$

$\mathbf{i}'$ denotes a spin operator composed of the same matrices as $\mathbf{i}$, but acting on the variable m_i'. From the relation (40) it follows that the density matrix behaves under Lorentz transformations like the wave function of a particle with the spin $\mathbf{i}+\mathbf{i}$. Therefore a finite Lorentz transformation for the matrix $\rho_{m_i m_i'}(\mathbf{p})$ is given by a formula analogous to Eq. (7):

$$\rho(\mathbf{p}) = D^i D^{i'} \sqrt{e_{p'}/e_p}\, \rho'(\mathbf{p}'). \tag{41}$$

In particular, a rotation of the polarization vector $\mathbf{P}$ is determined by the matrix a_{ij} of Eq. (9) and is given by

$$\mathbf{P} = \mathbf{P}' - \frac{\mathbf{p}(\mathbf{p}\ \mathbf{P}')(u_0-1)}{(e_p+\varkappa)(e_p u_0 - \mathbf{pu} + \varkappa)} + \frac{\mathbf{u}(\mathbf{p}\cdot\mathbf{P}')}{e_p u_0 - \mathbf{pu} + \varkappa} + \frac{\mathbf{p}(\mathbf{u}\cdot\mathbf{P}')(-e_p u_0 + 2\mathbf{up} - u_0\varkappa - e_p - \varkappa)}{(e_p+\varkappa)(e_p u_0 - \mathbf{pu} + \varkappa)(u_0+1)} - \frac{\mathbf{u}(\mathbf{u}\cdot\mathbf{P}')(e_p - \varkappa)}{(u_0+1)(e_p u_0 - \mathbf{pu} + \varkappa)} \tag{42}$$

We note that it is clear from Eq. (42) that the relativistic effects manifest themselves not only in single scattering but also in double scattering from unpolarized targets, since the polarization appearing after the first scattering is perpendicular to the plane of the scattering and consequently is not changed by the rotation (42). For the spin ½ this result was obtained in reference 10.

7. The exposition of the formal theory of scattering usually begins with the step of representing the wave function as a superposition of incident and scattered waves, $e^{ikz} + e^{ikr} f(\vartheta)/r$.

In the relativistic case, however, it is scarcely worthwhile to use this method, since in the coordinate representation the wave functions for a particle with spin as a rule have redundant components, which complicate the treatment, especially for higher spins. Furthermore a separate treatment has to be carried through for each value of the spin. The case of spin ½ has been treated in this way in reference 10. It must also be noted that the question of coordinates in relativistic quantum theory is not a simple one.[11]

The impression may arise that the discussion that has been given has not been formulated in a relativistically invariant way. This is untrue, however. The point is that four-dimensional tensors and spinors do not exhaust the possibilities for covariant physical quantities. Moreover, relativistic tensors and spinors transforming by nonunitary representations of the Lorentz group are, strictly speaking, in general not very suitable for the wave functions of relativistic quantum systems, since their norms are not definite. On the other hand, there exist unitary representations of the inhomogeneous Lorentz group, whose wave functions have positive definite norms. The functions (1), transforming according to Eqs. (2) and (3), are just such functions. These wave functions are just as covariant as tensors, and the part of the tensor indices is played by the set of variables $\mathbf{p}$, m_i. An essential point is that these functions are covariant only with respect to the set of spin and momentum variables, and not with respect to each of them separately.

The density matrix (37) is also a covariant quantity. According to Eq. (38) displacement transformations are unit operators for this matrix, since it transforms by a unitary representation of the homogeneous Lorentz group. A point of interest is the expansion of this representation in terms of irreducible representations, which will give a relativistically invariant classification of the possible angular distributions for particles with spin in an arbitrary reference system.

Finally, we shall make one further remark concerning the invariance of the parametrization of the S matrix in Eq. (31). The quantity

$$(\mathbf{i}+\mathbf{I})^2, \tag{43}$$

defined in an arbitrary coordinate system, is of course not an invariant. One finds, however, by direct verification that the quantity

$$\{(D^i)^{-1}\mathbf{i}D^i + (D^I)^{-1}\mathbf{I}D^I\}^2 = s(s+1) \tag{44}$$

is an invariant, and in the rest system the expression (44) is the same as (43). In a similar way one can give an invariant definition of the intrinsic orbital angular momentum *l*.

In conclusion I would like to thank Chou Kuang Chao and M. I. Shirokov for a helpful discussion and for information about their results.

---

[1] Chou Kuang Chao and M. I. Shirokov, J. Exptl. Theoret. Phys. (U.S.S.R.) **34**, 1230 (1958), Soviet Phys. JETP **7**, 851 (1958).

[2] J. M. Blatt and L. C. Biedenharn, Rev. Mod. Phys. **24**, 258 (1952).

[3] A. Simon, Phys. Rev. **92**, 1050 (1953).

[4] Iu. M. Shirokov, Dokl. Akad. Nauk SSSR **94**, 857 (1954).

[5] Iu. M. Shirokov, J. Exptl. Theoret. Phys. (U.S.S.R.) **33**, 1196 (1957), Soviet Phys. JETP **6**, 919 (1958).

[6] V. Bargmann and E. P. Wigner, Proc. Nat. Acad. Sci. **34**, 211 (1948). P. A. M. Dirac, Rev. Mod. Phys. **21**, 392 (1949).

[7] E. P. Wigner, Ann. of Math. **40**, 149 (1939).

[8] Iu. M. Shirokov, Dokl. Akad. Nauk SSSR **99**, 737 (1954).

[9] E. P. Wigner, Gruppentheorie und ihre Anwendung auf die Quantenmechanik der Atomspektren, p. 165. Braunschweig 1931.

[10] H. P. Stapp, Phys. Rev. **103**, 425 (1956).

[11] Iu. M. Shirokov, Dokl. Akad. Nauk SSSR **111**, 1223 (1956), Soviet Phys. "Doklady" **1**, 777 (1956).

Translated by W. H. Furry
210

SOVIET PHYSICS JETP VOLUME 35(8), NUMBER 4 APRIL, 1959

COHERENT ELECTRON RADIATION IN A SYNCHROTRON. I

L. V. IOGANSEN and M. S. RABINOVICH

P. N. Lebedev Physics Institute, Academy of Sciences, U.S.S.R., and Moscow State Pedagogical Institute

Submitted to JETP editor May 21, 1958

J. Exptl. Theoret. Phys. (U.S.S.R.) **35**, 1013-1016 (October, 1958)

The potential for the radiation field of a single relativistic electron moving in a circle and simultaneously executing small phase oscillations is considered. A general expression for the radiation generated by a bunch is obtained using the potential for a single phase-modulated electron and a distribution function for the particles in the bunch. The expression applies at low harmonics, in which case the radiation is coherent.

ELECTRONS in high-energy synchrotrons radiate over a wide frequency spectrum: this spectrum extends from the radio-frequency region, corresponding to wave lengths of the order of the orbital radius, to the ultraviolet or x-ray region.

In the region in which the wave lengths are much larger than the characteristic distance between the electrons in a bunch the radiation is partially coherent. The total intensity of the radiation in a given narrow portion of the spectrum is not proportional to the number of accelerated electrons N and is a strong function of the dimensions of the electron bunch and the nature of the particle distribution in a bunch.

The long dimension of a bunch (orbital direction) is determined by the phase oscillations. The transverse dimension, which is characteristic of the betatron oscillations, is small, being of the order of a millimeter in high-energy accelerators. Hence the coherent radiation in a synchrotron is affected primarily by the phase oscillations of electrons and is characteristic of the phase-oscillation distribution of the particles in a bunch.

A comprehensive experimental investigation of coherent radiation has been carried out by Prokhorov,[1] using a 5-Mev synchrotron. This author calculated the coherent radiation for several phase distributions for the particles in a bunch.[2] Somewhat later, Rytov (Report of the Institute of Physics, Academy of Sciences, U.S.S.R., 1950) calculated the coherent radiation assuming that all particles in a bunch execute phase oscillations of the same amplitude. Up to the present time no analysis has been made of the coherent radiation of a bunch with an arbitrary phase distribution for the particles. However, this problem is important because the coherent radiation can be used as a means of investigating various physical processes and particle loss during acceleration.

Before computing the radiation of a bunch we consider the radiation of a single electron which moves in a circle of radius r_0 with an angular velocity ω_0, simultaneously executing phase oscillations at an angular frequency $\Omega \ll \omega_0$.

We introduce a coordinate system with origin at the center of the circle and take the plane of the circle as the xy plane. The electron coordinates as functions of time are:

$$\begin{aligned} x(t) &= (r_0 - \rho_0 \cos \Omega t)\cos(\omega_0 t + \Phi \sin \Omega t), \\ y(t) &= (r_0 - \rho_0 \cos \Omega t)\sin(\omega_0 t + \Phi \sin \Omega t). \end{aligned} \tag{1}$$

Here Φ is the amplitude of the phase oscillations and ρ_0 is the amplitude of the radial oscillations.

We assume that the phase oscillations are harmonic and are given by the relation $\psi = \Phi \sin \Omega t$. The vector potential of the electron field can be expanded in a double Fourier series in the wave zone. Making use of the fact that $\rho_0/r_0 \sim \Omega/\omega_0 = 1/n_0 \ll 1$, we obtain the Fourier amplitudes of the potential of the electron field (to terms of order Ω/ω_0):

$$\begin{aligned} A_{xnm}(\mathbf{R}_0) &= -ie\beta \frac{e^{ik_{nm}R_0}}{R_0} J'_n(n\beta \sin\theta) J_m(n\Phi), \\ A_{ynm}(\mathbf{R}_0) &= \frac{e}{\sin\theta} \frac{e^{ik_{nm}R_0}}{R_0} J_n(n\beta\sin\theta) J_m(n\Phi). \end{aligned} \tag{2}$$

Here $k_{nm} = (n\omega_0 + m\Omega)/c$, $\mathbf{R}_0$ and θ are the radius vector and the polar angle of the point of observation, $\beta = v/c$, and the $J_n(x)$ are Bessel functions.

When $\Phi = 0$, (2) vanishes for $m \neq 0$ and becomes the well-known expression for the Fourier amplitude of the potential of a charge which moves with uniform motion when $m = 0$.[3]

We multiply (2) by $\exp\{-i(n\omega_0 + m\Omega)t\}$ and write the resulting vector in the form:

$$\mathbf{A}_{nm}(R_0, t) = \mathbf{A}_n(R_0, t)\exp\{-im\Omega(t - R_0/c)\}\, J_m(n\Phi), \tag{3}$$

where $\mathbf{A}_n(R_0, t)$ is the potential of the n-th harmonic in the spectrum of a uniformly rotating electron.

It is apparent from Eq. (3) that each harmonic in the spectrum of the uniformly rotating electron is to be associated with a band of frequencies in the spectrum of the phase-modulated electron. The amplitude distribution in the n-th band is given by the factor $J_m(n\Phi)$, as in the case of an ordinary phase-modulated signal. $J_m(n\Phi)$ falls off rapidly when $|m| > |n|\Phi$. Hence the number of lines in each branch of the n-th band is $|m| \leq |n|$ (usually $\Phi \leq 1$ in an accelerator). When $n > n_0$, adjacent bands start to overlap and the interpretation of the spectrum in terms of bands is no longer meaningful.

We now consider the phase-oscillation distribution for the particles.

We introduce a normalized particle distribution function in the phase plane: $w(\psi, \dot\psi, t)$ which gives the number of particles at a time t in an element $d\Gamma$ of the phase plane: $dn = Nw(\psi, \dot\psi, t)\,d\Gamma$. The function w is normalized to unity and the integration extends over the entire region of Γ which is enclosed by the stability boundaries. The nonlinearity of the phase oscillations cannot be neglected near the stability boundaries. We shall analyze the problem in the linear approximation, assuming that the amplitude of the oscillations is small compared with the region of stability; for this reason the exact form of the stability boundaries is not important. We shall assume that they are ellipses: $\psi^2 + \dot\psi^2/\Omega^2 = \Phi^2_{\max}$; $\Phi_{\max}$ is the amplitude of the largest nonlinear oscillation. The linear approximation is valid under the assumption that the mean amplitude in a bunch satisfies the condition $\Phi_0 \ll \Phi_{\max}$.

Starting from Liouville's theorem and the oscillatory nature of the particle motion, it is a simple matter to find the distribution function at any instant of time once it is known for the entire plane at some earlier time:

$$w(\psi, \dot\psi, t) = w(\Phi\sin(u - \alpha),\ \Omega\Phi\cos(u - \alpha),\ t_0),$$

$$\Phi = \sqrt{\psi^2 + \dot\psi^2/\Omega^2};\quad u = \arcsin(\psi/\Phi);\quad \alpha = \Omega(t - t_0).$$

In the simplest case the particle distribution is stationary, i.e., the distribution density at each point is independent of time, depending only on the amplitude of the phase oscillations: $w(\psi, \dot\psi, t) = w(\Phi)$. Frequently one uses a normalized distribution function (normalized to unity between 0 and $\Phi_{\max}$) for the amplitudes $f(\Phi)$; this function gives the number of particles with amplitudes in the range $d\Phi : dn = Nf(\Phi)\,d\Phi$. For a stationary distribution we have $f(\Phi) = 2\pi\Omega\Phi d(\Phi)$. We introduce another normalized (normalized to unity in the interval $-\Phi_{\max}$ to $+\Phi_{\max}$) particle phase distribution function $\varphi(\psi, t)$, which gives the number of particles at a time t in the angular interval $d\psi$: $dn = N\varphi(\psi, t)\,d\psi$.

For a stationary distribution:

$$\varphi(\psi) = \frac{1}{\pi}\int_{|\psi|}^{\Phi_{\max}} \frac{f(\Phi)}{\sqrt{\Phi^2 - \psi^2}}\,d\Phi.$$

For simplicity, we usually assume in the calculations a particle phase distribution of the form:

$$\varphi(\psi) = \begin{cases} {}^1/_4\ \Phi_0; & |\psi| \leqslant 2\Phi_0 \\ 0\quad ; & |\psi| > 2\Phi_0 \end{cases} \tag{4}$$

$$f(\Phi) = \Phi/2\Phi_0\sqrt{(2\Phi_0)^2 - \Phi^2},$$

or else assume that all particles execute phase oscillations of the same amplitude, i.e.,

$$f(\Phi) = \delta(\Phi - \Phi_0),\quad \varphi(\psi) = 1/\pi\sqrt{\Phi_0^2 - \psi^2}. \tag{5}$$

In Eq. (4) $2\Phi_0$ is a singularity and in Eq. (5) Φ_0 is a singularity, so that distributions of this type cannot apply to actual physical cases.

The true distribution in a bunch has not been studied in any detail. From the experimental amplitude-distribution curve for the 250-Mev synchrotron at the Institute of Physics, Academy of Sciences, U.S.S.R.,[4] it may be concluded that the particle phase distribution is essentially Gaussian, i.e.,

$$\varphi(\psi) = \frac{1}{2\Phi_0}\exp\left\{-\frac{\pi}{4}\left(\frac{\psi}{\Phi_0}\right)^2\right\},$$

$$f(\Phi) = \frac{\pi\Phi}{2\Phi_0^2}\exp\left\{-\frac{\pi}{4}\left(\frac{\Phi}{\Phi_0}\right)^2\right\}. \tag{6}$$

Here, in computing the normalized integral we set $\Phi_{\max} = \infty$, making use of the fact that $\Phi_{\max} \gg \Phi_0$.

We now consider the coherent radiation of a bunch; we shall analyze the low-wavelength region, where the radiation is coherent. In Eq. (3) we introduce the initial phase of the i-th electron $\psi_{0i} = \Phi\sin\Omega t_{0i}$ and integrate over the electrons in a bunch. The potential for a component in the bunch field designated by the numbers n and m is of the form

$$\bar{A}_{nm}(R_0, t) = NF_{nm}\mathbf{A}_{nm}(R_0, t), \tag{7}$$

where we have introduced the form factor

$$F_{nm} = \int J_m(n\Phi)\exp\{im\arcsin(\psi/\Phi)\}\, w(\psi, \dot\psi, t_0)\,d\Gamma \tag{8}$$

For a stationary distribution, using the variable

Φ and $u = \sin^{-1}(\psi/\Phi)$ in Eq. (8) and integrating with respect to u from 0 to 2π, we have

$$F_{nm} = 0 \text{ for } m \neq 0, \qquad F_{n0} = \int_0^{\Phi_{\max}} f(\Phi) J_0(nf)\, d\Phi. \tag{9}$$

The bunch spectrum contains only harmonics of the rotation frequency ω_0. The power in the n-th component of the bunch spectrum is $I_n = N^2 |F_{n0}|^2 \times I_{n0}$, where I_n is the power of the n-th component in the spectrum of the unmodulated electron (3).

We compute the integral in (9) for various distributions: for the distribution in (4) we find $F_{n0} = \sin 2n(\Phi_0)/2n\Phi_0$; for the distribution in (5) $F_{n0} = J_0(n\Phi_0)$; finally, for the Gaussian distribution (6) $F_{n0} = \exp(-n^2\Phi_0^2/\pi)$.

In the first two cases the form factor oscillates, falling off slowly as Φ_0 increases; this behavior is due to the singularities in the distributions. In the Gaussian case the function falls off rapidly without oscillating. By an appropriate choice of $f(\Phi)$ it is possible to obtain any intermediate case. Whence it follows that the energy variations in the coherent radiation observed by Prokhorov correspond to a well-defined distribution of particles over phase-oscillation amplitudes. These variations need not necessarily be found in other systems.

We now consider a non-stationary distribution. As a typical example we consider a distribution in which all the particles lie in the upper half of the phase plane at the starting time, i.e.,

$$\begin{aligned} w(\psi, \dot{\psi}, t_0) &= 2w(\Phi) & &\text{if } \dot{\psi} > 0, \\ w(\psi, \dot{\psi}, t_0) &= 0 & &\text{if } \dot{\psi} < 0. \end{aligned} \tag{10}$$

Substituting (10) in (8) and integrating with respect to u from 0 to π we have

$$\begin{aligned} F_{n0} &= \int_0^{\Phi_{\max}} f(\Phi) J_0(n\Phi)\, d\Phi, \qquad F_{nm} = 0;\ m = 2p, \\ F_{nm} &= \frac{2i}{m\pi} \int_0^{\Phi_{\max}} f(\Phi) J_m(n\Phi)\, d\Phi;\quad m = 2p + 1. \end{aligned} \tag{11}$$

The spectrum now contains the fundamental and the odd harmonics only. In the frequency region in which $n < n_0$ and the bands do not overlap it is meaningful to sum over all m harmonics which form a band. As a result we obtain a signal which is modulated in phase and also amplitude modulated at the frequency of the phase oscillations. This means that the energy radiated by a bunch in each band of the spectrum is modulated by the phase frequency.

The general properties of the spectrum are maintained for an arbitrary non-stationary particle distribution. The only changes are in the distribution of energy in the lines of each band and the form of the oscillations which modulate the radiation energy. This modulation of the energy of the coherent radiation at a frequency close to the calculated frequency of the phase oscillations has recently been observed at $\lambda = 3$ cm $(n = 170)$ by Iu. M. Ado at the synchrotron of the Institute of Physics, Academy ofSciences, U.S.S.R.

The authors wish to thank A. M. Prokhorov and Iu. M. Ado for valuable discussions and for communicating the results of their experimental work prior to publication.

---

[1] A. M. Prokhorov, Радиотехника и электроника (Radio Engineering and Electronics) 1, 71 (1956).

[2] A. M. Prokhorov, Dissertation, Institute of Physics, Academy of Sciences, Moscow 1951.

[3] L. D. Landau and E. M. Lifshitz, Теория поля (Theory of Fields) Gostekhizdat, Moscow 1948. (Addison-Wesley, 1951).

[4] Ускорители элементарных частиц (Elementary Particle Accelerators) Atomizdat, Moscow 1957.

Translated by H. Lashinsky
211

SOVIET PHYSICS JETP VOLUME 35 (8), NUMBER 4 APRIL, 1959

THE INELASTIC SCATTERING OF DEUTERONS BY Mg^{24}

T. I. KOPALEISHVILI and V. I. MAMASAKHLISOV

Physics Institute, Academy of Sciences, Georgian S.S.R.

Submitted to JETP editor May 20, 1958

J. Exptl. Theoret. Phys. (U.S.S.R.) 35, 1017-1019 (October, 1958)

The angular distribution of deuterons inelastically scattered from Mg^{24} with excitation of the 2^+ level (4.23 Mev), which results from excitation of a single quantum of deformation, is investigated. Both nuclear and electric interaction of the deuteron and nucleus are taken into account. The theory is compared with the experimental data.

A paper of Hinds, Middleton, and Parry[1] gives results of an experimental study of the inelastic scattering of 8.9 Mev deuterons by Mg^{24}, with excitation of the 2^+, 4^+, 2^+ levels which have energies of 1.37, 4.12, and 4.23 Mev respectively. The angular distributions of the scattered deuterons when the first level (2^+; 1.37 Mev) and the third level (2^+; 4.23 Mev) are excited differ both in shape and in magnitude. The probability of scattering with excitation of the 4.23-Mev level is smaller in order of magnitude than the probability for scattering with excitation of the 1.37 Mev level, even though the spin and parity of the levels are the same. The scattering of deuterons by Mg^{24} with excitation of the 1.37 Mev level was treated in our previous paper.[2] In the present paper we investigate the scattering of deuterons by Mg^{24} with excitation of the 4.23-Mev level.

The Mg^{24} nucleus is known to be highly deformed, so that it has a spectrum of rotational levels corresponding to the different values K of the projection of the total angular momentum I of the nucleus on its symmetry axis.

The lowest terms in the spectrum have $K = 0$ and $I = 0, 2^+, 4^+$, etc. In treating the inelastic scattering of deuterons by Mg^{24} with excitation of the 1.37-Mev level, we made the assumption that the target nuclei are excited to the $K = 0$, $I = 2^+$ rotational level, and that the deformation of the nucleus is not changed, i.e., no quanta associated with β and γ deformations are emitted ($n_\beta = 0$, $n_\gamma = 0$).

Since the cross section for inelastic scattering of deuterons by Mg^{24} with excitation of the 4.23-Mev state is smaller in order of magnitude than that for excitation of the 1.37-Mev state, it is natural to assume that the 4.23-Mev level arises from the creation of one quantum of γ deformation and therefore corresponds to $K = 2$. Thus this level is characterized by the quantum numbers $K = 2$, $I = 2$, $n_\beta = 0$ and $n_\gamma = 1$. (Values of the parameter γ different from 0 and π show that the nuclear shape deviates from axial symmetry.) An indication that the 4.23-Mev level in Mg^{24} corresponds to $K = 2$ is also contained in a paper of Rakavy.[3]

We shall calculate the inelastic scattering of deuterons by Mg^{24} on the basis of the above assumptions.

The interaction between the deuteron and the Mg^{24} nucleus is taken in the form

$$V = \left[\pm V_0 R_0 \delta(r_p - R_0) + \frac{3Ze^2R_0}{5r_p^3}\right] \times \sum_{\mu\nu} \alpha_{2\nu} D^{*2}_{\mu\nu}(\vartheta, \varphi, \psi)\, Y_{2\mu}(\vartheta_p, \varphi_p) \pm V_0 R_0 \delta(r_n - R_0) \sum_{\mu\nu} \alpha_{2\nu} D^{*2}_{\mu\nu}(\vartheta, \varphi, \psi)\, Y_{2\mu}(\vartheta_n, \varphi_n), \qquad (1)$$

where ϑ, φ, and ψ are the Euler angles which determine the position of the nuclear axis relative to a fixed system of coordinates; the subscripts p and n refer to the proton and neutron in the deuteron; $D^2_{\mu\nu}$ is the unitary matrix transforming the spherical functions; V_0 and R_0 are the familiar parameters of the uniform model; $\alpha_{2\nu}$ are the deformation parameters and are operators for the creation of phonons.

In Born approximation, the matrix element of the transition is

$$< 000\,\mathbf{k} \,|\, V \,|\, 2MK\mathbf{k}' > = \Pi^{1/2}(q) \times \sum_{\mu\nu} < 0 \,|\, \alpha_{2\nu} \,|\, 1 > \int \psi_{000} \psi^*_{2MK} D^{*2}_{\mu\nu}\, d\tau \times \left\{ \int \left[\pm V_0 R_0 \delta(r_p - R_0) + \frac{3Ze^2R_0^2}{5r_p^3}\right] e^{i\mathbf{q}\mathbf{r}_p} Y_{2\mu}(\vartheta_p, \varphi_p)\, d\mathbf{r}_p \pm V_0 R_0 \int \delta(r_n - R_0)\, e^{i\mathbf{q}\cdot\mathbf{r}_n} Y_{2\mu}(\vartheta_n \varphi_n)\, d\mathbf{r}_n \right\}, \qquad (2)$$

where ψ_{000} and ψ_{2MK} (M is the projection of I on the z axis of the fixed system), which are the wave functions of the nucleus in the initial and final states, have the form[4]

$$\psi_{000} = 1/\sqrt{8}\,\pi,$$

$$\psi_{2MK} = \sqrt{\frac{5}{16\pi^2}}\,[D^2_{MK}(\vartheta,\ \varphi,\ \psi) + D^2_{M-K}(\vartheta,\ \varphi,\ \psi)], \tag{3}$$

$$\Pi(q) = \left[\frac{4\alpha}{q}\ \tan^{-1}\frac{q}{4\alpha}\right]^2,$$

where $q = |\mathbf{k} - \mathbf{k}'|$ ($\mathbf{k}$ and $\mathbf{k}'$ are the wave vectors of the center of mass of the deuteron at the start and end of the process); α is the known size parameter of the deuteron; $\langle 0 | \alpha_{2\nu} | 1 \rangle$ is the matrix element for creation of a phonon and is equal to[4]

$$\langle 0 | \alpha_{2\nu} | 1 \rangle = (\hbar/2\sqrt{B_\nu C_\nu})^{1/2}, \tag{4}$$

where B_ν and C_ν are, respectively, the mass coefficient and the coefficient of deformability of the nucleus.

Using formulas (3) and (4) and the fact that the selection rules require $\nu = K$, we get for the matrix element (2)

$$\langle 000\ \mathbf{k} | V | 2MK\mathbf{k}' \rangle = (20\pi/\sqrt{2})\ \langle 2200 | 2200 \rangle \times \langle 22K-K | 2200 \rangle \sqrt{\frac{\hbar}{2\sqrt{B_K C_K}}}\, V_0 R_0^3 \Pi^{1/2}(q) \times \left[\pm\frac{J_{5/2}(qR_0)}{\sqrt{qR_0}} + \frac{0.3Ze^2}{R_0 V_0}\,\frac{J_{3/2}(qr_0)}{(qr_0)^{3/2}}\right]\delta_{M0}, \tag{5}$$

where $\langle \ldots | \ldots \rangle$ are Clebsch-Gordan coefficients, the J_n are Bessel functions, and r_0 is the electric radius of the nucleus.

We finally get for the differential cross section for inelastic scattering of deuterons by Mg^{24} (with K = 2)

$$\frac{d\sigma}{d\Omega} = \frac{2\mu^2 (V_0 R_0^2)^2 R_0^2 \Pi(q)}{\hbar^3 \sqrt{B_2 C_2}} \times \left[\pm\frac{J_{5/2}(qR_0)}{\sqrt{qR_0}} + \frac{0{,}3Ze^2}{V_0 R_0}\,\frac{J_{3/2}(qr_0)}{(qr_0)^{3/2}}\right]^2 \sqrt{1 + \frac{Q}{E_0'}}, \tag{6}$$

where μ is the reduced mass of the (d, Mg^{24}) system and E_0' is the energy of the incident deuteron in the center of mass system.

In order to compare our formulas with experimental data, we must choose values for the parameters. We evaluated the quantities B_2 and C_2 using the formulas[4]

$$B_2 = \frac{3}{8\pi} AMR_0^2, \quad C_2 = 4R_0^2 S - \frac{3}{10\pi}\frac{Z^2 e^2}{R_0},$$

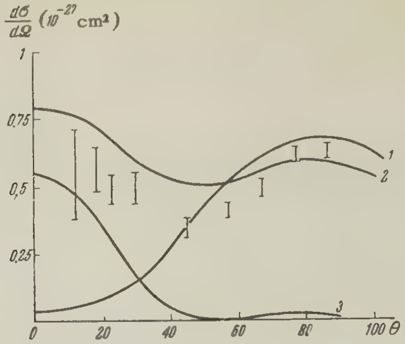

where $4\pi R_0^2 S = 15.4\ A^{2/3}$ Mev, A is the mass number of the nucleus, and M is the mass of the nucleon.

If we use the values of reference 2 for V_0 and r_0 ($V_0 = 1.84$ Mev, $r_0 = 6 \times 10^{-13}$ cm), take $R_0 = 3 \times 10^{-13}$ cm, and assume that the interaction of the deuteron with the nuclear vibrations is repulsive [i.e., choose the + sign before the nuclear term in formula (1)], the angular distribution of the deuterons, as shown in the figure, is in good agreement with the experimental data (curve 2).

Curve 1 corresponds to the inclusion only of the nuclear interaction of the deuteron and the nucleus, and curve 3 takes account only of their Coulomb interaction.

Thus, under our assumptions, simultaneous inclusion of both Coulomb and nuclear interactions gives satisfactory agreement with experiment. It is interesting that the occurrence of a second maximum in the deuteron distribution is explained.

It should be stated that there is some difference between the theoretical results and the experimental data with respect to the absolute value of the scattering cross section. However, since the coefficients B_2 and C_2 are evaluated approximately, no special significance should be attributed to this discrepancy.

---

[1] Hinds, Middleton, and Parry, Proc. Phys. Soc. **A70**, 900 (1957).

[2] V. I. Mamasakhlisov and T. I. Kopaleishvili, J. Exptl. Theoret. Phys. (U.S.S.R.) **34**, 1169 (1958), Soviet Phys. JETP **7**, 809 (1958).

[3] G. Rakavy, Nucl. Phys. **4**, 375 (1957).

[4] A. Bohr and B. Mottelson, Kgl. Danske Videnskab. Selskab Mat.-fys. Medd. **27**, No. 16 (1953).

Translated by M. Hamermesh
212

SOVIET PHYSICS JETP VOLUME 35(8), NUMBER 4 APRIL, 1959

POMERANCHUK EFFECT AND DIAGRAM OF STATE FOR He^3-He^4 SOLUTIONS

I. M. LIFSHITZ and D. G. SANIKIDZE

Khar' kov State University

Submitted to JETP editor May 26, 1958

J. Exptl. Theoret. Phys. (U.S.S.R.) **35**, 1020-1025 (October, 1958)

The influence of the Pomeranchuk effect upon equilibrium between the liquid and solid phases in He^3-He^4 solutions is investigated thermodynamically.

THE equilibrium diagram for the liquid and solid phases in He^3-He^4 solutions should show interesting features associated with the Pomeranchuk effect in He^3. It was shown by Pomeranchuk that the melting curve for He^3 should have a minimum in the P-T diagram, and that below the minimum point the heat of fusion should be negative.[1,2] This effect has been observed experimentally by Walters and Fairbank.[3] It follows from the experimental data on the entropy of He^3 that the minimum is located at $P_0 \approx 30$ atmos and $T_0 \approx 0.5°K$.

In the present paper we investigate the influence of the Pomeranchuk effect upon liquid-solid phase equilibrium in He^3-He^4 solutions is investigated.

1. WEAK SOLUTIONS OF He^4 IN He^3

Let us consider phase equilibrium in weak solutions of He^4 in He^3. The conditions for equilibrium between the liquid and solid phases can, as is well-known,[4] be written in the form:

$$\mu_0'(P, T) - x'kT = \mu_0''(P, T) - x''kT, \qquad (1)$$

$$kT \ln x' + \psi'(P, T) = kT \ln x'' + \psi''(P, T), \qquad (1')$$

where x' and x'' are the He^4 concentrations in the liquid and solid phases, respectively, $\mu_0'(P, T)$ and $\mu_0''(P, T)$ are the chemical potentials for the two phases in pure He^3, and $\psi'(P, T)$ and $\psi''(P, T)$ are functions characterizing the He^4 atoms in the solutions.

In Eq. (1) let us expand $\mu_0'(P, T)$ and $\mu_0''(P, T)$ in the neighborhood of the minimum, in powers of $P - P_0 = \Delta P$ and $T - T_0 = \Delta T$. Since at the minimum point both the chemical potentials and their first derivatives with respect to temperature are equal, the zero-order terms in (1) and the terms linear in ΔT will fall out. We obtain, therefore, for the difference between the concentrations in the two phases:

$$x' - x'' = \Delta x = \frac{v' - v''}{kT_0} \Delta P - \frac{c' - c''}{2kT_0^2} (\Delta T)^2, \qquad (2)$$

where c' and c'' are the specific heats, respectively, of liquid and solid He^3, and v' and v'' are the volumes (per particle) for pure He^3.

From (1') we see that the ratio of the concentrations in the two phases depends only upon P and T, and therefore that in the region near $x = 0$ this ratio may be regarded as a constant quantity

$$\varkappa = \frac{x'}{x''} = \exp\left\{\frac{\psi'(P_0, T_0) - \psi''(P_0, T_0)}{kT_0}\right\}. \qquad (3)$$

From (2) and (3) we obtain for the concentrations in the liquid and solid phases

$$x' = \frac{\varkappa}{\varkappa - 1} \Delta x, \qquad x'' = \frac{1}{\varkappa - 1} \Delta x. \qquad (4)$$

The pressure P_0 corresponding to the minimum in the P – T melting curve for He^3 is greater than the minimum pressure at which He^4 solidifies ($P \sim 25$ atmos). It is of interest therefore to consider three possible cases.

1. $\Delta P = 0$; then

$$x' = \frac{\varkappa}{\varkappa - 1} \frac{c'' - c'}{2kT_0^2} (\Delta T)^2, \qquad x'' = \frac{1}{\varkappa - 1} \frac{c'' - c'}{2kT_0^2} (\Delta T)^2. \qquad (5)$$

Thus, for $P = P_0$ the equilibrium curves in the limit of small concentrations are parabolas tangent to one another at the point $T = T_0$ (Fig. 1).

2. $\Delta P < 0$; it is then clear from (2) that $\Delta x < 0$ everywhere. The equilibrium curves in the small concentration region are parabolas, one lying within the other (Fig. 2). In this case the two curves do not intersect at any point and do not touch. The vertices of the parabolas are situated for $T = T_0$ at

$$x' = \frac{\varkappa}{\varkappa - 1} \frac{v' - v''}{kT_0} \Delta P, \qquad x'' = \frac{1}{\varkappa - 1} \frac{v' - v''}{kT_0} \Delta P,$$

The concentration difference is

$$\Delta x = \frac{v' - v''}{kT_0} \Delta P$$

(for $\Delta P \sim 1$ atmos, $\Delta x \sim 10^{-2}$).

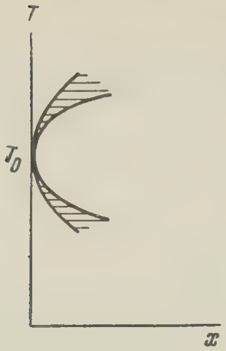

FIG. 1

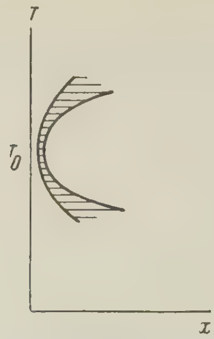

FIG. 2

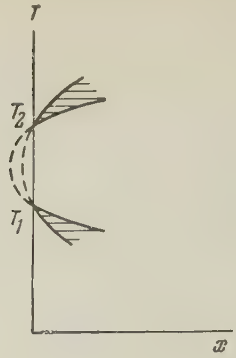

FIG. 3

3. If $\Delta P > 0$, the curves are parabolas intersecting at the points T_1 and T_2, which in the P-T diagram for pure He^3 correspond to the two melting temperatures for the pressure P (Fig. 3). From (2) we can readily obtain

$$T_{1,2} = T_0 \mp \left[\frac{2T_0(v' - v'')}{c' - c''} \Delta P\right]^{1/2}. \tag{6}$$

The concentration difference for a given T may be calculated from Eq. (2). It is more convenient, however, to employ the formula which is obtained if we expand in (1) the chemical potentials about the points (P, T_1) and (P, T_2). At T_1 and T_2 the first derivatives of the chemical potentials in the two phases are unequal, and the expansion begins with the term linear in ΔT. For small ΔP, where $T_2 - T_1 \ll T_0$, it is necessary to retain in the expansion the second-order term in ΔT as well, since the coefficient of the linear term is very small. We thus obtain for the concentration difference for $T < T_1$:

$$\Delta x = -\frac{Q_1}{kT_1^2}(T - T_1) + \frac{c''(T_1) - c'(T_1)}{2kT_1^2}(T - T_1)^2, \tag{7}$$

where Q_1 is the heat of fusion of pure He^3 at $T = T_1$. An analogous expression is obtained for $T > T_2$.

In the general case, for ΔP not small and $T_2 - T_1 \sim T_0$, we may confine ourselves to the term linear in ΔT. In this case the equilibrium curves, in the limit of small concentrations, are straight lines intersecting at T_1 and T_2. For the concentrations in the liquid and solid phases we obtain

$$x_1' = -\frac{\varkappa_1}{\varkappa_1 - 1}\frac{Q_1}{kT_1^2}(T - T_1), \quad x_1'' = -\frac{1}{\varkappa_1 - 1}\frac{Q}{kT_1^2}(T - T_1), \tag{8}$$

where κ_1 is determined from Eq. (3) at the point (P, T_1). Analogous equations are obtained for the curves intersecting at T_2.

As the pressure is further increased $T_1 \rightarrow 0$, and for $P \sim 40$ to 45 atmos the lower portion of the diagram vanishes completely.

2. "IMPURITY GAS" EXCITATION MODEL

Let us consider the energy spectrum for liquid He^3 containing a small number of He^4 atoms. The interaction of the He^4 atoms with the He^3 atoms leads to the appearance within the mixture of additional energy levels. Thus in addition to the fundamental He^3 energy spectrum there arises in the mixture a second branch due to the dissolved impurity atoms. Two forms of energy spectrum for the impurity particles are logically possible — in one case the energy minimum corresponds to a momentum equal to zero, in the other case, to nonzero momentum:

$$\varepsilon = \varepsilon_0 + p^2/2\mu, \tag{9}$$
$$\varepsilon = \varepsilon_0 + (p - p_0)^2/2\mu. \tag{9'}$$

The energy distribution for the impurity atoms is determined by Boltzmann statistics down to temperatures for which either the phenomenon of quantum degeneracy in the "impurity gas" or the interaction of the impurity particles with one another becomes significant. The conditions under which the deviation from classical statistics sets in have been established by Pomeranchuk.[5] For the case of a spectrum of the type (9), the degeneracy begins before it becomes necessary to consider the interaction, and the condition for applicability of classical statistics is $x \ll (T/T_d)^{3/2}$. The degeneracy temperature for a Bose gas:

$$T_B = 3.31\,(\hbar^2/\mu k)\,(\rho_3 x/m_3)^{2/3},$$

where ρ_3 is the density of He^3, m_3 is the mass of the He^3 atom, μ is the effective mass of the impurity particles, and x is the concentration of He^4 in the mixture.

For the case of a spectrum of the type (9′), however, the limit of applicability for classical statistics is determined by the condition $x \ll (kT/U)$, where U is an energy characterizing the interaction of the He^4 atoms, on the order of several degrees.

Applying the general formulas for the free energies of dilute solutions and of an ideal gas, we obtain,[5,2] respectively:

$$F' = F'_3 - xkT \ln \left[\frac{em_3}{\rho_3 x}\left(\frac{\mu kT}{2\pi\hbar^2}\right)^{3/2}\right] + x\varepsilon_0, \tag{10}$$

$$F' = F'_3 - xkT \ln \left[\frac{em_3}{\rho_3 x}\,\frac{p_0^2}{\hbar^3}\sqrt{\frac{\mu kT}{2\pi^3}}\right] + x\varepsilon_0, \tag{10'}$$

$$F'_3 = kT\left[-\frac{2I_{1/2}}{I_{-1/2}} + \ln A\right],$$

$$I_\alpha = \int\limits_0^\infty \frac{x^\alpha}{e^x/A+1}\,dx, \quad A = e^{\mu'/kT}.$$

From this we obtain for the entropy:[6]

$$s' = s'_3 + xk \ln\left[(m_3/\rho_3 x)(\mu k/2\pi\hbar^2)^{3/2} + 5/2\right]. \tag{11}$$

$$s' = s'_3 + xk \ln\left[(m_3 p_0^2/\rho_3 x\hbar^3)(\mu kT/2\pi^3)^{1/2} + 3/2\right], \tag{11'}$$
$$s'_3 = k\left[3I_{1/2}/I_{-1/2} - \ln A\right].$$

For a rough evaluation let us set μ in the spectrum (9) equal to the mass of He^4, (11) then yields

$$s' = s'_3 + xk \ln (1.2T^{3/2}/x). \tag{12}$$

In the case of the spectrum (9′), however, let us set for estimating purposes P_0 and μ equal to their values for rotons; (11′) then gives

$$s' = s'_3 + xk \ln (20\, T^{1/2}/x). \tag{12'}$$

From (12) and (12′) it is evident that the effect of impurities upon the entropy is more pronounced for the case $p_0 \neq 0$. The influence of the impurities upon the entropy of liquid He^3, however, (in contrast to the situation in liquid He^4) is negligibly small in the temperature region in which the impurities may be regarded as subject to classical statistics. This is explained by the fact that He^3, being a Fermi liquid, possess a very large entropy. The effect of the impurities upon the specific heat of He^3 is even weaker.

We turn now to consideration of liquid-solid phase equilibrium within the framework of the given model.

If one neglects the oscillatory term in the free energy (since $T \ll \Theta$), it is possible to write for the free energy of a weak solid solution of He^4 in He^3:

$$F'' = F''_3 + x\chi_4 + kT \ln (x/e), \tag{13}$$

where χ_4 is the zero-point energy of a single dissolved He^4 atom.

From the condition of equality of the chemical potentials of the dissolved particles, we obtain for the ratio of the concentrations in the two phases, using (10), (10′), and (13):

$$\varkappa = \frac{x'}{x''} = \frac{m_3}{\rho_3}\left(\frac{\mu kT}{2\pi\hbar^2}\right)^{3/2} e^{q/kT}, \tag{14}$$

$$\varkappa = \frac{x'}{x''} = \frac{m_3}{\rho_3}\,\frac{p_0^2}{\hbar^3}\left(\frac{\mu kT}{2\pi^3}\right)^{1/2} e^{q/kT}, \tag{14'}$$

where

$$q = \chi_4 - \varepsilon_0 + \int\limits_0^P \{v''_4(P, T) - v'_4(P, T)\}\, dP. \tag{15}$$

If μ is set equal to the mass of the He^4 atom, the factor preceding the exponential in (14) becomes $\sim 0.1\, T^{3/2}$. For $P = 30$ atmos we obtain from the experimental data[7] on pure He^4, $q/k \sim -0.1°$. For $T = 0.5°$, then, the concentration ratio $\kappa = x'/x'' \sim 1/30$. Thus for a spectrum of the type (9) with $T < T_0$ we will always have $x' < (T/T_d)^{3/2}$. The "impurity gas" is therefore subject to Boltzmann statistics down to $T = 0$, and it can readily be shown that $x' \rightarrow 0$ as $T \rightarrow 0$. In this case the liquidus curve will have a point of inflection, and will not reach the λ-transition curve. Such a conclusion, however, is not completely certain, since in the solution q/k may differ considerably from its value for pure He^4.

For the case of a spectrum of the type (9′), if we take p_0 and μ to be of the same order as for rotons, we have $x'/x'' \sim 1$ at $T \approx 0.5°$ and $P \approx 30$ atmos. Thus in this case the concentrations in the two phases increase rapidly with increasing $|\Delta T|$, and even for $\Delta T \gtrsim 0.1°K$ the model under consideration becomes unsuitable.

3. SOLUTIONS OF HIGH CONCENTRATION

At temperatures below 0.83°K liquid He^3-He^4 mixtures separate into two phases of differing He^3 concentration. This phenomenon must affect the form of the liquid-solid phase equilibrium diagram for He^3-He^4 solutions. In view of the fact that the solution separation has been experimentally investigated under the saturated vapor pressure of the solution,[9,10] while we are interested in pressures ~ 30 atmos, it is necessary to consider the influence of pressure upon this effect.

At the critical point the following conditions are fulfilled:[4]

$$\partial\mu'_3(T_c(P), x', P)/\partial x' = 0,$$
$$\partial^2\mu'_3(T_c(P), x', P)/\partial x'^2 = 0. \tag{16}$$

From this one readily obtains

$$\frac{dT_c}{dP} = \frac{\partial v_3}{\partial x'} \Big/ \frac{\partial s_3}{\partial x'}, \tag{17}$$

where s_3 and v_3 are the entropy and volume associated with a single He^3 atom in the solution.

From the existing experimental data on the concentration dependence of the solution density[11] we

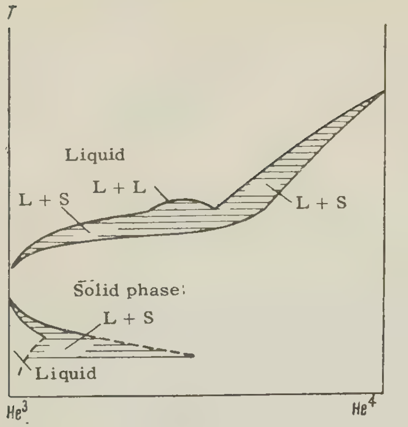

FIG. 4

may estimate that $dT_c/dp \sim 0.01 - 0.1$ deg/atmos.

It is not difficult also to evaluate the derivative $(dT/dP)_{x'}$ at any point on the separation diagram. We have:

$$(dT/dP)_{x'} = -(\partial T/\partial x')(\partial x'/\partial P). \qquad (18)$$

The derivative of the concentration with respect to pressure can readily be computed:

$$\left(\frac{dx'}{dP}\right) = -\left\{\frac{\partial v'(x_1')}{\partial x'} - \frac{v'(x_2') - v'(x_1')}{x_2' - x_1'}\right\} \Big/ \left(\frac{\partial^2 \varphi'}{\partial x'^2}\right)_{x_1'}, \qquad (19)$$

where x_2' and x_1' are the He^3 concentrations at the two separation points for a given temperature and $v'(x')$ is the volume per particle in a solution of concentration x'.

Using experimental data on the concentration dependence of the solution density, the value of $\partial\varphi/\partial x'^2$ calculated from the data on the concentration dependence of the saturated vapor pressure,[12] and the value of dT/dx' computed from the separation diagram, we obtain the estimate

$$(dT/dP)_{x'=0.07} \sim 10^{-2} \text{ deg/atmos}$$

As we observe, the separation of the solutions depends strongly upon pressure. For this reason it is impossible to state definitely whether or not limited solubility in the liquid phase will be observed for the pressures in which we are interested, on the order of 30 atmos. If the solubility remains limited at such high pressures, then a triple point will be observed on the upper part of the liquid-solid phase equilibrium diagram. The approximate form of such a diagram, for $P > P_0$, is shown in Fig. 4.

---

[1] I. Ia. Pomeranchuk, J. Exptl. Theoret. Phys. (U.S.S.R.) **20**, 919 (1950).

[2] Zh. G. Sanikdze, J. Exptl. Theoret. Phys. (U.S.S.R.) **35**, 279 (1958), Soviet Phys. JETP **8**, 192 (1959).

[3] G. K. Walters and W. M. Fairbank, Bull. Amer. Phys. Soc. Series II, **2**, 183 (1957).

[4] L. D. Landau and E. M. Lifshitz, Статистическая физика (Statistical Physics), Gostekhteorizdat, 1951.

[5] I. Ia. Pomeranchuk, J. Exptl. Theoret. Phys. (U.S.S.R.) **19**, 42 (1949).

[6] I. M. Khalatnikov and A. A. Abrikosov, J. Exptl. Theoret. Phys. (U.S.S.R.) **32**, 915 (1957), Soviet Phys. JETP **5**, 745 (1957).

[7] C. A. Swenson, Phys. Rev. **79**, 626 (1950).

[8] Schottky, Ulich, and Wagner, Thermodynamik, Springer, Berlin, 1929.

[9] G. K. Walters and W. M. Fairbank, Phys. Rev. **103**, 262 (1956).

[10] V. P. Peshkov and K. N. Zinov'eva, J. Exptl. Theoret. Phys. (U.S.S.R.) **32**, 1256 (1957), Soviet Phys. JETP **5**, 1024 (1957).

[11] T. P. Ptukha, J. Exptl. Theoret. Phys. (U.S.S.R.) **34**, 33 (1958), Soviet Phys. JETP **7**, 22 (1958).

[12] D. H. N. Wansink, Physica **23**, 140 (1947).

Translated by S. D. Elliott
213

SOVIET PHYSICS JETP VOLUME 35(8), NUMBER 4 APRIL, 1959

BINDING ENERGY OF LIGHT HYPERNUCLEI ACCORDING TO MESON THEORY

V. A. LIUL'KA and V. A. FILIMONOV

Moscow State University

Submitted to JETP editor May 31, 1958

J. Exptl. Theoret. Phys. (U.S.S.R.) 35, 1026-1030 (October, 1958)

The binding energy of Λ particles in the hypernuclei H_Λ^3, H_Λ^4, He_Λ^4, and He_Λ^5 has been computed in the second and fourth orders of perturbation theory. The theoretical results are in satisfactory agreement with experiment.

THE intensified study of hyperons in recent years has led to the discovery of many of their properties, such as the fact that the binding energy increases linearly with the atomic number,[1] and, in particular, to a more accurate measurement of the binding energy of the Λ particle in light hypernuclei. This opens new possibilities for the theoretical analysis of hyperon properties from the point of view of elementary particle interactions, say in terms of the π and K meson fields. Several papers[2-4] have investigated the binding energy of hypernuclei from field-theoretical considerations. Filimonov[4] tried to study the binding energy of the Λ particle in hypernuclei by using the elementary-particle systematics of Gell-Mann and Nishijima in the second and fourth orders of perturbation theory with a cutoff of the Chew type. This was done on the assumption that the K meson — baryon interaction is pseudoscalar and that g_Λ, the coupling constant for the interaction between the K meson and the Λ particle, is the same as g_Σ, the coupling constant for the interaction between the K meson and the Σ particle.

There exists at present no definitive data on the parity of K mesons or on the relative parity of baryons. For this reason theoretical investigations have assumed both scalar and pseudoscalar interactions between K mesons and baryons. Further, the study of K^+ meson scattering by nucleons leads to the conclusion that the interaction between the K^+ and the nucleon in the state with isotopic spin $T = 1$ is much stronger than the interaction in the state with $T = 0$. It has been suggested[5] that this is because $g_\Lambda \neq g_\Sigma$.

We shall use meson theory to study the binding energy of Λ particles in light hyperons, assuming that the K meson — baryon interaction is scalar, but making no assumptions as to the equality of g_Λ and g_Σ. The method used will be that of Filimonov.[4] We start with the interaction Hamiltonian[6]

$$\begin{aligned}\mathscr{H} = iG_\pi \{&\bar{N}\gamma_5\boldsymbol{\tau\pi}N + \bar{\Lambda}\gamma_5\boldsymbol{\pi\Sigma} + \bar{\boldsymbol{\Sigma}}\boldsymbol{\pi}\gamma_5\Lambda + [\bar{\boldsymbol{\Sigma}}\gamma_5\ \boldsymbol{\Sigma}]\boldsymbol{\pi}\\ &+ \bar{\Xi}\gamma_5\boldsymbol{\tau\pi}\Xi\} + G_\Lambda(\bar{N}K\Lambda + \text{Herm. conj.})\\ &+ G_\Sigma(\bar{N}\boldsymbol{\tau\Sigma}K + \text{Herm. conj.}) + G_{\Xi\Lambda}(\bar{\Xi}\tau_2K^*\Lambda + \text{Herm. conj.})\\ &+ G_{\Xi\Sigma}(\bar{\Xi}\tau_2\boldsymbol{\tau\Sigma}K^* + \text{Herm. conj.}).\end{aligned} \tag{1}$$

We assume that the coupling constants for the π meson — baryon interaction are equal, in agreement with symmetry considerations for strong interactions.[7] For baryons fixed at the points x_n, the interaction Hamiltonian becomes

$$\begin{aligned}\mathscr{H} = &\sqrt{4\pi}\, g_\pi \frac{i}{2V^{1/2}} \sum_{n=1}^{N} \sum_{k} \sum_{i=1}^{3} v(k)(\sigma_n\cdot\mathbf{k})\, T_i^{(\pi)\,(n)}\\ &\times \hat{a}^{(n)}(2\omega^{(\pi)})^{-1/2}(a_{ik} + \overset{*}{a}_{i,-k})\, e^{i\mathbf{k}\cdot\mathbf{x}_n}\\ &+ \sqrt{4\pi}V^{-1/2}\Big\{\sum_{n=1}^{N}\sum_{k}\sum_{i=1}^{2} v(k)\, T_i^{(K)(n)}(2\omega^{(K)})^{-1/2}\\ &\times (c_{ik} + \overset{*}{b}_{ik})\, e^{i\mathbf{k}\cdot\mathbf{x}_n} + \text{Herm. conj.}\Big\}.\end{aligned} \tag{2}$$

On going from (1) to (2) we have transformed from pseudoscalar coupling to pseudovector coupling; $v(k)$ is a function which gives the cutoff for the virtual meson momenta, and $\hat{a}^{(n)}$ is a diagonal matrix whose components are the reciprocals of the baryon masses.[4] The eight-by-eight matrices $T_i^{(\pi)}$ and $T_i^{(K)}$ have the following nonzero matrix elements:

$$\begin{aligned}&T_1^{(\pi)}:\ a_{12} = a_{21} = a_{34} = a_{43} = -ia_{56} = ia_{65} = a_{78} = a_{87} = 1;\\ &T_2^{(\pi)}:\ ia_{12} = -ia_{21} = a_{35} = a_{53} = ia_{46}\\ &\qquad = -ia_{64} = ia_{78} = -ia_{87} = 1;\\ &T_3^{(\pi)}:\ a_{11} = -a_{22} = a_{36} = a_{63} = -ia_{45}\\ &\qquad = ia_{54} = a_{77} = -a_{88} = 1;\end{aligned} \tag{3}$$

$$\begin{aligned}&T_1^{(K)}:\ a_{13} = g_\Lambda;\ a_{24} = -ia_{25} = a_{16} = g_\Sigma;\ a_{38} = -ig_{\Xi\Lambda};\\ &\qquad -ia_{47} = a_{57} = -a_{68} = g_{\Xi\Sigma};\\ &T_2^{(K)}:\ a_{23} = g_\Lambda;\ a_{14} = ia_{15} = -a_{26} = g_\Sigma;\ a_{37} = ig_{\Xi\Lambda};\\ &\qquad ia_{48} = a_{58} = a_{67} = g_{\Xi\Sigma};\end{aligned} \tag{4}$$

$g^2 = G^2/4\pi$ (we set $\hbar = 1$ and $c = 1$), and a_i, c_i, and b_i, and a_i^*, c_i^*, and b_i^* are annihilation and creation operators for the π_i, K_i, and $\tilde{K}_i$ mesons respectively.

Equation (2) can be used to obtain the Λ-nucleon interaction potentials in the second and fourth orders of perturbation theory by a previously developed method.[4,8] We call V^{1K} the potential due to exchange of a single virtual K meson, $V^{K\pi}$ the potential due to exchange of a π and K meson, V^{2K} the potential due to exchange of two K mesons, and $V^{2\pi}$ the potential due to exchange of two π mesons. These potentials are

$$V^{1K} = -g_\Lambda^2 \frac{4\pi}{(2\pi)^3} (\lambda_1\lambda_2^* + \lambda_2\lambda_1^*) \int \left\{ v^2(k) e^{i\mathbf{k}(\mathbf{x}_1-\mathbf{x}_2)} / \omega^{(K2)} (d\mathbf{k}) \right\}; \tag{5}$$

$$V^{K\pi} = -g_\pi^2 \frac{3(4\pi)^2}{4(2\pi)^6 M_\Lambda M_N} (\lambda_1\lambda_2^* + \lambda_2\lambda_1^*)$$

$$\times \iint v_1^2(k) v_2^2(\mathbf{k}) (\boldsymbol{\sigma}_1 \cdot \mathbf{k}_2)(\boldsymbol{\sigma}_2 \cdot \mathbf{k}_2) e^{i(\mathbf{k}_1+\mathbf{k}_2)\cdot(\mathbf{x}_1-\mathbf{x}_2)}$$

$$\times \left\{ \frac{1}{2}(g_\Lambda^2 + g_\Sigma^2)\left(\omega_1^{(\pi)-3}\omega_2^{(K)-2} + \omega_2^{(\pi)-2}\omega_1^{(K)-3}\right)\right.$$

$$\left. - \frac{1}{2}(g_\Lambda - g_\Sigma)^2 / \omega_2^{(\pi)2}\left(\omega_2^{(\pi)} + \omega_1^{(K)}\right)\omega_1^{(K)2} \right\} (d\mathbf{k}_1)(d\mathbf{k}_2); \tag{6}$$

$$V^{2K} = -\frac{(4\pi)^2}{4(2\pi)^6} \iint v_1^2(k) v_2^2(k) e^{i(\mathbf{k}_1+\mathbf{k}_2)\cdot(\mathbf{x}_1-\mathbf{x}_2)}$$

$$\times \{4g_{\Xi\Lambda}^2 (g_\Lambda^2 + 3g_\Sigma^2)\left(\omega_1^{(K)3}\left(\omega_1^{(K)} + \omega_2^{(K)}\right)\omega_2^{(K)}\right)^{-1}$$

$$+ [2g_{\Xi\Lambda}^2 (g_\Lambda^2 + 3g_\Sigma^2) + 2g_\Lambda^2 (g_\Lambda^2 + 3g_\Sigma^2)]$$

$$\times \left(\omega_1^{(K)2}\left(\omega_1^{(K)} + \omega_2^{(K)}\right)\omega_2^{(K)2}\right)^{-1}\} (d\mathbf{k}_1)(d\mathbf{k}_2). \tag{7}$$

The operators λ and λ^* transform the Λ particle into a nucleon, and the nucleon into a Λ particle, respectively. The expression for V^{2K} is simplified if we set $g_\Lambda = g_\Xi$, which is not in contradiction with the presently available data.

The potential due to two π mesons has been studied previously by one of the authors.[4] In order to calculate the interaction between the Λ particle and a nucleon in the core nucleus, we choose the nucleon and Λ particle wave functions in the form

$$\varphi_N(r) = (2\pi\gamma^2 r_c^2)^{-3} \cdot \exp[-r^2/4\gamma^2 r_c^2],$$

$$\varphi_\Lambda(r) = \eta^{3/2} (2\pi\gamma^2 r_c^2)^{-3/4} \exp]-r^2\eta^2/4\gamma^2 r_c^2], \tag{8}$$

$$r_c = \hbar/m_\pi c = 1.4 \cdot 10^{-13}\,\mathrm{cm},$$

where η is a parameter of variation.

Equation (8) can be used to calculate the potential energy in the singlet and triplet state of the Λ-nucleon pair for the forces given by Eqs. (5) to (7). We obtain

$$E_{\mathbf{singl}}^{1K} = -E_{\mathbf{tripl}}^{1K}$$

$$= -g_\Lambda^2 m_\pi c^2 \left\{ \frac{1}{\sqrt{\pi}\gamma_1} + [\Phi(\gamma_1\nu) - 1]\,\nu e^{\gamma_1^2\nu^2} \right\}, \tag{9}$$

$$E_{\mathbf{singl}}^{K\pi} = 3E_{\mathbf{tripl}}^{K\pi} = g_\pi^2 \frac{m_\pi^2}{M_\Lambda M_N} \frac{3}{4\pi^2\gamma_1^2}$$

$$\times m_\pi c^2 \left\{ \frac{g_\Lambda^2 + g_\Sigma^2}{2} F_1^{K\pi}(\gamma_1) - \frac{(g_\Lambda - g_\Sigma)^2}{2} F_2^{K\pi}(\gamma_1) \right\}, \tag{10}$$

$$F_1^{K\pi}(\gamma_1) = \int_0^{x_m'}\int_0^{x_m''} x_1 x_2^3 \varphi(\gamma_1, x_1, x_2)[(x_1^2 + \nu^2)^{-1}(x_2^2 + 1)^{-3/2}$$

$$+ (x_1^2 + \nu^2)^{-3/2}(x_2^2 + 1)^{-1}]\, dx_1\, dx_2, \tag{11}$$

$$F_2^{K\pi}(\gamma_1) = \int_0^{x_m'}\int_0^{x_m''} \frac{x_1 x_2^3 \varphi(\gamma_1, x_1, x_2)}{(x_1^2 + \nu^2)(x_2^2 + 1)\left(\sqrt{x_2^2 + 1} + \sqrt{x_1^2 + \nu^2}\right)}\, dx_1\, dx_2, \tag{12}$$

$$\varphi(\gamma_1, x_1, x_2) = \exp\{-\gamma_1^2 (x_1 - x_2)^2\} - \exp\{-\gamma_1^2 (x_1 + x_2)^2\}, \tag{13}$$

$$E_{\mathbf{singl}}^{2K} = E_{\mathbf{tripl}}^{2K} = -g_\Lambda^2 \frac{g_\Lambda^2 + 3g_\Sigma^2}{\pi^2} \frac{m_\pi c^2}{\gamma_1^2} F^{2K}(\gamma_1), \tag{14}$$

$$F^{2K}(\gamma_1) = \int_0^{x_m'}\int_0^{x_m''} \frac{x_1 x_2 \varphi(\gamma_1, x_1, x_2)}{(x_1^2 + \nu^2)(x_1^2 + \nu^2)^{3/2}}\, dx_1\, dx_2. \tag{15}$$

The expression for $E^{2\pi}$ was calculated previously,[4] and it is

$$x = r_c k,\ x_m = r_c k_m,\ \gamma_1^2 = \frac{1 + \eta^2}{2\eta^2}\gamma^2,\quad \nu = \frac{m_K}{m_\pi};$$

where k_m is the cutoff momentum. We are using a rectangular cutoff. The second term in (10) vanishes if $g_\Lambda = g_\Sigma$. When $g_\Lambda^2 = 3g_\Sigma^2$, it is about 1/30 of the first term and is therefore omitted in the calculations. The integrals $F_1^{K\pi}(\gamma_1)$ and $F_1^{2K}(\gamma_1)$ are found by numerical integration for $x_m = 6$.

For several values of γ_1^2 these integrals are

γ_1^2	0.75	1.00	1.25	1.50	1.75
$F^{K\pi}$	1.730	1.524	1.375	1.268	1.181
F^{2K}	0.0318	0.0279	0.0253	0.0232	0.0216

The kinetic energy of the Λ particle is

$$E_{\mathbf{kin}} = {}^3/_8\, \eta^2 (m_\pi / M_\Lambda' \gamma^2) m_\pi c^2, \tag{16}$$

where M_Λ' is the reduced mass of the Λ particle and the core.

A direct calculation of the potential energy of interaction in the singlet and triplet states of the Λ-nucleon pair shows that the singlet state is preferred. As in the case of pseudoscalar coupling, therefore, light hypernuclei in the ground state have the lowest possible spin.

Although experiments have been suggested for finding the spin of hypernuclei,[9,10] there exists as yet no relevant experimental data.

If the spins of H_Λ^3, H_Λ^4, He_Λ^4, and He_Λ^5 are $\frac{1}{2}$, 0, 0, and $\frac{1}{2}$, respectively, we obtain the following expressions for the energies of the Λ particles in the hypernuclei, as functions of the parameter of variation η:

$$\mathrm{H}_\Lambda^3 : E = E_{\mathbf{kin}} + 2E_c^{2\pi} + E_c^{1K} + \frac{5}{3}E_c^{K\pi} + 2E_c^{2K},$$

$$\mathrm{H}_\Lambda^4,\ \mathrm{He}_\Lambda^4 : E = E_{\mathbf{kin}} + 3E_c^{2\pi} + 2E_c^{K\pi} + 3E_c^{2K}, \tag{17}$$

$$\mathrm{He}_\Lambda^5 : E = E_{\mathbf{kin}} + 4E_c^{2\pi} - 2E_c^{1K} + 2E_c^{K\pi} + 4E_c^{2K}.$$

In $E^{2\pi}$ we have neglected the part depending on the spin of the hypernuclei.

The binding energy of the Λ particle is $B_\Lambda = -E_{\min}$, the minimum of the values in (17). We have found B_Λ for the four above hypernuclei using $g_\pi^2 = 16$, a value obtained from nucleon-nucleon forces, π meson photoproduction, etc.[11]

We shall make the two assumptions that $g_\Lambda^2 = g_\Sigma^2$ and $g_\Lambda^2 = 3g_\Sigma^2$. With the second of these assumptions the scattering amplitude of K^+ mesons on nucleons vanishes in the second order of perturbation theory for $T = 0$, as is required by experiment.[5] Further, Minami[13] has studied the relation between the K^+-proton scattering cross section with charge exchange and the sum of the scattering cross sections without charge exchange. If the ratio between these values is taken from experiment (about 0.2), we find that $x = g_\Sigma^2 / g_\Lambda^2 \approx 0.36$, which is in good agreement with the calculations.[5]

The results of the calculations are shown in the table. We have used the same values of γ^2 as before.[4]

Hypernucleus		H_Λ^3	H_Λ^4, He_Λ^4	He_Λ^5
B_Λ, Mev	$g_\Lambda^2=1.0$	<0	0.8	3.0
$g_\Lambda^2=g_\Sigma^2$	$g_\Lambda^2=1.2$	<0	0.9	2.7
B_Λ, Mev	$g_\Lambda^2=1.0$	~ 0	1.2	2.2
$g_\Lambda=3g_\Sigma^2$	$g_\Lambda^2=1.2$	0.1	1.1	2.1
B_Λ, Mev, exp.[12]		0.25 ± 0.31	1.44 ± 0.20 1.70 ± 0.24	2.56 ± 0.17

It is seen from the table that if we assume that $g_\Lambda^2 = 3g_\Sigma^2$, we obtain agreement with the experimental hypernucleon binding energies for g_Λ^2 between about 1.0 and 1.2, the range given by K^+-nucleon scattering experiments.[5] The assumption that $g_\Lambda^2 = g_\Sigma^2$ leads to a binding energy which increases more rapidly with the number of nucleons in the nucleus than does the result obtained for $g_\Lambda^2 = 3g_\Sigma^2$, and thus does not agree with the experimental data.

With our simplifying assumptions we cannot, of course, expect complete quantitative agreement with experiment; the overall agreement is, however, quite satisfactory.

The authors express their gratitude to Professor D. D. Ivanenko for encouragement during the performance of this work.

---

[1] D. D. Ivanenko and N. N. Kolesnikov, J. Exptl. Theoret. Phys. (U.S.S.R.) **30**, 800 (1956), Soviet Phys. JETP **3**, 955 (1956); R. Gatto, Nuovo cimento **3**, 499 (1956); G. Wentzel, Phys. Rev. **101**, 835 (1956).

[2] D. Lichtenberg and M. Ross, Phys. Rev. **103**, 1131 (1956).

[3] M. Dallaporta and F. Ferrari, Nuovo cimento **5**, 123 (1957).

[4] V. A. Filimonov, Научн. докл. Высш. школы (Sci. Papers of the Higher Schools) (in press).

[5] C. Ceolin and L. Teffaro, Nuovo cimento **5**, 435 (1957).

[6] A. Salam, Nuclear Phys. **2**, 173 (1956).

[7] M. Gell-Mann, Phys. Rev. **106**, 298 (1957).

[8] S. Gartenhaus, Phys. Rev. **100**, 900 (1955).

[9] K. Dalitz, Proceedings of the Sixth Annual Rochester Conference on High-Energy Physics, 1956 (Interscience, New York, 1956).

[10] Chou Kuang-Chao and M. I. Shirokov, Nuclear Phys. **6**, 10 (1958).

[11] G. Chew, Proceedings of the Seventh Annual Rochester Conference on High-Energy Physics, 1957 (Interscience, New York, 1957).

[12] V. Telegdi, Proceedings of the Seventh Annual Rochester Conference on High-Energy Physics, 1957 (Interscience, New York, 1957).

[13] S. Minami, Progr. Theoret. Phys. **16**, 66 (1956).

Translated by E. J. Saletan
214

SOVIET PHYSICS JETP VOLUME 35(8), NUMBER 4 APRIL, 1959

ON THE OVERHAUSER EFFECT IN NONMETALS. II.

G. R. KHUTSISHVILI

Tbilissi State University

Submitted to JETP editor May 31, 1958

J. Exptl. Theoret. Phys. (U.S.S.R.) 35, 1031-1038 (October, 1958)

An expression has been derived for the degree of stationary polarization of nuclei in the case of partial saturation of one of the components of hyperfine structure of paramagnetic resonance in a paramagnetic salt or in a semiconductor with a donor or an acceptor impurity. The degree of polarization for the same partial saturation of all the paramagnetic resonance components has also been computed. In the case I = $\frac{1}{2}$ the role of noncontact terms in nuclear relaxation has been taken into account. Methods of measuring polarization are considered.

1. During the last several years several articles have appeared in which different variants of the Overhauser method for polarizing nuclei in paramagnetic salts and in semiconductors have been proposed.[1-6] The authors of several of these articles have succeeded in producing nuclear polarization. In most of these cases the articles deal with the problem of obtaining a nonstationary dynamic nuclear polarization.

In an earlier article[7] the author gave an expression for the degree of stationary nuclear polarization obtained in the case of complete saturation of one of the components of the hyperfine structure of paramagnetic resonance. In the case examined in that article the relaxation of nuclear spin is due only to the hyperfine (contact) interaction with the spin of the electron shell.

In this article we generalize those results. We examine the case of partial saturation of one or more components of hyperfine structure of paramagnetic resonance, and take into account the role of other mechanisms of nuclear relaxation.

We note that unlike Jeffries[4] we consider the saturation of an allowed transition in the paramagnetic resonance spectrum.

2. We consider a system consisting of an electron shell with an effective spin S equal to $\frac{1}{2}$ and of a nucleus with spin I placed into an external magnetic field H (this includes the cases of a trivalent acceptor or a pentavalent donor impurity in silicon or in germanium, and also the cases of many paramagnetic salts). The Hamiltonian of the system has the form* (we neglect quadrupole effects, and also the direct effect of an external field on the nuclear spin):

$$V = \beta\{g_{\parallel} H_z S_z + g_{\perp}(H_x S_x + H_y S_y)\} + \{A S_z I_z + B(S_x I_x + S_y I_y)\} \tag{1}$$

(cf. Bleaney's paper;[8] we follow his notation and consider the case of axial symmetry).

We restrict ourselves to the consideration of the case of a strong field: $\beta H \gg A$, $\beta H \gg B$. In this case the components of the electron and the nuclear spins along the direction of the external field (M and m respectively) are good quantum numbers. For the energy levels we have[8] (up to terms of order A and B):

$$E_{Mm} = Mg\beta H + KMm, \tag{2}$$

$$g = (g_{\parallel}^2 \cos^2\vartheta + g_{\perp}^2 \sin^2\vartheta)^{1/2}, \tag{3}$$

$$Kg = [(Ag_{\parallel})^2 \cos^2\vartheta + (Bg_{\perp})^2 \sin^2\vartheta]^{1/2}. \tag{4}$$

Alternating fields of suitable frequencies will give rise to resonance transitions between the levels (2). In particular, the transitions $\Delta M = \pm 1$, $\Delta m = 0$ give rise to paramagnetic resonance, while the transitions $\Delta M = 0$, $\Delta m = \pm 1$ give rise to nuclear magnetic resonance. The paramagnetic resonance spectrum has the form $\beta gH + Km$, i.e., we obtain $2I + 1$ equally spaced (up to terms of order A and B) hyperfine-structure components.

We neglect the spin-spin interaction in calculating the Boltzmann distribution among the energy levels. In this approximation we obtain $2I + 1$ pairs of levels coincident in energy with the energy difference between the components of each pair equal to $g\beta H$.

We have four types of relaxation transitions:

I) $\Delta M = \pm 1$, $\Delta m = 0$ — relaxation of electronic spin;

II) $\Delta M = -\Delta m = \pm 1$ — relaxation due to the hyperfine (contact) interaction;

III) $\Delta M = \Delta m = \pm 1$;

---

*In the case of a pentavalent donor or a trivalent acceptor impurity in silicon or in germanium $g_{\parallel} = g_{\perp} = g \approx 2$, $K = A = B$.

IV) $\Delta M = 0$, $\Delta m = \pm 1$.*

Relaxation processes of type III and IV are not important compared with relaxation of type II in the case when the wave function of the electron (or more accurately of the electron shell with $S = \frac{1}{2}$) taken at the position of the nucleus is large, in other words if the s-part of the wave function of the electron is not small.[9] In the case of a pentavalent donor or a trivalent acceptor impurity in silicon or in germanium, this condition is satisfied. One would expect this condition to be fulfilled also in the case of many paramagnetic salts (indeed, according to Abragam and Pryce[10] the large value for the hyperfine structure of paramagnetic resonance indicates that the hyperfine interaction in a paramagnetic salt is due to the admixture of an excited state into the paramagnetic-ion ground state with an unpaired s-electron).

3. To be specific, we shall first consider the case $I = \frac{3}{2}$. We then have four pairs of levels (Fig. 1).

We denote by $W(a)$ the probability per unit time for the transition $a \longleftrightarrow a'$ brought about by an alternating field at right angles to the main field of frequency corresponding to this transition. It is well known that[11]

$$W(a) = \frac{\pi}{2}(\gamma_e H_1)^2 \varphi_a(\omega), \tag{5}$$

where γ_e is the gyromagnetic ratio for the spin of the electronic shell, $2H_1$ is the amplitude of the alternating field, ω is its (circular) frequency, while $\varphi_a(\omega)$ is the function which gives the line shape for the transition $a \longleftrightarrow a'$ (with $\int_0^\infty \varphi_a(\omega)\, d\omega = 1$).

We shall introduce the probabilities $W(b)$, $W(c)$ and $W(d)$ in an analogous manner. The frequencies of the corresponding four alternating fields differ from each other (they are equal to $(\beta g H + Km)/\hbar$, where $m = +\frac{3}{2}, +\frac{1}{2}, -\frac{1}{2}, -\frac{1}{2}, -\frac{3}{2}$).

We shall assume that only relaxation processes of types I and II occur.

We denote by $W(aa')$ the probability (per unit time) for the transition $a \rightarrow a'$ brought about by interaction with the lattice. In a similar manner we introduce $W(a'a)$, $W(bb')$ etc. We have

$$\begin{aligned} W(aa') &= W(bb') = W(cc') = W(dd') = We^{-\delta}, \\ W(a'a) &= W(b'b) = W(c'c) = W(d'd) = We^{\delta}, \end{aligned} \tag{6}$$

where W is some function of the temperature, while δ is given by the formula

$$2\delta = g\beta H / kT. \tag{7}$$

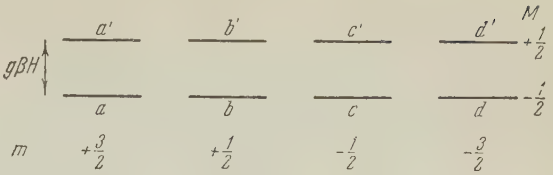

FIG. 1

We further denote by $N(a), \ldots$ the populations of the corresponding levels and by $N^0(a), \ldots$ the equilibrium populations. We use N to denote the total number of systems under consideration. We then have

$$N(a) + N(a') + N(b) + N(b') + N(c) + N(c') + N(d) + N(d') = N; \tag{8}$$

$$N^0(a) - N^0(a') = N^0(b) - N^0(b') = N^0(c) - N^0(c') = N^0(d) - N^0(d') = \frac{N}{4}\tanh\delta. \tag{9}$$

In the stationary case we obtain

$$\begin{aligned} N(a)/N(a') &= (W(a) + We^{\delta})/(W(a) + We^{-\delta}), \\ N(b)/N(b') &= (W(b) + We^{\delta})/(W(b) + We^{-\delta}), \\ N(c)/N(c') &= (W(c) + We^{\delta})/(W(c) + We^{-\delta}), \\ N(d)/N(d') &= (W(d) + We^{\delta})/(W(d) + We^{-\delta}), \end{aligned} \tag{10}$$

$$N(a)/N(b') = N(b)/N(c') = N(c)/N(d') = e^{2\delta}. \tag{11}$$

Formula (11) means that the hyperfine interaction establishes equilibrium between the levels a and b′, b and c′, c and d′.

In particular, let us assume that partial saturation of only the resonance $a \longleftrightarrow a'$ takes place. Then $W(b) = W(c) = W(d) = 0$, and the solution of (8), (10), and (11) yields

$$\begin{aligned} &N(a) = N(b) = N(c) = N(d) \\ &= N[W(a) + We^{\delta}]/[(5 + 3e^{-2\delta})W(a) + 4W(e^{\delta} + e^{-\delta})], \\ &N(b') = N(c') = N(d') \\ &= Ne^{-2\delta}[W(a) + We^{\delta}]/[(5 + 3e^{-2\delta})W(a) + 4W(e^{\delta} + e^{-\delta})], \\ &N(a') = N[W(a) + We^{-\delta}]/[(5 + 3e^{-2\delta})W(a) + 4W(e^{\delta} + e^{-\delta})]. \end{aligned} \tag{12}$$

We introduce the saturation parameter $s(a)$ for the resonance $a \longleftrightarrow a'$ by means of the following formula:

$$N(a) - N(a') = [1 - s(a)][N^0(a) - N^0(a')]. \tag{13}$$

We obtain

$$s(a) = (5 + 3e^{-2\delta})W(a)/[(5 + 3e^{-2\delta})W(a) + 4W(e^{\delta} + e^{-\delta})]. \tag{14}$$

For the degree of nuclear polarization we obtain

$$f = s(a)(1 - e^{-2\delta})/(5 + 3e^{-2\delta}). \tag{15}$$

---

*A quadrupole nuclear relaxation $\Delta M = 0$, $\Delta m = \pm 2$, is also possible, but we neglect it. This relaxation will be weak, since it is not associated with the interaction between the nuclear and the electronic spins.

In a completely analogous manner we can discuss the case of partial saturation of the resonance b ⟷ b′. In this case we introduce the saturation parameter s(b) for this resonance by means of

$$N(b) - N(b') = [1 - s(b)]\,[N^0(b) - N^0(b')]$$

and obtain after a simple calculation

$$s(b) = (5 + e^{2\delta} + 2e^{-2\delta})\,W(b)\,/\,[(5 + e^{2\delta} + 2e^{-2\delta})\,W(b) + 4W(e^{\delta} + e^{-\delta})], \tag{16}$$

$$f = s(b)\,(1 + 3e^{2\delta} - 4e^{-2\delta})\,/\,3\,(5 + e^{2\delta} + 2e^{-2\delta}). \tag{17}$$

4. The results obtained above can be easily generalized to include arbitrary I. If partial saturation is produced for the transition between two states with nuclear spin components equal to m, the saturation parameter for this resonance and the degree of nuclear polarization become

$$\begin{gathered} s(m) = \frac{[2(I+1) + (I-m)\,e^{2\delta} + (I+m)\,e^{-2\delta}]\,W(m)}{[2(I+1) + (I-m)\,e^{2\delta} + (I+m)\,e^{-2\delta}]\,W(m) + (2I+1)\,W\,(e^{\delta} + e^{-\delta})}, \\ f(m) = s(m)\,\frac{2m + (I-m)(I+1+m)\,e^{2\delta} - (I+m)(I+1-m)\,e^{-2\delta}}{2I\,[2(I+1) + (I-m)\,e^{2\delta} + (I+m)\,e^{-2\delta}]}, \end{gathered} \tag{18}$$

where W(m) is the probability (per unit time) of the transition between two states with nuclear spin components equal to m, produced by an alternating field of the corresponding frequency.

In particular, if $\delta \ll 1$, we obtain

$$s(m) = \frac{W(m)}{W(m) + W}, \quad f(m) = \frac{I(I+1) - m^2}{I(2I+1)}\,\delta s(m), \tag{18a}$$

while if $\delta \gg 1$:

$$s(m) = \frac{W(m)}{W(m) + (2I+1)\,We^{-\delta}}, \quad f(m) = \frac{I+1+m}{2I}\,s(m) \tag{18b}$$

when m ≠ I, and

$$s(I) = \frac{2(I+1)\,W(I)}{2(I+1)\,W(I) + (2I+1)\,We^{\delta}}, \quad f(I) = \frac{s(I)}{2I+1} \tag{18c}$$

when m = I.

From the results obtained above it follows, in particular, that for the complete saturation of the paramagnetic resonance that corresponds to the transition between levels with components of nuclear spin equal to I, it is necessary that the condition $W(I) \gg We^{\delta}$ be satisfied. In all the other cases (m ≠ I) it is necessary only that the weaker condition $W(m) \gg We^{-\delta}$ be satisfied. It is easy to understand the physical significance of this difference. To be specific, we consider the case I = 3/2 (Fig. 1). When the transition b ⟷ b′ is saturated the alternating field gives rise to more transitions of type b → b′ than of type b′ → b. But owing to the increase in the population of the b′ level, the hyperfine interaction gives rise to transitions of type b′ → a. Thus the hyperfine interaction transfers the systems from states b and b′ into states a and a′, facilitating the saturation of the resonance b ⟷ b′. We obtain the same result when the resonances c ⟷ c′ and d ⟷ d′ are saturated. But in the case of saturation of the a ⟷ a′ resonance this effect will not occur, since the level a′ is not connected to other levels by the hyperfine interaction.

5. Let us now consider, for arbitrary I, the case of the same partial saturation of all the 2I + 1 components of hyperfine structure of paramagnetic resonance. We again assume that only relaxation processes of types I and II take place. We denote by N(m) and N(m′) the populations of the states with nuclear spin components equal to m and spin components of the shell equal respectively to −½ and +½. In the stationary case we have

$$N(m)\,/\,N(m') = (W(m) + We^{\delta})\,/\,(W(m) + We^{-\delta}).$$

From this we obtain

$$\begin{aligned} N(m) - N(m') &= \frac{N(m)}{W(m) + We^{\delta}}\,W\,(e^{\delta} - e^{-\delta}) \\ &= \frac{N(m')}{W(m) + We^{-\delta}}\,W\,(e^{\delta} - e^{-\delta}), \end{aligned} \tag{19}$$

or, since all the resonances are saturated to the same degree,

$$N(m)\,/\,(W(m) + We^{\delta}) = N(m')\,/\,(W(m) + We^{-\delta}) = \text{const},$$

where the constant does not depend on m.

The hyperfine interaction establishes equilibrium between the levels m + 1 and m′. Thus

$$\begin{gathered} N(m+1)\,/\,N(m') \\ = (W(m+1) + We^{\delta})\,/\,(W(m) + We^{-\delta}) = e^{2\delta}. \end{gathered}$$

Therefore, for all the resonances to be saturated to the same degree it is necessary to have

$$W(m) = qe^{2m\delta}, \tag{20}$$

where q does not depend on m.

We introduce the saturation parameter s which, according to the assumed conditions, is the same for all the resonances. We then have

$$N(m) - N(m') = (1-s)[N^0(m) - N^0(m')] \\ = (1-s)\frac{N}{2I+1}\tanh\delta. \tag{21}$$

Thus, in accordance with (19) we obtain

$$\frac{N(m)}{W(m) + We^{\delta}} = \frac{N(m')}{W(m) + We^{-\delta}} = \frac{N}{2I+1}\,\frac{1-s}{W(e^{\delta}+e^{-\delta})} \tag{22}$$

From this we obtain

$$N(m) + N(m') = (1-s)\frac{N}{2I+1}\left[1 + \frac{2W(m)}{W(e^{\delta}+e^{-\delta})}\right]$$

By making use of the normalization condition

$$\Sigma[N(m) + N(m')] = N,$$

we can easily establish the relation between q and s

$$2\,\frac{1-s}{s}\,q = (2I+1)\,W(e^{\delta}+e^{-\delta})\frac{\sinh\delta}{\sinh(2I+1)\delta}, \tag{23}$$

and thus obtain

$$N(m) + N(m') = \frac{N}{2I+1}(1-s) + Nse^{2m\delta}\frac{\sinh\delta}{\sinh(2I+1)\delta} \tag{24}$$

The total component of nuclear spin is

$$\sum_m m[N(m) + N(m')]$$

and taking into account the fact that

$$\sum_m me^{2m\delta} = I\frac{\sinh(2I+1)\delta}{\sinh\delta}B_I(2I\delta)$$

(B_I is the Brillouin function) we obtain for the degree of nuclear polarization

$$f = sB_I(2I\delta).$$

6. We state without proof an expression for the degree of nuclear polarization in the case I = ½ (Fig. 2), when partial saturation (generally speaking with different degrees of saturation) of both components of paramagnetic resonance is produced (we here again assume that relaxation processes of only types I and II occur):

$$f = \frac{2W(a)W(b)(e^{\delta}-e^{-\delta}) + 2W[W(a) - W(b)] -}{2W(a)W(b)(e^{\delta}+e^{-\delta}) + 2W[W(a) + W(b)] +} \tag{25}$$
$$\rightarrow \frac{-W[e^{-\delta}W(a) - e^{\delta}W(b)]\,(e^{\delta}+e^{-\delta})}{+W[e^{-\delta}W(a) + e^{\delta}W(b)](e^{\delta}+e^{-\delta}) + 2W^2(e^{\delta}+e^{-\delta})}$$

7. Finally we consider, for the case I = ½, the effects produced by relaxation processes of types III and IV. For the probabilities of transitions produced by interaction with the lattice we may write (Fig. 2):

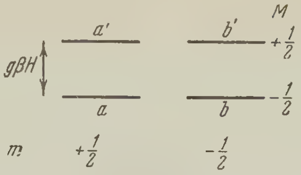

FIG. 2

$$W(a'a) = W(b'b) = We^{\delta}, \quad W(aa') = W(bb') = We^{-\delta},$$
$$W(b'a) = \lambda We^{\delta}, \qquad W(ab') = \lambda We^{-\delta},$$
$$W(a'b) = \lambda_1 We^{\delta}, \qquad W(ba') = \lambda_1 We^{-\delta},$$
$$W(ab) = W(ba) = W(a'b') = W(b'a') = \lambda_2 W, \tag{26}$$

where λ, λ_1, λ_2 and W are functions of the temperature.

In the stationary case we obtain

$$N(a')(\lambda_1 e^{\delta} + \lambda_2) + N(a)(\lambda e^{-\delta} + \lambda_2)$$
$$= N(b')(\lambda e^{\delta} + \lambda_2) + N(b)(\lambda_1 e^{-\delta} + \lambda_2),$$
$$N(a')[W(a) + We^{\delta}] + N(b')\lambda We^{\delta} + N(b)\lambda_2 W$$
$$= N(a)[W(a) + W(1+\lambda)e^{-\delta} + \lambda_2 W],$$
$$N(b)[W(b) + We^{-\delta}] + N(a)\lambda We^{-\delta} + N(a')\lambda_2 W$$
$$= N(b')[W(b) + W(1+\lambda)e^{\delta} + \lambda_2 W]. \tag{27}$$

From the normalization condition we have

$$N(a) + N(a') + N(b) + N(b') = N. \tag{28}$$

We first consider the case of complete saturation of both components of paramagnetic resonance. The N(a) = N(a′), N(b) = N(b′) and we obtain

$$\frac{N(a)}{N(b)} = \frac{\lambda e^{\delta} + \lambda_1 e^{-\delta} + 2\lambda_2}{\lambda e^{-\delta} + \lambda_1 e^{\delta} + 2\lambda_2}, \quad f = \frac{(\lambda - \lambda_1)\sinh\delta}{(\lambda+\lambda_1)\cosh\delta + 2\lambda_2}. \tag{29}$$

If, in particular, $\delta \ll 1$, we obtain

$$\frac{N(a)}{N(b)} = 1 + 2\delta\frac{\lambda - \lambda_1}{\lambda + \lambda_1 + 2\lambda_2}, \quad f = \delta\frac{\lambda - \lambda_1}{\lambda + \lambda_1 + 2\lambda_2}. \tag{29a}$$

(the first of these formulas agrees with Abragam's result[2]). For $\delta \gg 1$ we obtain

$$\frac{N(a)}{N(b)} = \lambda/\lambda_1, \quad f = (\lambda - \lambda_1)/(\lambda + \lambda_1). \tag{29b}$$

However, if (complete) saturation is produced only for the resonance a ⟷ a′, we obtain for the degree of nuclear polarization

$$f = \frac{\lambda_2(\lambda-\lambda_1)(e^{\delta}-e^{-\delta}) + (\lambda+\lambda_1+2\lambda\lambda_1) - \lambda_1(1+\lambda)e^{2\delta} - \lambda(1+\lambda_1)e^{-2\delta}}{\lambda_2(1+\lambda)(3e^{\delta}+e^{-\delta}) + \lambda_2(1+\lambda_1)(e^{\delta}+3e^{-\delta}) + (3\lambda+3\lambda_1+2\lambda\lambda_1+4\lambda_2^2) + \lambda_1(1+\lambda)e^{2\delta} + \lambda(1+\lambda_1)e^{-2\delta}}, \tag{30}$$

which gives for $\delta \ll 1$

$$f = \delta(1+\lambda_2)(\lambda-\lambda_1)/2[\lambda + \lambda_1 + 2\lambda_2 + \lambda_2^2 + \lambda\lambda_1 + \lambda\lambda_2 + \lambda_1\lambda_2]. \tag{30a}$$

For $\delta \gg 1$ (30) gives $f = -1$, which is easily understood since, if $\lambda_1 \neq 0$ in the case of complete saturation of the resonance $a \leftrightarrow a'$, all the systems will accumulate in level b.

8. In conclusion, we consider the question of the possibility of a direct measurement of the degree of nuclear polarization in the case of the effects considered above. It is desirable to have methods by which f can be determined without applying the results obtained above (since these results are associated with certain assumptions).

We consider the case $I = 3/2$. We have

$$f = \{3[N(a) + N(a')] + [N(b) + N(b')] - [N(c) + N(c')] - 3[N(d) + N(d')]\}/3N,$$

or

$$f = \{3[N(a) - N(b)] + 3[N(a') - N(b')] + 4[N(b) - N(c)] + 4[N(b') - N(c')] + 3[N(c) - N(d)] + 3[N(c') - N(d')]\}/3N. \quad (31)$$

If we measure experimentally, for example, the signal due to the nuclear resonance $a \leftrightarrow b$, we can find $N(a) - N(b)$. Thus, by measuring experimentally the nuclear resonances $a \leftrightarrow b$, $a' \leftrightarrow b'$, $b \leftrightarrow c$ etc. we can determine f.

We also note that some of the differences $N(a) - N(b)$, $N(a') - N(b')$, $N(b) - N(c)$ must increase strongly when at least one of the components of the hyperfine structure of paramagnetic resonance is saturated, even if $\delta \ll 1$ [this can be seen, for example, from (12)]. Thus, nuclear magnetic-resonance measurements afford a check, at high temperatures, on the validity of the above theoretical results.

However, the actual situation is more complicated. According to (2) the energies of all the nuclear-resonance transitions are the same up to terms proportional to A and B, and are equal to K/2. In the next approximation the terms differ by an amount of order $B^2/g\beta H$. But to prevent the different components of nuclear magnetic resonance from overlapping the experiments have to be conducted at relatively weak external fields.

Moreover, according to Valiev,[12] nuclear magnetic resonance experiments on nuclei of paramagnetic atoms will be successful apparently only at liquid-helium temperatures. Such experiments are of considerable interest for their own sake.

It can be seen from (31) that when one of the components of paramagnetic resonance is saturated it is not possible to find f directly by measuring the paramagnetic resonance of the unsaturated components. However, such measurements may be carried out to check theoretical results.

For example, when the resonance $b \leftrightarrow b'$ is completely saturated

$$N(a) - N(a') = N(e^{2\delta} - 1)/(e^{2\delta} + 5 + 2e^{-2\delta}),$$

while in the absence of saturation

$$N^0(a) - N^0(a') = \frac{N}{4}\tanh\delta.$$

Thus, if δ is of the order of or greater than unity, then in the case of complete saturation of the resonance $b \leftrightarrow b'$ the signal corresponding to the resonance $a \leftrightarrow a'$ must increase significantly (in particular, if $\delta \gg 1$, it will increase by a factor of four).

Finally, we note that in the case of polarization of radioactive nuclei the degree of polarization can be found directly from the angular anisotropy of γ radiation from these nuclei.

---

[1] A. Abragam, Phys. Rev. **98**, 1729 (1955).

[2] A. Abragam, Compt. rend. **242**, 1720 (1956). A. Abragam and J. Combrisson, Compt. rend. **243**, 650 (1956); suppl. Nuovo cimento **6**, 1197 (1957). Abragam, Combrisson, and Solomon, Compt. rend. **245**, 157 (1957). A Abragam and W. G. Proctor, Compt. rend. **246**, 2253 (1957).

[3] G. Feher, Phys. Rev. **103**, 500 (1956). G. Feher and E. A. Gere, Phys. Rev. **103**, 501 (1957).

[4] C. D. Jeffries, Phys. Rev. **106**, 164 (1957). Abraham, Kedzie, and Jeffries, Phys. Rev. **106**, 165 (1957).

[5] Pines, Bardeen, and Slichter, Phys. Rev. **106**, 489 (1957).

[6] F. M. Pipkin and J. W. Culvahouse, Phys. Rev. 109, 319, 1423 (1958).

[7] G. R. Khutsishvili, J. Exptl. Theoret. Phys. (U.S.S.R.) **34**, 1653 (1958), Soviet Phys. JETP **7**, 1136 (1958).

[8] B. Bleaney, Phil. Mag. **42**, 441 (1951).

[9] J. Korringa, Physica **16**, 601 (1950).

[10] A. Abragam and M. H. L. Pryce, Proc. Roy. Soc. **A205**, 135 (1951).

[11] Bloembergen, Purcell, and Pound, Phys. Rev. 73, 679 (1948).

[12] K. A. Valiev, Thesis, University of Kazan', 1958.

Translated by G. Volkoff
215

SOVIET PHYSICS JETP VOLUME 35 (8), NUMBER 4 APRIL, 1959

Letters to the Editor

ANALOGY BETWEEN THE MECHANICAL AND THERMODYNAMICAL EQUATIONS OF MOTION AND THE ONSAGER RECIPROCITY RELATION

I. FENYES

Institute of Theoretical Physics, L. Eotvos University, Budapest

Submitted to JETP editor May 23, 1958

J. Exptl. Theoret. Phys. (U.S.S.R.) **35**, 1039-1041 (October, 1958)

1. In many works by Popov[1]* and Karanikolov,[2] the Onsager reciprocity relations[3] are derived from a proposed analogy between classical mechanics and irreversible thermodynamics. The fundamental equations of irreversible thermodynamics can be written[4] in the following convenient notation:

$$X = -g\alpha, \tag{1}$$

$$\dot{\alpha} = LX, \quad X = R\dot{\alpha}\,(R = L^{-1}). \tag{2}$$

Here X is the force vector, α the state vector, $L(R)$ the conductivity ("resistance") matrix, and g is a symmetrical matrix,

$$g = \tilde{g}, \tag{3}$$

(the tilde denotes transposition), whose elements, are the negatives of the second-order derivatives

$$g_{ik} = -\partial^2 S/\partial\alpha_i\partial\alpha_k \tag{4}$$

of the entropy

$$S = S(\alpha_1, \alpha_2, \ldots, \alpha_n) = S(\alpha). \tag{5}$$

We note that in matrix notation X and α are columns, while their transposed values $(\tilde{X}, \tilde{\alpha})$ are rows

Since Eqs. (1) and (2) do not permit a determination of the symmetry properties of the matrix L, Popov proposes that the following equation holds:†

$$X = \ddot{\alpha}. \tag{6}$$

Using Eq. (6), Popov and Karanikolov[1,2] succeed, through rather lengthy computations, in deriving the reciprocity relation of Onsager

$$L = \tilde{L}. \tag{7}$$

In the present article we prove the following.

(1) Popov's results can be obtained in a considerably simpler form.

(2) Relation (6) of Popov is a very restrictive and, generally speaking, unfounded condition, which reduces to

$$L^{-2} = g, \quad L = g^{-1/2}. \tag{8}$$

(3) Instead of (6), it is necessary to use a general relation that can be considered with full justification as the thermodynamic analogy of Newton's equations of motion. Equation (6) and its equivalent, the expressions in (8), can be valid only in a few rather particular cases. It will be shown that Eq. (7) unfortunately no longer follows from the above-mentioned general relation.

2. The Onsager relation can be obtained very simply from Eqs. (6), (1), (2), and (3). We differentiate Eqs. (1) and (2) with respect to time

$$\dot{X} = -g\dot{\alpha}, \quad \dot{X} = L^{-1}\ddot{\alpha};$$

we use again Eq. (2)

$$L^{-1}\ddot{\alpha} = -g\dot{\alpha} = -gLX$$

and furthermore

$$-X = (LgL)^{-1}\ddot{\alpha} = Rg^{-1}R\ddot{\alpha}. \tag{9}$$

It is obvious that by deriving this relation we have solved the above problem. In fact, since Eq. (9) follows from (1) and (2), it is equivalent to these two equations. Furthermore, (9) has the same form as Newton's equation of motion

$$F = m\ddot{r}.$$

It is clear that Popov's relation holds only when

$$LgL = 1,$$

hence,

$$L^2 = g^{-1}, \quad L = g^{-1/2}, \quad |g| \neq 0.$$

It is obvious that if $g = \tilde{g}$, $g^{-1/2}$ is also symmetrical, i.e.,

$$L = g^{-1/2} = (\tilde{g}^{-1/2}) = \tilde{L}.$$

Since the equation of motion (9) results from Eqs. (1) and (2), and since the symmetry relation (7) does not follow from (1) and (2), it cannot follow from (9). Relation (7) is obtained only if we assume that L is a symmetrical function of the matrix g. At the present time we know of not one thermodynamic system for which L depends on g, so that this assumption is quite unfounded.

In analogy with Eq. (9), or with Eqs. (1) and (2), with Newtonian mechanics it can be followed by making the following comparisons:

F	$-X$
m	$(LgL)^{-1}$
r	α
$F = m\ddot{r}$	$-X = (LgL)^{-1}\ddot{\alpha}.$

Further comparisons pertain to the motion of a point under the influence of friction:

$$F = -\varkappa \ddot{r} \qquad -X = -R\dot{x}$$

$$\varkappa \qquad R.$$

The resistance matrix corresponds to the coefficient of friction.

There exists also an analogy in that respect, that the positive definite matrices $(LgL)^{-1}$ and R correspond, in the case of $|g| \neq 0$ and $|L| \neq 0$ to positive values of m and κ. The analogy remains in full force also in that case when we consider, instead of the motion of a point under the influence of friction, the rotation of a solid body in the presence of an anisotropic friction force.

Thus, the mechanical model of irreversible thermodynamics comprises rotation of a solid about a certain point in the presence of anisotropic friction. This model, to the extent that it is practically realizable, can be used to integrate the equation of motion of irreversible processes.

---

*For other work by Popov on this subject see the literature of reference 1.

†See Eq. (10) of reference 1.

---

[1] K. Popov, J. Exptl. Theoret. Phys. (U.S.S.R.) 28, 257 (1955), Soviet Phys. JETP 1, 336 (1955).

[2] Kh. Karanikolov, J. Exptl. Theoret. Phys. (U.S.S.R.) 28, 283 (1955), Soviet Phys. JETP 1, 265 (1955).

[3] L. Onsager, Phys. Rev. 37, 405 (1931), 38, 2265 (1931).

[4] S. R. de Groot, Thermodynamics of Irreversible Processes, Amsterdam, North Holland Publ. Co., 1952.

Translated by J. G. Adashko
216

---

*ON THE POSSIBILITY OF APPLYING THE BELEN'KII-TAMM EQUILIBRIUM SPECTRUM TO THE DETERMINATION OF (γ, n) REACTIONS**

V. A. SHKODA-UL' IANOV

The Uzhgorod State University

Submitted to JETP editor May 31, 1958

J. Exptl. Theoret. Phys. (U.S.S.R.) 35, 1041-1042 (October, 1958)

THE measurement of photonuclear cross sections in the energy range of 25 to 80-100 Mev with presently-known methods involves many difficulties. These difficulties are in a large measure due to the smallness of cross section of the (γ, n) reaction and to the relatively high neutron background in experiments of this kind.

A further difficulty is connected with the necessity of knowing the sensitivity of the monitor as a function of the photon energy. In contrast to earlier work, where the (γ, n) excitation functions were determined with thin specimens, we propose a new method of determination of photonuclear cross sections. The basic idea of this method is the utilization of the equilibrium photon spectrum obtained when the original monoenergetic electron beam strikes a target so thick that practically the full electron-photon shower can develop.

The number of photoneutrons thus generated in the thick block of the investigated material is connected with the equilibrium photon spectrum and with the cross section $\sigma_{\gamma n}(E)$ by the integral equation (see, e.g., reference 1)

$$Q(E_0) = \int_{E_t}^{E_0} \sigma_{\gamma n}(E)\,\Gamma_p(E_0 E)\,dE,$$

which in our case has a solution

$$\sigma_{\gamma n}(E_0) = \sigma_T(E_0) f(0)\left[\frac{E_0\beta}{f(0)}\frac{d^2 Q(E_0)}{dE_0^2} + E_0\frac{dQ(E_0)}{dE_0} - Q(E_0)\right], \tag{1}$$

where $\sigma_{\gamma n}(E_0)$ is the photoneutron production cross section, $\sigma_T(E_0)$ the total photon absorption cross section at energy E_0, β the critical energy, $Q(E_0)$ the neutron yield per primary electron of energy E_0, $f(0) = 2.29$, E_t the energy of the (γ, n) threshold in the material under investigation, $\Gamma_p(E_0E)$ the so-called equilibrium photon spectrum[2] which results when electrons of energy E_0 bombard a target of such thickness that practically the full electron-photon shower can develop.

Equation (1) was obtained by using the explicit expressions for $\Gamma_p(E_0E)$ given in reference 2.

It was reported in reference 3 that the uncertainties connected with the monitor problem alone can lead to errors in the cross section of (γ, n) reactions of the order of 100% in the 30 to 80 Mev energy region. In the same energy range, the cross sections can have additional errors of 50% due to errors in the determination of the photoneutron yield. In the presently proposed method the monitoring can be performed on the electron beam with greater accuracy (e.g., by means of a Faraday cup) than is possible on the bremsstrahlung beam.

We hope that our proposed method of the determination of the excitation functions of (γ, n) reactions in the region of relatively high energies will eliminate such large errors.

The author is deeply indebted to V. I. Gol'danskii and L. E. Lazareva for valuable discussion of a number of questions.

---

*Presented as a short communication on the All-Union Conference on Low- and Medium-Energy Nuclear Reactions, Moscow, 1957.

[1] V. I. Gol'danskii and V. A. Shkoda-Ul'ianov, J. Exptl. Theoret. Phys. (U.S.S.R.) 28, 623 (1955), Soviet Phys. JETP 1, 579 (1955).

[2] S. Z. Belen'kii, Лавинные процессы в космических лучах (Cascade Processes in Cosmic Rays) Gostekhizdat, Moscow (1948).

[3] L. W. Jones and K. M. Terwilliger, Phys. Rev. 91, 699 (1953).

Translated by M. Danos
217

DETERMINATION OF THE MOMENTUM AND EXCITATION ENERGY ACQUIRED BY A HEAVY NUCLEUS IN THE INTERACTION WITH A FAST NUCLEON

A. I. OBUKHOV

Radium Institute, Academy of Sciences, U.S.S.R.

Submitted to JETP editor June 2, 1958

J. Exptl. Theoret. Phys. (U.S.S.R.) 35, 1042-1044 (October, 1958)

ACCORDING to the model proposed by Serber,[1] particles with energy ~100 Mev and higher interact with the individual nucleons of the nucleus. As a result of the cascade of nucleon-nucleon collisions, the nucleus that remains after the emission of a few fast nucleons acquires a momentum and an excitation energy which, on the average, amount to a fraction of the momentum and the energy of the incident particle. Steiner and Jungerman[2] measured the component of the momentum of the nucleus along the direction of incidence of the proton for the interaction of uranium nuclei with protons of energy 190 and 340 Mev. The value found is ~⅓ of the momentum of the incident proton. The calculations of Porile and Sugarman[3] lead to the conclusion that, in the interaction of bismuth with protons of energy 468 Mev, the nucleus acquires a perpendicular momentum component which is of the same order of magnitude as the parallel component.

We determined experimentally the mean value of the parallel as well as the perpendicular component of the momentum of the nucleus for the interaction of 660-Mev protons with uranium nuclei. The photo-emulsion technique was used. We have assumed, in first approximation, that the angular distribution of the fission fragments is isotropic in the system of the fissioning nucleus. The parallel component of the nuclear momentum $P_{\parallel} = Mv_{\parallel}$ was determined from the expression $N_f/N_b = (1 + \eta_{\parallel})/(1 - \eta_{\parallel})$, where N_f, N_b are the numbers of fragments in the forward and backward hemispheres, respectively, $\eta_{\parallel} = v_{\parallel}/V$ is the ratio of the mean transfer velocity of the nucleus to the mean velocity of the fission fragments, and M is the mass of the nucleus after the emission of the cascade nucleons. Corrections were made for the failure of the apparatus to register fissions with an angle of inclination of $\leq 15°$ to the vertical. The perpendicular component of the momentum of the nucleus was determined from the angle between the tracks of the fragments which make an angle of $\leq 5°$ with the plane of the plate. The plate was exposed to a proton beam perpendicular to its surface:

$$P_{\perp} = Mv_{\perp}, \ \eta_{\perp} = \frac{v_{\perp}}{V} = \frac{\pi}{2} \tan \frac{\gamma_{\perp}}{2} \approx \frac{\pi\gamma_{\perp}}{4},$$

where $\gamma_{\perp}$ is the mean value of the complement to the angle between the fragments. Both equalities presuppose $M_h = M_l$. The effect of the scattering of the fission fragments from the nuclei of the emulsion is much smaller than the effect we are looking for. It was assumed that nucleon evaporation occurs until fission sets in, and that the former is isotropic. In the discussion we exclude fissions accompanied by the emission of particles with $Z \geq 2$, since the momentum of these particles is larger than or equal to the momentum we want to measure, and thus "smears out" the picture. The values found are: $\eta_{\parallel} = 0.039 \pm 0.010$ and $\eta_{\perp} = 0.049 \pm 0.007$. In the table we list the values of the components of the momentum of the nucleus and their ratio, calculated from the experimental values for $\eta_{\parallel}$ and $\eta_{\perp}$, where we assume $V = 0.04c$. We also list

	$P_{\parallel}$ (Mev/c)	$P_{\perp}$ (Mev/c)	$P_{\perp}/P_{\parallel}$
Experiment	340	430	1.26
Computation	280	380	1.35

the corresponding values computed from the data of Ivanova and P'ianov[4] on the angular and energy distributions of the cascade nucleons. These data were obtained in the calculation of the cascade for uranium at the proton energy of 660 Mev with the Monte Carlo method. In the calculation the creation of mesons was neglected.

The table shows qualitative agreement between the computed and experimental values. It should be kept in mind that the experimental values refer only to fission experiments.

From the experimental value for the parallel component of the momentum of the nucleus we can determine the excitation energy of the nucleus under the assumption, as in references 5 and 6, that the momenta of the cascade nucleons are transferred by way of one fast cascade particle in the direction of the incident proton beam. With our data, this gives $\overline{E}_f = 240$ Mev for uranium with $\overline{E}_p = 660$ Mev. This surpasses the value ~ 160 Mev of reference 6. Under the assumption that two fast cascade nucleons are emitted in the direction of the proton beam and perpendicular to it the measured values for the parallel and perpendicular components of the nucleus momentum yield for the excitation energy the value $\overline{E}_f =$ 145 Mev. It is seen that the presence of the perpendicular momentum component leads to a significantly lower value for E_f. It is obvious, however, that the second variant represents an extreme approximation just as the first variant does. It must also be pointed out that the perpendicular component of the momentum of the nucleus should be considered in the investigation of the angular distributions. The irregularity in the angular distribution of the fission fragments of bismuth in the 60 to 90° region in the laboratory system, found by Wolke and Gutman,[7] may possibly be explained by this fact, as these authors also noted.

In conclusion the author expresses his gratitude to Prof. N. A. Perfilov for a number of critical remarks, and to N. S. Ivanova and I. I. P'ianov for making available the computational data on the angular and energy distributions of the cascade nucleons of uranium.

---

[1] R. Serber, Phys. Rev. 72, 1114 (1947).

[2] N. M. Steiner and J. A. Jungerman, Phys. Rev. 101, 807 (1956).

[3] N. T. Porile and N. Sugarman, Phys. Rev. 107, 1410 (1957).

[4] N. S. Ivanova and I. I. P'ianov, J. Exptl. Theoret. Phys. (U.S.S.R.) 31, 416 (1956); Soviet Phys. JETP 4, 367 (1957).

[5] V. I. Ostroumov, Dokl. Akad. Nauk SSSR **103**, 409 (1955).

[6] V. P. Shamov, **Физика деления атомных ядер. Приложение №1 к журн. Атомн. энергия за** 1957 г. (The Physics of Nuclear Fission. Supplement No. 1 to the "Atomic Energy," 1957), Atomizdat, M., 1957, p. 129.

[7] R. L. Wolke and J. R. Gutman, Phys. Rev. **107**, 850 (1957).

Translated by R. Lipperheide
218

ON THE MULTIPLE INTERACTION IN QUANTUM FIELD THEORY

L. I. PODLUBNYI

Odessa Pedagogical Institute

Submitted to JETP editor June 7, 1958

J. Exptl. Theoret. Phys. (U.S.S.R.) **35**, 1044-1045 (October, 1958)

THE problem of constructing the nucleon potential with the inclusion of multiple interactions by summing over the corresponding terms in the perturbation expansion was considered in reference 1 in the framework of pair mesodynamics.

In the present paper, an expression for the effective potential for the multiple interaction of two particles is found in closed form. The discussion is based on the usual methods of Feynman and Dyson under the assumption $||E| - m| \ll m$. In the expansion for the energy of the free particle (e.g., the electron)

$$|E_n| = m + p_n^2/2m + \ldots \qquad (1)$$

(here, as in the following, $\hbar = c = 1$) we can therefore restrict ourselves to the first term $|E_n| \approx m$. It is easily seen[1] that in this case the Green's function for the electron has the form

$$\begin{aligned} S^F(2,1) &\approx \frac{1+\beta}{2}\,\delta(r_1 - r_2)\,e^{-im(t_2-t_1)}, \quad t_2 > t_1 \\ S^F(2,1) &\approx \frac{1-\beta}{2}\,\delta(r_1 - r_2)\,e^{im(t_2-t_1)}, \quad t_2 < t_1. \end{aligned} \qquad (2)$$

We note that the approximation (2) does not imply a transition to a theory with fixed sources $(m \to \infty)$, since the Green's function S^F would then depend only on the time.

Using (2) and carrying out all calculations in the coordinate representation, we obtain for the case of a process of order 2n, where the interacting particles interchange n virtual quanta,

$$S^{(2n)} = e^2\left(-\frac{e^2}{m^2}\right)^{n-1}\iint d^3r_1 d^3r_2\,|\varphi(r_1, r_2)|^2 \times \iint\limits_{-\infty}^{\infty} dt_1 dt_2\,[D^F(x_1 - x_2)]^n. \tag{3}$$

Summing over n and introducing the effective potential,[2]

$$S_{i\to f} = \sum_{n=1}^{\infty} S^{(2n)} = -i\iint d^3r_1 d^3r_2 \varphi_f^*(r_1, r_2) \times U(|r_1 - r_2|)\,\varphi_i(r_1, r_2)\lim_{t\to\infty}\int_{-\infty}^{t} e^{i\nu t_1}\,dt_1, \tag{4}$$

where $\nu = \epsilon_f - \epsilon_i = 0$. We find, finally,

$$U(r) = ie^2\int_{-\infty}^{\infty} D_F'(r, t)\,dt, \quad D_F' = \frac{D^F}{1 + r_0\lambda D^F}, \tag{5}$$

where r_0 is the classical electron radius, λ is the Compton wavelength (in our notation S^F and D^F are equal to $\frac{1}{2}S^F$ and $\frac{1}{2}D^F$ in reference 2, respectively).

Such simple results were obtained only by excluding the poles of type $[m^2 - (\omega_2 + \ldots + \omega_k)^2]^{-1}$ for processes involving n virtual quanta, keeping in mind the character of the approximation, i.e., $|\omega_2 + \ldots + \omega_k| < m$. It can be shown that these restrictions have, in any case, no bearing on the finiteness of the potential at the origin, which follows from (5):

$$U(r) = e^2/\sqrt{r^2 + R^2}, \quad R = \sqrt{r_0\lambda/\pi} \tag{6}$$

The form of expression (6) agrees with the potential proposed in reference 3. We have

$$U(r)|_{r=0} = m\sqrt{\pi\alpha}, \quad \alpha = 1/137.$$

In the calculations for the pseudoscalar mesodynamics with pseudoscalar coupling the order of the time integrations has to be changed; but the final result agrees with Eqs. (3) to (5): the nucleon potential depends on the distance like $\int_{-\infty}^{\infty}\Delta_F'(r, t)\,dt$, where

$$\Delta_F' = \Delta^F/[1 + (G/M)^2\Delta^F],$$

M is the mass of the nucleon, and G is the coupling constant.

---

[1] A. Klein, Phys. Rev. **91**, 740 (1953); **92**, 1017 (1953).

[2] A. I. Akhiezer and V. B. Berestetskii, Квантовая электродинамика (Quantum Electrodynamics), M. Gostekhizdat, 1953. [Engl. Transl. Publ. by U. S. Dept. of Commerce].

[3] D. D. Ivanenko and V. Lebedev, J. Exptl. Theoret. Phys. (U.S.S.R.) **22**, 639 (1952).

Translated by R. Lipperheide
219

LEVEL WIDTHS OF π-MESONIC ATOMS

A. I. LEBEDEV

P. N. Lebedev Physics Institute, Academy of Sciences, U.S.S.R.

Submitted to JETP editor June 14, 1958

J. Exptl. Theoret. Phys. (U.S.S.R.) **35**, 1045-1047 (October, 1958)

IF the interaction between slow negative pions and nuclei is considered as a perturbation to the Coulomb potential of a point source (see references 1 and 2), it is possible to estimate the potential of the meson-nucleus interaction. Denoting by v(r) the deviation of the interaction potential from its Coulomb value, we obtain, to first order of perturbation theory, the total shift ΔE_{nl} of the mesonic-atom level

$$\Delta E_{nl} = \int_0^{\infty} |\Psi_{nl}(r)\,{}^2 v(r)\,r^2 dr, \tag{1}$$

and the phase τ_{kl} of scattering of a slow pion by a nucleus denoted by I_l in reference 1), becomes

$$\tau_{kl} = -\frac{\pi\mu}{\hbar^2}k\int_0^{\infty}|\varphi_{kl}(r)|^2 v(r)\,r^2 dr. \tag{2}$$

Here k is the wave number of the meson, and v(r) differs from zero only when $r \leq r_Z$ [$r_Z = (\hbar/\mu c)A^{1/3}$ is the nuclear radius] and depends little on the energy in the low-energy region (~1 Mev); $\Psi_{nl}(r)$ is the wave function of the bound state in the Coulomb field, which has the following form as $r/R_{nZ} \to 0$ $\left(2R_{nZ} = \frac{\hbar^2}{\mu e^2}\frac{n}{Z}\right)$

$$\Psi_{nl}(r) = \left[\frac{(n+l)!}{2n(n-l-1)!}\right]^{1/2}\frac{1}{(2l+1)!}\left(\frac{1}{R_{nZ}}\right)^{3/2}\left(\frac{r}{R_{nZ}}\right)^l \tag{3}$$

and $\varphi_{kl}(r)$ is the regular wave function of the continuous spectrum in the Coulomb attraction field, which becomes, as $(kr) \to 0$

$$\varphi_{kl}(r) = \sqrt{\frac{2}{\pi}}\,C_l\,\frac{(kr)^l}{(2l+1)!!}, \tag{4}$$

$$C_l^2 = \frac{2\pi|\alpha|}{1 - \exp\{-2\pi|\alpha|\}}\prod_{s=1}^{l}\left(1 + \frac{\alpha^2}{s^2}\right); \quad \alpha = -\frac{Ze^2}{\hbar c}\sqrt{\frac{\mu c^2}{2E_\pi}}.$$

Considering in mesonic atoms only levels with values of n such that $r_Z/R_{nZ} \ll 1$, but to which perturbation theory is still applicable (n bounded from above), considering in the continuous spectrum such slow mesons for which $kr_Z \ll 1$, and using furthermore Eqs. (3) and (4), we obtain in lieu of (1) and (2)

$$\Delta E_{nl} = \frac{(n+l)!}{2n\,(n-l-1)!\,[(2l+1)!]^2}\left(\frac{1}{R_{nZ}}\right)^{2l+3}\int_0^{r_Z} r^{2(l+1)}\,v(r)\,dr, \tag{5}$$

$$\tau_{kl} = -\frac{2\mu}{\hbar^2}\,\frac{C_l^2}{[(2l+1)!!]^2}\,k^{2l+1}\int_0^{r_Z} r^{2(l+1)}\,v(r)\,dr. \tag{6}$$

Comparison of formulas (5) and (6) shows a simple connection between the level shift in the mesonic atom and the phase of scattering of a low-energy meson by a nucleus. This connection is a particular case of the more general relation obtained by Byers.[3]

In what follows we shall treat the imaginary part of the interaction potential Im v, which leads to a broadening of the levels (particularly by the 1S level) in mesonic atoms and to the absorption of pions when scattered by nuclei. We shall assume the imaginary part of the potential to be independent of r (the results of the calculations depend little on the shape of the potential and depend on r_Z, the average radius of the nuclear matter). Then, using (5) and using for Im ΔE_{1S} the value (0.45 ± 0.07) kev* measured experimentally by West and Bradley[4] for beryllium-9, we obtain for the S state Im v ≈ 1.5 Mev. An analogous estimate can be made using the two-nucleon model of absorption of pions by nuclei.[5] In this case (see, for example, reference 3), we obtain for the S state

$$\operatorname{Im}\tau = \Gamma\,\frac{Z}{6\pi}\left(\frac{\mu c}{\hbar}\right)10^{-27}\,C_0^2\,k\ \text{cm}^2, \tag{7}$$

where the parameter Γ characterizes the probability of absorption of a pion by a pair of nucleons in the nucleus, referred to the absorption in deuterium. Comparing this expression with formula (6) at $l = 0$ and taking $\Gamma = \sim 5$ (see reference 6), we get Im v = 0.28Γ ≈ 1.4 Mev, which is in approximate agreement with the quantity obtained above. Thus the complex portion of the potential, responsible for the absorption of slow mesons, is small.

Knowing the width of the 1S level, we can estimate the lifetime of the negative pion at this level for nuclear capture, and compare it with the lifetime for decay. This is of interest because Fry and White[7] reported observed cases of decay of negative pions stopped in emulsion and gave an approximate value of 10^3 for the ratio of the decay probability to the nuclear-absorption probability (for the light elements C, N, and O). Taken together with an approximate pion lifetime of 10^{-8} seconds, this gives approximately 10^{-11} seconds for the lifetime for nuclear capture. This contradicts, as noted by Gol'danskii and Podgoretskii,[8] the strong interaction between the pion and the nuclear matter. Since the time that the meson hits the 1S orbit of the mesonic atom amounts to approximately 10^{-13} seconds, the observed decay should occur obviously on this orbit. Yet the lifetime for nuclear capture, obtained by West and Bradley from a measurement of the level width (Δt Im $\Delta E \approx \hbar$) is approximately 10^{-18} seconds, which contradicts the results of Fry and White.

I am grateful to A. M. Baldin for a discussion of the above problems.

---

*Reference 4 gives the total level width $\gamma = (8/3)$ Im $\Delta E_{1S} = (1.2 \pm 0.2)$ kev.

---

[1] A. M. Baldin and A. I. Lebedev, J. Exptl. Theoret. Phys. (U.S.S.R.) **33**, 1221 (1957), Soviet Phys. JETP **6**, 940 (1958).

[2] S. M. Bilen'kii, J. Exptl. Theoret. Phys. (U.S.S.R.) **32**, 624 (1957), Soviet Phys. JETP **5**, 517 (1957).

[3] N. Byers, Phys. Rev. **107**, 843 (1957).

[4] D. West and E. F. Bradley, Phil. Mag. **2**, 957 (1957).

[5] Brueckner, Serber, and Watson, Phys. Rev. **84**, 258 (1951).

[6] F. H. Tenney and J. Tinlot, Phys. Rev. **92**, 974 (1953).

[7] W. F. Fry and G. R. White, Phys. Rev. **93**, 1427 (1954).

[8] V. I. Gol'danskii and M. I. Podgoretskii, J. Exptl. Theoret. Phys. (U.S.S.R.) **28**, 620 (1955), Soviet Phys. JETP **1**, 571 (1955).

Translated by J. G. Adashko
220

EXCHANGE EFFECTS IN FERROMAGNETIC RESONANCE

M. A. GINTSBURG

Submitted to JETP editor June 18, 1958;
resubmitted July 4, 1958

J. Exptl. Theoret. Phys. (U.S.S.R.) **35**, 1047-1049 (October, 1958)

In the present paper we find a single dispersion law for transverse electromagnetic waves and for spin waves, which takes into account both relativistic and exchange interactions. When the wavelength is shortened (at constant ω) the relative role of the displacement currents becomes less and less; on the contrary, the contribution from the exchange forces increases, and instead of transverse electromagnetic waves we get spin waves.

1. We start with the usual equations of motion for the magnetization,[1]

$$dM/dt = \gamma \{(H_{ex}a^2/M_S)[M\Delta M] + [MH]\}, \qquad (1)$$

where H_{ex} is the effective field of the exchange forces, a the lattice constant, M_S the saturation magnetization, H the magnetic field intensity in the sample, γ the ratio of the magnetic moment of the electron to its spin: $\gamma = 2.8$ Mcs/Oe. We shall put $M = M_S + m$, $H = H_i + h$ ($M_S \parallel H_i \parallel OY$), where H_i is the internal magnetic field inside the specimen, while h and m are the high-frequency components of the magnetic field and the magnetization. If $|m| \ll |M_S|$, $|h| \ll |H_i|$ we get from (1) for the waves E, H ~ $\exp i[k(y\cos\theta + x\sin\theta) + \omega t]$ the linear equations,

$$i\omega m_x = \gamma\{-H_{ex}a^2k^2m_z + M_sh_z - H_im_z\};$$
$$i\omega m_z = \gamma\{H_{ex}a^2k^2m_x - M_sh_x + H_im_x\},$$

from which we find the components of the magnetic susceptibility tensor,

$$\mu_{xx} = \mu_{zz} = \mu_1 = 1 - \frac{(\sigma_0 + \alpha k^2)\,p}{1 - (\sigma_0 + \alpha k^2)^2}; \qquad (2)$$
$$\mu_{xz} = -\mu_{zx} = i\mu_2 = \frac{ip}{1 - (\sigma_0 + \alpha k^2)^2},$$

where $\alpha = \gamma H_{ex}a^2/\omega$, $\sigma_0 = \gamma H_i/\omega$, $p = 4\pi M_S\gamma/\omega$. As $\alpha \rightarrow 0$ expression (2) goes over into the well known equations of Polder's.[2]

Absorption can be taken into account by substituting for ω, $\omega - i\gamma\Delta H$, where ΔH is the halfwidth of the resonance curve.

2. Substituting (2) into the general Eq. (4) of reference 3, which describes the propagation of electromagnetic waves in gyrotropic media, we find a connection between ω and k, the dispersion law,

$$\omega^6 - \omega^4[(\gamma B + \beta k^2)^2 + 2\omega_0^2] + \omega^2\{(\gamma B + \beta k^2)[2(\gamma H + \beta k^2) + 4\pi M_S\gamma\sin^2\theta] + \omega_0^2\}\omega_0^2 - (\gamma H + \beta k^2 + 4\pi M_S\gamma\sin^2\theta)(\gamma H + \beta k^2)\omega_0^4 = 0 \qquad (3)$$

($\omega_0 = ck/\sqrt{\epsilon}$, c is the velocity of light, $\beta = \alpha\omega$), which describes both transverse electromagnetic waves and spin waves. This equation is of the third degree in ω^2 and has three roots, corresponding to three branches of the dispersion curve. If we neglect the displacement currents (as $\omega\sqrt{\epsilon}/ck \rightarrow 0$), (3) goes over into the equation of the static approximation,

$$\omega^2 = (\gamma H + \beta k^2)(\gamma H + \beta k^2 + 4\pi M_S\gamma\sin^2\theta), \qquad (4)$$

i.e., into the spin wave dispersion relation found in reference 1.

3. The character of the dispersion curves can most conveniently be observed from the particular cases $\theta = 0$ and $\theta = \pi/2$.

(1) $\theta = 0$. In this case (3) has three positive solutions,

$$k_1^2 = \frac{1}{2\beta}\left\{-\left(\omega + \gamma H - \frac{\omega^2}{c^2}\varepsilon\beta\right) + \left[\left(\omega + \gamma H - \frac{\omega^2}{c^2}\varepsilon\beta\right)^2 + 4\frac{\omega^2}{c^2}\beta\varepsilon(\omega + \gamma B)\right]^{1/2}\right\}, \qquad (5)$$

$$k_{2,3}^2 = \frac{1}{2\beta}\left\{\left(\omega - \gamma H + \frac{\omega^2}{c^2}\varepsilon\beta\right) \pm \left[\left(\omega - \gamma H + \frac{\omega^2}{c^2}\varepsilon\beta\right)^2 + 4\frac{\omega^2}{c^2}\beta\varepsilon(\gamma B - \omega)\right]^{1/2}\right\}. \qquad (6)$$

Expression (5) describes the ordinary wave, (6) the extraordinary one. The (ω, k) plane can be divided into three regions: region A ($\omega < \gamma H$), region R ($\gamma H \le \omega \le \gamma B$), and region D ($\omega > \gamma B$). In region A only one of the extraordinary waves is propagated [the one corresponding to the plus sign before the radical in Eq. (6)], while the spin wave propagates in region R. In region D the spin wave branch is retained, but added to it is one branch of the transverse electromagnetic waves, the one corresponding to the minus sign in front of the square root in Eq. (6).

(2) $\theta = \pi/2$. In that case two waves are possible: type E and type H.[4] For waves of type E $k^2 = (\omega^2/c^2)\epsilon$. Dividing Eq. (3) by $k^2 - (\omega^2/c^2)\epsilon$ we get the dispersion law for waves of type H,

$$2\omega^2 = (\gamma B + \beta k^2)^2 + \omega_0^2 \pm \{[(\gamma B + \beta k^2)^2 + \omega_0^2]^2 - 4\omega_0^2(\gamma B + \beta k^2)(\gamma H + \beta k^2)\}^{1/2}. \qquad (7)$$

The ω(k) curves for intermediate values of θ lie between the dispersion curves corresponding to $\theta = 0$ and $\theta = \pi/2$. The line $\omega^2 = \gamma^2 H(H + 4\pi M_S\sin^2\theta)$ is the lower boundary of the region R, and the line $\omega = \gamma B$ its upper boundary.

---

[1] C. Herring and C. Kittel, Phys. Rev. 81, 869 (1951).

[2] D. Polder, Phil. Mag. 40, 99 (1949).

[3] M. A. Gintsburg, Dokl. Akad. Nauk SSSR, 95, 489 (1954).

[4] M. A. Gintsburg, Izv. Akad. Nauk SSSR, Ser. Fiz. 18, 444 (1954) [Columbia Techn. Transl. 18, 136 (1954)].

Translated by D. ter Haar
221

HOLE BANDS IN NaCl

T. I. KUCHER

Physics Institute, Academy of Sciences, Ukrainian S.S.R.

Submitted to JETP editor July 23, 1958

J. Exptl. Theoret. Phys. (U.S.S.R.) **35**, 1049-1050 (October, 1958)

In a recent paper[1] the author presented, in general form, a calculation of hole bands and of effective masses in them for NaCl-type crystals. The many-electron problem was solved by the Hartree-Fock method, in the tight-binding approximation. Because of the threefold degeneracy of the p-state of the halogen, there are three hole bands; the principal band has four minima at the points $\{\pm\pi/d;\ \pm\pi/d;\ \pm\pi/d\}$. Expressions were given previously[1] for the energy $E(\mathbf{k})$, the width of the principal band, the effective masses etc., in terms of two exchange integrals D and $\mathscr{E}$. The latter was calculated for KCl only in reference 1.

Analogous calulations (see reference 1) have been made for NaCl. The expression for the energy $E(\mathbf{k})$ as a function of the wave number $\mathbf{k}$ is:

$$E(\mathbf{k}) = \frac{2e^2}{d}\{B - 4D \underset{x \neq y}{\mathrm{S}} \cos k_x \cos k_y$$

$$+2(\mathscr{E}+D)\ [\underset{x \neq y}{\mathrm{S}}\ b^2 \cos k_x (\cos k_y + \cos k_z) \tag{1}$$

$$-2 \underset{x \neq y}{\mathrm{S}}\ bc \sin k_x \sin k_y]\},$$

where

$$B = \mathrm{const};$$

$$D = \frac{d}{6}\iiint \{Q(\mathbf{r}_s^{l'}) + P(\mathbf{r}_s^{l'})\}\, \psi_1^*(\mathbf{r}_s^{l})\, \psi_1(\mathbf{r}_s^{l'})\, d\tau = 1.57\cdot 10^{-2},$$

$$\mathscr{E} = -\frac{d}{6}\iiint \{Q(\mathbf{r}_s^{l'}) + P(\mathbf{r}_s^{l'})\}\, \psi^*_3(\mathbf{r}_s^{l})\, \psi_3(\mathbf{r}_s^{l'})\, d\tau = 6.7\cdot 10^{-2},$$

$$Q = \frac{\hbar^2}{2me^2}\left\{\alpha^2 - 2\alpha/|\mathbf{r}_s^{l'}| - 2/|\mathbf{r}_s^{l'}|^2\right\}, \tag{2}$$

$$P(\mathbf{r}) = \frac{2\alpha}{5}\left\{\frac{5}{\rho} + \frac{6}{\rho^3}\right.$$

$$\left. - 8\rho^2 \,\mathrm{Ei}(-2\rho) - e^{-2\rho}\left[4\rho + 13 + \frac{17}{\rho} + \frac{12}{\rho^2} + \frac{6}{\rho^3}\right]\right\},$$

$$\psi_1(\mathbf{r}) = (3\alpha^3/\pi\sqrt{2})\, e^{-\alpha r} \sin\vartheta\, e^{i\varphi},$$

$$\psi_3(\mathbf{r}) = (3\alpha^3/\pi)\, e^{-\alpha r} \cos\vartheta, \qquad \rho = \alpha r.$$

For NaCl, as for KCl, $\alpha = \alpha(\mathrm{Cl}) = 1.54 \times 10^8\ \mathrm{cm}^{-1}$, but $d(\mathrm{NaCl}) = 5.64 \times 10^{-8}$ cm.

The coefficients $\{b, c, a\} \equiv \mathbf{a}$ appear in Eq. (1) through the ψ function of the crystal

$$\psi = A \sum_{l=1}^{M} e^{i\mathbf{k}\mathbf{r}_s^l}\{b\psi_{s1}^l + c\psi_{s2}^l + a\psi_{s3}^i\}, \tag{3}$$

and in the last equation through the ψ function of the chlorine atom which is in the sl-th site, the ground state of which is threefold degenerate. These coefficients are determined (to satisfy the normalization condition $b^2 + c^2 + a^2 = 1$) from the condition for minimizing the energy [Eq. (1)], which leads to a third-order secular equation. On substituting the values of b, c and a, found in this way, into (1) we obtain (see reference 1):

1. The width of the principal band

$$(2e^2/d)\, 4\, (2\mathscr{E} - D) = 2.17 \text{ ev}. \tag{4}$$

2. The effective-mass tensor at the point $\{\pi/d;\ \pi/d:\ \pi/d\}$:

(a) parallel to the diagonal of the cube [111] — the longitudinal mass

$$\mu = \mu_{\min} = 6.38\cdot 10^{-2}/(2\mathscr{E} - D) = 0.539,$$

(b) perpendicular to the cube diagonal — the transverse mass

$$\mu = \mu_{\max} = 6.38\cdot 2\cdot 10^{-2}/(4\mathscr{E} + D) = 0.98.$$

Some of the increase in width of the principal band in NaCl, compared with KCl, comes from the smaller lattice constant of NaCl; the exchange integrals increase exponentially and this leads to a broadening of the band. Since the radial wave function of the Cl^- ion in Eq. (3) agrees with the Hartree value[2] only at distances $R > 1$ A,[1] the calculations are more accurate for NaCl than for KCl.

Casella[3] obtained a qualitatively similar result for the properties of hole bands in NaCl within the framework of the one-electron problem. A spherically-symmetrical potential was built up, by Slater's method, from the atomic 3p wave functions of argon, which Casella substituted for the ψ function of chlorine. As he took into account the threefold p-degeneracy of argon, his band behavior is analogous to reference 1. He obtained ~1.2 ev for the width of the principal hole band in NaCl, which is smaller than the value of 1.5 ev obtained by the present author for KCl.[1] Mention should be made of the old work of Shockley,[4] in which the Wigner-Seitz cellular method gave the hole band width of NaCl as 4.4 ev.

I take this opportunity to thank V. I. Fedorchenko for checking part of the calculations.

---

[1] T. I. Kucher, J. Exptl. Theoret. Phys. (U.S.S.R.) **34**, 394 (1958), Soviet Phys. JETP **7**, 274 (1958).

[2] D. R. Hartree and W. Hartree, Proc. Roy. Soc. **156**, 45 (1936).

[3] R. C. Casella, Phys. Rev. **104**, 1260 (1956).

[4] W. Shockley, Phys. Rev. **50**, 754 (1936).

Translated by R. Berman

ANGULAR DISTRIBUTION FOR THE DIFFRACTION SCATTERING OF DEUTERONS

I. I. IVANCHIK

P. N. Lebedev Physics Institute, Academy of Sciences, U.S.S.R.

Submitted to JETP editor June 27, 1958

J. Exptl. Theoret. Phys. (U.S.S.R.) **35**, 1050-1052 (October, 1958)

THE angular distribution of elastically scattered deuterons was considered in reference 1. However, as the authors themselves pointed out, their formula (10) is valid only for $\kappa' \ll p$. Here, κ is the transverse momentum acquired by the deuteron as a result of the scattering, $\kappa' = R$, R is the nuclear radius, R_d is the radius of the deuteron, and $p = R/R_d$. The theory of diffractional scattering is valid up to $\kappa \sim \mu c$, i.e., up to $\kappa' \sim 2p$. It is therefore of interest to obtain a formula covering the whole angular range.

We turn to the derivation of the angular distribution. We have

$$d\sigma = |A_x|^2 d\varkappa/(2\pi)^2,$$

where

$$A_\varkappa = \int e^{-i\varkappa\rho} d\boldsymbol{\rho} \int d\mathbf{r}\, \varphi^2{}_0(\mathbf{r}) \left[\omega\left(\boldsymbol{\rho} + \frac{\mathbf{r}}{2}\right) + \omega\left(\boldsymbol{\rho} - \frac{\mathbf{r}}{2}\right)\right. \tag{1}$$

$$\left. - \omega\left(\boldsymbol{\rho} + \frac{\mathbf{r}}{2}\right)\omega\left(\boldsymbol{\rho} - \frac{\mathbf{r}}{2}\right)\right], \qquad \omega(\boldsymbol{\rho}) = \begin{cases} 1 & \text{for} \quad \rho < R \\ 0 & \text{for} \quad \rho > R \end{cases}$$

Here, $\boldsymbol{\rho}$ is the radius vector of the center of mass of the deuteron in the plane perpendicular to the axis of the incident beam, $\mathbf{r}$ is the radius vector of the relative distance in the deuteron, $\varphi_0(\mathbf{r}) = \sqrt{\alpha/2\pi}\, e^{-\alpha r}/r$ is the internal wave function of the deuteron in the approximation of zero-range nuclear forces $(\alpha = 1/2R_d)$. We consider the case $R_d \ll R$, and replace the nucleus by a flat disk with a straight edge, as in references 2 and 3. We note that the expression inside the square bracket in (1) is equal to zero for $\rho < R$, while, for $\rho > R$, it equals unity in a band of width $2(\rho - R)$ and zero elsewhere. After these remarks, the integral (1) is easily evaluated with the result

$$A_\varkappa = 2\pi R^2 \left\{\frac{J_1(\varkappa')}{\varkappa'} + \frac{1}{2p}\int_0^\infty dx\, J_0\left[\varkappa'\left(1 + \frac{x}{2p}\right)\right] \mathscr{E}_1(x)\right\}$$
$$= 2\pi R^2 a_p(\varkappa'). \tag{2}$$

Here $J_0(x)$ and $J_1(x)$ are the Bessel functions, $\mathscr{E}_1(x)$ is the Gold integral:

$$\mathscr{E}_1(x) = \int_1^\infty e^{-xt}\, dt/t^2.$$

With the help of the formula

$$\int_0^\infty \varkappa' d\varkappa' J_0\left[\varkappa'\left(1 + \frac{x}{2p}\right)\right] J_0\left[\varkappa'\left(1 + \frac{x'}{2p}\right)\right] = \frac{2p\delta(x - x')}{1 + x/2p},$$

we easily verify that

$$\int d\sigma = \int |A_\varkappa|^2\, 2\pi\varkappa d\varkappa = \pi R^2 + \frac{2\pi}{3}(1 - \ln 2) R R_d.$$

This total cross section agrees with the total cross section of reference 1.

The function $a_p(\kappa')$ was tabulated for $p = R/R_d = 3$, which corresponds to $A = 216$:

$\varkappa' =$	0	1	2	3	4	5
$a_3(\varkappa') =$	0.5833	0.5691	0.3154	0.0656	—0.0796	—0.0797

$\varkappa' =$	6	7	8	9
$a_3(\varkappa') =$	0.0177	0.0356	0.0402	0.0088.

V. S. Popov pointed out to the author that the function (2) can be represented approximately (with accuracy ~ 10%) by the following expression:

$$a_p(\varkappa') = \frac{J_1(\varkappa')}{\varkappa'} + pJ_0(\varkappa') \frac{\ln(1 + \varkappa'^2/4p^2)}{\varkappa'^2}$$
$$+ \frac{J_1(\varkappa')}{\varkappa'^2}\left(1 - \frac{2p}{\varkappa'}\tan^{-1}\frac{\varkappa'}{2p}\right).$$

In terms of the angular variables, the required angular distribution has the following form:

$$d\sigma(\theta) = 2\pi R^2 |a_p(p_0 R\theta/h)|^2 (p_0 R/h)^2\, \theta d\theta, \tag{3}$$

where p_0 is the momentum of the incident deuteron. This distribution decreases much more slowly with increasing angles than the distribution in reference 1. We note that the width of the secondary maxima in the distribution (3) is one half of that for the diffraction of point particles.

---

[1] A. I. Akhiezer and A. G. Sitenko, J. Exptl. Theoret. Phys. (U.S.S.R.) **32**, 794 (1957), Soviet Phys. JETP **5**, 652 (1957).

[2] R. Glauber, Phys. Rev. **99**, 1515 (1955).

[3] R. Serber, Phys. Rev. **72**, 1008 (1947).

Translated by R. Lipperheide
223

GALVANO-MAGNETIC EFFECTS IN METALS WITH NEARLY EQUAL NUMBERS OF ELECTRONS AND HOLES

M. I. KAGANOV and V. G. PESCHANSKI

Physico-Technical Institute, Academy of Sciences, Ukrainian S.S.R. and Khar'kov State University

Submitted to JETP editor July 8, 1958

J. Exptl. Theoret. Phys. (U.S.S.R.) **35**, 1052-1053 (October, 1958)

A general theory of galvanomagnetic effects in metals, which explains the asymptotic behavior of the resistance tensor ρ_{ik} in high magnetic fields, is developed in reference 1. It has been shown that all metals (with closed Fermi surfaces) can be divided into two groups; one (Cu, Na, In, Al, . . .) with unequal number of electrons (n_1) and holes (n_2), and one (Bi, Be, Zn, Mg, . . .) with $n_1 + n_2$.*

Besides these limiting cases, we would expect approximate equality of the number of electrons and holes (i.e., $n_1 \approx n_2$) for a number of metals with small impurity content.[2] The relative difference $\Delta n/n$ ($\Delta n = n_1 - n_2$; $n = (n_1 + n_2)/2$) is a parameter which enables us to express the dependence of the resistance tensor on the magnetic field.

A calculation analogous to that described in reference 1 leads to the following results for the resistance ρ and the Hall constant R:

$$\rho \approx \rho' \frac{(H/H_1)^2}{1+\left(\frac{\Delta n}{n}\frac{H}{H_1}\right)^2}, \qquad H \gg H_1; \qquad (1)$$

$$R \approx \frac{1}{nec}\,\frac{a+\frac{\Delta n}{n}(H/H_1)^2}{1+\left(\frac{\Delta n}{n}\frac{H}{H_1}\right)^2}, \qquad H \gg H_1; \qquad (2)$$

$H_1 \sim m^*c/et_0$ (the notation is the same as in reference 1). The parameters ρ', H_1, and a depend on the angle between the magnetic field and the crystallographic axes, with a on the order of unity.

From (1) and (2) we obtain

$$\rho = \begin{cases} \rho'(H/H_1)^2 & (H_1 \ll H \ll H_1\,|n/\Delta n|) \\ \rho'(n/\Delta n)^2 & (H \gg H_1\,|n/\Delta n|) \end{cases}, \qquad (3)$$

$$R = \begin{cases} \frac{a}{nec} + \frac{\Delta n}{n^2 ec}(H/H_1)^2 & (H_1 \ll H \ll H_1\,|n/\Delta n|) \\ \frac{1}{\Delta nec} & (H \gg H_1\,|n/\Delta n|) \end{cases} \qquad (4)$$

We note furthermore that the present results agree well with the experiments of Alekseevskii, Brandt, and Kostina[2] on bismuth with small concentrations of impurities. In fact, independently of the law of dispersion, the ratio $HE_y/E_x = H^2R/\rho$ (see reference 2) varies linearly with the square of the magnetic field, and the sign of the coefficient of H^2 is determined by the sign of Δn.

---

*Note added in proof (September 1, 1958). Recent results of I. M. Lifshitz and V. G. Peschanskii on the one hand, and of N. E. Alekseevskii and Iu. P. Gadukov on the other, show that the division of metals into two groups is very provisional.[1] Apparently many metals have open Fermi surfaces.

---

[1] Lifshitz, Azbel', and Kaganov, J. Exptl. Theoret. Phys. (U.S.S.R.) **31**, 63 (1956), Soviet Phys. JETP **4**, 41 (1957).

[2] Alekseevski, Brandt, and Kostina, Dokl. Akad. Nauk SSSR **105**, 46 (1955).

Translated by R. Berman
224

TRANSITION FROM THE ANTIFERROMAGNETIC INTO THE FERROMAGNETIC STATE IN $CoSO_4$

A. S. BOROVIK-ROMANOV and N. M. KREINES

Institute of Physical Problems, Academy of Sciences, U.S.S.R.; All-Union Institute for Physico-Technical and Electronic Measurements

Submitted to JETP editor July 16, 1958

J. Exptl. Theoret. Phys. (U.S.S.R.) **35**, 1053-1055 (October, 1958)

We have investigated, jointly with Karasik,[1] the magnetic properties of anhydrous polycrystalline $CoSO_4$. We have established that this substance goes into an antiferromagnetic state near 15°K. In the present investigation we prepared single crystals of anhydrous $CoSO_4$ by weighing approximately 1.5 milligrams, using a procedure previously described.[2,3] The magnetic properties of these single crystals have been investigated at temperatures from 1.3 to 70°K. The crystals were obtained in bipyramidal form. The measurements were made along the axis joining the vertices of the pyramid (the c axis) and along axes that are coincident with the sides of the base

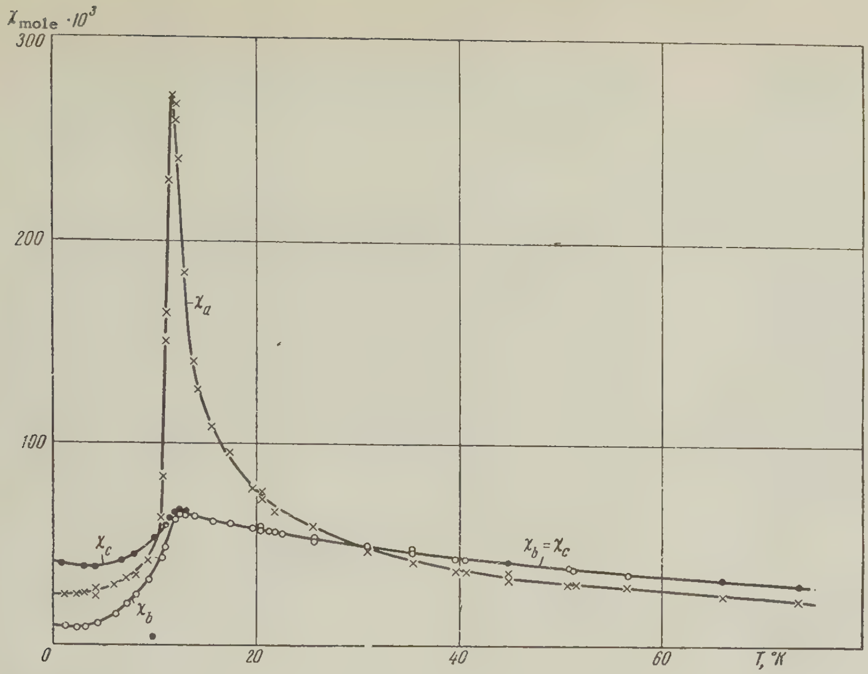

FIG. 1. Temperature dependence of molar susceptibility of single crystal of $CoSO_4$.

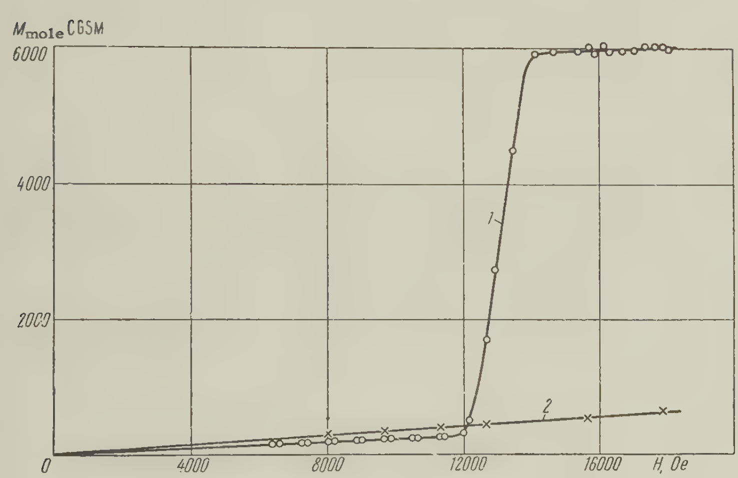

FIG. 2. Dependence of molar magnetic moment of $CoSO_4$ on the magnetic field at T = 4.2°K. 1) along a axis, 2) along b axis.

(the a axis corresponds to the smaller side and the b axis to the larger).

The magnetic susceptibility is independent of the field at all temperatures, up to fields of ~ 4 kilo-oersteds. The measured values of the susceptibility along all three axes of the crystal are shown in Fig. 1. The character of the resultant curves confirms that $CoSO_4$ goes into an anti-ferromagnetic state at $T_N = 12°K$. Attention must be called to the very sharp susceptibility peak along the a axis. It is probably due to the character of splitting of the Co^{++} in the crystal field. Another feature of the results is that as $T \rightarrow 0°K$ the susceptibility does not tend to zero along any of the axes.

The most interesting are the results obtained in strong fields. We have found that while the susceptibility along the b and c axes is independent of the field up to 18 kilo-oersteds, the magnetic properties along the a axis exhibit a sharp anomaly. Figure 2 shows the dependence of the molar magnetic moment on the field for two directions (a and c axes) at 4.2°K. We see that when a field is applied along the a axis the moment increases linearly until the field reaches 12 kilo-oersted. Increasing the field one kilo-oersted more causes a sharp jump in the moment, to ~ 6,000 cgs magnetic units, followed by a continuing very slight rise. The observed anomaly is obviously connected with the reversal of the magnetization vectors of the sublattices and the transition of the substance from anti-ferromagnetic into ferromagnetic state. Two interesting facts should be noted here. First the ferromagnetic moment does not reach saturation even at ~ 18 kilo-oersteds. Second, the value of the ferromagnetic moment amounts to merely 30% of the nominal moment, calculated under the assumption that the orbital moments are completely frozen.

An anomaly analogous to that observed by us for $CoSO_4$ was previously observed for $FeCl_2$ by Shalyt[4] in polycrystals and by Bizette et al.[5] in single crystals. However, $FeCl_2$ is a layered antiferromagnet with strong ferromagnetic interaction inside the layer and weak antiferromagnetic interaction between layers, a fact that manifests itself in the ferromagnetic sign of the constant Θ in the Curie-Weiss law. The reversal of the moments of the layer is quite natural in such a structure, even in weak fields. A similar behavior was also observed in the metallic $MnAu_2$, compound.[6] $CoSO_4$ is the first ionic crystal with such an antiferromagnetic sign of Θ that the antiferromagnetism is destroyed by a relatively weak magnetic field ($\mu H \ll kT_N$).

A detailed discussion of the observed anomaly will be made after a thorough study is completed of the phenomenon over the entire temperature range and after the structures of the crystals are established.

The authors express their deep gratitude to Academician P. L. Kaptiza for a continuous interest in this work and to Professor P. G. Strelkov for many valuable hints.

---

[1] Borovik-Romanov, Karasik, and Kreines, J. Exptl. Theoret. Phys. (U.S.S.R.) **31**, 19 (1956), Soviet Phys. JETP **4**, 109 (1957).

[2] A. S. Borovik-Romanov and N. M. Kreines, J. Exptl. Theoret. Phys. (U.S.S.R.) **33**, 1119 (1957), Soviet Phys. JETP **6**, 862 (1958).

[3] N. M. Kreines, J. Exptl. Theoret. Phys. (U.S.S.R.) **35**, 1391 (1958), Soviet Phys. JETP **8** (in press).

[4] S. S. Shalyt, J. Exptl. Theoret. Phys. (U.S.S.R.) **15**, 246 (1945).

[5] Bizette, Terrier, and Tsai, Compt. rend. **243**, 895 (1956).

[6] A. Y. P. Meyer and P. Taglang, Compt. rend. **239**, 961 (1954).

Translated by J. G. Adashko
225

COULOMB EXCITATION OF ALUMINUM

D. G. ALKHAZOV, A. P. GRINBERG, G. M. GUSINSKII, K. I. EROKHINA, and I. Kh. LEMBERG

Leningrad Physico-Technical Institute, Academy of Sciences, U.S.S.R.

Submitted to JETP editor July 9, 1958

J. Exptl. Theoret. Phys. (U.S.S.R.) **35**, 1055-1056 (October, 1958)

WE have investigated the Coulomb excitation of Al^{27} using heavy ions accelerated in a cyclotron — 15.9-Mev triply charged nitrogen ions and 18.1-Mev triply-charged oxygen ions. The γ radiation emitted during the bombardment of aluminum was studied using a scintillation γ spectrometer having a NaI (T1) crystal 40 mm in diameter and 40 mm high. A detailed description of the method, as well as the procedure for calculating $B(E2)\uparrow$, i.e., the reduced probability for electric quadrupole transition of the nucleus from its ground state to an excited state, was given earlier.[1,2]

The figure shows the spectrum of γ lines obtained from Coulomb excitation of aluminum by nitrogen ions. Two lines are observed, with $E = 0.84$ and 101 Mev. A study of the low energy region of the spectrum under the same conditions showed that the relative intensity η of the 0.84 + 0.17 Mev cascade does not exceed 4% of the direct transition to the ground state. According to reference 3, η is 2.2%.

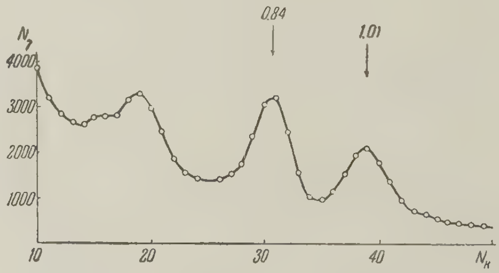

An attempt to excite the two levels of Al^{27} using 25-Mev nitrogen ions was unsuccessful, owing to the marked increase in γ-ray background from nuclear reactions.

The results obtained using nitrogen and oxygen ions are in good agreement with one another.

In computing the values of $B(E2)\uparrow$ from the yield of γ quanta from a thick target we assumed, on the basis of reference 4, that the stopping power of aluminum for nitrogen ions is 5.9 Mev-cm^2/mg. The values of $B(E2)\uparrow$ for the levels with $\Delta E = 0.84$ and 1.01 Mev are, respectively, 0.0019 and $0.0031\, e^2 \times 10^{-48}$ cm^4. Using the known values of the spins of the ground state and first two excited states of Al^{27},[5] we find that the partial lifetime

τ (E2) of the level at $\Delta E = 1.01$ Mev is 1.7×10^{-11} sec, while the lifetime of the level at $\Delta E = 0.84$ Mev is 1.7×10^{-11} sec. Previously only an upper limit of $\tau < 10^{-10}$ sec was known[6] for these levels in Al^{27}.

---

[1] Alkhazov, Andreev, Grinberg, and Lemberg, Izv. Akad. Nauk SSSR, ser. fiz. **20**, 1365 (1956). [Columbia Techn. Transl. **20**, 1249 (1956)].

[2] Alkhazov, Andreev, Erokhina, and Lemberg, J. Exptl. Theoret. Phys. (U.S.S.R.) **33**, 1347 (1957), Soviet Phys. JETP **6**, 1036 (1958).

[3] Almqvist, Bromley, Gove, and Litherland, Bull. Am. Phys. Soc. **2**, 178 (1957).

[4] Webb, Reynolds, and Zucker, Phys. Rev. **102**, 749 (1956).

[5] van der Leun, Endt, Kluyver, and Vrenken, Physica **22**, 1223 (1956).

[6] C. P. Swann and W. C. Porter, J. Frankl. Inst. **261**, 371 (1956).

Translated by M. Hamermesh
226

LIFETIME OF THE FIRST EXCITED STATE OF Mg^{24}

D. G. ALKHAZOV, A. P. GRINBERG, G. M. GUSINSKII, K. I. EROKHINA, and I. Kh. LEMBERG

Leningrad Physico-Technical Institute, Academy of Sciences, U.S.S.R.

Submitted to JETP editor July 9, 1958

J. Exptl. Theoret. Phys. (U.S.S.R.) **35**, 1056-1058 (October, 1958)

THE study of Coulomb excitation of nuclear levels enables us to calculate their lifetimes. For even-even nuclei the formula relating the lifetime τ of the excited state and the reduced probability $B(E2)\uparrow$ for transition from the spin 0 ground state to the first excited state (which has spin 2), has the form:

$$1/\tau = 2.46 \cdot 10^{-3} (\Delta E)^5 B(E2)\uparrow,$$

where ΔE is the energy of the level in kev, and $B(E2)$ is in units of $e^2 \times 10^{-48}$ cm^4.

Previously all attempts to excite the first level in Mg^{24} have been unsuccessful, because in this case $\Delta E = 1.37$ Mev and the energies of the α particles or protons necessary for Coulomb excitation of the level are so high that there is a marked increase in the interfering background from nuclear reactions.

In our work we used triply-charged ions of nitrogen and oxygen with energies of 15.9 and 18.1 Mev, respectively, and also quadruply-charged nitrogen ions having energies of 25.6 and 36 Mev.

The investigation of the Coulomb excitation of the first level of Mg^{24} using nitrogen and oxygen ions is made more complicated by the fact that, in the γ spectra we have investigated from Coulomb excitation of various elements, a parasitic line is always present at 1.37 Mev, i.e., a line coinciding with the one we are studying here. This line is apparently related to nuclear interaction of the nitrogen and oxygen ions with carbon deposited on the target during the operation of the cyclotron. We showed that if a target of carbon is irradiated with nitrogen or oxygen ions the intensity of the peak corresponding to a 1.37-Mev γ line increases approximately a hundredfold. We noted that, despite the spread of values of absolute yields of γ lines in the parasitic peaks, the ratio of the peak amplitude to the background changed only slightly during irradiation of targets of various materials with heavy ions.

The figure shows the γ spectrum from bombardment of natural magnesium by 15.9-Mev nitrogen ions. The dotted curve is the parasitic peak calculated on the basis of the observations mentioned above. We estimate that the maximum error in the determination of the area of the parasitic peak does not exceed ±5% of the area of the true peak. The average value of $B(E2)\uparrow$, determined from six different experiments, is $0.054\, e^2 \times 10^{-48}$ cm^4. This gives a value of $\tau = (1.5 \pm 0.4) \times 10^{-12}$ sec.

The lifetime of the first excited state of Mg^{24} was determined in reference 1 from data on inelastic scattering of 187 Mev electrons. According to reference 1, $\tau = 1.9 \times 10^{-12}$ sec; however the author points out that the method is not very accurate and that the result could be changed by a factor of the order of unity. At the Eighth Annual Conference on Nuclear Spectroscopy there were two reports[2,3], of measurements of τ (Mg^{24}). The lifetime of the first excited state of Mg^{24} was determined in these experiments by studying resonance scattering of γ-rays. The results of references 2 and 3 differ from one another by about a factor of 10. Our value of τ is close to the value of $\tau = (1.7 \pm 0.4) \times 10^{-12}$ sec reported in reference 2.

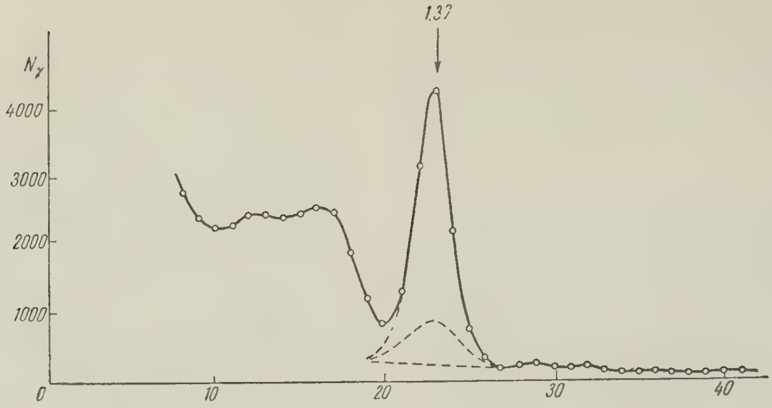

[1] R. H. Helm, Phys. Rev. **104**, 1466 (1956).

[2] N. N. Deliagin and V. S. Shpinel'. Report at the Eighth Annual Conference on Nuclear Spectroscopy, Leningrad, 1958.

[3] N. A. Burgov and Iu. V. Terekhov. Report at the Eighth Annual Conference on Nuclear Spectroscopy, Leningrad, 1958.

Translated by M. Hamermesh
227

FOCK'S CYCLIC SYMMETRY CONDITION AND YOUNG'S PATTERNS

G. I. ZEL'TSER

Leningrad Agricultural Institute

Submitted to JETP editor March 23, 1958

J. Exptl. Theoret. Phys. (U.S.S.R.) 35, 1058-1059 (October, 1958)

In constructing the wave function of an n-electron system by Fock's method,[1] the following conditions are imposed on the coordinate wave function Ψ:
(1) antisymmetry in the first k arguments,
(2) antisymmetry in the remaining n-k arguments,
(3) the cyclic-symmetry condition

$$(1 - \sum_{i=k+1}^{n} P_{ik})\Psi = 0 \qquad (1)$$

(P_{ik} is the operator for transposition of the arguments i and k.) It is assumed that $k \leq n-k$; then $s = n/2 - k$ is the total spin of the system.

It is known[2] that every function constructed from a Young pattern with two columns satisfies these conditions. In other words, it has been shown that the Young operator

$$Y_{n-k,k} = A(1,\ldots,k)\,A(k+1,\ldots,n)\prod_{m=1}^{k} S(m, k+m) \qquad (2)$$

(where S and A are the operators for symmetrization and antisymmetrization with respect to their arguments), corresponding to the pattern with two columns shown in Fig. 1, satisfies the cyclic symmetry condition

$$(1 - \sum_{i=k+1}^{n} P_{ik})\,Y_{n-k,k} = 0. \qquad (3)$$

In the present note we want to show that this result is easily generalized to Young patterns of arbitrary shape, containing any number of columns.

Let us consider a Young pattern of the most general type (Fig. 2), having p columns of lengths $\lambda_1, \lambda_2, \ldots \lambda_p$, where

$$\lambda_1 \geqslant \lambda_2 \geqslant \ldots \geqslant \lambda_p > 0 \text{ and } \lambda_1 + \lambda_2 + \ldots + \lambda_p = n.$$

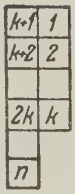

FIG. 1

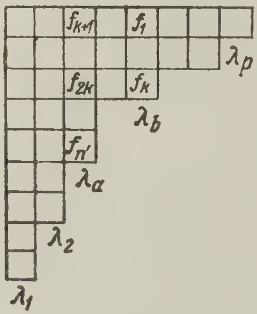

FIG. 2

In this case the Young operator consists of a symmetrization with respect to the arguments in the rows followed by antisymmetrization with respect to columns. We shall show that this operator satisfies the cyclic symmetry condition with respect to any pair of columns, say the columns a and b ($\lambda_a \geq \lambda_b$). For convenience of comparison with the case of two columns, we shall set $\lambda_b = k$ and $\lambda_a = n' - k$, and denote the arguments in the cells of these two columns by $f_1, f_2, \ldots f_k$ and $f_{k+1}, \ldots f_{n'}$, while the set of arguments in the other columns are denoted by g. The Young operator corresponding to our pattern can be written as

$$Y_{\lambda_1\lambda_2,\ldots,\lambda_p} = A'(g)\,A(f_1\ldots f_k) \times A(f_{k+1}\ldots f_{n'}) \prod_{m=1}^{k} S(f_m, f_{k+m})\, S'(f,\ g). \tag{4}$$

$A'(g)$ is the product of the antisymmetrizers for all columns except a and b. We have extracted from the row symmetrizers factors containing the symmetrization with respect to the pairs of arguments in columns a and b, and have denoted the product of the remaining factors by $S'(f, g)$.

We want to show that

$$\Big(1 - \sum_{i=k+1}^{n'} P_{f_i f_k}\Big)\, Y_{\lambda_1,\lambda_2,\ldots,\lambda_p} = 0. \tag{5}$$

But once the Young operator for the general case has been put in the form (4), relation (5) follows immediately from the already proven cyclic symmetry for the case of two columns, since the operator (. . .) in (5) commutes with the operator $A'(g)$.

A condition equivalent to (5), namely the impossibility of increasing the antisymmetry of a function which is antisymmetric with respect to groups of $\lambda_1, \lambda_2, \ldots \lambda_p$ arguments by adding to a larger group of arguments some argument from a shorter group (or a group of the same length) was the basis of Hund's[3] classification of the types of permutation symmetry of functions. Hund describes such a symmetry character as having the A-normal form $A(\lambda_1 + \lambda_2 + \ldots + \lambda_p)$. The case of $p = 4$ is of interest in treating the coordinate wave function of the nucleus when the forces are assumed to be independent of the spin and charge of the nucleons.[4]

Thus we have shown in the present note that a function symmetrized according to a general Young pattern has the A-normal form of Hund. The fact that Fock's condition is satisfied for Young patterns with two columns is an important special case of this result.

---

[1] V. A. Fock, J. Exptl. Theoret. Phys. (U.S.S.R.) **10**, 961 (1940).

[2] Iu. N. Demkov, J. Exptl. Theoret. Phys. (U.S.S.R.) **34**, 714 (1958), Soviet Phys. JETP **7**, 491 (1958).

[3] F. Hund, Z. Physik **43**, 788 (1927).

[4] F. Hund, Z. Physik **105**, 202 (1937).

Translated by M. Hamermesh
228

MEASUREMENT OF THE HALF-LIFE OF THE NEUTRON

A. N. SOSNOVSKII,* P. E. SPIVAK, Iu. A. PROKOF'EV, I. E. KUTIKOV, and Iu. P. DOBRYNIN*

Submitted to JETP editor July 11, 1958

J. Exptl. Theoret. Phys. (U.S.S.R.) **35**, 1059-1061 (October, 1958)

THE present work, the purpose of which is to measure the neutron half-life with an accuracy considerably greater than that of previous experiments,[1-3] was undertaken by us in view of the special interest at present in the form of the β interaction.

The measurements were made in an apparatus shown in longitudinal section in Fig. 1. A well-collimated beam of neutrons from the RFT reactor (Physics and Engineering Reactor) passed through the evacuated chamber 1; decay protons appearing in the part of the beam opposite the diaphragm 2 passed through a field-free space to the grid 3 and were focused on the window of the proportional counter 5 by an electric field applied between grids 3 and 4. The strength of the electric field was considerably greater than the computed value for 100% focusing of the protons. The neutron half-life T, in minutes, is given by the formula $T = Jk\alpha \ln 2/n$, where J is the integral of the neutron density over the cross section of the beam, n is the number of decay protons recorded per minute, α is the transmission of the grids, and k is a coefficient whose value is determined only by the geometry of the apparatus and the distribution of the neutron density in the beam and is independent of the shape of the proton spectrum.

The neutron density was determined from activation of gold targets, making the appropriate corrections for the effect of resonance neutrons, and also from activation of targets of sodium, which follows a $1/v$ law. In both cases, the standardization was done by absolute β counting on gold.

The neutron density measured at the center of the beam was 2.17×10^3 neutrons/cm^3 in these experiments, while the integral of the neutron density over the cross section of the beam was $J = 7.68 \times 10^4 \pm 2\%$. The number of decay protons was determined from the difference of the counter readings with and without electric field. As a result of many series of measurements at the value of J cited above, we found the value $n = 30.0 \pm 0.4$ min^{-1}. The transmission α of the grids,

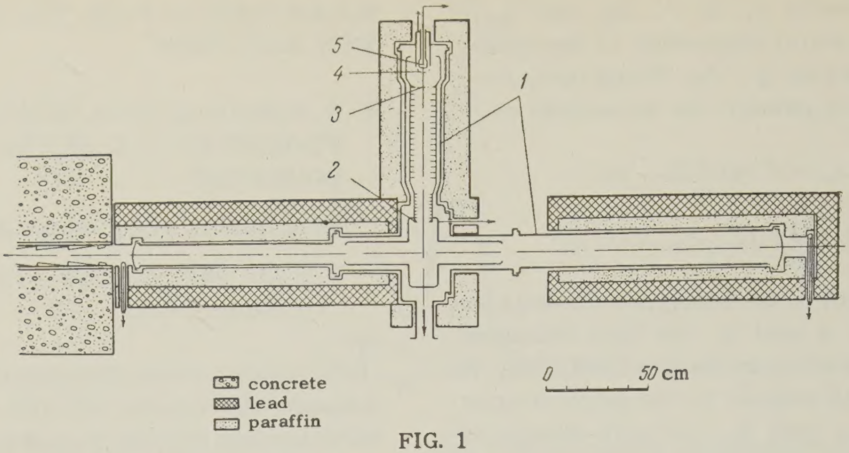

FIG. 1

taking account of the slight correction $(\sim 1 - 1.5\%)$ due to its dependence on the angle of incidence of the protons, was $0.84 \pm 0.5\%$. The coefficient k was determined on a computer† and was equal, to 7.87×10^{-3}. The uncertainty in this number was determined mainly by the lack of precision in fixing the geometry of the apparatus, and did not exceed a few tenths of a percent.

Inserting these values in the expression for T gives a value of $T = (11.7 \pm 0.3)$ min for the neutron half-life. This half-life leads to an ft value for the neutron of 1180 ± 35. If we make use of the relation between the ft value and the ratio of the coupling constants g_{GT} and g_F, we find from a comparison of the neutron ft value and that of O^{14} (ft = 3100[4]) the value $|g_{GT}/g_F|^2 = 1.42 \pm 0.08$ for this ratio.

*Deceased.

†The authors express their thanks to E. S. Kuznetsov, M. R. Shura-Bura, and their co-workers I. G. Krutikov, V. N. Toroptsev and O. B. Moskalev, who made these computations.

---

[1] Snell, Pleasonton, and McCord, Phys. Rev. 78, 310 (1950).

[2] J. M. Robson, Phys. Rev. 83, 349 (1951).

[3] A. N. Sosnovskii and P. E. Spivak. Report at the International Conference, Geneva, 1955; vol. II, p. 38.

[4] J. B. Gerhart, Phys. Rev. 109, 897 (1958).

Translated by M. Hamermesh
229

POLARIZATION OF RaE *ELECTRONS AND TIME REVERSAL INVARIANCE*

A. I. ALIKHANOV, G. P. ELISEEV, and V. A. LIUBIMOV

Submitted to JETP editor August 20, 1958

J. Exptl. Theoret. Phys. (U.S.S.R.) 35, 1061-1062 (October, 1958)

IN a previous paper by the authors[1] it was shown that for β decays in heavy nuclei corresponding to first forbidden transitions (so-called Coulomb transitions, $\Delta J \neq 2$, as well as unique transitions $\Delta J = 2$, yes) the longitudinal polarization of the electrons should equal $-v/c$ accurate to 5%, and should be energy independent. However there exists a Coulomb transition, namely RaE $(1^- \rightarrow 0^+)$, for which the shape of the β-spectrum is anomalous.

To explain this anomaly, Yamada[2] postulated an accidental cancellation of matrix elements such that the large energy independent terms determining the β spectrum are reduced by destructive interference down to 1% of their value; thus the small energy dependent terms become important and are responsible for the anomaly in the β-spectrum shape. Two parameters, x and y, are introduced, representing the ratios of two matrix elements to a third one and by an appropriate choice of these parameters the normal β-spectrum shape is changed to fit the experimental shape for RaE.

The fit is obtained by the introduction of a correction factor $C(R_0, \epsilon, x, y)$[3-6] where R_0 is the nuclear radius and ϵ the total energy. It is to be expected that if the accidental-cancellation hypothesis is valid the magnitude of longitudinal polarization $(-\langle\sigma\rangle c/v)$ of electrons will also exhibit an anomaly in the exceptional case of RaE.

This case is of particular interest since, as was noted by Lewis[6] and Fujita et al,[7] the Yamada hypothesis permits limits to be set on the violation of time-reversal invariance.

The additional term arising from the assumption that the β decay coupling constants are complex affects the correction factor and narrows down the range of possible fits to the experimental spectrum shape.

We have measured the longitudinal polarization of electrons of average energy $\overline{E} = 125$ and 350 kev using the apparatus and technique previously described.[1]

The source of Ra(D + E) of 5 millicurie intensity was approximately 0.8 mg/cm^2 thick. We obtained $-\langle\sigma\rangle\ c/v = 0.733 \pm 0.06$ and 0.725 ± 0.06 (average: 0.73 ± 0.04) for $\overline{E} = 125$ and 390 kev respectively.

Geshkenbein, Nemirovskaia, and Rudik,[8] drawing on the above mentioned papers, calculated the longitudinal polarization for RaE electrons for the VA and ST covariants allowing for parity nonconservation, and assuming time reversal invariance either to be valid or to be violated.

In the case of the VA covariants, the two parameters entering into the correction factor are

$$x = (iC_V/C_A)\int \mathbf{r} \Big/ \int [\sigma\times\mathbf{r}], \qquad y = (C_V/C_A)\int \alpha \Big/ \int [\sigma\times\mathbf{r}].$$

Under the assumption of time reversal invariance ($F^2 = 0$) the parameter x is limited by the spectrum shape to lie in the range $2 > x > 0.2$, and the theoretically-possible values for $-\langle\sigma\rangle\ c/v$ at E = 250 kev lie between 0.67 and 0.835. The experimental value 0.73 ± 0.04 lies within these narrow limits which serves as confirmation of Yamada's hypothesis and limits x to the range $2 > x > 1$, i.e., reduces the uncertainty in x by a factor of 5. The magnitude of the polarization is very sensitive to time reversal invariance violation. Taking the same range of values $2 > x > 1$ and $F^2 = 6 \times 10^{-3}$, $F < 0$ (where F is the imaginary part of C_A) we have: $0.63 > -\langle\sigma\rangle\ c/v > 0.57$ and for $F > 0$: $0.85 > -\langle\sigma\rangle\ c/v > 0.79$. Both cases are in disagreement with experiment.

However, it is possible to fit the experiment with $F^2 = 6 \times 10^{-3}$, $F < 0$ provided $0.2 < x < 0.5$; the polarization then lies in the range $0.71 > -\langle\sigma\rangle\ c/v > 0.67$ and $x = 0.2$ is the minimum value of the parameter x that will yield a fit for the spectrum. From this the maximum possible value of F and, consequently, of time reversal invariance violation turns out to be less than 7.5% which coresponds to an angle $\Delta\theta$ between A and V of $\sim 4.5°$. At this time this appears to be the most precise determination of time reversal invariance.

A greater precision would be possible if an independent determination (e.g., by use of shell model calculations) were made of at least the order of magnitude of the parameter x or if the energy dependence in the range from 100 to 700 kev of the longitudinal polarization of RaE electrons were measured.

---

[1] Alikhanov, Eliseev, and Liubimov, J. Exptl. Theoret. Phys. (U.S.S.R.) **34**, 1045 (1958), Soviet Phys. JETP **7**, 723 (1958).

[2] M. Yamada, Progr. Theoret. Phys. Japan **10**, 252 (1953).

[3] G. E. Lee-Whiting, Phys. Rev. **97**, 463 (1955).

[4] E. A. Plassman and L. M. Langer, Phys. Rev. **96**, 1593 (1954).

[5] Takebe, Nakamura, and Taketani, Progr. Theoret. Phys. (Japan) **14**, 317 (1955).

[6] R. R. Lewis, Phys. Rev. **108**, 904 (1957).

[7] Fujita, Yamada, Matumoto, and Nakamura, Phys. Rev. **108**, 1104 (1957).

[8] Geshkenbein, Nemirovskaia, and Rudik, J. Exptl. Theoret. Phys. (U.S.S.R.) (in press).

Translated by A. Bincer
230

A NOTE ON d-d REACTIONS

I. Sh. VASHAKIDZE and O. D. CHEISHVILI

Tbilisi (Tiflis) State University

Submitted to JETP editor April 25, 1958

J. Exptl. Theoret. Phys. (U.S.S.R.) **35**, 1062-1063 (October, 1958)

RECENTLY D. I. Blokhintsev[1] made the suggestion that the formation of "sub-barrier" fragments in the disintegration of nuclei by high energy nucleons can be explained by assuming that during the motion of the nucleons in the nucleus a close agglomeration of nucleons can result from fluctuations. As a result of a direct collision of the incident particle with such a cluster, "sub-barrier" fragments are produced. The results were compared with experiments on the scattering of 675-Mev protons by light nuclei.

A test of these ideas can be made with a variety of nuclear reactions, including the d + d reactions at these same energies. These reactions can proceed via the following channels:

$$d + d\ (1),\quad d + n + p\ (2),\quad 2n + 2p\ (3),$$
$$\mathrm{He}^3 + n\ (4),\quad \mathrm{H}^3 + p\ (5),\quad \mathrm{He}^4 + \gamma\ (6). \qquad (1)$$

If we denote the total cross section for the d + d reaction by σ_t, and the probability that it proceeds via the i-th channel by W_i, the cross sections for the reactions enumerated above can be written as $\sigma_i = \sigma_t W_i$, where σ_i is the cross section for the i-th reaction, and each W_i can be expressed as

$$W_1 = W_d^2,\quad W_2 = 2W_d(1 - W_d),\quad W_3 = (1 - W_d)^2,$$
$$W_4 = W_{\mathrm{He}^3},\quad W_5 = W_{\mathrm{H}^3},\quad W_6 = W_{\mathrm{He}^4}.$$

Here W_d is the probability for finding the two nucleons in the deuteron so close to one another that the impinging high energy particle cannot break up the deuteron and transfers its energy to the system as a whole;[1] W_{He^3} is the probability that in the "intermediate" state of the reaction a tightly bound system of two protons and a neutron is formed (this probability is different from that considered in Blokhintsev's paper); the probabilities W_{H^3} and W_{He^4} are defined similarly.

If we use the numerical value $W_d \approx 7 \times 10^{-3}$, we find for the ratio of the first three reactions: $\sigma_1/\sigma_3 \approx 5 \times 10^{-5}$, $\sigma_2/\sigma_3 \approx 1.4 \times 10^{-2}$.

Concerning the other reactions one can only assert that the ratio σ_4/σ_5 will be close to unity, its value being dependent on the extent to which the nuclear forces are charge independent at high energies, as is indicated by the experimental data.[2] Apparently at these energies the reactions are due mainly to indirect processes. The determination of their cross sections would enable one to estimate the role of indirect interactions in these processes.

---

[1] D. I. Blokhintsev, J. Exptl. Theoret. Phys. (U.S.S.R.) **33**, 1295 (1957); Soviet Phys. JETP **6**, 995 (1958).

[2] C. S. Godfrey, Phys. Rev. **96**, 1621 (1954).

Translated by M. Hamermesh
231